Understanding the lubrication mechanisms of ionic liquids when used as additives or as neat lubricants

By

Waleed Tareq Ibrahim Al-Sallami

Submitted in accordance with the requirements for the degree of
Doctor of Philosophy

The University of Leeds
Institution of Functional Surfaces
School of Mechanical Engineering

October, 2019

Publication Statement

The candidate confirms that the work submitted is his/her own, except where work which has formed part of jointly-authored publications has been included. The contribution of the candidate and the other authors to this work has been explicitly indicated below. The candidate confirms that appropriate credit has been given within the thesis where reference has been made to the work of others. *Further details of the jointly-authored publications and the contributions of the candidate and the other authors to the work should be included below this statement.*

Work Formed Jointly Authored Publication

During my PhD study the publications have been written with the help of my supervisors and colleagues. The contribution of the authors will be stated for each paper:

1- Al-Sallami W, Parsaeian P, Dorgham A, Neville A. Reactivity of oil-soluble IL with silicon surface at elevated temperature. Lubrication Science. 2019 Jun.
   This paper is presented in chapter 4. The candidate has done the experimental work, the analysis and the writing. The co-authors are the supervisors and a colleague Dr. Abdel Dorgham who contributes in the revision process before the submission.

2- Al-Sallami W, Parsaeian P, Neville A. An appraisal of the thermal decomposition mechanisms of ILs as potential lubricants. Lubrication Science. 2019 Apr.
   This paper is presented in chapter 6. The candidate has done the experimental work, the analysis and the writing. The co-authors are the supervisors.

3- Conference publication (The IET new challenges in tribology): “Can PP Ionic liquid be a replacement for ZDDP in some conditions?”. A poster has been presented. The work is taken from this thesis (chapter 5). The candidate is the author and the co-authors are the supervisors.

4- Conference publication (46th Leeds-Lyon): “Effect of ILs’ chemistry on their lubrication mechanism under various sliding distances”. The work is presented orally. The work is presented in chapter 7. This work will be submitted as a full paper. The candidate is the author and the co-authors are the supervisors.

5- Conference publication (ITC 2019 in Japan): “Effect of ILs’ chemistry on their lubrication mechanism”. The work is presented orally. A summary for chapters 6 and 7 will be presented. The candidate is the author and the co-authors are the supervisors.

6- Conference publication (TriboUK 2019 in Leeds): “The reactivity of neat ILs lubricants with silicon surfaces at elevated temperatures”. It is part from the material presents in chapter 6.

Work to be Submitted Soon:

1- Journal paper will be submitted in the tribology international journal. The paper is titled: “Effect of ILs’ chemistry on their lubrication mechanism under various contact pressures”. Al-Sallami W, Parsaeian P, Dorgham A, Neville A. This paper is part from the material presented in chapter 7.

2- Journal paper will be submitted in the tribology international journal. The paper is titled: “Oil-soluble IL to lubricate silicon”. Al-Sallami W, Parsaeian P, Dorgham A, Neville A. This paper presents the whole material presented in chapter 5.

3- The paper that accepted in Leeds-Lyon conference 2019 will be submitted in the tribology international journal.

4- A journal paper titled “The reactivity of neat ILs lubricants with silicon surfaces at elevated temperatures” is written. Al-Sallami W, Parsaeian P, Dorgham A, Neville A. The paper is part of the material presented in chapter 6.

Acknowledgements

Firstly, in the name of Allah, the Most Gracious and the Most Merciful, all praises to Allah for the strength and His blessing in completing this thesis.

I would like to express my pleasure to work under supervision of professor Anne Neville and Dr. Pourya Parsaeian. I would like to say thanks a lot for everything that you have done for me. Your unlimited support is the key point to achieve this work. Also, I would like to thank Dr. Filippo Mangolini for his help in the first part of this work.

To my family, I have to say that nothing can be achieved without your support in every single step in my life. To my parents in particular, you have sacrificed a lot and spent all your lives to provide me a proper education. Thus, I think this work is simply yours. My brothers, my sister and my wife also deserve a very big thanks for their help and support.

To all friends, I would like to thank you all for all your support. Your support helps me to overcome any unexpected trouble in my life during my study.

To my colleagues, in iFS, I would say it is the best working atmosphere that I have ever been. Thanks for all staff, PhD students and the technicians for their gentle help. We worked together and I can confirm that all researchers in the iFS are extreme cooperative.

Abstract

The promising properties of ionic liquids have attracted many tribologists to use them as lubricants. They have been used as either neat lubricants or as anti-wear additives. The results show that ionic liquids reacted/adsorbed with the lubricated surfaces and form a protective layer (tribofilm). A large number of previous studies have examined the tribological performance of ionic liquids. However, the relationship between the tribological performance and ionic liquids' chemistry is still not fully understood. The previous studies focused on the suggestion of various ionic liquids as lubricants and study their tribological behaviour. The effect of ionic liquids' chemistry, including anion and cation chain lengths, anion type and cation type, on their lubrication mechanism is still not fully understood. This lack of knowledge is the motivation to conduct the first part of this study (using neat ionic liquids as lubricants).

In terms of effective anti-wear additives, Zinc Dialkyl Dithio Phosphate (ZDDP) is one of the most common. However, the production of ash when it is decomposed and the emission of harmful gases push researchers to identify alternatives which can provide comparable anti-wear performance. Therefore, ashless additives are proposed as anti-wear additives instead of ZDDP. Soluble ILs are also suggested to be an effective alternative to ZDDP, especially when lubricating light alloys. Phosphonium phosphate (PP) ionic liquid is oil-soluble. Recent studies showed that this ionic liquid provided a superior anti-wear performance than ZDDP at some conditions (high temperature and sliding distance over 40 m). However, the reason behind this superior performance is still vague. This lack of knowledge is the motivation to conduct the second part of this study. It compares the reactivity and the tribological performance of both anti-wear additives (ZDDP and PP).

The lubrication mechanism is studied by considering the formation mechanisms of both *thermal* and *tribo* films. The durability of both films are studied. A nanotribometer is used to conduct the tribological experiments. Two tribopairs are utilized; borosilicate against silicon to simulate the working of Micro Electro Mechanical Systems.

Silicon against steel to simulate the working of the internal combustion engines (piston ring versus cylinder). Al-Si is commonly used as a cylinder liner material and the counter face is steel based piston rings. Previous studies showed that tribochemical studies using Si can be a good analogue for the Al-Si.

PP ionic liquid is used as a sample of oil-soluble ionic liquid and compared with ZDDP. Five ionic liquids are used as neat lubricants which are ethyl methyl imidazolium ethyl sulfate, ethyl methyl imidazolium octyl sulfate, butyl methyl imidazolium octyl sulfate, ethyl methyl imidazolium ethyl phosphate and butyl methyl phosphonium ethyl sulfate. Surface morphology of the thermal and tribo films is analysed by using Scanning Electron Microscopy, Atomic Force Microscopy and white light interferometry. Besides, surface chemistry is analysed using Energy Dispersive Spectroscopy, Fourier-transform infrared spectroscopy and X-ray Photoelectron Spectroscopy.

The results show that the formation rate of thermal/tribo films for Zinc Dialkyl Dithio Phosphate is higher than the formation rate for phosphonium phosphate. The absence of the positive cation after the decomposition of phosphonium phosphate leads to a self-limited formation of its thermal/tribo film. In contrast, the presence of zinc cation maintains the formation of thermal/tribo film. This causes a higher consumption of Zinc Dialkyl Dithio Phosphate (faster depletion). This leads to phosphonium phosphate can provide higher protection against wear at the highest sliding distance.

The results of the use of ionic liquids as neat lubricants show that their chemistry strongly affects their tribological performance. The reactivity of ionic liquids and hence the thickness of the thermal/tribo films is strongly affected by their chemistry. Further, the ionic liquids' chemistry also affects the viscosity and thermal stability. All the examined ionic liquids reacted with silicon surfaces and formed thermal films. Lastly, the formation of tribofilms by ionic liquids enhances the tribological behaviour of the lubricated surfaces.

Table of Contents

Acknowledgements ... iv

Abstract ... v

Table of Contents ... vii

List of Tables ... xii

List of Figures ... xiv

1. Chapter 1: Introduction and Background ... 1

- 1.1 Energy Losses and Fuel Economy ... 1
- 1.2 Ionic Liquids for Lubrication ... 2
- 1.3 Aim and Objectives ... 4
- 1.4 Thesis Chapters Layout ... 5
- 1.5 General Background ... 5
  - 1.5.1 Tribology ... 5
  - 1.5.2 Lubricants ... 6
  - 1.5.3 Lubrication Regimes ... 9
  - 1.5.4 Ionic Liquids (ILs) ... 10

2. Chapter 2: Literature Review ... 13

- 2.1 Introduction ... 13
- 2.2 ILs Lubricants ... 14
  - 2.2.1 ILs as Potential Lubricants ... 14
    - 2.2.1.1 Imidazolium Based ILs ... 14
    - 2.2.1.2 Ammonium Based ILs ... 19
    - 2.2.1.3 Phosphonium Based ILs ... 20
    - 2.2.1.4 Studies Using Various Cations ... 20
  - 2.2.2 Using ILs as Additives ... 24
    - 2.2.2.1 Imidazolium Based ILs ... 24
    - 2.2.2.2 Ammonium Based ILs ... 25
    - 2.2.2.3 Phosphonium Based ILs ... 26
    - 2.2.2.4 Studies using Various Cations ... 28
- 2.3 Nano/Micro Scale Studies and the Lubrication of MEMS ... 32
- 2.4 Summary and the Current Gap of Knowledge ... 36

3. Chapter 3: Methodology ... 38

- 3.1 Introduction ... 38
- 3.2 Instruments ... 38
  - 3.2.1 Hot Plate ... 38

3.2.2 Nano Tribometer 39
3.2.3 AFM 42
3.2.4 ATR-FTIR (Attenuated Total Reflection Fourier Transform Infrared) ……………………………………………… 44
3.2.5. SEM-EDS (SEM-EDS Scanning Electron Microscopy Energy Dispersive Spectroscopy) ……………………………… 46
3.2.6 XPS (X-ray Photoelectron Spectroscopy) 48
3.2.7 White Light Interferometry (NPFLEX) 51
3.2.8 TGA (ThermoGravimetric Analysis) 51
3.2.9 Rheometer 52
3.3 Materials.. 52
3.3.1 Lubricants 52
3.3.2 Materials 54
3.4 Experiments Procedures 55
3.4.1 Blending Lubricants 55
3.4.2 Thermal Film Experiments 56
3.4.3 Thermal Decomposition Experiments 56
3.4.4 Micro Scale Experiments 56
3.5 Summary... 59
4. Chapter 4: Reactivity of oil-soluble IL with the silicon surfaces at elevated temperature 60
4.1 Introduction 60
4.2 Experimental Conditions 61
4.3 Results 61
4.3.1Thermal Decomposition of Lubricants... 61
4.3.2ZDDP Thermal Film Results.. 63
4.3.3PP Thermal Film 69
4.3.4The Durability of Thermal Films 72
4.4 Discussion 76
4.4.1Film Formation Mechanism 76
4.4.2Film Thickness 77
4.4.3Tribological Behaviour... 77
4.5 Conclusions.. 78
5. Chapter 5: Oil-soluble IL to lubricate silicon 79
5.1 Introduction 79
5.2 Experimental Conditions 79
5.3 Results 81

5.3.1 Effect of Contact Pressure 81
5.3.1.1 Friction Coefficient 81
5.3.1.2 Wear Coefficient 83
5.3.1.3 Surface Chemistry 85
5.3.2 Effect of Temperature 88
5.4.2.1 Friction Coefficient 88
5.4.2.2 Wear Coefficient 90
5.4.2.3 Surface Chemistry 91
5.3.3 Effect of Sliding Distance 92
5.4.3.1 Friction Coefficient 92
5.4.3.2 Wear coefficient 93
5.4.3.3 Surface Chemistry 94
5.4 Discussion 95
5.5.1 Friction Coefficient 95
5.5.2 Wear Coefficient 96
5.5.3 Lubrication Mechanism 97
5.5 Conclusions 97

6. Chapter 6: Thermal stability of neat ILs and their reactivity with the silicon surfaces at elevated temperature 99
6.1 Introduction 99
6.2 Experimental Conditions 100
6.3 Results 102
6.3.1 Thermal Decomposition of ILs 102
6.3.1.1 Dynamic Thermal Decomposition 102
6.3.1.2 FTIR Results at Room Temperature 104
6.3.1.3 FTIR Results After Heating Process 108
6.3.2 Reactivity of ILs with Silicon Surface at Elevated Temperature 112
6.3.2.1 Thermal Decomposition of ILs in the Presence of Silicon Surface 112
6.3.2.2 Thermal Film Chemistry 114
6.3.2.3 Thermal Film Morphology 118
6.3.2.4 Thermal Films Durability 119
6.4 Discussion 121
6.4.1 Comparison Between Dynamic and Static Thermal Decomposition 121
6.4.2 Thermal Decomposition Mechanism 121

6.4.3 Effect of Time and Temperature on the Decomposition Process ... 122

6.4.4 Film Formation Mechanism ... 123

6.4.5 Effect of IL Chemistry on the Formation of the Thermal Film. 125

6.5 Conclusions ... 126

7. Chapter 7: Lubrication mechanism of neat ILs in various tribological conditions ... 128

7.1 Introduction ... 128

7.2 Experimental Conditions ... 130

7.3 Results ... 131

7.3.1 Viscosity ... 131

7.3.2 Effect of Contact Pressure ... 132

7.3.2.1 Friction ... 132

7.3.2.2 Wear ... 135

7.3.2.3 Surface Chemistry ... 137

7.3.3 Effect of Sliding Distance ... 141

7.3.3.1 Friction ... 141

7.3.3.2 Wear ... 144

7.3.3.3 Surface Chemistry ... 145

7.3.4 Effect of Temperature ... 148

7.3.4.1 Friction ... 148

7.3.4.2 Wear ... 151

7.3.4.3 Surface Chemistry ... 153

7.4 Discussion ... 155

7.4.1 Friction Coefficient ... 155

7.4.2 Wear and Lubrication Mechanism ... 156

7.5 Conclusions ... 157

8. Chapter 8: Discussion ... 159

8.1 Chapter Overview ... 159

8.2 The Link between Thermal and Tribo Films of Neat ILs (The Lubrication Mechanism of IL as Potential Lubricant To Lubricate MEMS) ... 159

8.3 Effect of Neat ILs Chemistry on Their Lubrication Mechanism .. 163

8.4 The Link between Thermal and Tribo Films of Oil-Soluble IL (The Lubrication Mechanism of Oil-Soluble IL). ... 164

9. Chapter 9: Conclusions and Future Work ... 169

9.1 Conclusions ... 169

9.2 Future Work 171
10. References... 172
11. Appendix 1: XPS data process 189

List of Tables

Table 2-1: The differences between macro and nano tribology (108).

Table 3-1: The utilized lubricants in this study.

Table 3-2: Properties of solid materials.

Table 4-1: The applied conditions to generate the thermal films of anti-wear additives.

Table 5-1: The applied conditions to examine the formation mechanism of tribofilm for PP and ZDDP at various contact pressures.

Table 5-2: The applied conditions to examine the formation mechanism of tribofilm for PP and ZDDP at various sliding distances.

Table 5-3: The applied conditions to examine the formation mechanism of tribofilm for PP and ZDDP at various temperatures.

Table 5-4: EDS results at contact pressure 700 MPa.

Table 5-5: Surface roughness inside wear track at various contact pressures.

Table 6-1: The applied conditions in the static thermal decomposition experiments.

Table 6-2: The applied conditions to generate thermal film.

Table 6-3: The assigned peaks for EMIM ESU at room temperature.

Table 7-1: The applied conditions to investigate the effect of contact pressure on the lubrication mechanism.

Table 7-2: The applied conditions to investigate the effect of sliding distance on the lubrication mechanism.

Table 7-3: The applied conditions to investigate the effect of temperature on the lubrication mechanism.

Table 7-4: Surface roughness inside wear tracks at various contact pressures.

Table 7-5: Surface roughness inside wear tracks at various sliding distances.

Table 7-6: Surface roughness inside wear tracks at various temperatures.

List of Figures

Figure 1-1: The average energy consumption in heavy duty vehicles based on average values from the four categories of trucks and buses (1). 1

Figure 1-2: Performance properties of lubricants (31). 7

Figure 1-3: The classification of additives based on their functions (27). 8

Figure 1-4: The lubrication regimes (32). 9

Figure 1-5: The molecular structure of common ILs lubricants (5). 11

Figure 2-1: The proposed procedure by (45) to decrease or eliminate tribocorrosion. 16

Figure 2-2: Relationship between cation chain length and film thickness (60). 18

Figure 2-3: The Imidazolium cation, the phosphonium cation and the FAP anion. 22

Figure 2-4: Chemical structure of oil-soluble phosphonium phosphate IL. 26

Figure 2-5: The chemistry of tribofilms formed by additives in (104). 29

Figure 2-6: The chemical structure of choline phosphate IL. 30

Figure 2-7: The chemical structures of additives that examined in [105]. 31

Figure 2-8: Configuration of the use of AFM as tribometer (108). 32

Figure 2-9: Micro tribometer designed by Leong [114]. 34

Figure 2-10: Micro tribometer designed by Reddyhoff *et al* [112]. 35

Figure 2-11: A summary to the use of ILs as lubricants in the literature and the current gaps. 37

Figure 3-1: The working principle of WiseStir hot plate. 39

Figure 3-2: A bespoke sample holder for room temperature experiments. 40

Figure 3-3: A bespoke sample holder containing two perforations. 41

Figure 3-4: High temperature experiment configuration using nano tribometer. 42

Figure 3-5: The working principle of AFM; (a) scanning process and (b) force behaviour (131). 43

Figure 3-6: Representing of the AFM cantilever as spring (131). 44

Figure 3-7: The typical FT-IR spectrum (134). 45

Figure 3-8: The molecules vibration types (137). 45

Figure 3-9: SEM-EDS main components [144]. 47

Figure 3-10: Photoemission process (146). 48

Figure 3-11: Clarify the meaning of work function (147). 49

Figure 3-12: Ball on plate contact. 57

Figure 3-13: The summery for the utilized methodology. 59

Figure 4-1: FTIR results for all lubricants at; (a) Room temperature and (b) 150 ^oC for 24 h. 62

Figure 4-2: FTIR results for silicon substrate before the generation of thermal film and after the formation of PP thermal film. 63

Figure 4-3: FTIR results for ZDDP thermal film at the following conditions: (a) 150 ^oC and 2 hours, (b) 175 ^oC and 2 hours, (c) 150 ^oC and 6 hours, (d) 175 ^oC and 6 hours and (e) 150 ^oC and 24 hours. 64

Figure 4-4: Surface morphology of (a) Si substrate before test; (b) Si in ZDDP 150 ^oC 2h; (c) Si in ZDDP 175 ^oC 2h; (d) Si in ZDDP 150 ^oC 6h (e) Si in ZDDP 175 ^oC 6h and (f) Si in ZDDP 150 ^oC 24h. 65

Figure 4-5: The EDS result of ZDDP thermal film at 150 ^oC and for 24 h. 66

Figure 4-6: S2s peak for (a) silicon before experiment, (b) ZDDP thermal film formed at 2h and 150 ^oC and (c) ZDDP thermal film formed at 6h and 175 ^oC. 67

Figure 4-7: Zn2p peak for (a) ZDDP thermal film formed at 2h and 150 ^oC and (b) ZDDP thermal film formed at 6h and 175 ^oC. 68

Figure 4-8: P2s peak for (a) silicon before experiment, (b) ZDDP thermal film formed at 2h and 150 ^oC and (c) ZDDP thermal film formed at 6h and 175 ^oC. 68

Figure 4-9: Surface morphology of (a) Si substrate before test; (b) Si in PP 150 ^oC 2h; (c) Si in PP 175 ^oC 2h; (d) Si in PP 150 ^oC 6h (e) Si in PPIL 175 ^oC 6h and (f) Si in PPIL 150 ^oC 24h. 70

Figure 4-10: The EDS results of PP thermal film at 150 ^oC and for 24 h. 71

Figure 4-11: P2s peak for (a) silicon before experiment, (b) PP thermal film formed at 2h and 150 ^oC and (c) PP thermal film formed at 6h and 175 ^oC. 72

Figure 4-13: Friction coefficient behaviour during experiment. 73

Figure 4-12: Average friction coefficients on surfaces of silicon in PAO before and after the formation of either ZDDP or PP thermal films. 73

Figure 4-14: The wear coefficients of silicon surfaces before and after the formation of thermal films. 74

Figure 4-15: Surface morphologies of: (a) Silicon substrate without before the formation of thermal film, (b) silicon substrate contains PP thermal film and (c) silicon substrate contains ZDDP thermal film. 75

Figure 4-16: PP thermal film formation mechanism. 76

Figure 5-1: The average friction coefficient under various contact pressures. 82

Figure 5-2: Evolution of friction coefficient during experiment at contact pressure: (a) 220 MPa, (b) 474 MPa, (c) 597 MPa and (d) 700 MPa. 83

Figure 5-3: Wear coefficient at various contact pressures. 84

Figure 5-4: A 3D view for wear tracks at contact pressure 700MPa when lubricate with: (a) Neat PAO, (b) PAO+PP and (c) PAO+ZDDP. 84

Figure 5-5: SEM images for wear tracks of silicon substrates when lubricated by: (a) neat PAO, PAO+PP and PAO+ZDDP. 85

Figure 5-6: XPS results for Zn2p from inside wear track for samples lubricated by ZDDP at; (a) contact pressure 700 MPa, 25 ^{o}C and sliding distance 14.4 m, (b) contact pressure 700 MPa, 80 ^{o}C and sliding distance 14.4 m and (c) contact pressure 700 MPa, 25 ^{o}C and sliding distance 36 m. 87

Figure 5-7: XPS results of P2s peak for: (a) silicon before experiments, the rest are inside wear track that resulted from (b) ZDDP tribofilm at contact pressure 700 MPa, 25 ^{o}C and sliding distance 14.4 m, (c) ZDDP tribofilm at contact pressure 700 MPa, 80 ^{o}C and sliding distance 14.4 m and (d) ZDDP tribofilm at contact pressure 700 MPa, 25 ^{o}C and sliding distance 36 m, (e) PP tribofilm at contact pressure 700 MPa, 25 ^{o}C and sliding distance 14.4 m, (f) PP tribofilm at contact pressure 700 MPa, 80 ^{o}C and sliding distance 14.4 m and (g) PP tribofilm at contact pressure 700 MPa, 25 ^{o}C and sliding distance 36 m. 88

Figure 5-8: The average friction coefficients for PAO+ZDDP and PAO+PP at room temperature and at high temperature. 89

Figure 5-9: The evolution of friction coefficients for both PAO+ZDDP and PAO+PP at high temperature (80 ^{o}C). 90

Figure 5-10: Wear coefficients for PAO+ZDDP and PAO+PP at room temperature and at high temperature. 91

Figure 5-11: The average friction coefficients for both additives at various sliding distances. 92

Figure 5-12: Friction coefficient evolution of both additives at three various sliding distances. 93

Figure 5-13: Wear coefficient behaviour of both additives at two various sliding distances. 94

Figure 6-1: Dynamic thermal decomposition of the examined ILs to reveal the effect of: (a) anion chain length, (b) cation chain length, (c) cation type and (d) anion type. 102

Figure 6-2: First derivative of the weight loss against surface temperature curve for: (a) EMIM ESU, (b) EMIM OSU, (c) BMIM OSU, (d) PSU and (e) EMIM EP. 104

Figure 6-3: IR spectra of five ILs at room temperature; (a) spectra between 4000 cm^{-1} and 2000 cm^{-1} and (b) spectra between 2000 cm^{-1} and 650 cm^{-1}. 105

Figure 6-4: ILs after heating them into 80 ^{o}C and for 2 hours. 108

Figure 6-5: IR spectra of five ILs after heating into 100 ^{o}C for five hours; (a) spectra between 4000 cm^{-1} and 2000 cm^{-1} and (b) spectra between 2000 cm^{-1} and 650 cm^{-1}. 111

Figure 6-6: Effect of time and temperature on BMIM OSU IR spectra; (a) spectra between 4000 cm^{-1} and 2000 cm^{-1} and (b) spectra between 2000 cm^{-1} and 650 cm^{-1}. 112

Figure 6-7: FTIR spectra for BMIM OSU IL at room temperature, 100 ^{o}C for 2h (HT) in the absence of silicon substrate and 100 ^{o}C for 2h (HT Si) in the presence of silicon substrate for (a) wave number between 4000 and 2000 cm^{-1} and (b) wave number between 2000 and 650 cm^{-1}. 113

Figure 6-8: FTIR results for silicon substrate before after the generation of thermal films of all examined ILs. 114

Figure 6-9: N1s peaks for: (a) EMIM ESU at 80 ^{0}C 2h, (b) EMIM ESU at 100 ^{o}C 2h, (c) BMIM OSU at 100 ^{o}C 5h, (d) EMIM OSU at 80 ^{o}C 2h, (e) EMIM OSU at 100 ^{o}C 2h, (f) EMIM OSU at 100 ^{o}C 5h, (g) BMIM OSU at 100 ^{0}C 2h, (h) EMIM EP at 100 ^{0}C 2h, (i) EMIM ESU at 100 ^{0}C 5h, (j) EMIM OSU at 100 ^{0}C 5h, (k) BMIM OSU at 100 ^{0}C 5h and (l) EMIM EP at 100 ^{0}C 5h. 115

Figure 6-10: S2s peaks for: (a) EMIM ESU, (b) EMIM OSU, (c) BMIM OSU and (d) PSU. 116

Figure 6-11: P2s peak for: (a) silicon before experiment, (b) EMIM EP 80 ^{o}C 2h, (c) EMIM EP 100 ^{o}C 2h, (d) EMIM EP 100 ^{o}C 5h, (e) PSU 80 ^{o}C 2h, (f) PSU 100 ^{o}C 2h and (g) PSU 100 ^{o}C 5h. 118

Figure 6-12: The surface morphology of (a) silicon before formation of thermal film and for thermal films that formed at 100 ^{o}C for 5 hours for: (b) EMIM ESU, (c) EMIM OSU, (d) BMIM OSU, (e) EMIM EP and (f) PSU. 119

Figure 6-13: Friction coefficients for silicon before and after the generation of ILs' thermal films. 120

Figure 6-14: Wear coefficients for silicon before and after the generation of ILs' thermal films. 120

Figure 6-15: Thermal decomposition mechanism for: (a) EMIM ESU, (b) EMIM OSU and (c) BMIM OSU. 122

Figure 6-16: The formation mechanism of thermal film of imidazolium based ILs. 123

Figure 6-17: The formation mechanism of thermal film of PSU. 124

Figure 6-18: The formation mechanism of thermal film of EMIM EP. 124

Figure 7-1: ILs viscosity at various temperatures. 132

Figure 7-2: Friction coefficient values for five ILs at various contact pressures. 133

Figure 7-3: Variation of friction coefficient with sliding distance at various contact pressures; (a) 142 MPa, (b) 306 MPa, (c) 386 MPa and 451 MPa. 134

Figure 7-4: Wear coefficient values for five ILs at various contact pressures. 136

Figure 7-5: Surface topography of wear track for samples lubricated by EMIM ESU IL. 137

Figure 7-6: Surface topography of wear track for samples lubricated by EMIM EP IL. 137

Figure 7-7: XPS results of N1s for samples lubricated by imidazolium sulfate ILs. 138

Figure 7-8: XPS result of S2s peak for all imidazolium sulfate ILs and phosphonium sulfate IL at three contact pressures; 306, 386 and 451 MPa. 139

Figure 7-9: P2s peaks for silicon before test and inside the wear tracks of samples lubricated by either EMIM EP or PSU. 140

Figure 7-10: P2s to Si2s ratio for silicon before test and inside wear tracks of samples lubricated by either PSU or EMIM EP. 140

Figure 7-11: Friction coefficient at various sliding distances. 142

Figure 7-12: Friction coefficient behaviour at three various sliding distances. 143

Figure 7-13: A 3D view of surface morphology and wear track for: (a) EMIM ESU after 14.4 m of sliding and (b) EMIM ESU after 36 m of sliding. 145

Figure 7-14: Wear coefficient at various sliding distances. 145

Figure 7-15: XPS scan of N1s inside wear track for samples lubricated by: (a) BMIM OSU at sliding distance 14.4 m, (b) BMIM OSU at sliding distance 36 m and (c) typical result of EMIM ESU, EMIM OSU and EMIM EP at both sliding distances. 146

Figure 7-16: Typical result of XPS scan of S2s inside wear track of all imidazolium sulfate ILs and PSU at both sliding distances. 147

Figure 7-17: P2s peaks for: (a) silicon before experiment, (b) inside wear track of sample lubricated by EMIM EP at distance 14.4 m, (c) inside wear track of sample lubricated by PSU at distance 14.4 m, (d) inside wear track of sample lubricated by EMIM EP at distance 36 m and (e) inside wear track of sample lubricated by PSU at distance 36 m. 148

Figure 7-18: Friction coefficient values for five ILs at various contact pressures. 149

Figure 7-19: Variation of friction coefficient with sliding distance at: (a) at room temperature (25 ^oC) and (b) at high temperature (80 ^oC). 150

Figure 7-20: Wear coefficient values for five ILs at temperatures. 151

Figure 7-21: Surface morphologies for: (a) sample lubricated by EMIM OSU at room temperature, (b) sample lubricated by EMIM OSU at high temperature, (c) sample lubricated by PSU at room temperature and (d) sample lubricated by PSU at high temperature.. 152

Figure 7-22: XPS results of N1s peak for: (a) sample lubricated by BMIM OSU at room temperature, (b) sample lubricated by BMIM OSU at high temperature and (c) The typical N1s peak for the samples that lubricated by EMIM ESU, EMIM OSU and EMIM EP at both temperatures. 153

Figure 7-23: S2s typical peak for the samples that lubricated by EMIM ESU, EMIM OSU, BMIM OSU and PSU at both temperatures. 154

Figure 7-24: P2s peaks for: (a) silicon before test, (b) inside wear track of EMIM EP at contact pressure 386 MPa, (c) inside wear track of PSU at room temperature, (d) inside wear track of PSU at high temperature (e) inside wear track of EMIM EP at high temperature.. 154

Figure 8-1: The relationship between the formation of the tribofilm and the tribological performance of ILs at various contact pressures: (a) at 306 MPa, (b) at 386 MPa and (c) at 451 MPa..... 160

Figure 8-2: The relationship between the formation of the tribofilm and the tribological performance of ILs at various conditions: (a) at 386 MPa, sliding distance 14.4 ma and 25 ^oC, (b) at 386 MPa, sliding distance 36 m and 25 ^oC and (c) at 386 MPa, sliding distance 14.4m and 80 ^oC.. 162

Figure 8-3: The tribological properties of PP and ZDDP thermal films.. 165

Figure 8-4: The relationship between the ZDDP and PP tribofilms formation with their tribological behaviour at: (a) 597 MPa and (b) at 700 MPa... 166

Figure 8-5: The relationship between the ZDDP and PP tribofilms formation with their tribological behaviour at: (a) 14.4 m and (b) 36 m. 168

1. Chapter 1: Introduction and Background

1.1 Energy Losses and Fuel Economy

In tribology current studies are predominantly focused on the reduction of both fuel consumption and the emission of gases and products that impact negatively on the environment. These two aims can be achieved by increasing system efficiency, which means mitigating wear and friction, since the mitigation of friction will decrease the required energy. Similarly, the reduction of wear will prolong the life time of the component which means less waste. For instance, the latest development in tribology in terms of reducing friction can lead to 14% and 18% reduction in the consumed fuel in the heavy machines and passenger automobiles respectively. Concurrently, CO_2 emissions could be reduced by 200 and 290 million tons for heavy machines and passenger automobile respectively (through the reduction of the consumed fuel) [1, 2]. This advance in tribology includes the utilizing of advanced lubricants [3-6], advanced coatings [7] and surface texturing [8].

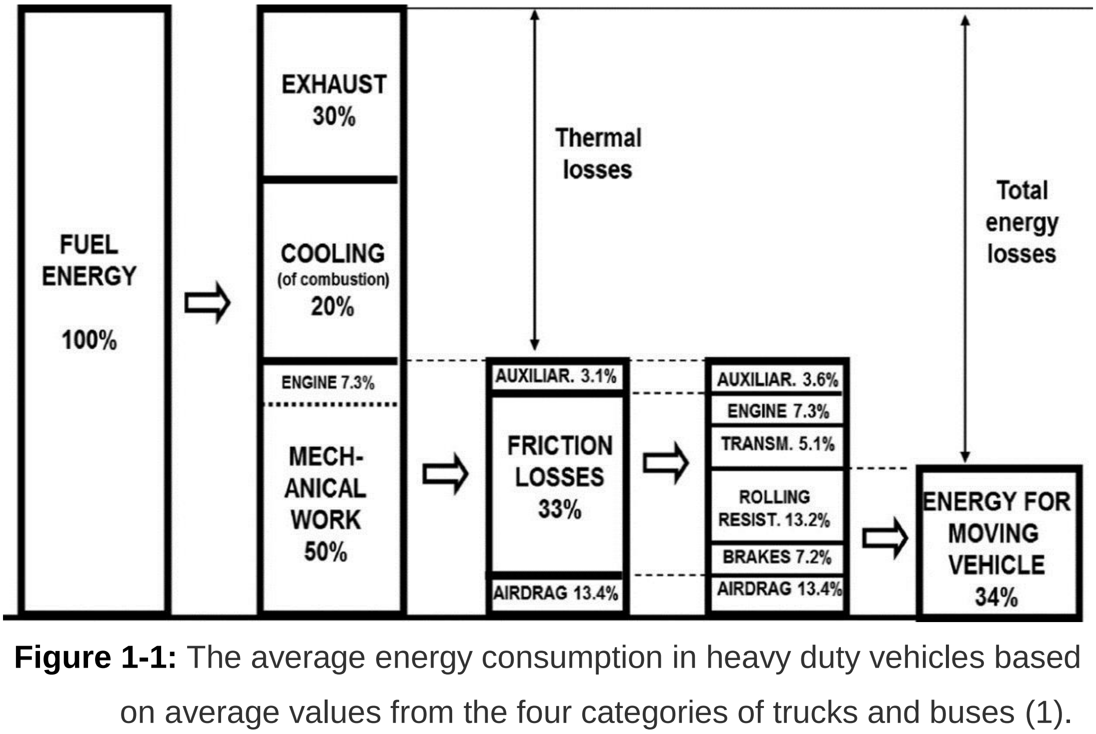

Figure 1-1: The average energy consumption in heavy duty vehicles based on average values from the four categories of trucks and buses (1).

1.2 Ionic Liquids for Lubrication

Ionic Liquids (ILs) demonstrate an extremely low vapour pressure, high thermal stability, non-flammability and their ability to adsorb and react with different surfaces. In addition, the use of ILs as lubricants can mitigate the utilization of additives such as detergents, anti-oxidants and anti-wear. ILs are solvents, having very high thermal stability and they are able to produce anti-wear films (tribofilms). However, in some cases, for halogenic ILs, anti-corrosion additives must be employed [9].

Using ILs as lubricants started in 2001 when Ye *et al* [10] suggested a few ILs as neat lubricants for various surfaces and they showed an excellent tribological performance for all the examined surfaces. The reduction of wear and friction results due to the chemical reaction/adsorption of ILs with the lubricated surfaces. After that, due to their negligible vapor pressure, ILs were used at vacuum condition in which they showed better tribological performance than PerFlouroPolyEther (PFPE), which is commonly used at vacuum condition [11-16]. A new group of ILs was proposed by Shah *et al* [17] referred to halogen-free, which were developed to avoid tribocorrosion that was observed in halogenic ILs. Many researchers have examined various halogenic-free ILs and the results showed that they exhibited better tribological performance than halogenic ILs [18-21]. Phillips *et al* [22] added various ILs into water to lubricate ceramic tribopairs and suggested that using ILs as additives can penetrate the market faster and easier than as neat lubricants. Their results revealed that adding ILs can provide a significant enhancement in the tribological performance due to their ability to react/adsorb with the lubricated surfaces. Fully oil-soluble ILs have been proposed by Yu *et al* [23] and their results suggested that oil-soluble ILs can provide higher wear protection than ZDDP. The findings of the aforementioned studies confirmed that ILs can react with the rubbed surfaces and form a protective layer (tribofilm).

Hence, due to the high cost of ILs; their use as neat lubricants is limited to two main applications. The first one is in aerospace applications since the cost can be tolerated. The second application is the lubrication of Micro Electro Mechanical Systems (MEMS).

On the other hand, the use of ILs as anti-wear additives is proposed to be an effective alternative to ZDDP when lubricating engines [3-6]. Therefore, in this study, the lubrication of MEMS and engines will be simulated when using ILs as potential lubricants or additives, respectively.

Previous studies have mainly focused on the use of various ILs as lubricants regardless of their chemistry [3-6]. Nevertheless, few studies compared the tribological performance of halogenic and non-halogenic ones [18-21]. In addition, few studies reported that the increase of anion/cation chain length enhances the tribological performance [24-27]. However, the reason behind this enhancement is vague, especially in the absence of any tribocorrosion. Besides, in terms of the use of IL as an additive. The reason behind the superior anti-wear performance of oil-soluble IL than ZDDP at a particular condition (high temperature) is not understood [28, 29].

This research aims to provide a comprehensive understanding for the lubrication mechanism of ILs. To understand the effect of IL chemistry on their tribological performance. To find why PP can provide better tribological performance that ZDDP at elevated temperature. Lastly, to reveal at which conditions the oil-soluble IL can be a replacement anti-wear additive to ZDDP.

These objectives can be conducted by studying the lubrication mechanism of ILs when they are used as potential lubricants or additives. The influence of anion type, anion chain length, cation type and cation chain length on the lubrication mechanism will be studied. The effect of various conditions including contact pressure, temperature and sliding distance on the lubrication mechanism will be considered to obtain a consistent study.

1.3 Aim and Objectives

The main aim of this research is to develop a fundamental understanding of the lubrication mechanism of a class of advanced lubricants, i.e., ILs. Their use as either neat lubricants or additives is investigated. To reach this aim, the objectives are as follows:

1. Understanding the anti-wear mechanism (the formation mechanism of the protective layer, i.e., thermal/tribo film) of oil-soluble IL in comparison with ZDDP. This can be achieved by:
    a- Comparing the reactivity of oil-soluble IL with ZDDP on silicon surfaces at elevated temperature (no tribomotion) and their ability to form a thermal film.
    b- Comparing the reactivity of oil-soluble IL with ZDDP on silicon surfaces at various tribological conditions and their ability to form a tribofilm.
2. Understanding the lubrication mechanism of ILs when they are used as potential lubricants and study the effect of ILs chemistry on their lubrication mechanism. This can be achieved by:
    a- Studying the effect of ILs chemistry on thermal stability and viscosity.
    b- Studying the effect of ILs chemistry on their reactivity on silicon surfaces at elevated temperature (no tribomotion).
    c- Studying the effect of ILs chemistry on their reactivity on silicon surfaces at various tribological conditions and their ability to form a tribofilm.

1.4 Thesis Chapters Layout

This thesis is divided into nine chapters. **Chapter 1** presents a brief introduction, the aim and objectives of this work and a general background. **Chapter 2** presents the literature review that is related to the use of ILs as either potential lubricants or additives and the previous studies that simulate the lubrication of MEMS. **Chapter 3** demonstrates the methodology that is used in this project with a brief background about the utilized techniques. After that, **chapter 4** illustrates the results of the reactivity of oil-soluble IL with silicon surface at elevated temperature. **Chapter 5** presents the results of the lubrication mechanism of oil-soluble IL when lubricating silicon surfaces. **Chapter 6** presents the results of the thermal stability of neat ILs and their reactivity with the silicon surfaces at elevated temperature. **Chapter 7** demonstrates the results of the lubrication mechanism of neat ILs when lubricating MEMS. Then, **chapter 8** is a discussion that will discuss the proposed lubrication mechanism of ILs based on the obtained results. Lastly, **chapter 9** shows the conclusions of the whole work and the suggested work to be conducted in the future.

1.5 General Background

1.5.1 Tribology

It is the subject that deals with friction, wear and lubrication of the interacting surfaces when they are in relative motion. The motion can be sliding, rolling, spinning, reciprocating or a combination of two of the aforementioned motions. Friction is the resistance to motion that is initiated by surface asperities. The presence of friction causes an increase in the required energy to achieve the required work. This means that the reduction of friction leads to a decrease of the energy consumption. Besides, wear can be defined as the progressive damage that results in a loss of mass or a plastic deformation in the rubbed surfaces. Wear causes a failure in the system. The use of proper lubricant aims to provide efficient lubrication that leads to decrease friction and wear. Lower wear and friction means better tribological performance (tribological behaviour) [30].

1.5.2 Lubricants

They can be defined as an effective materials in the form of liquid, solid or gas which are inserted between two rubbing surfaces to achieve certain aims. Reduction of both friction and wear is the main aim of lubricants. However, there are several other functions such as to dissipate heat, separate interacting surfaces, transmit power, inhibit corrosion, provide sealing and decrease noise and vibration. The ability of lubricants to dissipate heat is strongly related to their thermal conductivity and specific heat capacity. Further, it is a crucial property since the friction which takes place between the sliding surfaces will increase the temperature and may lead to either softening or melting the interacting surfaces. Besides, the power transmission is required in limited applications such as in hydraulic systems. In contrast, the lubricant must inhibit corrosion by covering the rubbing surfaces and preventing them from being exposed to a corrosive environment, for instance, oxygen and water. Again, to minimize wear and friction the two surfaces have to be separated by lubricant to avoid dry contact that is the worst tribological scenario. Lastly, the contaminants and wear debris should be removed by the working lubricant to reduce wear [31].

The selection of the proper lubricant that can achieve a certain function mainly depends on lubricant’s properties [32]. Some properties are desirable for all lubricants such as long life and environmental properties. The former includes inhibiting of corrosion, oxidation stability and hydrolytic stability. The environmental properties include those that negatively affect the environment. For example, toxicity, renewability and biodegradability [33, 34]. On the other hand, the rest properties are called performance properties, aforementioned, each group is required for a particular application, see Fig.1-2 [31].

Fig.1-2 summarizes the performance properties. Viscosity is the most crucial property since it controls the separation distance between the sliding surfaces. It is influenced by both temperature and pressure. The increase of temperature decreases viscosity. Furthermore, high viscosity in lubricant decreases wear and friction because it provides high separation (in full film lubrication regimes). However, it needs higher pumping power than low viscosity ones [33, 34].

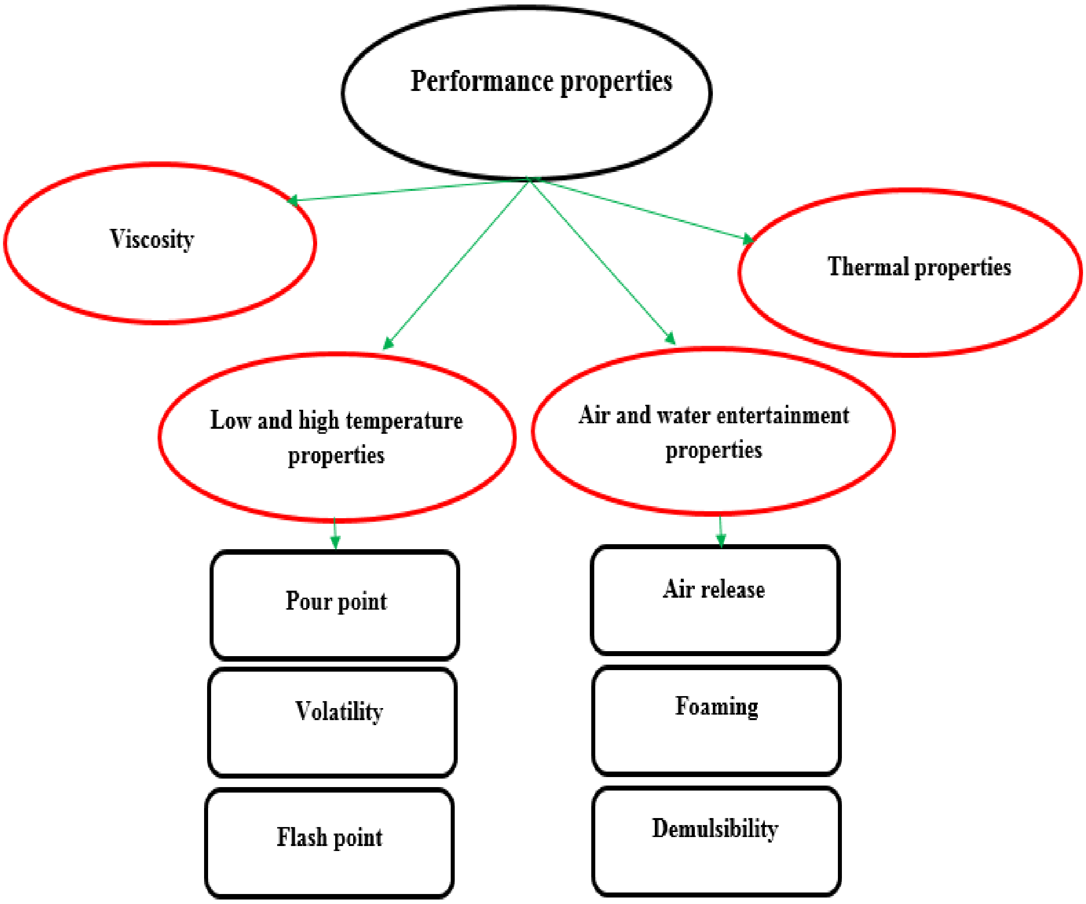

Figure 1-2: Performance properties of lubricants (31).

Temperature can directly affect the performance of lubricants. The decrease of temperature may lead to solidify the working lubricant and then stop its flowing which causes failure. The pour point is the lowest temperature at which fluid can keep flowing. In contrast, the volatility is the ability of lubricant to evaporate. This feature is strongly related to vapour pressure when lubricants with high vapour pressure could be evaporated easily. The last property with respect to temperature is called flash point, which is the temperature at which the mixture of lubricant vapour and air is ignitable [35]. Besides, water and air retainment properties should be considered since the air bubbles may cause cavitation in the working pump. The presence of water can cause corrosion. Dispersant is used to separate water [36]. Lastly, thermal properties are substantial properties especially when the lubricant is utilized as a coolant [31].

Base lubricants (pure without additives) are usually not able to achieve the desirable duties, i.e., low friction, low wear, working over a wide range of temperatures and etc.

Thus, additives are added to the base lubricants to enhance their properties. A wide range of additives are available and each one has special function such as to inhibit corrosion, reduce wear, and reduce friction and many others. Fig. 1-3 depicts the classification of additives based on their functions. Essentially, they can be divided into two groups; surface active and bulk active. The former additives are utilized to protect the interacting surfaces while the latter group is utilized to enhance both chemical and physical properties of lubricants [31].

Surfaces can be protected by preventing corrosion, reducing wear, reducing friction and the preventing the dry contact. Corrosion inhibitor additives are used to prevent corrosion by either acting as acid neutralizers or form a protective film to prevent the direct contact between surface and oxygen [36]. Also, friction can be reduced at low loads using Friction Modifier (FM) additives by forming a physical adsorbed layer. They usually consist of either oxygen or nitrogen atom [37]. Besides, at high loads when the FM additives cannot perform properly; Anti-Wear (AW) additives are utilized. These additives are able to produce protective films by chemically reacted/adsorbed with/on the lubricated surfaces.

Only 1-3% of AW additives in the base lubricant is adequate to substantially mitigate wear. Currently, the most common AW additive is ZDDP [38]. Lastly, Extreme Pressure (EP) additives are suitable for extreme conditions such as high load and/or high temperature under boundary lubrication regime [36].

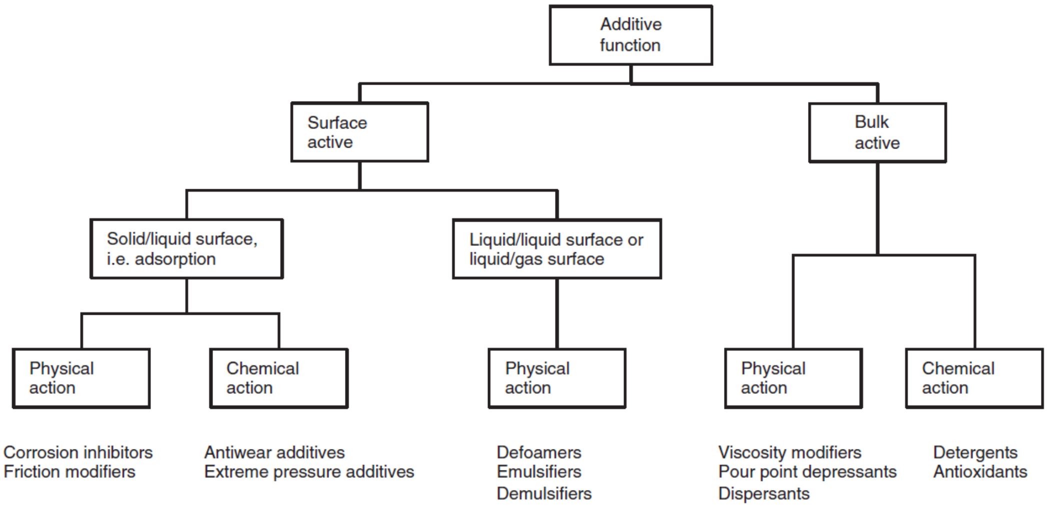

Figure 1-3: The classification of additives based on their functions (27).

Bulk active additives are added to enhance either physical or chemical properties of the base lubricants. Physical properties include viscosity, pour point depressants and dispersant. The additives can decrease the influence of temperature on lubricant's properties. In other words, increase the thermal stability of lubricants, decrease the influence of temperature on viscosity and keep the fluidity of lubricants at low temperature. In addition, detergents and antioxidants are utilized to modify the chemical properties of lubricants since the former is used to maintain the lubricated surfaces clean while the latter additives are utilized to prevent oxidation [31].

1.5.3 Lubrication Regimes

Based on the Stribeck curve [32], the lubrication regimes can be divided into four regions; boundary friction, mixed film friction, elastohydrodynamic lubrication and hydrodynamic lubrication, see Fig. 1-4.

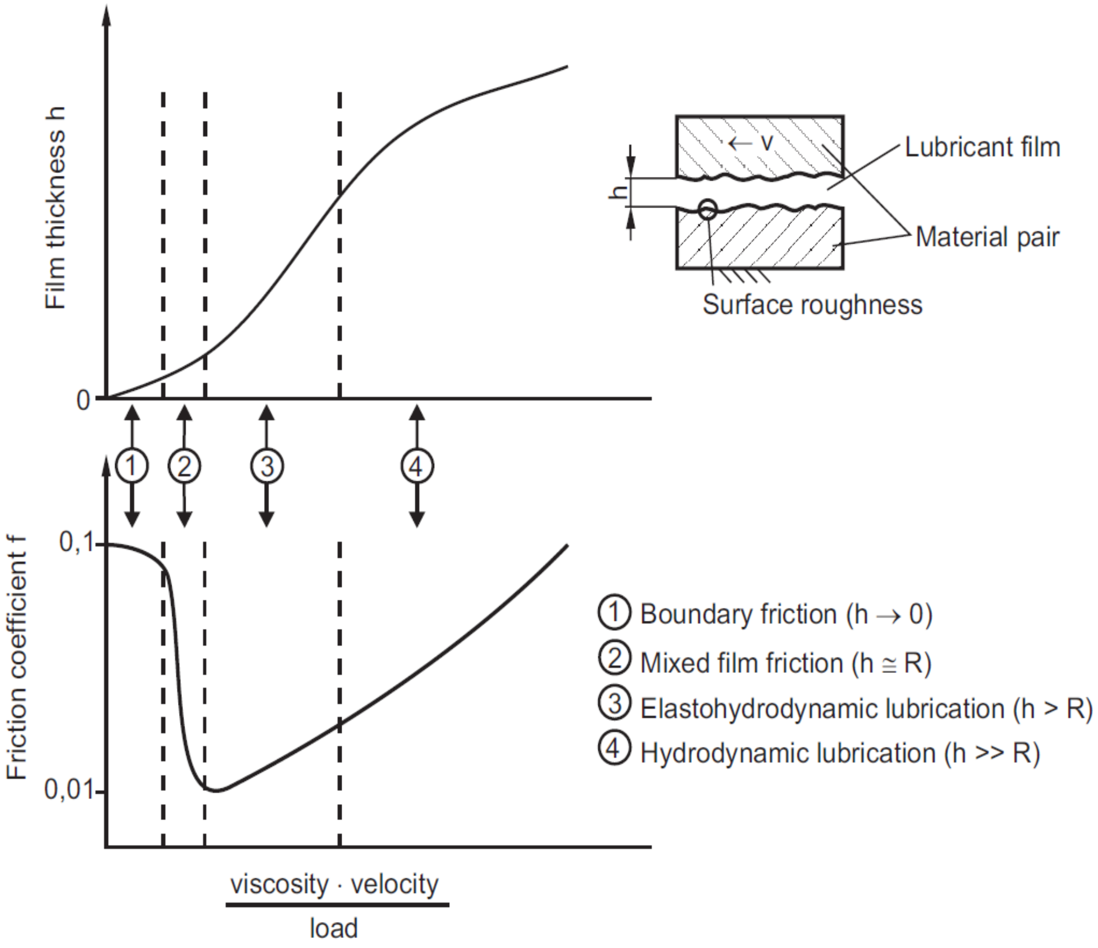

Figure 1-4: The lubrication regimes (32).

In the boundary lubrication regime, the two interacting surfaces will be separated by only a thin protective film which is formed by surface active additives. This film can by created by either chemical reaction, chemical adsorption or physical adsorption. Much effort in research have been conducted to enhance the understanding of the ability of lubricants to form this protective layer [39, 40]. Secondly, the mixed film friction is the regime in which that the rubbing surfaces will experience both elastohydrodynamic and boundary scenarios. This means that the formation of the protective film is still crucial since the boundary regime is still taken place in some regions. Besides, the two surfaces are fully separated by lubricant in both elastohydrodynamic and hydrodynamic regimes. In these two regimes, the frictional resistance is occurred due to the presence of fluid friction.

Finally, there is another scenario that is the worst tribological scenario which is called dry contact. The two surfaces become in direct contact and neither lubricant film nor protective layer is existed to mitigate wear and friction [32].

1.5.4 Ionic Liquids (ILs)

ILs are molten salts which are available at liquid phase at a temperature below 100 ^{o}C or even at standard ambient temperature (25 ^{o}C). In contrast to solid salts, ILs cannot form crystalline structure due to both the large ions radii and asymmetry [41]. ILs have been discovered in 1914, and then in 1970 they have been employed in limited scopes. This limitation was existed due to their instability in both air and water media. Then, in 1992, the first stable IL was produced with promising properties. After that, in 2001, the first paper that used ILs as potential lubricants was published [10].

ILs exhibit promising properties such as negligible vapour pressure, high thermal stability, high thermal conductivity, high electrical conductivity, tuneable miscibility and tuneable physical properties. The combination of ions can be optimized to obtain reusable, biodegradable and minimize toxicity. Many ILs have been considered as environmental friendly [3-6]. Based on these unique properties, they have been utilized in various applications, for instance, as battery electrolytes, in metal extraction, biomass applications solar cells and as lubricants.

However, some challenges could be faced when utilizing ILs due to their ecotoxicity, degradation, moisture sensitivity and cost [42].

These properties are strongly influenced by the chemistry of ILs. Essentially, ILs consist of a positively charged ions called the cations and negatively charged ions called the anions. Thus, the combination of anion-cation and the chemistry of each ion are crucial in the determination of IL properties. For example, the imidazolium cation is more viscous than the ammonium cation while it exhibits lower electrical conductivity than the ammonium cation. Furthermore, the variation in the alkyl chain length of either cation or anion can change the physical properties of IL. For instance, the increase of cation alkyl chain in all cations leads to increase viscosity, decrease electrical conductivity and decrease surface tension [43]. The most common anions and cations of ILs lubricants are demonstrated in Fig. 1-5.

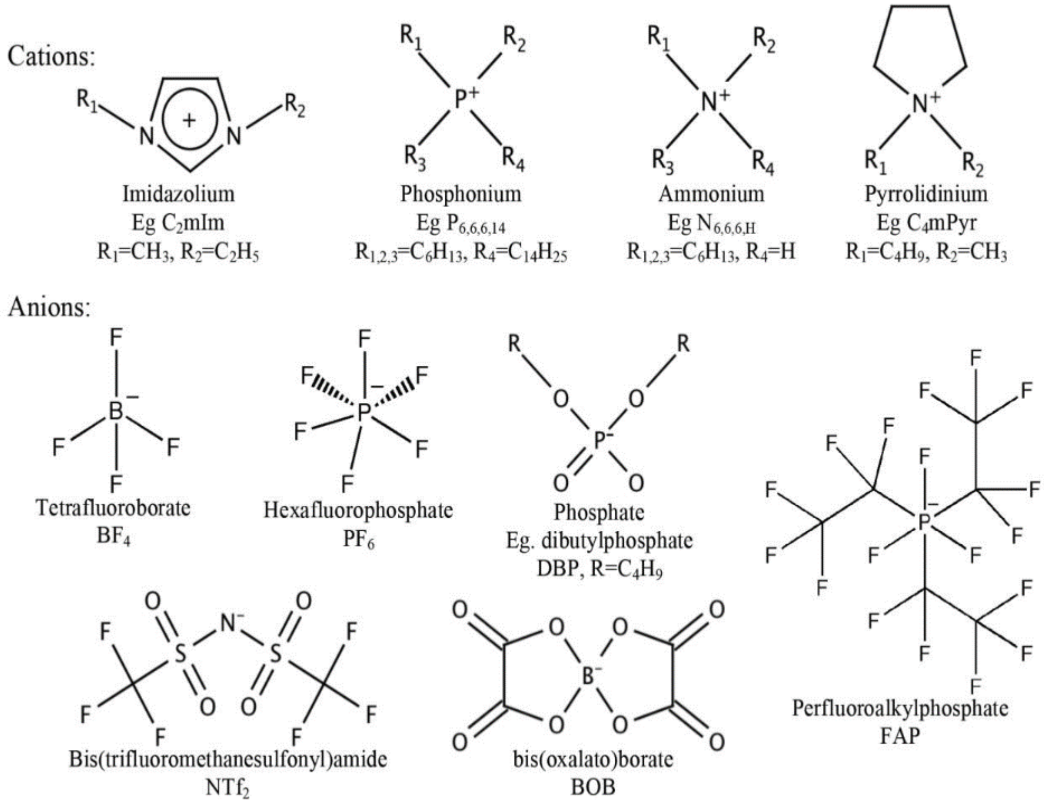

Figure 1-5: The molecular structure of common ILs lubricants (5).

It can be observed the presence of nitrogen in the majority of cations. This element has been utilized for corrosion inhibition, FM and AW additives. Also, the existence of phosphorus and sulfur in either anion or cation moieties is aimed to decrease wear and corrosion. These two elements have been used in the manufacturing of FM and AW additives.

Moreover, the presence of fluorine in the anion was reported as beneficial in the formation of protective film. However, in the humid environment it may interact with hydrogen and form hydrofluoric acid and then corrode the tribopair [4].

Lastly, ILs chemistry can influence on their cost as well. A new class of IL has been suggested to be used as lubricant by Qu *et al* [44] which is called protic IL. Protic Il is cheaper and easier to synthesis than the conventional ILs.

2. Chapter 2: Literature Review

2.1 Introduction

A large number of previous studies has been published to investigate the tribological performance of ILs lubricants when they have been used as either potential lubricants or additives. However, these studies mainly focused on the use/propose of various ILs as lubricants regardless to their chemistry [3-6]. Nevertheless, few studies compared the tribological performance of halogenic and non-halogenic ones [18-21]. In addition, few studies reported that the increase of anion/cation chain length enhances the tribological performance [24-27]. However, the reason behind this enhancement is still vague, especially in the absence of any tribocorrosion. Besides, in terms of the use of IL as an additive. The reason behinds the superior anti-wear performance of oil-soluble IL than ZDDP at a particular condition (high temperature) is still not fully understood [28, 29].

This research aims to fill the lack of consistency in the previous studies by conducting the following studies:

- Understand the effect of ILs chemistry on their tribological performance.
- Understand the reason behind the superior anti-wear performance of oil-soluble IL than ZDDP at high temperature.
- Reveal at which conditions the oil-soluble IL can be a replacement anti-wear additive to ZDDP.

The use of ILs lubricants as potential lubricants is mainly limited to two applications; aerospace applications (where high cost can be tolerated) and to lubricate Micro Electro Mechanical Systems (MEMS) [3-6]. In this study ILs are used as either additives or potential lubricants.

This chapter aims to cover the previous studies that used ILs as either potential lubricants or additives and also the lubrication of MEMS. This chapter is divided into four sections; introduction, IL lubricants, lubrication of MEMS and the summary of the literature with the current gap of knowledge.

2.2 ILs Lubricants

ILs have been used as either potential lubricants or additives. This section will be divided further into two subsection; using ILs as potential lubricants and using ILs as additives.

2.2.1 ILs as Potential Lubricants

The high cost of the production of ILs makes the use of ILs as potential lubricants mainly limited to two applications only; in aerospace and to lubricate MEMS. The cost can be tolerated in the former application and only a small amount is required in the latter application [3-6]. Nevertheless, a large number of previous studies have been conducted to investigate the use of IL as potential lubricants to lubricate various tribopairs.

The literature will be presented based on the cation type.

2.2.1.1 Imidazolium Based ILs

The use of ILs as lubricants was started in 2001 when Ye *et al* [10] proposed that ILs can lubricate a wide range of tribopairs. This is not applicable in the conventional lubricants. For instance, the suitable lubricant for steel/steel contact is either not suitable or inefficient for steel/aluminium contact. IL (imidazolium tetrafluoroborate) was utilized to lubricate steel/steel, steel/aluminium, steel/copper, steel/ceramic, steel/silicon, steel/sialon and ceramic/sialon. IL demonstrated a significant reduction in both wear and friction in comparison with PerFluroPolyEther (PFPE) and cyclic phosphines lubricant (X-1P) for all surfaces at different loads. In addition, IL showed better tribological performance than PolyTetraFluorEthylene (PTFE) when lubricating PolyEther Ether Ketone (PEEK) due to the high reactivity of IL with steel counter face and the formation of tribofilm. The superior thermal conductivity of IL also enhanced their ability to lubricate PEEK. The superior tribological performance of the imidazolium based ILs than PFPE was also observed by Lu *et al* [45] when lubricating steel surface. The enhancement of the tribological performance was mainly occurred due to the formation of tribofilm that caused by chemical adsorption of anion moieties into steel surface.

This finding was confirmed by Lopez-Sánchez *et al* [46] when their analysis of surface chemistry demonstrated that the concentration of the sulfate anion inside wear track was higher than the imidazolium cation.

The lubrication of light alloys is an interesting topic in tribology since these alloys exhibit high strength to density ratio [47]. However, the conventional lubricants and their additives cannot lubricate them efficiently [48-50]. ILs have been proposed to lubricate these alloys [3-6]. Bermudez *et al* [51] examined the ability of imidazolium based IL to lubricate aluminium-titanium tribopairs. The results demonstrated that the increase of temperature decreased wear volume since IL reacted and formed tribofilm that lead to decrease wear volume.

Due to their negligible vapour pressure, IL were used to lubricate steel-steel tribopairs in vacuum conditions by Liu *et al* [13]. The results presented that ILs exhibited better tribological performance than conventional vacuum lubricants such as PFPE in terms of exhibiting less wear volume and lower friction coefficient. The very low vapour pressure of ILs and their high reactivity with the lubricated surfaces are behind this superior performance.

The high thermal stability of ILs and their availability at liquid state even at very low temperature attracted the researchers to use them at extreme conditions. Jimenez *et al* [52] compared the use of the imidazolium tetrafluoroborate ILs with Propylene Glycol Dioleate (PGDO) when lubricating steel-aluminium contact at extreme conditions. At very low temperature, -30 ^{o}C ILs exhibited the lowest friction coefficient and wear volume. However, the highest wear volume and friction coefficient were obtained at this temperature due to the freezing of the water content. The increase of temperature to 100 ^{o}C, 150 ^{o}C and 200 ^{o}C caused a thermal decomposition of (PGDO) while ILs showed an enhancement in their tribological performance. This finding was also confirmed by Jimenez *et al* [53] when they reported that the increase of temperature from 100 ^{o}C to 200 ^{o}C lead to enhance the tribological performance. The further increase of temperature to 300 ^{o}C lead to decrease friction coefficient by 50%. However, wear volume was significantly increased at this temperature (300 ^{o}C) due to the increase of tribocorrosion.

Despite the excellent tribological performance of ILs, the presence of tribocorrosion increases wear volume especially at high temperatures [50, 53]. Tribocorrosion is mainly caused by hydrofluoric acid that produced in the presence of water and fluorine [54]. In order to decrease or eliminate tribocorrosion; either less fluorine or fluorine free ILs must be employed instead. Further, the hydrophobic ILs can reduce tribocorrosion due to the reduction of water content [45].

A new class of anions was proposed by Liu *et al* [45] that either contains less fluorine such as TriFluoromethylSulfonImide (TFSI) or they are more hydrolysis stable such as perFluoroAlkylPhosphate (FAP), see Fig. 2-1. These new anions showed an enhancement in the tribological performance of ILs in terms of exhibiting less friction coefficient and less wear volume.

Another solution was proposed by Chen *et al* [55] by adding water into IL. They added 5 wt% water in the imidazolium tetrafluoroborate IL and the results showed that corrosion was inhibited. However, a slight increase in the friction coefficient was obtained. Adding water lead to increase the hardness of the aluminium surface and thus decreased the tribocorrosion.

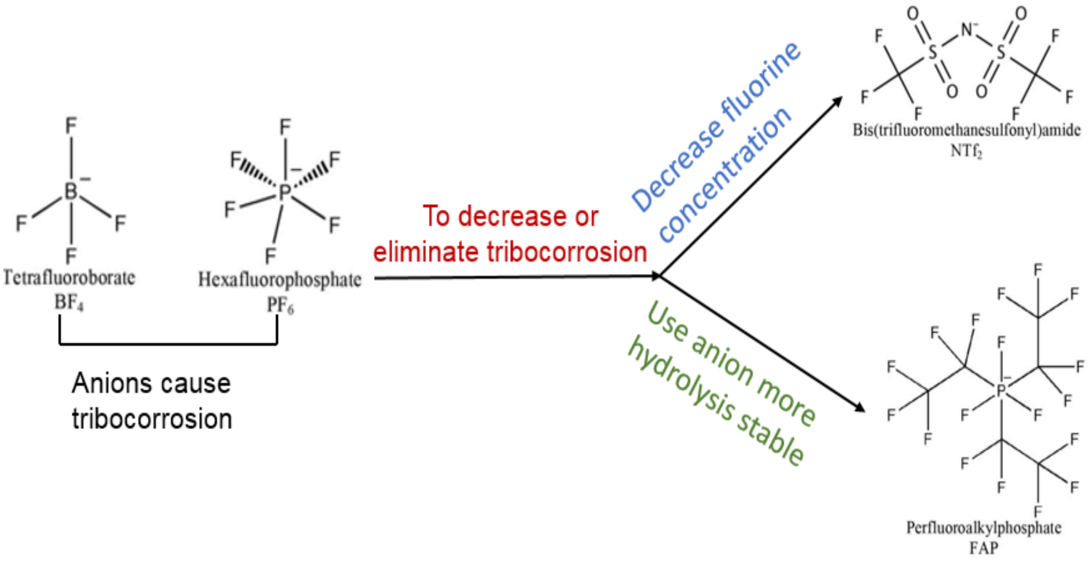

Figure 2-1: The proposed procedure by (45) to decrease or eliminate tribocorrosion.

In addition to tribocorrosion, fluorine has a negative impact on the environment since it reacts with ozone layer and contributes in the ozone depletion layer process [3-5].

To overcome these two issues together, a new class of anions was proposed by Zhang *et al* [56] that is called halogen free IL (hf). They compared hf, the phosphate anion, with the tetrafluoroborate anion and the results revealed that hf IL exhibited better tribological performance. A humid environment was used to check the presence of tribocorrosion. The results confirmed that tribocorrosion is occurred only by the halogenic IL. Another hf IL was proposed by Song *et al* [57] which is called the imidazolium ibuprofen IL. They stated that the manufacturing process of this IL is simpler than halogenic ILs. The results revealed that IL contained the ibuprofen anion implied superior tribological performance than that contained the hexafluorophosphate anion.

In contrast, the use of halogenic anion in the lubrication of light alloys such as copper and nickel can lead to form a film of metal fluorides layer that inhibits corrosion. However, this scenario is not valid for iron surfaces when iron fluoride causes corrosion due to the formation of hydrogen fluoride. Therefore halogenic free anions are the versatile solution for tribocorrosion of various tribopairs [54].

The effect of either cation or anion chain length was previously investigated. Bermudez *et al* [58] studied the influence of cation chain length of imidazolium tetrafluoroborate. The results revealed that the increase of cation chain length decreased friction coefficient despite of the reduction in the IL reactivity. The results also showed that tribocorrosion can be controlled by anion chain length rather than cation chain length. Lu *et al* [59] confirmed that the increase of cation chain length decreased the IL reactivity and the enhancement in the tribological performance was resulted from the reduction of tribocorrosion [45, 49].

Xiao *et al* [60] found that the increase of cation chain length increased the thickness of the protective layer (tribofilm thickness) see Fig. 2-2. In addition, the increase of cation chain length decreased thermal stability of ILs [61]. This means that the increase of cation chain length will cause a faster decomposition in IL and then it might lead to enhance the reactivity of IL. Further, the increase of cation chain length enhanced the tribological behaviour in the absence of any tribocorrosion in [57].

These results suggested that the increase of cation chain length enhanced the tribological performance due to the reduction of tribocorrosion in halogenic ILs. In halogen free ILs the enhancement was obtained due to the increase of the reactivity of cation moiety. This means that the increase of cation chain length decreased the reactivity of anion moieties and increased the reactivity of cation moieties.

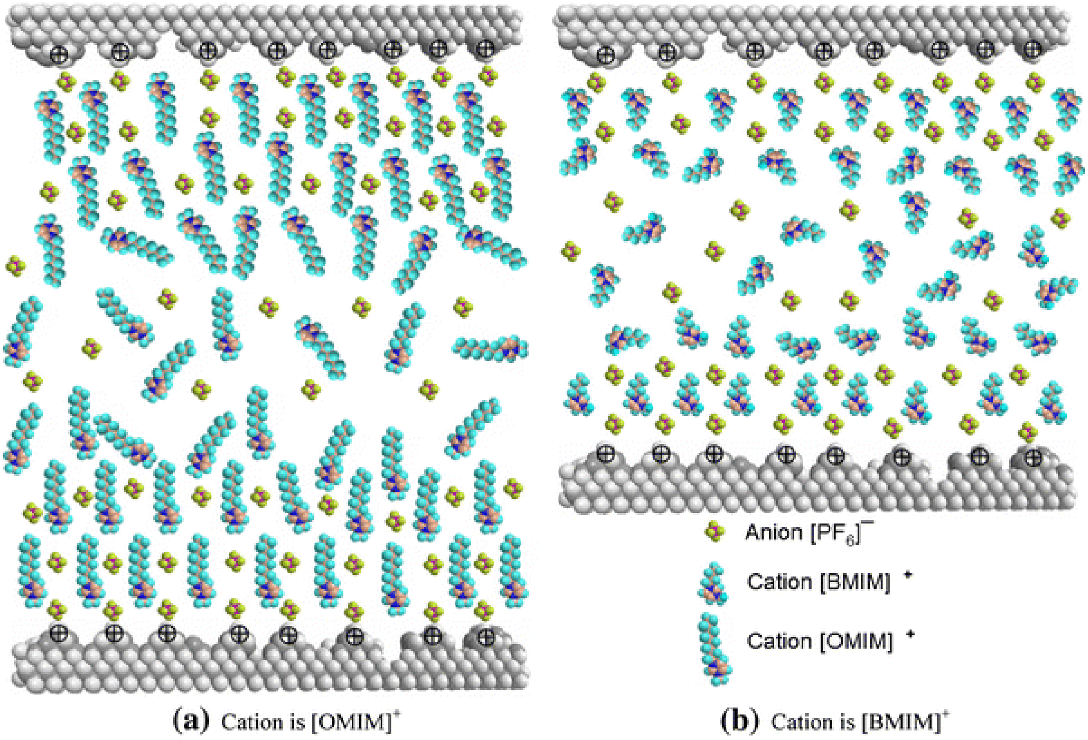

(a) Cation is $[OMIM]^+$ (b) Cation is $[BMIM]^+$

Figure 2-2: Relationship between cation chain length and film thickness (60).

ILs were also proposed to be used as lubricants for polymer-steel tribopairs at elastohydrodynamic lubrication. They provided better tribological performance than PTFE. The high load carrying capacity, high viscosity and high thermal conductivity of ILs are behind this superior performance of ILs at elastohydrodynamic lubrication regime [62].

Lastly, Jiang *et al* [63] suggested the use of the functionalized imidazolium based ILs as potential lubricants. The results of corrosion test implied that the use of functionalized cation mitigated corrosion by forming a hydrophobic layer that prevented water to be absorbed. Thus, the formation of hydrofluoric acid was prevented. In addition, the functionalized cation ILs demonstrated better tribological performance than PFPE.

Mu *et al* [64, 65] compared the tribological performance of the functionalized ILs with the imidazolium tetrafluoroborate IL and X-1P when lubricating aluminium. The results showed that the functionalized imidazolium exhibited superior tribological performance than both X 1P and the imidazolium tetrafluoroborate IL.

2.2.1.2 Ammonium Based ILs

The physical properties, the reactivity and the solubility of ILs can be controlled by changing their chemistry [3-6]. Ammonium based ILs were mainly proposed as additives since the ammonium cation showed higher solubility than imidazolium [66]. However, some previous studies examined the tribological performance of ammonium based IL when use it as potential lubricant.

Yagi *et al* [15] examined the tribological performance of this IL when lubricating aluminium, copper, iron and titanium at vacuum condition. The results revealed that in comparison with dry contact; the highest reduction in friction coefficient obtained in copper while the lowest reduction obtained in titanium. Battez *et al* [67] also used ammonium based IL but when lubricating steel-steel tribopairs. The results demonstrated that at both the lowest load and the highest load; no tribofilm was detected since the destruction rate was higher than the formation rate. The tribofilm was only detected at moderate load since the formation rate outweigh the destruction rate.

Qu *et al* [68] studied the tribofilm formation mechanisms of the ammonium trifluoromethylsulfony IL when lubricating steel, cast iron or aluminium. The highest amount of fluorine detected inside the wear track was obtained in steel while the lowest was obtained in aluminium. The formation of tribofilm was stopped when the film became thick and the substrate stops feeding the tribofilm by the positive cation to sustain the formation process. This finding was also confirmed when the thickest film was obtained in aluminium substrate since the highest amount of wear debris produced in aluminium due to its soft nature.

2.2.1.3 Phosphonium Based ILs

The phosphonium cation was proposed due to the presence of phosphorus atom that is existed in the AW additives and it shows desirable tribological performance [31]. In addition, this cation does not corrode the substrate [17], and also a recent study revealed that this cation offers high solubility [69].

Liu [70] in 2006 was firstly proposed phosphonium based IL and examined its tribological performance when lubricating steel-aluminium tribopairs. They compared between phosphonium based IL and imidazolium based IL. The results implied that phosphonium cation exhibited better tribological performance. However, each cation was combined with different anion; the phosphonium cation with the tetrafluoroborate anion and the imidazolium cation with the hexafluorophosphate anion.

In the lubrication of light alloys, Somers *et al* [71] and Shah *et al* [17] compared between the tribological performance of phosphonium based IL and 15W-50 engine oil. The results demonstrated that IL exhibited lower friction coefficient and lower wear volume. Besides, Saurin *et al* [72] investigated the tribological performance of hf ILs consist of phosphonium sulfonate when lubricating steel-ceramic and steel-polymer tribopairs. The results showed that the cation controlled the relation between viscosity and temperature. For all the examined tribopairs; the results showed that these hf IL provided very efficient lubrication (low wear and friction coefficients).

2.2.1.4 Studies Using Various Cations

This subsection will mainly present studies which either used other cations (different to those mentioned above) or papers utilized more than one cation to examine the effect of the cation type or to compare the tribological performance of two different ILs.

Firstly, pyrrolidinium cation has been utilized in few previous studies as the only cation combined with various anions [73-75]. The results of these studies showed that pyrrolidinium based IL exhibited better tribological performance than conventional lubricant (PFPE) in terms of exhibiting lower friction coefficient and lower wear volume.

Phosphazene based IL was also suggested by Omotowa *et al* [14] to be used as lubricant in aircrafts. This suggestion was made due to its unique properties such as it exhibits very low pour point (about -50 ^{o}C), high load carrying capacity and they can be used for various tribopairs. This IL showed an excellent tribological performance in terms of providing a high reduction in both friction coefficient and wear volume.

Guanidinium was combined with the tetrafluoroborate anion and form IL lubricant by Yu *et al* [76]. The results showed that it exhibited better tribological performance than the liquid paraffin. However, the imidazolium tetrafluoroborate IL showed better tribological performance.

Further studies were conducted to investigate the influence of cation type on the tribological behaviour of ILs when lubricating various tribopairs [27, 48, 77]. Qu *et al* [48] compared between the ammonium cation and the imidazolium cation when combined with the trifluoromethylsulfony anion and lubricating aluminium alloy. The results showed that the ammonium cation exhibited lower friction coefficient and lower wear volume. In addition, the extra reduction of wear volume by ammonium was obtained due to the significant reduction in the tribocorrosion. This finding suggests that the cation type is also crucial in the determination of tribocorrosion. Jimenez *et al* [78] also confirmed these findings when compared between ammonium based IL and imidazolium based IL when lubricating steel-titanium tribopair.

However, Guo *et al* [79] demonstrated that imidazolium exhibited comparable tribological performance with ammonium when combined with the phosphate anion and lubricating ceramic at room temperature. The increase of temperature to 100 ^{o}C showed that the imidazolium cation exhibited lower friction coefficient while wear volume was comparable.

In similar manner, Itoh *et al* [27] compared between the imidazolium cation and the phosphonium cation when combined with the sulfate anion and lubricating steel-steel tribopairs. The results demonstrated that the phosphonium cation exhibited superior tribological performance in terms of providing lower friction coefficient.

This finding was confirmed by Otero *et al* [77] when the phosphonium cation exhibited lower friction coefficient and lower wear volume than the imidazolium cation when both cations combined with the FAP anion as shown in Fig. 2-3.

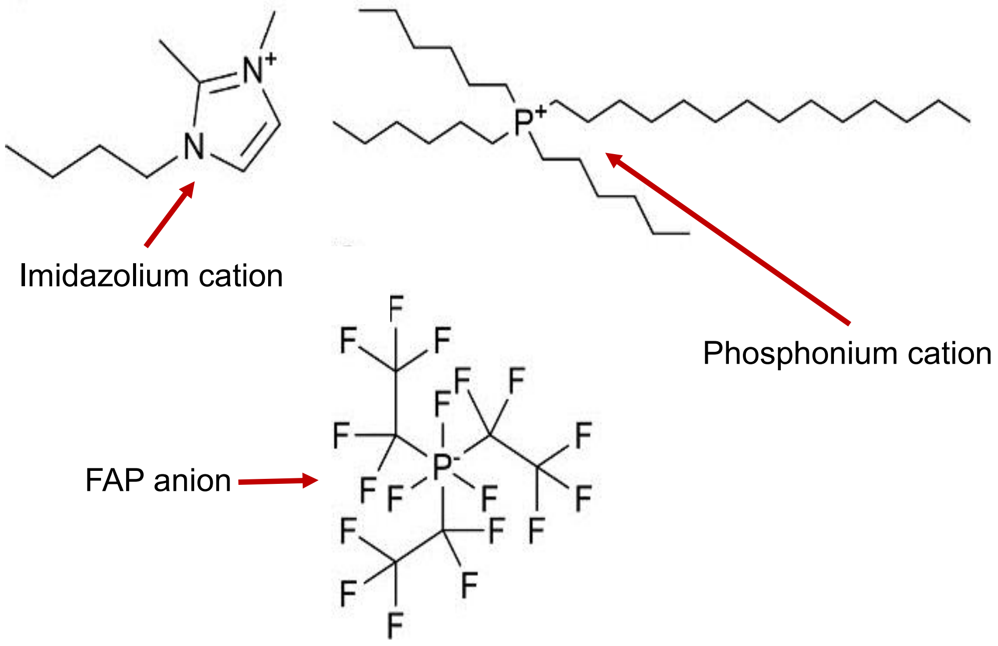

Figure 2-3: The Imidazolium cation, the phosphonium cation and the FAP anion.

Weng *et al* [80] again confirmed that the phosphonium cation exhibited better tribological performance than the imidazolium cation due to the presence of the phosphorus element in the formed tribofilm that lead to decrease friction coefficient. The increase of temperature from room temperature to 100 °C lead to increase the presence of phosphorus which means that the formation rate of the tribofilm was increased. Wu *et al* [19] compared between imidazolium and phosphonium when lubricating polymer-steel tribopairs at elevated temperature. The results implied that both cations exhibited very comparable friction coefficients at 80 °C while phosphonium cation implied slightly lower friction coefficient at 160 °C.

In contrast, Minami *et al* [81] reported that both cations (imidazolium and phosphonium) exhibited very comparable friction coefficients when combined with FAP. However, they stated that the phosphonium cation reacts with the utilized surface before fluorine and then prevents fluorine to react with the employed surface.

On the other hand, Fan *et al* [82] compared the ammonium and the phosphonium cations when lubricating steel, copper or aluminium. The results showed that both cations exhibited comparable friction coefficients when lubricating steel surfaces. Phosphonium showed lower friction coefficient than ammonium when lubricating copper while ammonium showed lower friction coefficient when lubricating aluminium. For wear volume, very comparable behaviour to that observed in friction coefficient was obtained.

A very recent study conducted by Matczak *et al* [83] compared between phosphonium, imidazolium and ammonium cations when lubricating steel-steel contact. The results showed that ammonium exhibited the highest friction coefficient while it was comparable for the rest two ILs. Imidazolium demonstrated the highest wear volume while the wear volumes of the rest two ILs were comparable.

Another technique was utilized to enhance the tribological behaviour of ILs by using dicationic ILs. Dicationic means that two cations are combined by either oxygen or hydrocarbon to form dicationic IL. Dicationic ILs are thermally more stable than monocationic ILs. Pagano *et al* [25] investigated the tribological performance of twelve dicationic ILs. Dications were synthesized from imidazolium and pyrrolidinium cations when combined with four anions which were Tf2N, chloride, methanesulfunate and butansulfunate at three temperatures; 50 ^{o}C, 100 ^{o}C and 150 ^{o}C. The results demonstrated that all the examined ILs had comparable friction coefficients and wear volumes. However, in order to investigate whether dicationic IL can provide better tribological performance than monocationic IL or not; at least one monocationic IL supposed to be examined for comparison purposes.

2.2.2 Using ILs as Additives

Due to the high cost of the manufacturing process of ILs, using them as base lubricants in macro scale is very costly. The use of ILs as additives to enhance the tribological performance in terms of reducing wear volume and friction coefficient can penetrate lubricants market faster [84]. In addition, using IL as additive can provide comparable reduction in the wear volume and friction coefficient to that obtained by neat ILs [44]. However, the majority of ILs are not soluble in non-polar lubricants due to their high polarity [3-6]. In this subsection, the related literature to the use of ILs as additives in either polar or non-polar base lubricants are presented. It is also divided based on the cation type.

2.2.2.1 Imidazolium Based ILs

ILs have been proposed as additives firstly by Phillips *et al* [22] when they added imidazolium hexafluorophosphate in water to lubricate ceramic. The results confirmed that adding IL can provide a considerable enhancement in the tribological performance, especially in the friction coefficient during the running-in period. Mistry *et al* [85] added both imidazolium tetrafluoroborate and tritolyl phosphate (TTP) to mineral oil. The results showed that friction coefficient was decreased by 81% when adding these two additives together, while adding IL only decreased friction coefficient by 62%. Surface analysis results implied that both the anion moiety (fluorine) and the cation moiety (nitrogen) were detected at the worn area.

ILs were also added to grease. Cai *et al* [86] added imidazolium hexafluorophosphate and imidazolium tetrafluoroborate to grease base lubricant. The results showed that both additives lead to a decrease in wear and friction coefficients and both additives exhibited comparable tribological performance. The increase of temperature was lead to a decrease in wear and friction and increased the formation rate of tribofilm. In contrast, Battez *et al* [87] reported that the tetrafluoroborate anion exhibited better tribological performance than the hexafluorophosphate anion when they were added in mineral oil with the same concentration. The results showed that in contrast to temperature; the increase of load was lead to increase wear mass and friction coefficient.

The effect of the anion type on the solubility of IL in PolyEthylene Glycol (PEG) was studied by Cai *et al* [88]. They compared between the solubility of tetrafluoroborate, hexafluorophosphate and trifluoromethylsulfony. The highest solubility was obtained in the trifluoromethylsulfony and the lowest one in the tetrafluoroborate. The tribological performance of PEG + hexafluorophosphate only was examined and the results showed that friction coefficient was decreased with the increase of IL concentration. Jimenez *et al* [49, 89] utilized the same ILs as in [88] at room temperature and at 100 ^{o}C. The results showed that these ILs were not soluble in Propylene Glycol DiOleate (PGDO) and therefore adding ILs was only decreasing friction coefficient at high temperature since they became fully soluble.

Pejakovic *et al* [90] studied the influence of the imidazolium sulfate IL concentration in glycerol base oil on its tribological performance. Among three concentrations; 0.63 wt%, 2.5 wt% and 8 %wt, the highest reduction in the wear volume and friction coefficient was obtained when adding 0.63 wt%. However, moving from pure sliding in [90] to mixed sliding rolling in (50) showed a converse behaviour. The increase of IL concentration lead to enhance the tribological performance. The results also demonstrated that the tribofilm thickness was increased with IL concentration.

Lastly, imidazolium ibuprofen was examined by Wang *et al* [91]. They added IL to Water–Ethylene Glycol liquid when lubricating steel-steel tribopairs. The results showed that the imidazolium ibuprofen IL can provide a considerable reduction in the wear volume due the formation of tribofilm.

2.2.2.2 Ammonium Based ILs

Blanco *et al* have conducted two studies [92, 93] using the ammonium-FAP IL as additive in Poly-Alpha-Olefin 6 (PAO6) base lubricant to lubricate various coatings and compared the results with ZDDP. The first study utilized CrN PVD coat while the second one used TiN PVD coat. The results showed that both additives provided a reduction in the wear volume and friction coefficient of both coats. However, ZDDP provided higher reduction in both wear volume and friction coefficient and for both coats.

Fan *et al* [66] also reported that adding the ammonium sulfosuccinate IL in PAO10 lead to a decrease in friction coefficient and wear volume. However, it is not fully soluble in PAO10 and the increase of the cation chain length enhanced its solubility.

A new oil miscible IL was proposed very recently by Zheng *et al* [94]. The ammonium phosphite IL was added to both fatty acid and vegetable oil. The results implied that this IL is fully soluble and can provide a reduction in the wear volume and friction coefficient due to the formation of tribofilm that detected by surface chemistry analysis.

2.2.2.3 Phosphonium Based ILs

The first fully soluble IL in non-polar lubricants is the phosphonium based ILs. Qu *et al* [84] proposed the phosphonium phosphate IL as the first fully soluble IL. It is presented in Fig. 2-4. They added this IL to PAO and also to 5W-30 engine oil. The results showed that the phosphonium phosphate IL is thermally stable and does not cause tribocorrosion. The friction coefficient and wear volume were substantially decreased by adding IL. The highest reduction in wear volume was 70% when IL added to the engine oil. This reduction was obtained due to the formation of thin tribofilm; about 40-60 nm.

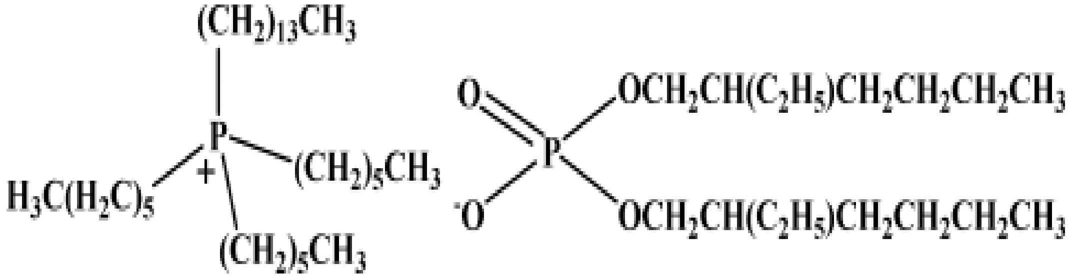

Figure 2-4: Chemical structure of oil-soluble phosphonium phosphate IL.

Qu *et al* [95] compared between ZDDP and the phosphonium phosphate IL when they are both added to the engine oil to lubricate steel-DLC tribopairs. The results showed that friction coefficients of both additives were very comparable while IL exhibited lower wear volume. Again, Qu *et al* [29] conducted a comparative study to compare the anti-wear performance of the phosphonium phosphate IL and ZDDP when added them in PAO under various temperatures.

As expected, the results implied that when add either ZDDP or IL a comparable and significant reduction in both wear volume and friction coefficients was obtained.

However, at elevated temperature, IL demonstrated better anti-wear performance. Huang *et al* [96] confirmed this finding when reported that the phosphonium phosphate IL provided superior performance than ZDDP in terms of both anti-wear additive and anti-corrosion additive.

Another approach was proposed; mixing the phosphonium phosphate IL with ZDDP together as anti-wear additives. Qu *et al* [97] reported that the mixture of phosphonium phosphate with ZDDP provided higher wear reduction that obtained by only phosphonium phosphate. The mixture of ammonium based IL with phosphonium phosphate did not show any extra enhancement to the anti-wear property of phosphonium phosphate.

Landauer *et al* [98] investigated the relation between the anti-wear property and the mechanical properties of tribofilms that formed by ZDDP, phosphonium phosphate and their combination. The mechanical properties which considered in this study were hardness, modulus of elasticity and the resistance to plastic deformation. The results implied that add ZDDP+IL significantly reduced the effect of temperature on mechanical properties. The increase of modulus of elasticity lead to a substantial enhancement in the tribological performance. The tribofilm hardness had no influence on tribological properties. In contrast, surprisingly, the increase of tribofilm resistance to plastic deformation reduced its anti-wear.

Phosphonium phosphate was also incorporated with silica nanoparticles and used together as anti-wear additive in mineral oil by Seymour *et al* [99]. A chemical reaction was conducted between these two additives and it was detected by XPS. The combination of these two additives showed higher reduction in both friction coefficient and wear volume than that obtained when either only IL or only silica particles was used.

Yu *et al* [23] studied the influence of the anion chain length on the solubility of phosphonium phosphate IL. The results showed that the decrease of the anion chain length enhanced IL solubility.

The tribological behaviour in terms of wear volume and friction coefficient was also significantly enhanced when adding 5 wt% of IL to engine oil. Otero *et al* [69] compared between phosphate and trifluorophosphate anions when combined with phosphonium and utilized as additives. The results showed that phosphate exhibited lower friction coefficient while trifluorophosphate exhibited lower wear volume.

Another comparison between the phosphonium phosphate IL and amine phosphate (both are biocompatible additives) was conducted by Khemchandani *et al* [100]. Both additives were added to Safflower oil to lubricate bio systems. The results showed that both additives provided a considerable reduction in the wear volume and friction coefficient. However, IL showed higher reduction in both friction coefficient and wear volume. Surface analysis results revealed that IL formed thicker tribofilm due to its higher reactivity.

The phosphonium phosphate additive was added to grease as well by Wang *et al* [101]. The results demonstrated that a significant reduction in the wear volume and friction coefficient was obtained.

Lastly, the phosphonium phosphate IL was added to the imidazolium borane IL by Totolin *et al* [20] to enhance its tribological performance. The results demonstrated that adding phosphonium phosphate lead to decrease friction coefficient and wear volume due to the formation of tribofilm. Minami *et al* [18] also suggested adding phosphonium phosphate IL to imidazolium based IL base lubricant. They added it to the imidazolium tetrafluoroborate IL. The results showed that a significant reduction in the tribocorrosion, friction coefficient and wear volume were obtained when add phosphonium phosphate.

2.2.2.4 Studies using Various Cations

Pyrrolidinium based IL was also employed as additive when the pyrrolidinium sulfate IL added to glycerol. The experiments were conducted at four temperatures; 20 ^oC, 50 ^oC, 100 ^oC and 150 ^oC. Despite the reduction of wear volume and friction coefficient especially at high temperatures (above 50 ^oC). The results implied that this IL caused corrosion.

Gonzalez *et al* [75] also used the pyrrolidinium trifluorophosphate IL as additive in PAO6 when lubricating DLC, TiN and CrN coats. The results showed that this IL is not fully soluble in PAO6 and only slight reduction in the friction coefficient and wear volume was obtained.

The increase of the cation chain length of pyrrolidinium was lead to increase friction coefficient and wear volume when added to PEG [74].

Pejakovic *et al* [102] compared between pyrrolidinium and ammonium cations when combined with the sulfate anion and added to glycerol with various concentrations; 0.625 wt%, 2.5 wt% and 8 wt%. The results showed that the increase of IL concentration lead to increase wear volume for both cations. Friction coefficient was decreased slightly with the increase of IL concentration.

The influence of the cation type on the solubility of IL was investigated by Schneider *et al* [103]. The solubility of imidazolium, ammonium, thiazolium and uranium cations when combined with the trifluoromethylsulfony anion and added to either PAO or Easter. The results implied that the highest solubility was obtained in the uranium cation while the solubility of the rest cations was very comparable.

Sharma *et al* [104] used choline phosphate IL as additive and compared it with ZDDP when added to either mineral oil or to fully formulated oil. They focused on the formed tribofilms as presented in Fig. 2-5.

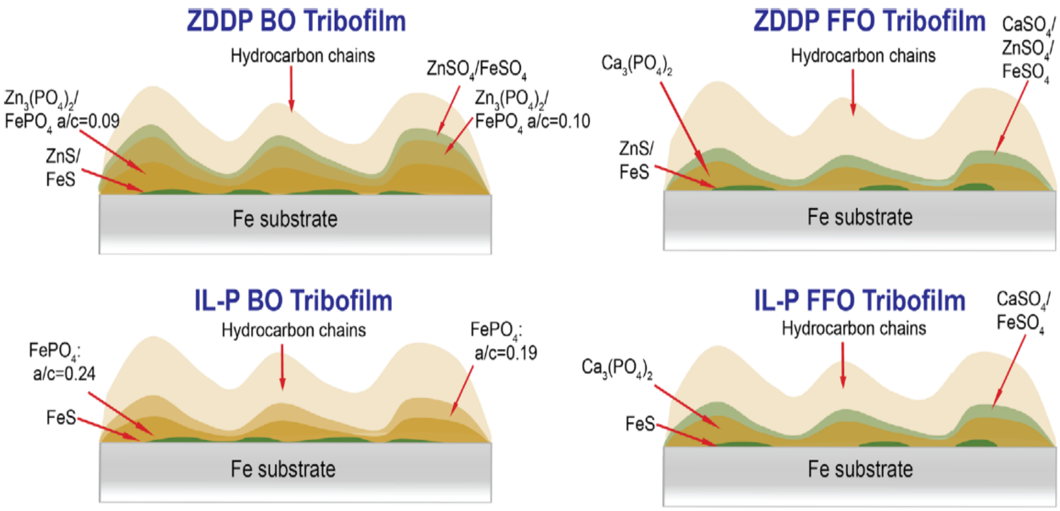

Figure 2-5: The chemistry of tribofilms formed by additives in (104).

The results showed that IL formed glassy polyphosphate tribofilm with longer chain length than ZDDP polyphosphate tribofilm at the identical tribological conditions. However, only one more layer was created by ZDDP which was $ZnSO_4/FeSO_4$.

In addition, they stated that FeS is also created by choline phosphate IL. This assumption cannot be accepted when IL was added to mineral oil since sulfur was not existed in neither base oil nor in the additive, the chemical structure of choline phosphate is presented in Fig. 2-6.

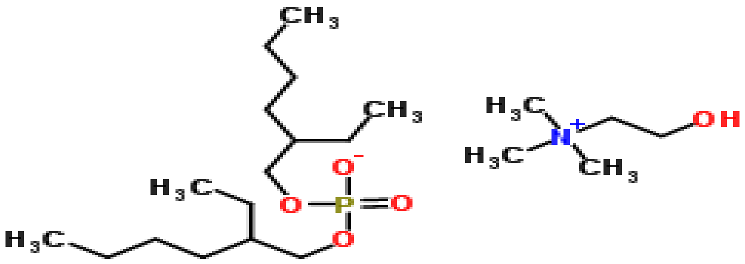

Figure 2-6: The chemical structure of choline phosphate

Again, Sharma *et al* [105] compared the anti-wear performance between ZDDP and six ILs which were either phosphonium based or choline based ILs, as shown in Fig. 2-7. The results showed that in addition to ZDDP all ILs were decomposed firstly and then reacted and formed tribofilms. The hardness of all tribofilms was increased with tribofilm depth.

Lastly, some more studies were conducted to investigate the enhancement in the tribological properties that results when add IL to PEG in [21], to paraffinic-naftenic in [106] and to glycol in [107]. The results implied that add IL lead to decrease both wear volume and friction coefficient.

Coded name	Chemical name	Chemical structure	Onset decomposition temperature (°C)
	ZDDP	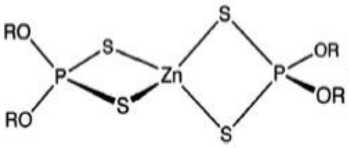	206
	Choline bis(ethylhexyl)-phosphate IL	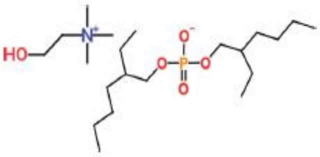	258
	Choline dibutyl-dithiophosphate	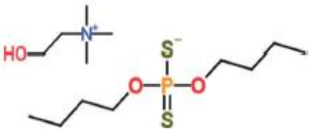	172
	Phosphonium Phosphinate	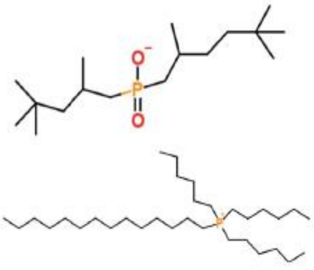	362
	Phosphonium TFSI	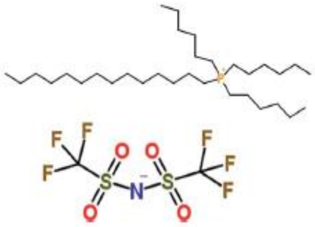	413
	Methyl-tributyl-Phosphonium dimethyl-phosphate	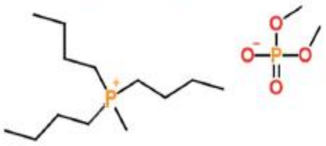	326
	Tetra-butyl-Phosphonium diethyl-dithiophosphate	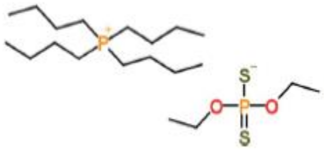	261

Figure 2-7: The chemical structures of additives that examined in [105].

2.3 Nano/Micro Scale Studies and the Lubrication of MEMS

Nano tribology has been introduced after the invention of new techniques that could characterize surface topography and measure friction in nano scale. Also, the development of super computer allows researchers to simulate nano tribology. The main differences between conventional (macro) tribology and nano tribology are illustrated in table 2 [108].

Table 2-1: The differences between macro and nano tribology (108).

Macro tribology	Nano tribology
Large mass	Small mass
Heavy load	Light load
Controlled by weight	Controlled by interfacial forces
Rely on bulk material properties	Rely on surface properties

In contrast to the macro scale when a large number of asperities of tribopair become in contact. In nano tribology; a single sharp asperity of scanning tunnelling microscope STM or Atomic Force Microscopy (AFM) slides over the sample [108] (see Fig. 2-8). In micro scale studies a few asperities become in contact instead [109].

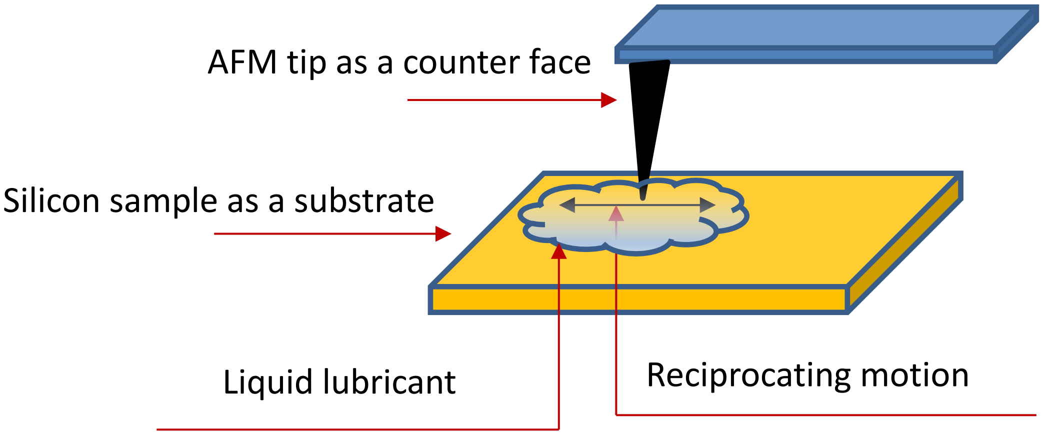

Figure 2-8: Configuration of the use of AFM as tribometer (108).

A few previous studies were conducted to examine the tribological performance of ILs at nano scale. Li *et al* [110] conducted a nano scale study using AFM to compare between octane, octane+1 wt% phosphonium based IL and neat phosphonium based IL. The results showed that add only 1 wt% of IL lead to significant reduction in the friction coefficient. This supports that IL is an effective additive to reduce friction coefficient even at nano scale. A comparison between the phosphonium phosphate IL and ZDDP when both were added to hexadecane at both nano scale and macro scale was conducted by Li *et al* [47]. The results showed that when the contact pressure was the same at both scales, a high agreement between friction coefficient results was observed. The phosphonium phosphate IL exhibited lower friction coefficient than ZDDP in both scales.

Hijalmarsson *et al* [111] conducted a nano scale investigation to study the influence of temperature on both normal and frictional force when lubricating mica with the ammonium nitrate IL. The results implied that the increase of temperature was lead to decrease lubricant viscosity. Therefore, both normal and lateral forces have been influenced by temperature change since the latter force was decreased with increasing temperature. The results showed that IL was strongly adsorbed into mica surface and formed an adsorbed protective layer.

On the other hand, the nano tribology is also feasible to simulate the working of the components have either micro or nano scale of contact such as MEMS/NEMS. In addition, the lubrication of MEMS is a current challenge that is facing the tribologists. The reduction of both wear and friction is strongly aimed in order to elongate the life cycles of MEMS [108]. The use of coating can provide a significant reduction in the wear and friction coefficients but once its wear out and a dry contact is taken place, failure occurs. Liquid lubricant can be employed to provide a longer life for MEMS [24].To simulate the working of MEMS either silicon-silicon or silicon-borosilicate tribopairs must be employed [24].

Two previous approaches were employed to simulate the working of MEMS in order to evaluate their lubrication behaviour. The first approach using on demand designed micro tribometer to characterize wear and friction coefficients in MEMS [112-114]. The second approach using commercially available tribometers including micro scale tribometer (nanotribometer) [115] and nano scale tribometer (AFM) [24, 116] to evaluate both wear and friction coefficients.

Leong [114] designed a tribometer that is shown in Fig. 2-9. They studied the use of either PFPE or hexadecane + Multiply Alkylated Cycloparffins (MACs) to lubricate MEMS. They proposed a new method to keep liquid lubricant only within the moving parts by modifying silicon surface. The results showed that hexadecane + MACs exhibited lower friction coefficient and wear volume than PFPE.

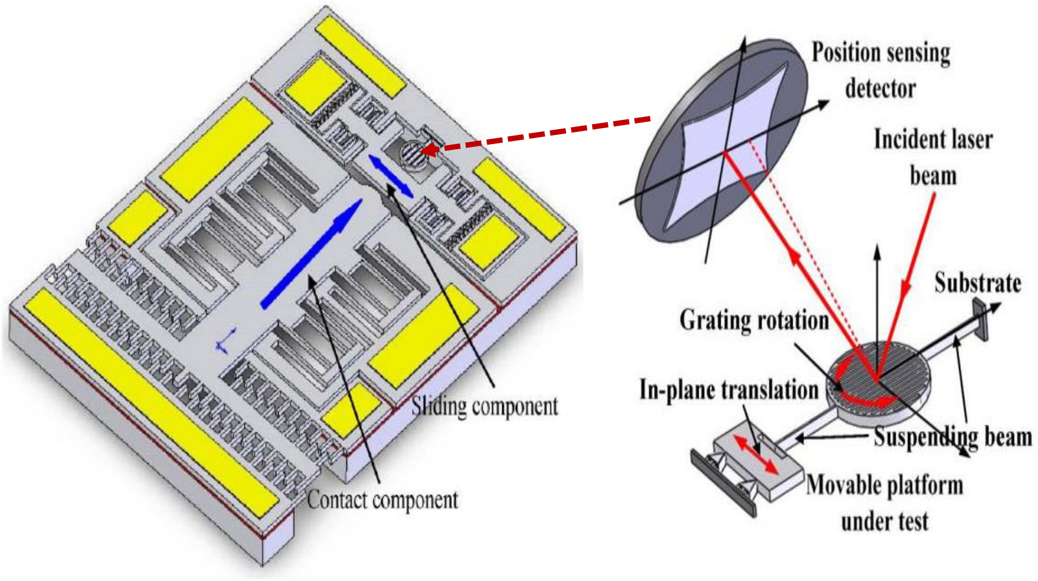

Figure 2-9: Micro tribometer designed by Leong [114].

Reddyhoff *et al* [112] manufactured a micro tribometer that simulates the working of micro bearing as presented in Fig. 2-10. They examined the reduction of friction coefficient that might be obtained when a friction modifier Octadecylamine was added to the silicon base oil. The results showed that a considerable reduction in the friction coefficient was obtained when added this friction modifier.

The use of commercial rigs to simulate the working of MEMS is also done previously. Bhushan *et al* [116] conducted a nano scale study to investigate the tribological performance of imidazolium combined with either hexafluorophosphate or sulfate when lubricating silicon. The aim was to simulate the working of MEMS. However, silicon substrate was employed against silicon nitride tip, which is different to the real tribopair in MEMS. The results implied that both friction coefficient and adhesive force were substantially decreased when using ILs due to the protective layer that was formed by the chemical adsorption of ILs into silicon surface.

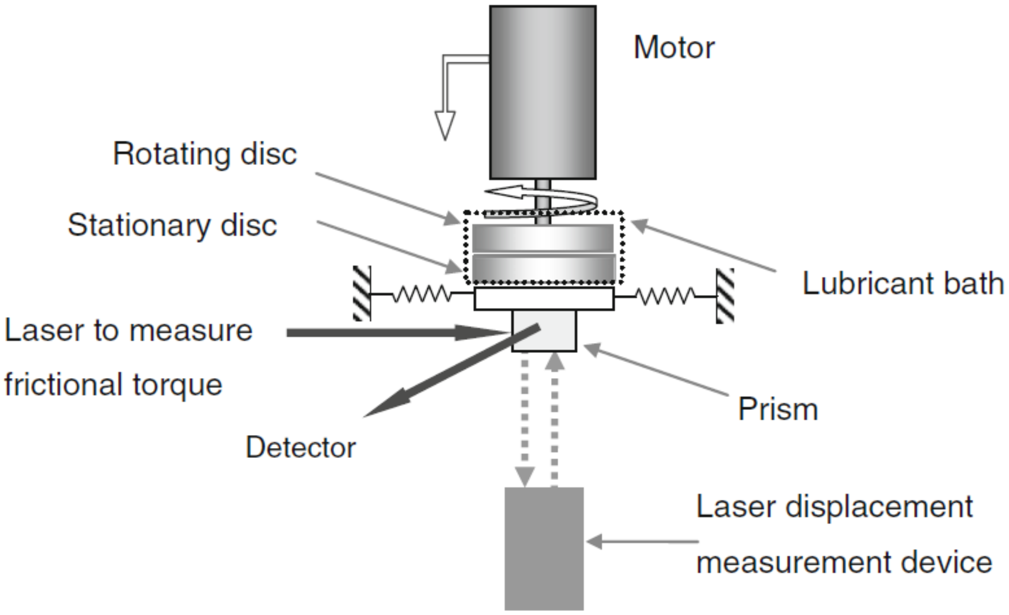

Figure 2-10: Micro tribometer designed by Reddyhoff *et al* [112].

Kondo *et al* [117] proposed ammonium based IL as an effective lubricant for MEMS. AFM was employed to conduct the experiments in order to simulate the working of MEMS. The results showed that the increase of the adsorbed film thickness decreased friction coefficient.

Nainaparampil *et al* [24] also employed AFM to simulate the lubrication of MEMS with ILs. They stated that only silicon based materials must be employed to simulate MEMS. Therefore, they utilized silicon against borosilicate tribopair. The results showed that IL chemistry is crucial in the determination of the tribological performance. The increase of the cation chain length enhanced the tribological performance while the cation type was not effective. However, both cations, imidazolium and pyridinium, have the same atom which is nitrogen.

A few issues have been pointed out when use AFM as a tribometer to simulate MEMS. A complex set up procedure and long-time are required to conduct the experiment in comparison with conventional tribometers [108]. The contact pressure can be varied during experiment due to either the variation of tip geometry or the formation of tribofilm. The former reason occurred as a result of wear and the latter one causes a variation in the Young's modulus [118]. In addition, the real contact in MEMS is in micro meter order rather than nano meter which is easier to achieve by micro scale tribometer [109].

A micro scale study was also conducted very recently by Amorim *et al* [115] using commercial nanotribometer (NTR). The results implied that add 2 wt% of IL to the PEG base oil, lead to a considerable reduction in the friction coefficient. The addition of IL lead to make the friction coefficient very comparable in both humid and dry environments. However, the utilized tribopair was steel ball against silicon surface which does not match the tribopair in the real MEMS.

2.4 Summary and the Current Gap of Knowledge

A large number of previous studies that proposed ILs as lubricants and examined their tribological performance were published. In addition, other studies have been conducted to study the tribological performance of ILs as coatings [119-122], in confined geometry [123-125] or as corrosion inhibitors [126, 127]. Fig. 2-11 depicts a brief summary for the story of the use of ILs as lubricants. The general story is presented in the middle diagrams. The two diagrams on each side highlight the current gaps of knowledge.

A clear lack for a consistent microscale study that covers the effect of IL chemistry on its lubrication mechanism (relationship between the formation of tribofilm and the tribological performance) at various conditions. In addition, no previous study considered the reactivity of ILs with solid surfaces at elevated temperature, i.e.; the formation of thermal film in the absence of any tribological motion. The understanding of the thermal film formation mechanism strongly helps to understand the lubrication mechanism of ILs.

Besides, the reason behind the superior tribological performance of oil-soluble IL than ZDDP at particular conditions (especially at high temperature) is still vague. Thus, a comprehensive comparison between the lubrication mechanism of ZDDP and oil-soluble will be conducted.

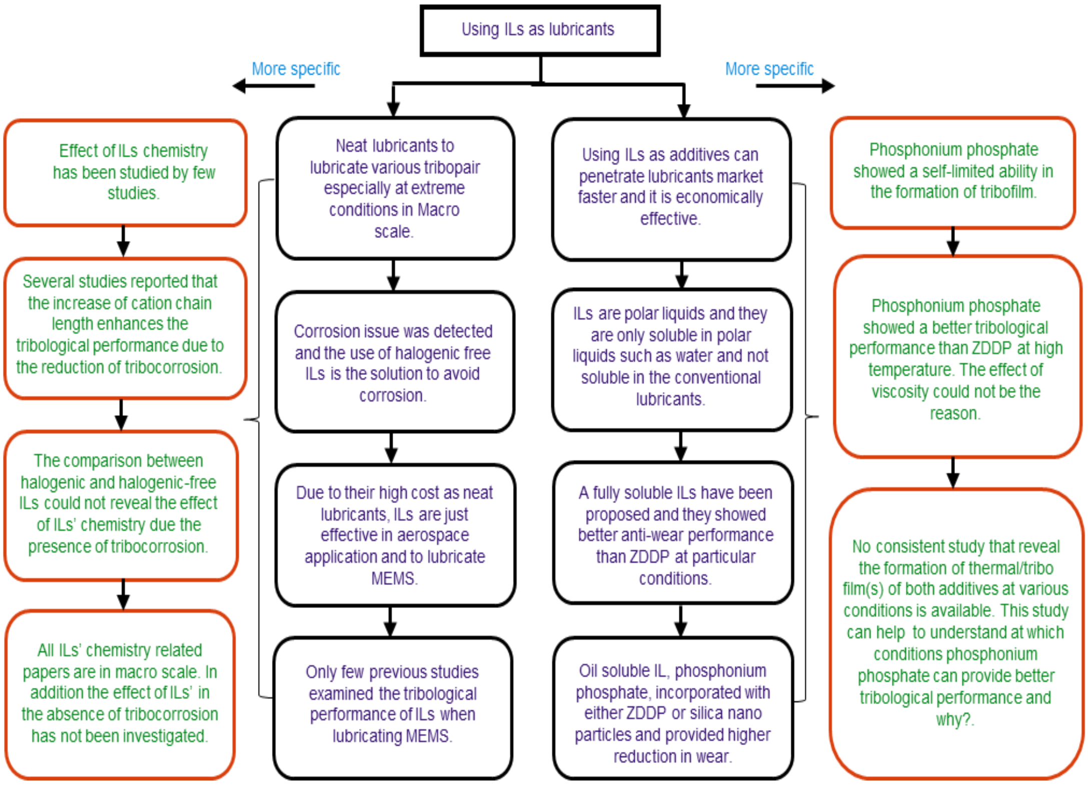

Figure 2-11: A summary to the use of ILs as lubricants in the literature and the current gaps.

3. Chapter 3: Methodology

3.1 Introduction

This chapter illustrates a description of the instruments, ILs and materials that are used in this project. Basically, the instruments can be divided into two groups; the first one includes those used to conduct the experiments while the second group includes the instruments that are used for surface analysis. The utilized ILs and materials are also depicted including those used when using IL as additive and those used when using IL as neat lubricant.

In addition, the methodologies of the blending process of lubricants, tribological experiments and thermal film formation experiments will be presented. Mainly, the procedure of the aforementioned experiments will be demonstrated. The experiments' conditions will be presented in the results chapters.

3.2 Instruments

The instruments are classified into two types; experiment conducting instruments and surface analysis instruments. The former group includes hot plate and nano tribometer. Surface analysis instruments include; SEM-EDS, ATR FTIR, XPS and AFM. These will be demonstrated starting from the first group and going in the same order as presented in this paragraph.

3.2.1 Hot Plate

WiseStir hot plate with feedback control system was used to blend lubricants, conduct the thermal film formation experiments and static thermal decomposition experiments. The stirring was used just for blending lubricants process. The schematic diagram of WiseStir with an elucidation of the working of the feedback control is presented in Fig. 3-1. Both temperature and stirring can be regulated manually. When the lubricant reach the pre-set temperature, the heater is turned off. Once the temperature is dropped to a temperature lower than the pre-set limit, the heater works again. An additional beaker contains PAO lubricant was employed to control temperature and avoid any direct contact between the examined lubricants and the temperature sensor to avoid chemical contamination.

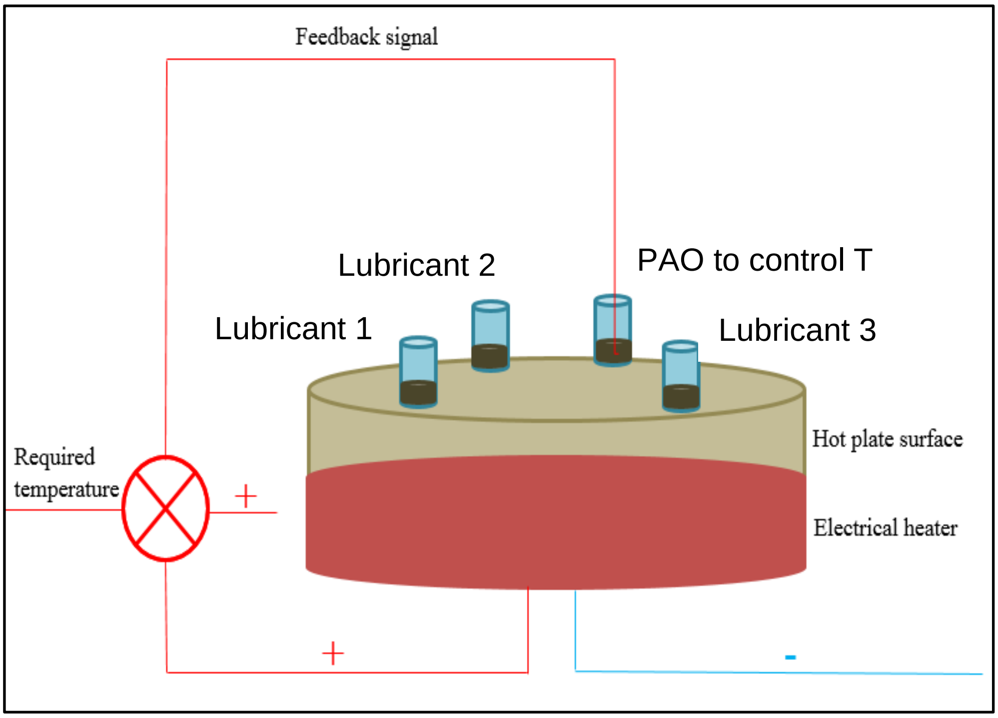

Figure 3-1: The working principle of WiseStir hot plate.

3.2.2 Nano Tribometer

Tribometers are equipments in which are designated to simulate the tribological motion of various applications. Friction is measured in-situ during the experiment by measuring the ratio of the tangential force to the normal force. Wear is usually measured after conducting the experiment using either optical or X-ray scanning microscopy [128].

A wide range of tribometers are available, for example, pin on disk, and pin on plate and four balls. Further, each type is designated to simulate a group of applications and working at certain conditions. In order to simulate the working of the desired application properly, the feasible tribometer must be used to eliminate the deviations in the obtained results. The majority of tribometers exhibit a precise simulation of wear and friction by offering a high control of operating conditions such as humidity, temperature and applied load. Lastly, tribometers are utilized instead of using the full size equipment due to their ability to offer high control and their low cost in comparison with the full size equipment [128].

A commercial nanotribometer from Anton Paar is utilized in this study. The need for micro scale study in order to simulate the working of MEMS leads to select of this tribometer.

The tribological experiments are conducted by applying reciprocating motion with ball-on-plate configuration. The high load cell is employed when the maximum applicable load is 1N and the minimum is 0.5 mN with load resolution 3 µN.

A bespoke sample holder was designed to minimize the required amount of IL in each test, and avoid using glue to hold the silicon wafers during experiments (Fig. 3-2). Eight sample holders have been manufactured at the University of Leeds, UK. Each sample holder was specified for a particular lubricant to avoid chemical contamination that might be occurred when using same sample holder for different lubricants.

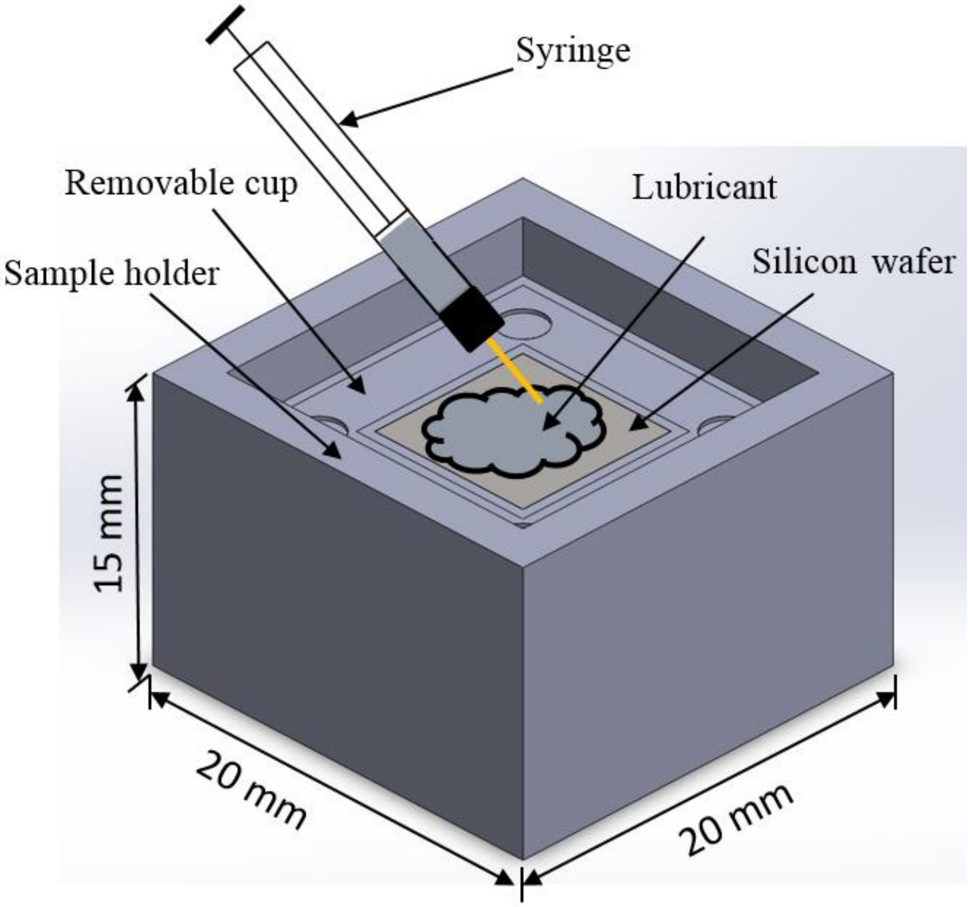

Figure 3-2: A bespoke sample holder for room temperature experiments.

This tribometer is designed to conduct experiment only at room temperature. In order to conduct high temperature experiment; an engineering modification has been applied. However, the highest temperature that can be applied is 100 ^{o}C.

The further increase in temperature can lead to a deviation in the sensors sensitivity that measure normal and tangential forces. Another bespoke component was designed which contains two perforations for both heater and sensor, see Fig. 3-3.

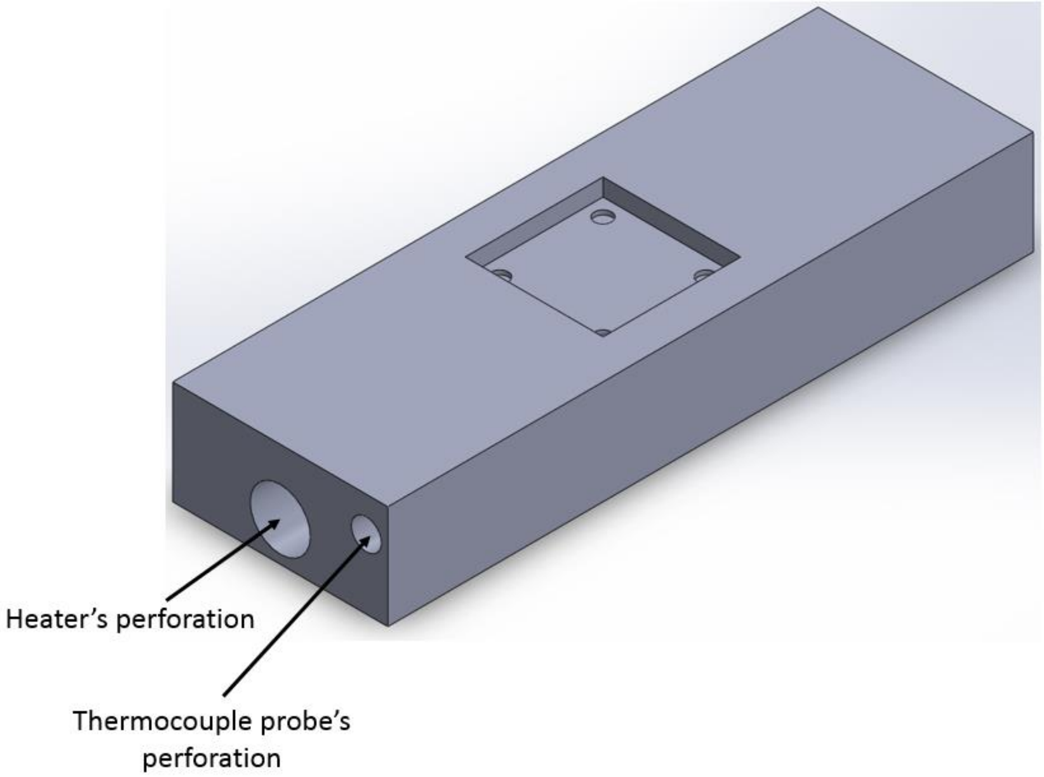

Figure 3-3: A bespoke sample holder containing two perforations.

A cartridge heater was inserted in the larger perforation and the probe of the thermocouple was inserted in the second perforation. A super conductive glue was utilized to minimize the thermal resistance. Both the cartridge heater and the K-type thermocouple were purchased from Thermosense, UK. A digital controller was incorporated to control the temperature by comparing between the pre-set temperature and the signal that comes from the thermocouple. The controller was also purchased from Thermosense, UK.

Lastly, a manual calibration was done to eliminate the error that might be occurred due the presence of thermal resistances result from the glue and the body of the sample holder. The full configuration of high temperature set up is depicted in Fig. 3-4.

The manual calibration reveals that the difference between IL temperature and body temperature (sample holder) is 5 ^{o}C. Therefore in order to obtain 80 ^{o}C in IL; 85 ^{o}C must be specified as a pre-set temperature. However, an error about -1 ^{o}C +5 ^{o}C is unavoidable since the heater cannot work unless the temperature becomes below 85 ^{o}C. Despite the cut out of electricity to heater once the temperature becomes 85 ^{o}C, the temperature is rise up to about 90 ^{o}C due to the presence of stored heat in the heater.

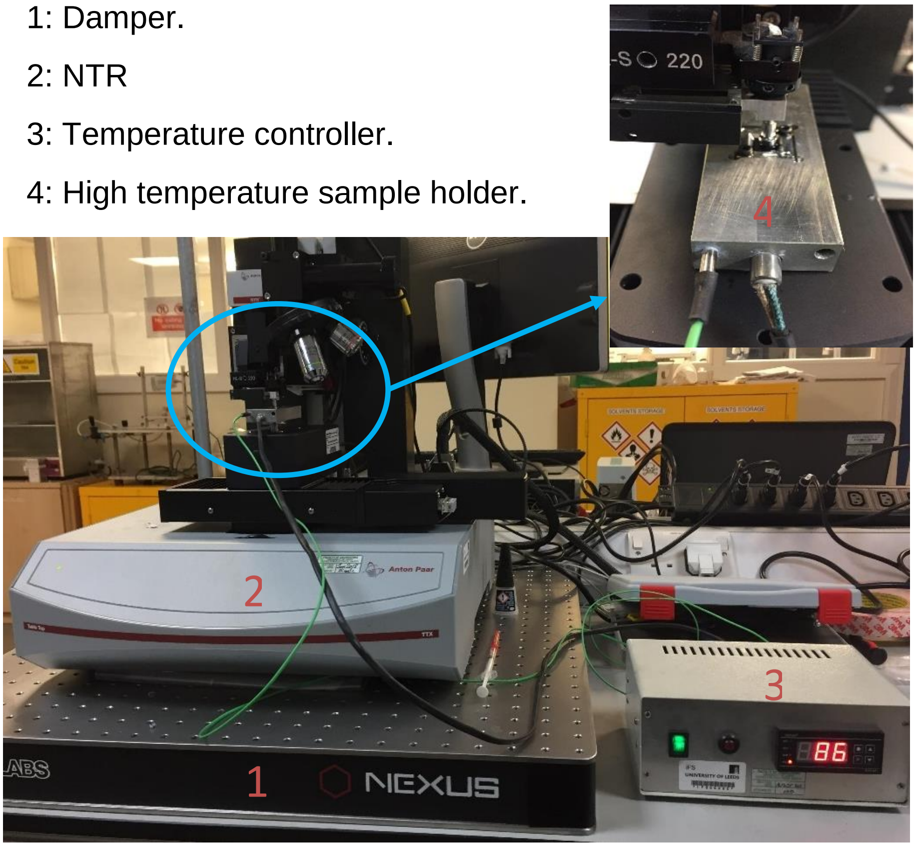

1: Damper.
2: NTR
3: Temperature controller.
4: High temperature sample holder.

Figure 3-4: High temperature experiment configuration using nano tribometer.

3.2.3 AFM

It can be defined as a blind microscopy which can scan both conductor and insulator substrates using a sharp probe. It can be considered as non-destructive [129]. AFM attracted many researchers in various subjects since it offers [130]: a very high lateral resolution (5-10 nm), it can be operated under a wide range of environment conditions, it can image any material regardless to its mechanical and electrical properties and it can be utilized to study the nanomechanical properties of surfaces such as nano-friction.

Three operation modes are available; contact, non-contact and tapping when the first mode will be used in this research. The working principle of AFM relies on the atomic force between AFM tip and the examined substrate, see Fig. 3-5 [131].

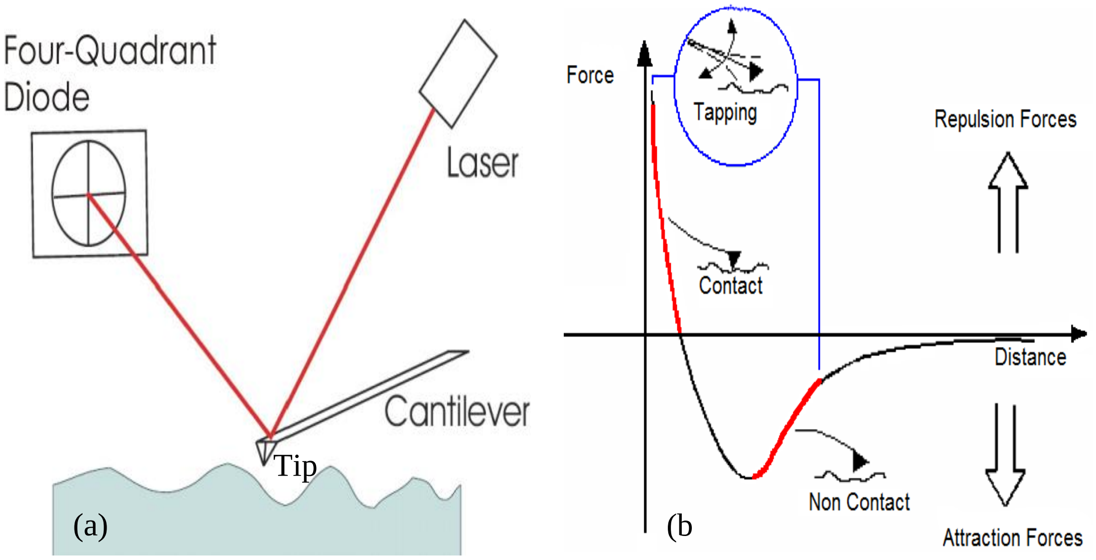

Figure 3-5: The working principle of AFM; (a) scanning process and (b) force behaviour (131).

Based on Fig. 3-5, when the two surfaces, tip and substrate, come close enough the attraction force gets start, after that, this force reaches the maximum negative value when tip just gets in contact with substrate. Then, the repulsive force takes place and the separation between tip and substrate occurs. In other word, AFM cantilever falls and raises based on the distance between tip and substrate asperities. This movement is reflected from the back of cantilever into Quadrant Photo Detector (QDP) by laser ray and then, the obtained signal is analysed [131].

There are two types of cantilevers: V-shape and rectangular cantilevers. The former one is always made of silicon nitride, coated with gold, have tip radius between 20 to 50 nm, thinner than rectangular and has smaller stiffness than rectangular. Besides, the rectangular cantilever is made of silicon, coated with aluminium and having tip radius less than 10 nm [132]. The cantilever is considered as a spring and the calibration process is basically the calculation of spring stiffness of both normal and lateral directions, see Fig. 3-6 [131].

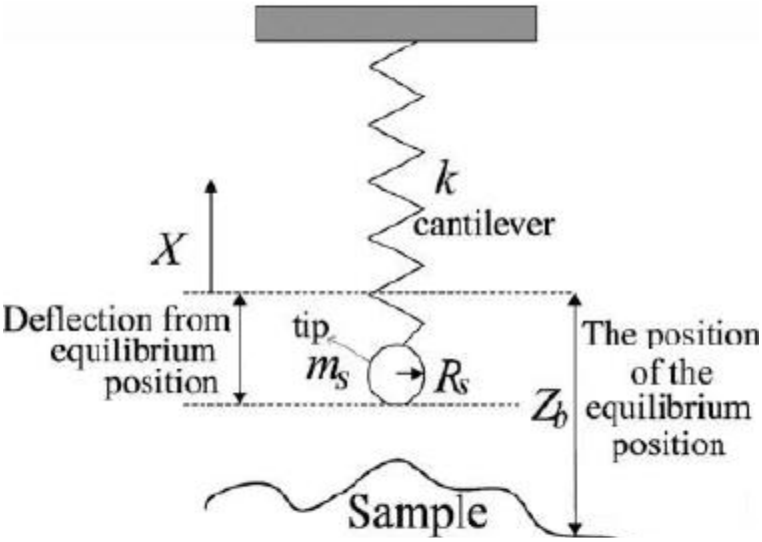

Figure 3-6: Representing of the AFM cantilever as spring (131).

Lastly, AFM has been utilized extensively to characterize surface properties when lubricating with ILs and obtain 3D images [62, 102, 133], to study the tribological behaviour of ILs in nano scale [47, 110, 111, 116, 134]. In this study, the morphologies of the ILs thermal films are characterized by AFM.

3.2.4 ATR-FTIR (Attenuated Total Reflection Fourier Transform Infrared)

In this project, PerkinElmer ATR-FTIR is utilized. This technique could be utilized to elucidate the chemical structure of both organic and inorganic compounds and in either gas, liquid or solid state. The working principle of this method relies on the interaction between the electromagnetic radiations, at infrared region, with molecules. It results a vibrational motion of molecules [135].

This motion is detected by analysing the reflected waves, thus, it will be presented as a function of either transmitted or absorbed waves, see Fig. 3-7 [136]. However, the vibration cannot be occurred unless the dipole moment is changed [137].

To understand the factors that influence on the molecules vibration, let us consider that we have a molecule consists of three atoms which are connecting with each other in different manners, as shown in Fig. 3-8.

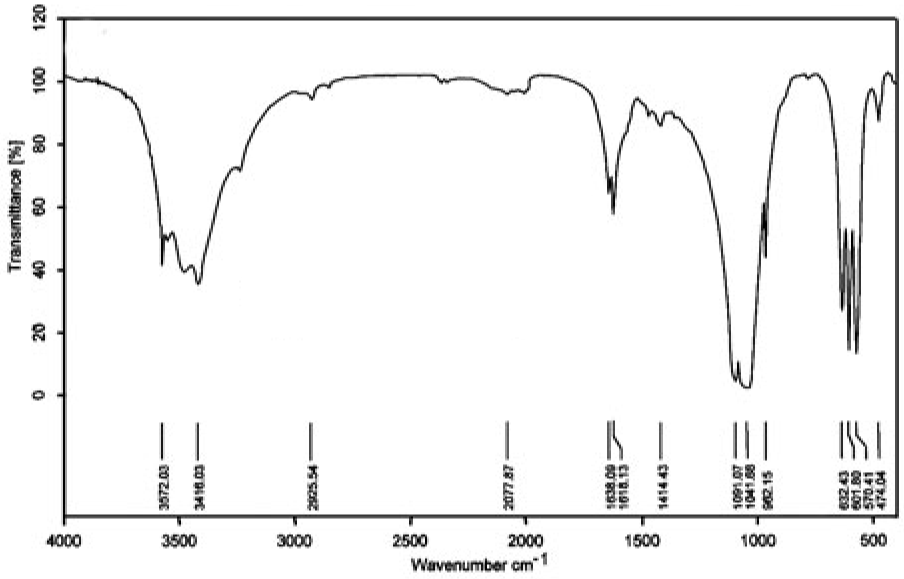

Figure 3-7: The typical FT-IR spectrum (134).

The vibration wave number is related to two factors; atoms’ mass (m) and the stiffness (k) of the connecting bonds, based on the following relation: $wave\ number = 4.12\frac{\sqrt{k}}{m}$. Therefore, the increase of bond stiffness increases vibration frequency. In other word, if the atoms are connected with double bond will be vibrated at higher frequency. In contrast, the increase of atoms’ mass decrease vibration frequency. Lastly, the vibration motion could be stretching vibration, bending, waging or twisting, see Fig. 3-8 [137].

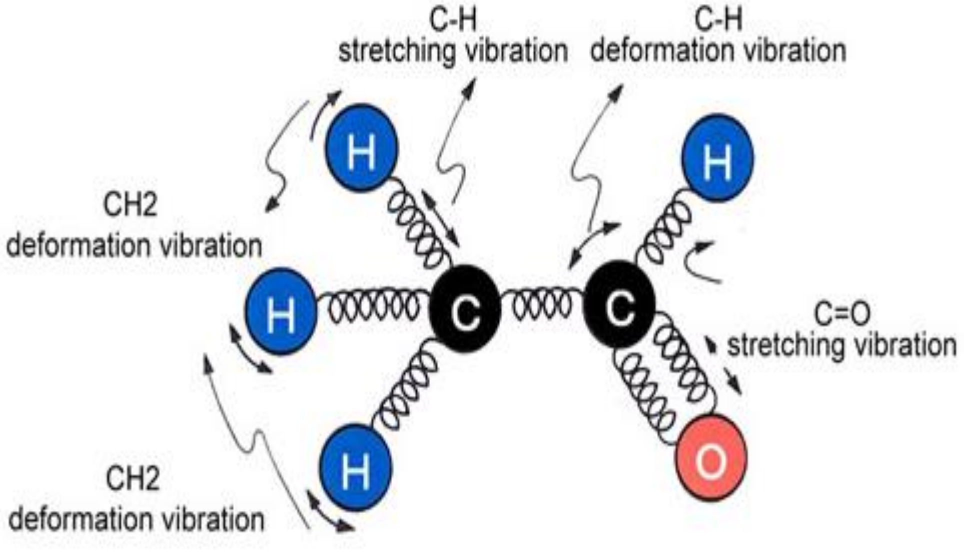

Figure 3-8: The molecules vibration types (137).

In order to analyse FTIR results, the chemical formula of the examined lubricant/additive is written and compared with the obtained data. The presence of additive/lubricant is confirmed when at least one of its related bonds is existed. In the addition, based on Beer-Lambert law, the decrease of transmissivity of FTIR peak is proportional to the increase of its concentration [138]. However, FTIR is usually employed for only qualitative analysis since a quite complex procedure is required to obtain a quantitative analysis [137].

The main limitations of ATR FTIR are the difficulty of revealing compounds with low concentration, the minimum measurable film thickness is about 0.5 µm and the dipole moment must be changed to detect the variation in frequency [135].

In this study, FTIR is used to analyse lubricants and their thermal decomposition mechanism. The chemistry of thermal film is also examined by FTIR. However, the formation of tribofilm cannot be examined by FTIR because of the small dimensions of wear track which is difficult to be oriented to the measurable area over the crystal. The following conditions were applied in this study: the signal was collected within the range of 650 to 4000 cm^{-1} and an average of 25 scans was utilized when the resolution was 2 cm^{-1}. The obtained spectra were analysed using the handbook for IR spectra for both organic and inorganic compounds [135] in addition to the available data in the literature [139-143].

3.2.5 SEM-EDS (SEM-EDS Scanning Electron Microscopy Energy Dispersive Spectroscopy)

In this study Hitachi SU8230 is utilized. It is a common technique which is mainly used to define surface morphology and find surface chemical composition. In addition, it’s a non-destructive method and the measurement can be achieved quickly. However, this method is valid just for solids and a high vacuum is required inside the test chamber. Fig. 3-9 illustrates the main components of SEM-EDS. The electron gun, usually thermionic cathode, is used to generate electrons, these electrons will be accelerated by anode. However, the generated beam in this case is very wide and it can strike both sample and sample holder. Thus, the electromagnetic lens are used to focus the electrons beam on sample.

The sample will emit secondary electrons as a result of the striking of primary ones. This means that surface morphology will be obtained from the emission of the secondary electrons. To achieve that, a secondary electrons (SE) detector is utilized, and also a positive charge could be added at the head of SE to increase the number of the absorbed electrons. Finally, the raster scan generator allows the user to move the primary electrons beam to scan the whole sample [144].

The brightness is proportional linearly with the number of electrons. It depends on the geometry; for instance, the protrusion, spherical and edges can emit a large number of electrons while holes produce lower number.

Additionally, the chemical composition could be obtained by detecting the X-ray energy that released due to the transition of electrons from higher level of electron shell to lower one. The X-ray detector reveals the type of material based on the absorbed energy since each particular material will release a particular energy. The necessity of vacuum can be summarized just in two points, which are to maintain the sample clean and to avoid any interaction between either the secondary electrons or X-ray with air [144].

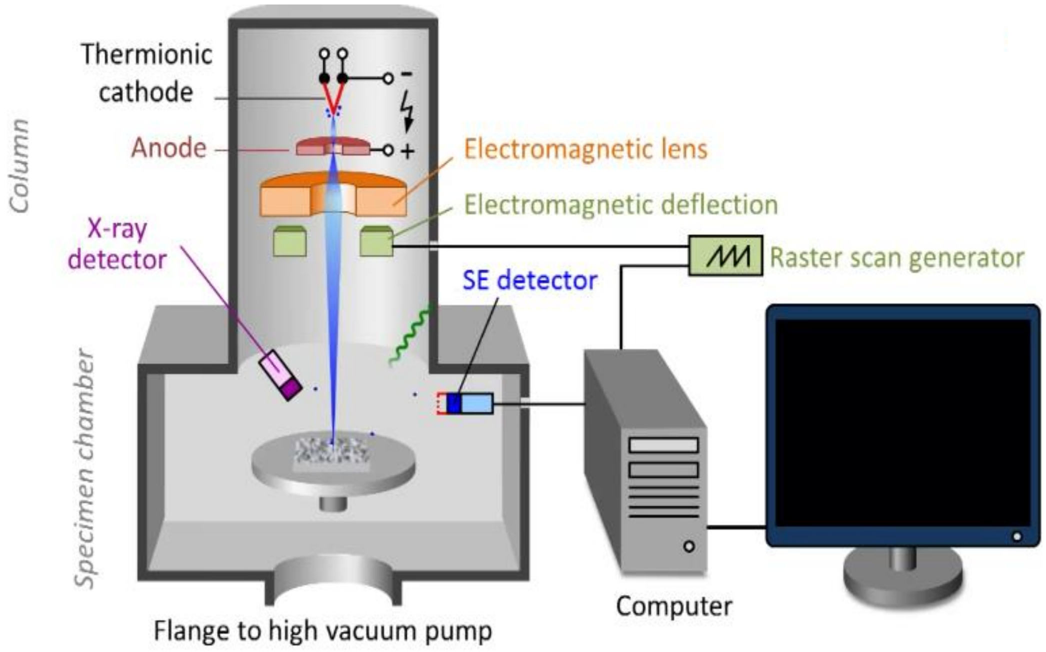

Figure 3-9: SEM-EDS main components

In this study SEM-EDS is utilized to reveal surface morphology of the thermal films and wear tracks and their chemical compositions. 2 KeV and 15 KeV are applied in order to obtain surface morphology and surface chemical composition respectively.

Carbon coating must be applied to low conductive materials to enhance their conductivity and then improve the obtained image [145]. Further, the surface chemistry of thin films could not be detected by EDS. In this study, the use of SEM-EDS is limited only in the study of IL as additive. For the study of the lubrication mechanism of neat ILs; AFM, optical microscopy and XPS are employed to investigate surface morphology of thermal film, surface morphology of wear tracks and surface chemistry respectively.

3.2.6 XPS (X-ray Photoelectron Spectroscopy)

This technique relies on the fact that the incident X-ray encourages the photoemission process, which means that an electron, or more than one, is ejected from atom after absorbing this energy, see Fig 3-10 as an illustration. This electron is analysed using electron energy analyser to obtain chemical composition, chemical formula and chemical state of the element that the electron ejected from [146].

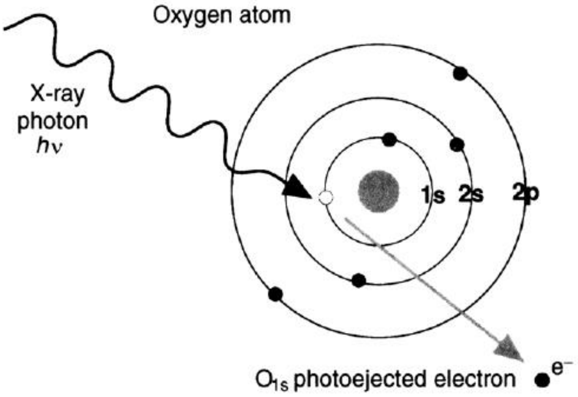

Figure 3-10: Photoemission process (146).

The ejected electron is detected based on its binding energy (B.E). It is the energy between electron and atom, since electron kinetic energy (K.E) cannot be considered because it can be varied with the change of the incident x-ray.

The binding energy is calculated from $B.E = hv - K.E - \emptyset$, when hv is the photon energy and Ø is the work function, see Fig. 3-11. The work function relates to the required energy for the ejected electron to escape from solid; transfers from fermi level to the vacuum level [147].

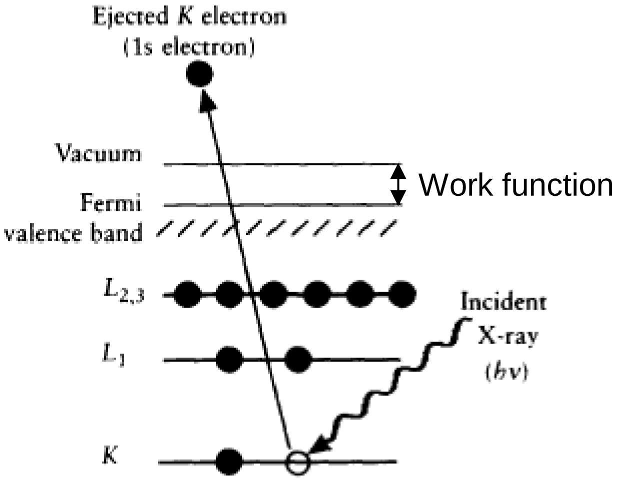

Figure 3-11: Clarify the meaning of work function (147).

As all other techniques, XPS exhibits some advantages and disadvantages. The advantages are: non-destructive, surface sensitive and it provides quantitative measurement. Besides, the disadvantages are: expensive, high vacuum is required, slow processing and helium and hydrogen elements cannot be detected. Further, the sampling depth is between 3-10 nm since electrons scatter in higher depth [146].

The interpretation of the obtained spectrums are divided into qualitative and quantitative. The former is usually conducted firstly to get an idea about the existed elements. The spectrums are quantified by calculating peak areas or measuring peaks' intensity [146].

In this study, XPS is used to characterize the surface chemistry of both thermal films and tribofilms. Two facilities are utilized. NEXUS facility at the university of Newcastle and XPS facility at the school of physics at the University of Leeds. The former facility is only used to characterize the thermal films of additives and the latter is used for the rest samples.

In NEXUS facility, a Kratos AXIS Nova XPS at the University of Newcastle, UK, is utilized. A monochromatic Al Kα (1486.6 eV) beam is utilized and the spot size was 300 µm. Three spots are scanned in each sample to investigate the homogeneity of the formed films.

This XPS system also contains an optical microscope which allows users to obtain 700 × 300 micron images and the scanned area can be specified from this image.

The second facility that is utilized in this study is Thermo Escalab 250 XPS at the University of Leeds, School of Physics and Astronomy, UK. A monochromatic Al Kα (1486.6 eV) beam is used and the spot size is 500 µm when the position of spot is specified at the centre of silicon sample using the incorporated optical microscopy.

In both facilities; three sweeps are applied to obtain the survey and ten sweeps for the high resolution regions and the pass energies are 160 eV and 20 eV for survey and high resolution regions respectively. For all samples, first of all, the survey is collected in the range of binding energy between 0 and 1200 eV and based on the obtained results the high resolution regions are specified.

However, to avoid the interference between silicon electrons, that resulted from the Plasmon effect, and both phosphorus and sulfur electrons; P2s and S2s are scanned in high resolution regions instead of P2p and S2p since the recognition with silicon electrons is easier in the former ones [115, 148].

After that, CasaXPS is used for curve fitting using Gaussian-Lorentzian method. The calibration to achieve charge correction is fulfilled based on Carbon spectrum when it is shifted to 285 eV. Appendix 1 shows the curve fitting process step by step.

On the other hand, the quantitative analysis are conducted using corrected area A_0 by dividing the obtained area by the sensitivity factor Sf. This factor can be calculated using the following equation; $Sf = \sigma. \Lambda. B. T$, when σ is photoionization cross-section and it can be obtained from [149], Λ inelastic mean free path and the calculation method is available in [150], B is the asymmetry parameter and it is obtained from [151] and lastly, T is representing analyser transmission function.

3.2.7 White Light Interferometry (NPFLEX)

The characterization of surface morphology of samples’ contain wear track is achieved by NPFLEX. In contrast to SEM, quantitative data can be obtained to quantify wear volume and the samples can be examined directly without any pre-preparation. In this study, White Light Interferometry, 3D optical microscopy, (Bruker, University of Leeds, UK) is employed.

A vertical optical scanning using 10x lens is employed to obtain a 3D map of surface topography, surface roughness and quantitate wear volume. Further, in order to quantify wear volume, a stitching scan is applied to cover 3 × 0.82 mm^2 scanning area, with spatial resolution 100 µm. After that, the software Vision64 is utilized to present and analyze data when the wear volume is calculated by applying a special filter, mask filter, to subtract wear track from the rest area in the surface and then quantify wear track width, length, depth and lastly wear volume.

3.2.8 TGA (ThermoGravimetric Analysis)

It is defined as a common technique that is used to measure the effect of temperature on mass; it measures the reduction of mass as a function of temperature change. In addition, the influence of pressure on mass change can also be involved, in this situation the technique is called pressurized TGA (PTGA). TGA reveals the variation of composition and thermal stability of the measured sample from weight loss curve. The reduction of weight might be resulted from either chemical reaction, physical transitions or both together. Chemical reaction represents by the loss of water, decomposition and the reduction of metal oxide due to combustion, while physical transitions represents by evaporation or absorption [152].

In this study, the TGA at the University of Leeds, school of chemical and process is used. The obtained curves are exported to Origin pro and the first derivative is evaluated to find the onset temperature. The dynamic thermal decomposition of neat ILs are examined by TGA.

3.2.9 Rheometer

The dynamic viscosity of the selected ILs are measured at various temperatures using Kinexus rheometer, University of Leeds, UK. Basically, the dynamic viscosity is varied as a function of shear rate, pressure, temperature and time. However, just viscosity of non-Newtonian fluids are changed with shear rate while ILs behave as Newtonian fluids [153, 154].

3.3 Materials

3.3.1 Lubricants

In this study, ILs are used as either additive or neat lubricants. A soluble IL; phosphonium phosphate is used as additive in PAO6 and compared with the common anti wear additive ZDDP when also added to PAO6. For the second part, using ILs as neat lubricants; five ILs are used. Table 3-1 depicts the utilized lubricants and additives in this study.

The selection of neat ILs is aimed to cover the effect of cation chain length, anion chain length, anion type and cation type in order to obtain the relation between IL chemistry and its lubrication mechanism. The effect of anion chain length is studied by comparing between EMIM ESU and EMIM OSU. The effect of cation chain length is studied by comparing between BMIM OSU and EMIM OSU. The effect of anion type is studied by comparing between EMIM ESU and EMIM EP. Lastly, the effect of anion type is studied by comparing between PSU and EMIM ESU.

In addition, halogenic ILs are avoided since a large number of previous studies considered them [3-6]. The selection also aims to investigate the effect of the presence of phosphorus atom in either phosphonium cation or phosphate anion. All ILs are utilized in as-received condition without any extra treatment.

Table 3-1: The utilized lubricants in this study.

Lubricant/additive	Vendor	Structure
Poly Alpha Olefin 6 (PAO6)	Ineos Oligomers	
Zinc Dialkyl Dithio Phosphate (ZDDP)	Afton chemicals	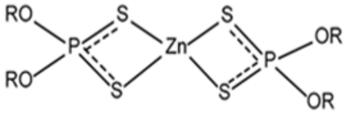
Phosphonium Phosphate (PP)	Sigma-Aldrich	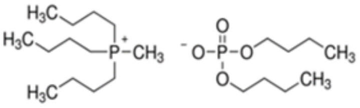
Ethyl Methyl Imidazolium Ethyl Sulfate (EMIM ESU)	Merck	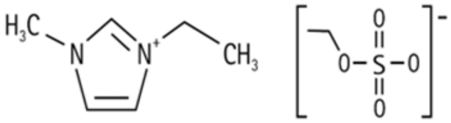
Ethyl Methyl Imidazolium Octyl Sulfate (EMIM OSU)	Merck	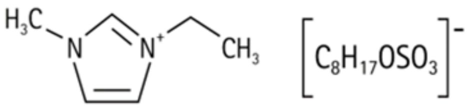
Butyl Methyl Imidazolium Octyl Sulfate (BMIM OSU)	Merck	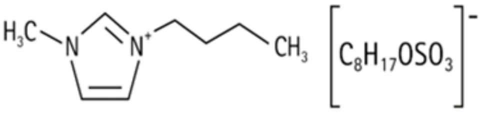
Ethyl Methyl Imidazolium Diethyl Phosphate (EMIM EP)	Sigma Aldrich	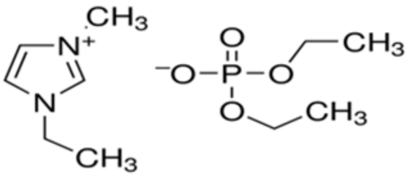
Butyl Methyl Phosphonium Methyl Sulfate (PSU)	Santa Cruz	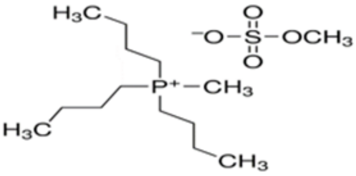

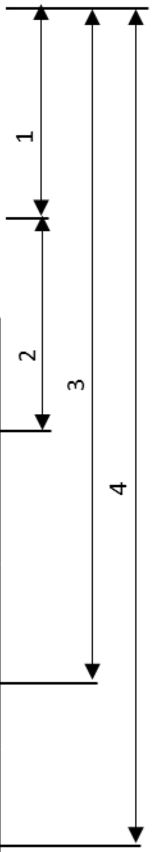

1: Anion chain length is increased, 2: cation chain length is increased, 3: Anion type is changed and 4: cation type is changed.

3.3.2 Materials

Two tribopairs are utilized in the current study in order to simulate two various applications. The use of ILs as anti-wear additive is aimed to be used in engines. Thus, the first tribopair is silicon substrate against steel ball. Silicon showed a very comparable tribological behaviour to Aluminium-Silicon alloy (the dominant material in the manufacturing of cylinders) [155]. The mechanical properties and surface roughness of both silicon and steel ball are illustrated in table 3-2.

Aforementioned, neat ILs can be used as potential lubricants in two applications; in aerospace and to lubricate MEMS since the cost can be tolerated in the first application and only few amount is required in the latter one [3-6]. Therefore, the second application is simulated in this study. Silicon based materials must be used in order to simulate the lubrication of MEMS [24]. Silicon substrate against borosilicate ball is utilized in this study.

Silicon wafers are cut into small square samples; 7.5 mm × 7.5 mm, and then placed in the sample holder, see section 3.2.2. The diameter of both steel and borosilicate balls is 2 mm.

All samples have been sonicated for 2 minutes in acetone solvent and dried by nitrogen gas flow before the experiment. After each experiment, the samples have been sonicated for 30 second and dried by nitrogen gas flow. Then, all samples have been stored at vacuum in order to avoid contaminations.

Table 3-2: Properties of solid materials.

AISI 5200 Chromes Steel balls	Silicon substrate	Borosilicate ball
Mechanical properties		
Elastic modulus 211 GPa	Elastic modulus 129.5 GPa	Elastic modulus 64 GPa
Poisson’s ratio 0.3	Poisson’s ratio 0.25	Poisson’s ratio 0.2
Average roughness		
125 nm	0.25 nm	45 nm
Hardness (HRC)		
60	65	64

3.4 Experiments Procedures

This section will present the methodology of each phase of experiments and their related calculations. The conditions of each phase of experiments will be presented in the related results’ chapter.

3.4.1 Blending Lubricants

The first step is to blend the anti-wear additives (PP and ZDDP) with the base lubricant PAO6. Both PP and ZDDP are added into PAO6 with 1.08 wt% and 0.74 wt% respectively. These percentages are selected to keep the phosphorus content same in both mixtures. It is 800 PPM which is the maximum permitted percentage [98]. The procedure starts with the weighting of PAO6 to obtain its mass and the following equation is used to find additives masses:

$$required\ percentage = \frac{(additive\ mass)}{(base\ lubricant\ mass + additive\ mass)}$$

The required mass to achieve the aimed percentages of both additives are defined. Each mixture is heated to 60 ^oC and stirred at 200 RPM for 2 hours.

3.4.2 Thermal Film Experiments

These experiments have been conducted using the hot plate presented in section 3.2.1. All beakers are cleaned by soap firstly and then rinsed by methanol and lastly dried in a hot zone (40 ^oC). They kept there until starting the experiment. The silicon substrates were sonicated for 10 minutes before each test and then inserted in the previously cleaned beakers. After that, the beakers (with silicon wafers inside them) are filled with about 1 ml of lubricant and then all beakers are seated over the hot plate surface. All together are placed in a well ventilated area to ensure that the produced fumes are directly exhausted.

3.4.3 Thermal Decomposition Experiments

Two types of thermal decomposition experiments are conducted in this study; dynamic thermal decomposition and static thermal decomposition. TGA is used for dynamic thermal decomposition. A 70 µl alumina oxide crucibles from Mettler-Toledo are utilized. The crucibles are weighted before and after filling them with lubricant. To obtain a precise measurement; a comparable amounts of lubricant is utilized in all experiments. Then all crucibles are placed inside TGA.

For static thermal decomposition experiments (temperature is kept constant and the time is varied), the same procedure that is followed for thermal film formation is conducted. However, all beakers are filled with lubricant only, no silicon wafers in these experiments are needed.

3.4.4 Micro Scale Experiments

Aforementioned, nano tribometer is utilized in micro scale study and it has been described in details in section 3.2.2. A few calculations must be conducted to evaluate the contact radius, contact pressure and check whether the lubrication regime is boundary one or not.

In this study, the boundary lubrication regime will be used in all experiments, since the sever condition encourages the formation of tribofilm.

Based on Stribeck diagram that is presented in Fig. 1-3, the lubrication regime is considered boundary when the specific film thickness (λ) is less than 1. λ is calculated using the following equation [32]:

$$\lambda = \frac{h_{min}}{\sum R_a} = \frac{h_{min}}{\sqrt{R_{q_1}^2 + R_{q_2}^2}}$$

Ra and Rq refer to the centre line average roughness and root mean square roughness respectively. They can be measured experimentally using either AFM or NPFLEX [156].

Besides, hmin is the minimum film thickness and it is calculated utilizing the following equation [156]:

$$\frac{h_{min}}{R} = 3.63 \left(\frac{U\eta_0}{E^{\prime}R}\right)^{0.68} \left(\alpha E^{\prime}\right)^{0.49} \left(\frac{W}{E^{\prime}R^2}\right)^{-0.073} \left(1 - e^{-0.68k}\right)$$

When U is the entraining surface velocity, η_0 is the dynamic viscosity, $E^{\prime}$ is the reduced Young's modulus, W is the contact load, α is the pressure-viscosity coefficient, R is the reduced radius of curvature and k is the ellipticity parameter. It is clear that some parameters are varied based on the contact geometry, in this particular study, a ball on plate configuration is used as shown in Fig. 3-12 [156].

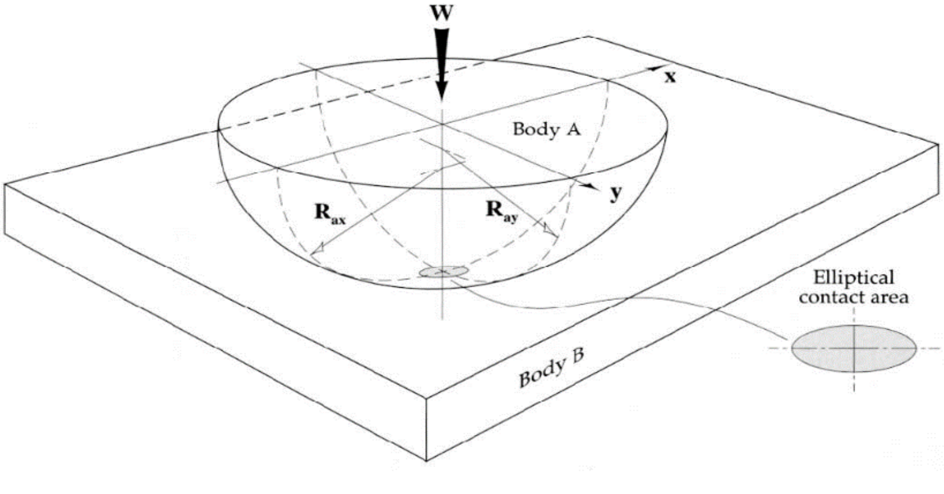

Figure 3-12: Ball on plate contact.

In this case, the body B, silicon wafer, is considered that has infinity radiuses in both directions x and y. Therefore, just the radiuses of body A will be considered in the determination of reduced radius of curvature, as demonstrated in the following equation [156]:

$$\frac{1}{R} = \frac{1}{R_{ax}} + \frac{1}{R_{ay}}$$

Since the body A is a ball, thus, both radiuses have the same value which is 1 mm, hence, R = 0.0005 mm. The reduced Young's modulus is calculated utilizing the following equation [156]:

$$E^{'} = \frac{2E_a E_b}{(1 - v_a^2)E_b + (1 - v_b^2)E_a}$$

Ʊ represents the Poisson's ratio.

The pressure viscosity coefficient cannot be measured unless using viscometer contains a pressure cell to measure the variation of viscosity with pressure.

However, this value has a slight influence on the calculation of minimum film thickness. It can be estimated based on the available data in the literature [157]. Due to the high dependency of viscosity on cation type, rather than anion type, as reported before by Saurin [72] and also confirmed in this research. Therefore, the values of pressure viscosity coefficient of ILs having same cations, that are reported in the literature [9, 158, 159] will be used here. For BMIM is 10 GPA and for EMIM and Phosphonium based IL is 8.5 GPA.

The last parameter that must be determined to find the hmin is the ellipticity parameter (k) which is determined from the following equation [156]:

$$k = 1.0339 \left(\frac{R_y}{R_x}\right)^{0.636}$$

After calculating hmin and measuring Ra, the calculation of λ becomes straight forward. Lastly, the calculations of contact pressure and the contact radius (r) are achieved using the following equations respectively [156]:

$$P_{mean} = \left(\frac{3 \times W \times R}{E'}\right)^{0.333}$$

$$r = \left(0.10616 \times 3 \times W \times E'^2 \times \left(\frac{1}{\mathrm{R}^2}\right)\right)^{0.333}$$

3.5 Summary

This chapter has presented the methodology of the current study in details. The schematic diagram below (see Fig. 3-13) summarizes the utilized equipments to conduct experiments and the utilized techniques for post experiments analysis.

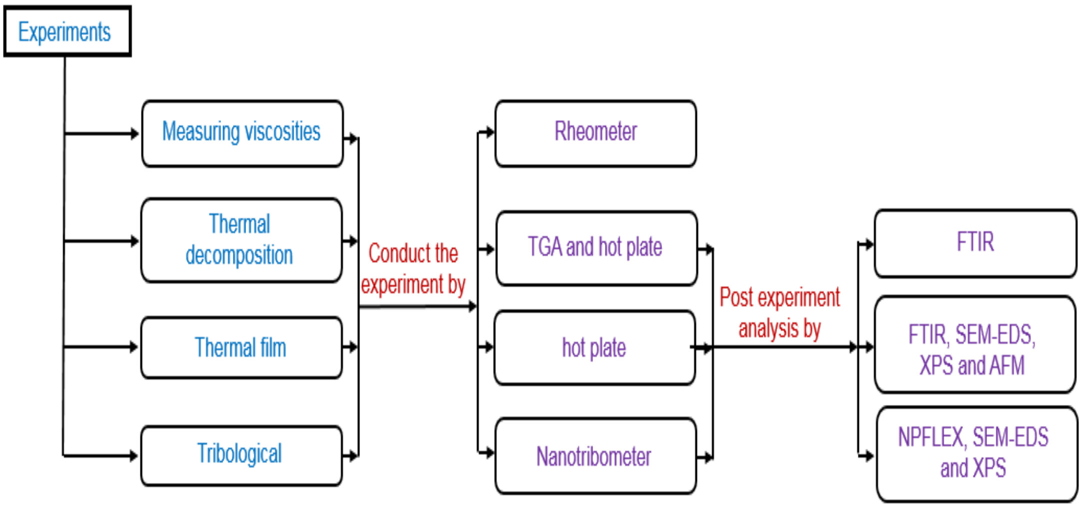

Figure 3-13: The summery for the utilized methodology.

Further, the working principle and the utilized procedure of each equipment have been illustrated in details. Lastly, the materials and the related calculations for tribological experiments have been also demonstrated.

4. Chapter 4: Reactivity of oil-soluble IL with the silicon surfaces at elevated temperature

4.1 Introduction

Oil-soluble IL, phosphonium phosphate (PP), has been proposed as an effective anti-wear additive. It is also proposed to be used as an alternative to ZDDP. The latter additive can provide a good protection against wear and it is one of the most common anti-wear additives. However, the production of ash as a result of ZDDP decomposition pushes the researchers to find an effective alternative [160, 161].

The previous studies as presented in the literature showed that both additives (PP and ZDDP) can provide a comparable anti-wear performance at room temperature. The increase of temperature showed that PP can provide superior anti-wear performance to ZDDP [23, 28, 29, 162]. However, the reason behind this finding was suggested to be due to the effect of viscosity. The increase of temperature decreases lubricants' viscosity which leads to a decrease in its load-carrying capacity. Nevertheless, both mixtures, PAO+ZDDP and PAO+PP, exhibit same viscosity as pointed out in the [23, 28, 29, 162].

To investigate the reason behind the superior performance of PP at elevated temperature; this study is conducted to compare the reactivity of PP and ZDDP with the silicon surfaces at elevated temperature. In addition, the durability of both thermal films (ZDDP and PP) is examined by applying a reciprocating tribological motion using steel against silicon to simulate the working of a cylinder bore/piston ring interface in engine [155]. The AL-Si lines is used and the steel piston ring will be running on the large Si grains.

The chapter is divided into six sections as follows: overview, introduction, experimental conditions, results, discussion and conclusions.

4.2 Experimental Conditions

The reactivity of both additives is investigated at various temperatures and after various periods. Table 4-1 depicts the applied conditions. The selection of high temperature is to simulate the working temperature in engines.

Table 4-1: The applied conditions to generate the thermal films of the anti-wear additives.

Time (hours)	Temperature (°C)
2	150 and 175
6	150 and 175
24	150

The durability of the generated thermal films is examined by comparing their tribological properties (wear and friction) with the silicon surface before the formation of the thermal films. The tribological properties of the thermal films that are created by after 2 hours and at 150 °C are examined. A neat PAO is utilized as a lubricant and the experimental conditions are: 14.4 m sliding distance, average contact pressure 600 MPa and lambda ratio 0.004 which means it is at the boundary lubrication regime.

4.3 Results

4.3.1 Thermal Decomposition of Lubricants

Fig. 4-1 presents the FTIR peaks for PAO, PAO+ZDDP and PAO+PP at room temperature. Firstly, as expected, all lubricants have the same peaks with the same intensities. The differences between the oils cannot be discerned due to their low concentrations [163]. Therefore, the obtained peaks are assigned to hydrocarbon bonds which might result from either PAO, additives or both together. The lowest frequency peak at 721 cm^{-1} is assigned to the rocking vibration of CH_2. The second peak at 1378 cm^{-1} is assigned to the deformation vibration of CH_3 while the peak exhibits wave number 1465 cm^{-1} can be related to either asymmetric deformation of CH_3 or deformation of CH_2. The last two peaks at 2853 cm^{-1} and 2921 cm^{-1} are assigned to the symmetric stretching of CH_2 and asymmetric stretching of CH_2 respectively.

These assignments are in agreement with the previous work conducted by Mangolini *et al* [164].

When the temperature is increased to 150 °C for two hours, the decomposition is initiated and a new peak appears at 1720 cm^{-1} which is assigned to the symmetric stretching of C=O. Further increase in temperature by 25 °C, for the same period, does not show any changes in the obtained peaks.

To examine the effect of time on the decomposition process, the time is increased from 2 to 6 hours at two different temperatures; 150 °C and 175 °C. The results reveal that no new peaks are initiated. However, a slight change occurs in the region between 850 and 1350 cm^{-1}. This change could be assigned to C-O stretching as mentioned before by Mangolini *et al* [164]. Time was increased to 24 h for only one temperature; 150 °C. As expected, this increase creates new peaks related to the oxidation process. From the FTIR results in Fig. 4-1b, it is clear that the formation of a new peak at wave number 1170 cm^{-1} is related to the stretching vibration of C-O. Also, a very clear wide peak extends from 850 to 1300 cm^{-1} due to the stretching vibration of C-O.

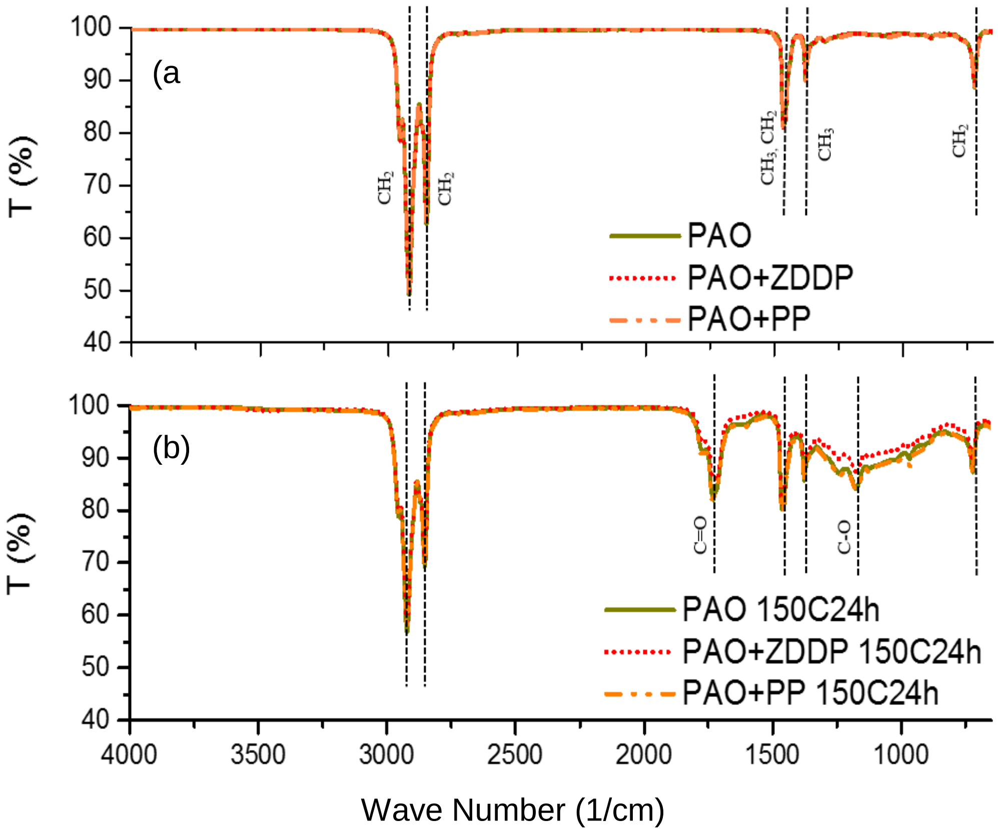

Figure 4-1: FTIR results for all lubricants at; (a) Room temperature and (b) 150 °C for 24 h.

4.3.2 ZDDP Thermal Film Results

Fig. 4-2 depicts the FTIR results for the silicon surfaces before the generation of the ZDDP thermal film. It is clear that silicon surface is clear of any compounds that can be detected by FTIR. Fig. 4-3 demonstrates the FTIR results of silicon samples after the generation of ZDDP thermal films. The results show that among the five conditions only for 2h 175 ^oC, 6h 175 ^oC and 24h 150 ^oC, were peaks detected and that showed the presence of a thermal film. The peak at 926 cm^{-1} can be assigned to either stretching vibration of P=O [163] or the asymmetric vibration of P-O-P [165]. A peak at 1087 cm^{-1} is detected and it can be assigned to the asymmetric vibration of either PO_3 or SO_4 [165, 166]. The peak at 1125 cm^{-1} can be assigned to either the stretching vibration of P-O-Si [163], asymmetric vibration of PO_3^{-2} [165, 166] or an overlap of both peaks. For the longest period, 24 h, a new weak peak is obtained at 750 cm^{-1} which can be assigned to the symmetric vibration of P-O-P [163]. Also, a peak at 1640 cm^{-1} can be assigned to C=C [163].

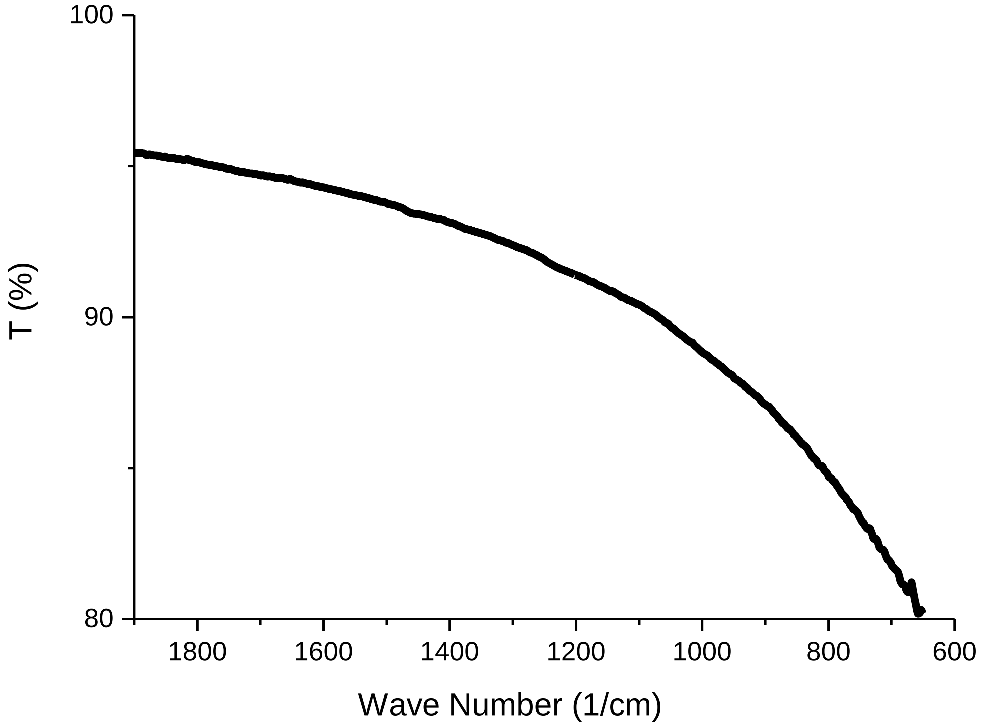

Figure 4-2: FTIR results for silicon substrate before the generation of thermal film and after the formation of PP thermal film.

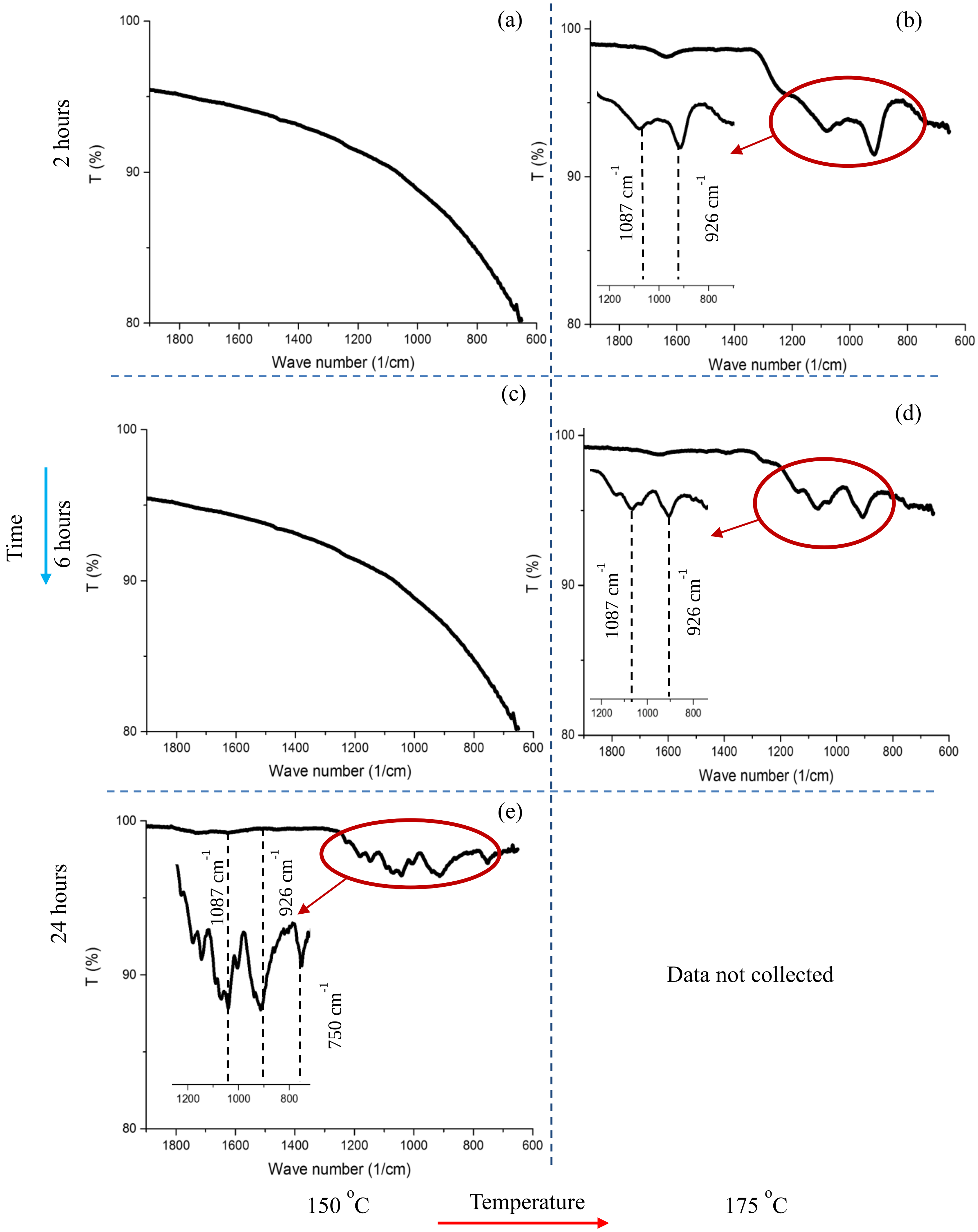

Figure 4-3: FTIR results for ZDDP thermal film at the following conditions: (a) 150 °C and 2 hours, (b) 175 °C and 2 hours, (c) 150 °C and 6 hours, (d) 175 °C and 6 hours and (e) 150 °C and 24 hours.

SEM enables the physical nature of surface to be examined. The surface morphologies of Si before and after the formation of ZDDP thermal film under all applied conditions are demonstrated in the SEM images in Fig. 4-4. It can be seen clearly that both film thickness and film consistency are increased with the increase of either temperature or time. In addition, the elemental mapping of the created films from EDS analysis showed that all surfaces have the same elements; phosphorus, zinc, carbon, silicon and oxygen. Fig. 4-5 depicts EDS results of ZDDP thermal film after the longest period at 24h. It can be seen that the presence of silicon significantly decreased when the thermal film is formed. The presence of oxygen, zinc and phosphorus is increased with the formation of thermal film. The presence of carbon is comparable before and after the formation of thermal film.

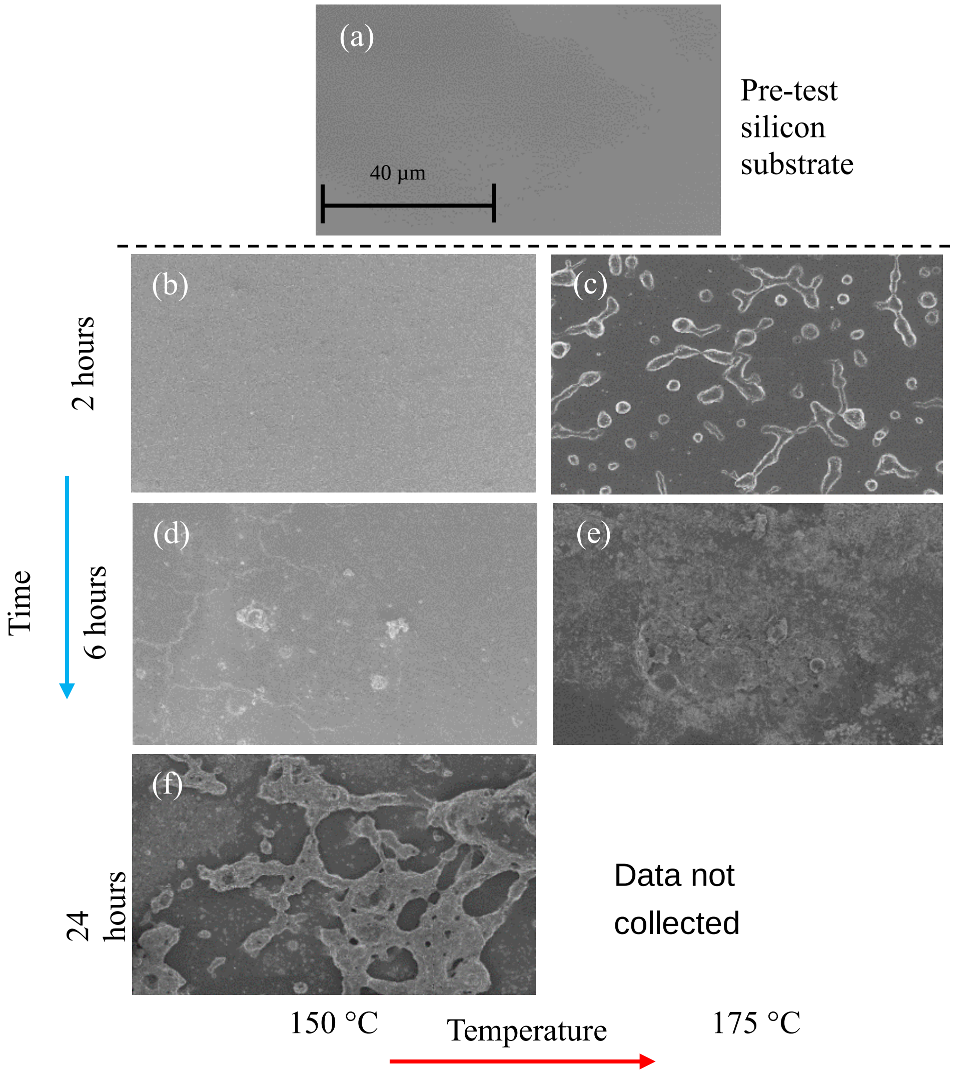

Figure 4-4: Surface morphology of (a) Si substrate before test; (b) Si in ZDDP 150 ^{o}C 2h; (c) Si in ZDDP 175 ^{o}C 2h; (d) Si in ZDDP 150 ^{o}C 6h (e) Si in ZDDP 175 ^{o}C 6h and (f) Si in ZDDP 150 ^{o}C 24h.

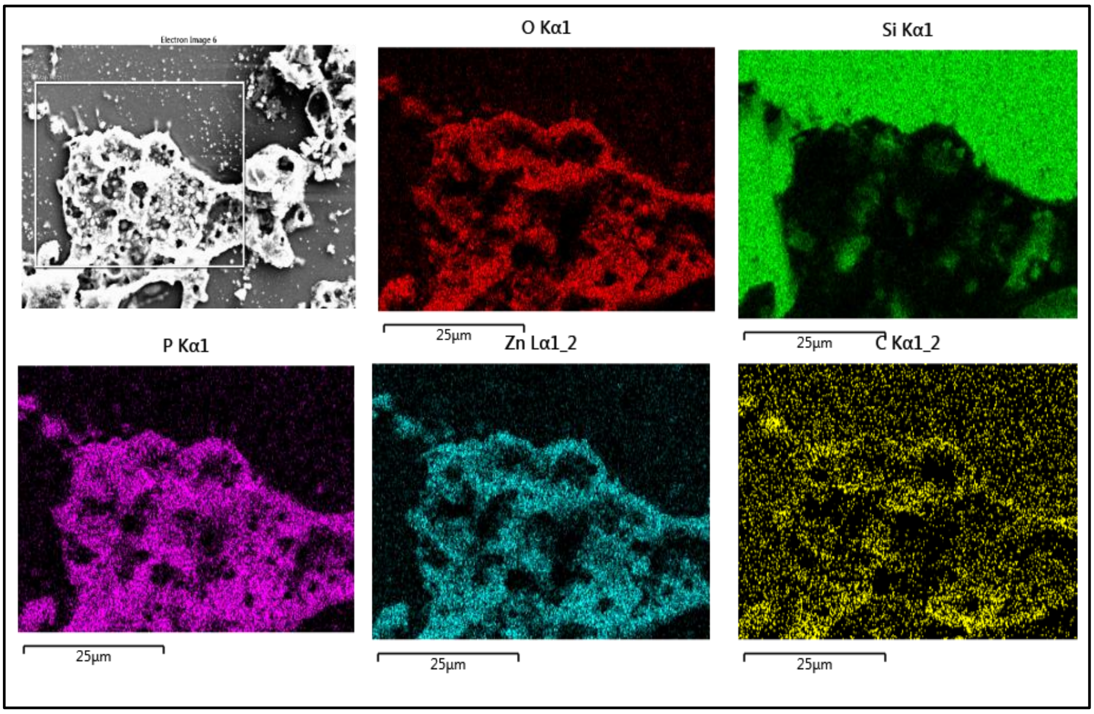

Figure 4-5: The EDS result of ZDDP thermal film at 150 °C and for 24 h.

The results of XPS again confirm the formation of the thermal film when zinc, phosphorus and sulfur are detected. Three spectra are collected; P2s, S2s, Zn2p which are the elements that resulted from the chemical reaction between ZDDP and silicon surface.

Sulfur is detected only at 2h and 150 °C, see Fig. 4-6. S2s at 226.6 eV is fitted with one peak and assigned to ZnS [167], which is also confirmed by the Zn2p peak. The S2s peak is diminished with the increase of time and temperature which means that sulfur in ZnS is dissociated.

Zinc is detected at both conditions; 150 °C (2 hours) and 175 °C (6 hours), and Zn2p is scanned at the high resolution region. Fig. 4-7 presents the Zn2p peaks, fitted into two peaks (Zn2p 3/2 and Zn2p 1/2). At lower temperature the Zn2 p3/2 at 1022 ev is assigned to ZnS [168] which is in agreement with the sulfur assignment. The increase of both time and temperature lead to a shift the peak by 0.6 eV which means that the chemical state has been changed.

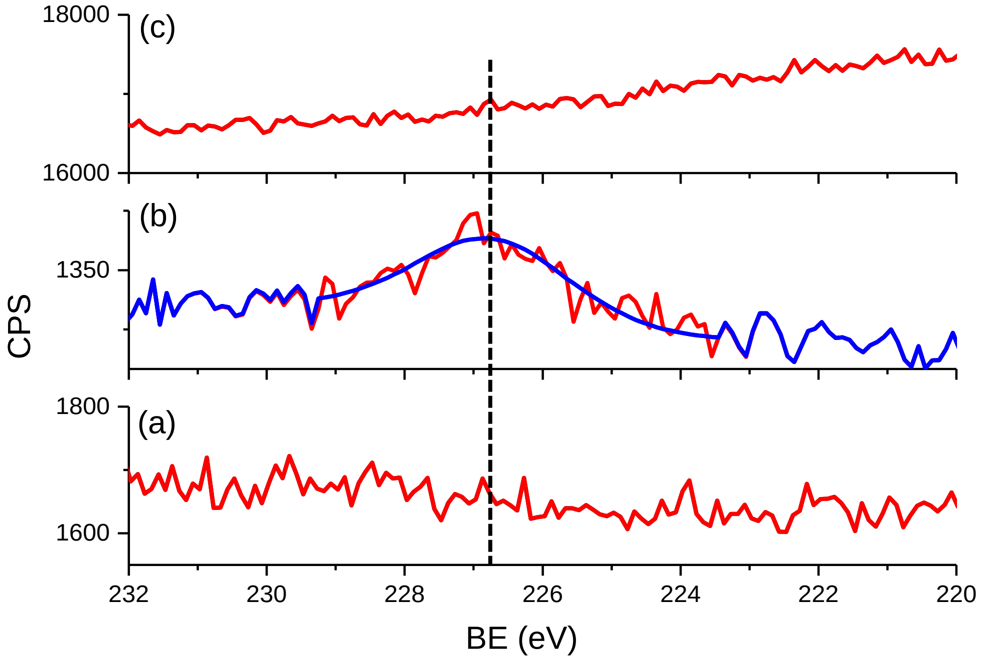

Figure 4-6: S2s peak for (a) silicon before experiment, (b) ZDDP thermal film formed at 2h and 150 ^{o}C and (c) ZDDP thermal film formed at 6h and 175 ^{o}C.

This shifting is as a result of the oxidation of Zn and the new peak is assigned to ZnO [168]. The Zn2p of ZnO and ZnS are close to each other (1022 eV and 1022.6 eV) respectively; in this chapter the XPS results of Zn and S have been used to suggest that there is a change from ZnS to ZnO.

P2s is also detected at both conditions as shown in Fig. 4-8. However, phosphorus already exists in the n-type silicon. In order to distinguish between phosphorus created by the thermal film and phosphorus element that exists in the substrate; both the intensity ratio of P2s to Si2s and the binding energy are utilized. The intensity ratio of P2s to Si2s, that existed due to plasmon effect, is 0.5 and the binding energy of P2s is 187.7 eV which is in agreement with [148].

After the formation of the thermal film; both the silicon plasmon peak and the phosphorus peak are diminished. Two new peaks are obtained at 188.6 eV and at 191.5 eV. The interpretation of these two peaks is done using information from FTIR results and the available data in [148]. The first peak at 188.6 eV can be assigned to phosphate as shown in FTIR results. The second peak at 191.5 eV can be assigned to P-O-Si which is in agreement with [148], FTIR results in the current study and FTIR results in [163].

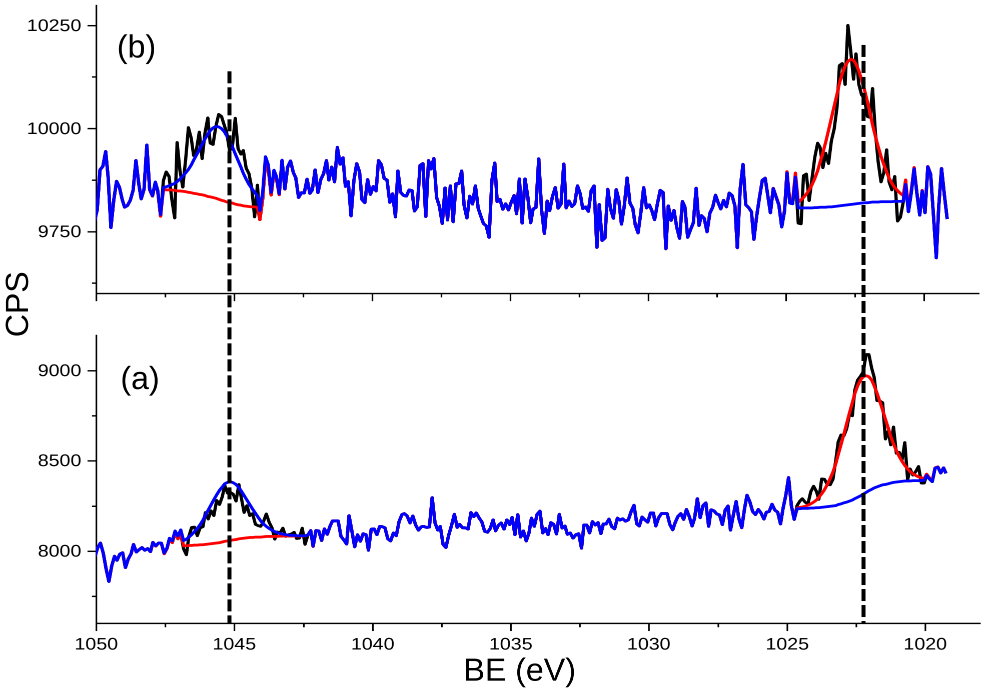

Figure 4-7: Zn2p peak for (a) ZDDP thermal film formed at 2h and 150 °C and (b) ZDDP thermal film formed at 6h and 175 °C.

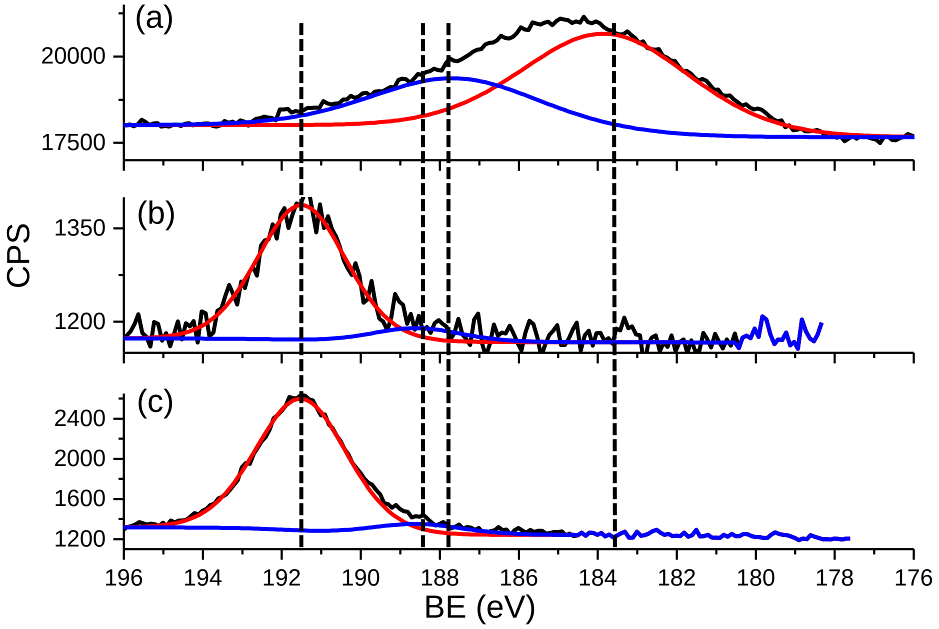

Figure 4-8: P2s peak for (a) silicon before experiment, (b) ZDDP thermal film formed at 2h and 150 °C and (c) ZDDP thermal film formed at 6h and 175 °C.

4.3.3 PP Thermal Film

Using ATR-FTIR, the thermal film of PP could not be detected under any of the applied conditions (as shown in Fig.4-2). This means that the created film is not thick enough to be detected by FTIR. The sampling depth of the ZnSe crystal is about 1.66 µm [169].

SEM-EDS is used in order to characterize the topography of the silicon surface before test and after the formation of PP thermal films under various circumstances as shown in Figs. 4-9. and 4-10. It is clear that PP creates a thermal film. The SEM results confirm that a few changes occur in the surface morphology, especially, when the temperature is increased to 175 °C.

EDS results in Fig. 4-10 shows that the presence of oxygen and carbon is significantly increased in the silicon surface after the generation of PP thermal film. However, phosphorus still could not be detected and a more surface sensitive technique was employed to confirm the formation of PP thermal film.

XPS results confirm that there is a thermal film present at the lowest applied temperature with the lowest period; 150 °C and 2h. The film is detected by comparing P2s peak (Figure 11) with silicon substrate before the formation of thermal film. Again, as observed in the ZDDP thermal film, phosphorus element and Si2s related peaks are diminished compared with the P2s peak for silicon before the formation of thermal film.

Two peaks are obtained at 150 °C, 2h with their binding energies are 188.6 eV and 191.5 eV respectively. The former can be assigned to phosphate comparable to a ZDDP thermal film. The second peak at 191.5 eV is assigned to P-O-Si [148]. Only one peak at 191.5 eV is obtained in the second examined condition, 175 °C and 6h which means that P-O-Si solely exists at this condition.

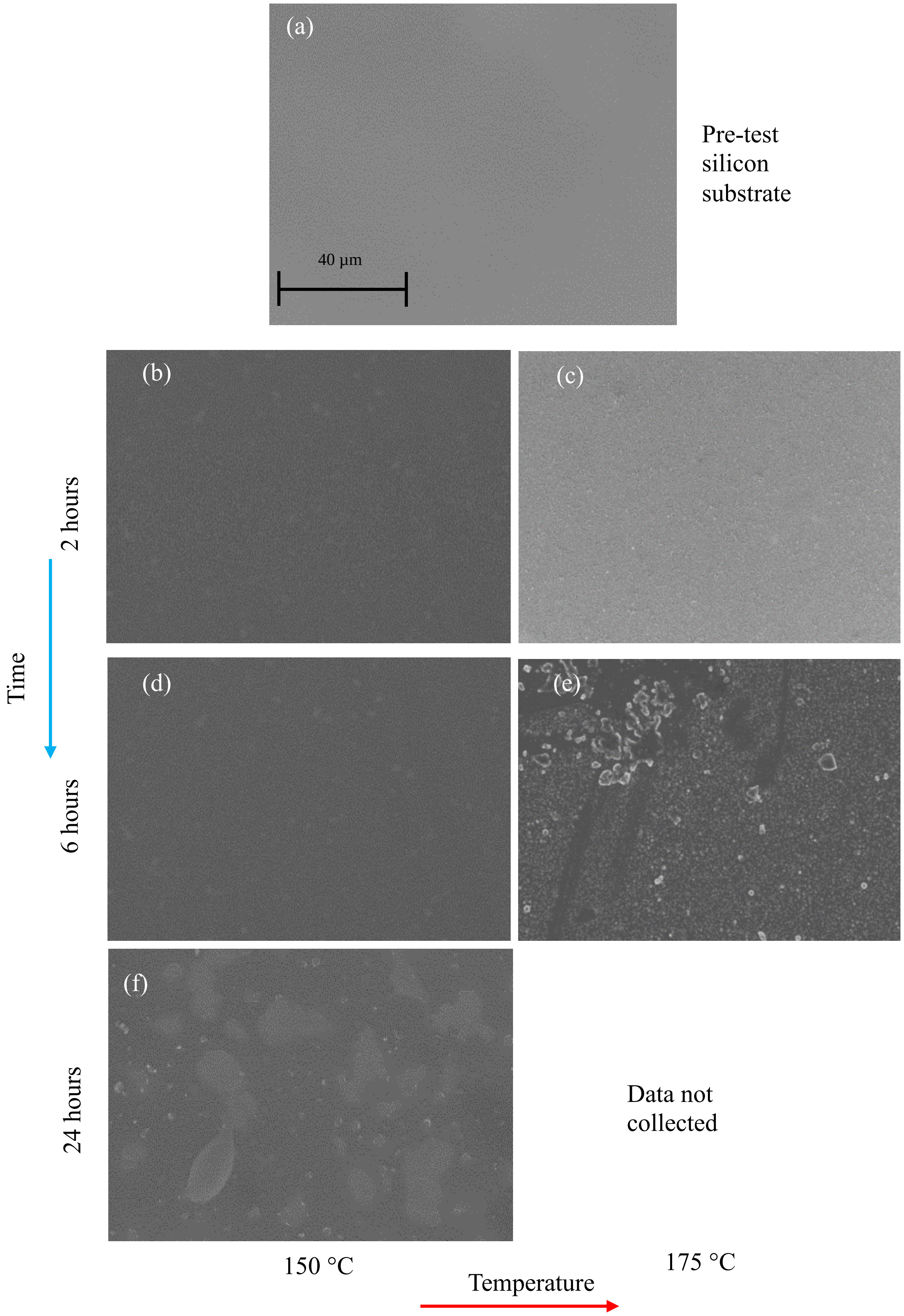

Figure 4-9: Surface morphology of (a) Si substrate before test; (b) Si in PP 150 ^{o}C 2h; (c) Si in PP 175 ^{o}C 2h; (d) Si in PP 150 ^{o}C 6h (e) Si in PPIL 175 ^{o}C 6h and (f) Si in PPIL 150 ^{o}C 24h.

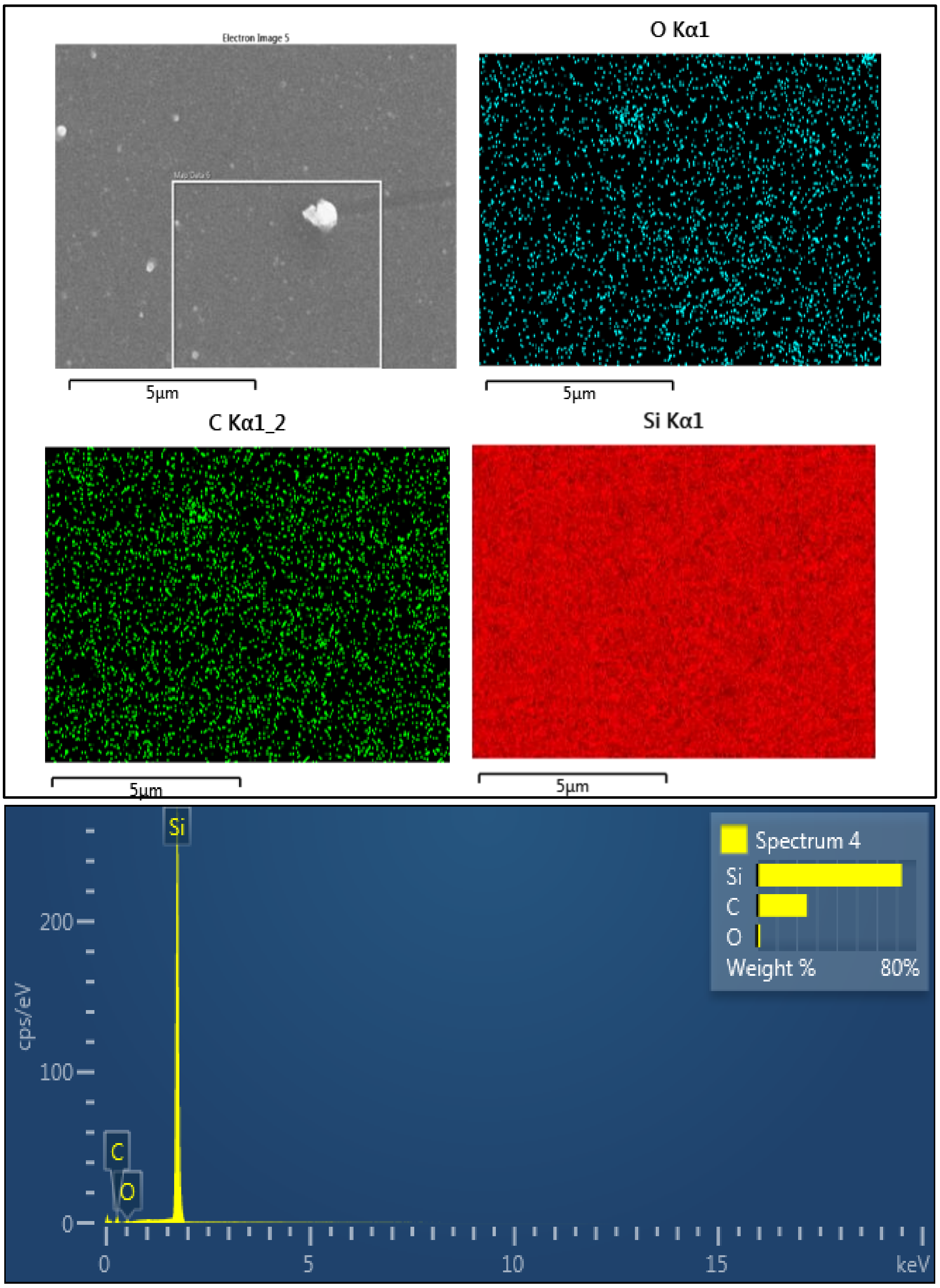

Figure 4-10: The EDS results of PP thermal film at 150 ºC and for 24 h.

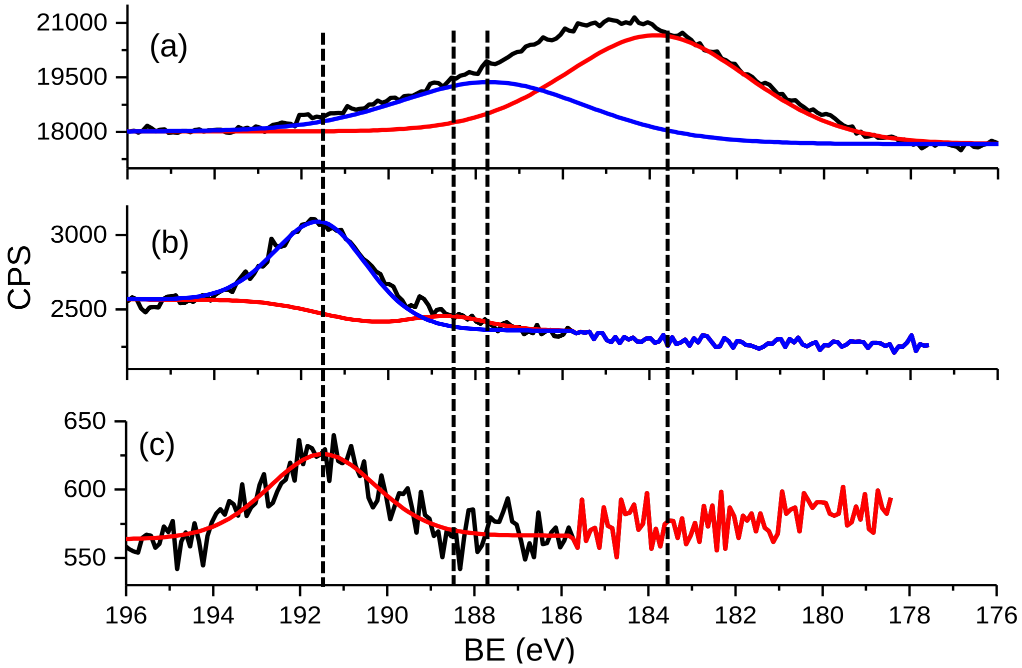

Figure 4-11: P2s peak for (a) silicon before experiment, (b) PP thermal film formed at 2h and 150 °C and (c) PP thermal film formed at 6h and 175 °C.

4.3.4 The Durability of Thermal Films

The durability of PP and ZDDP thermal films is investigated in order to understand their roles in the reduction of friction and wear coefficients. The experiments are conducted in the presence of PAO lubricant for silicon before the generation of the thermal film, silicon containing the PP thermal film and silicon containing the ZDDP thermal film. The results of friction coefficients are presented in Figs. 4-12 and 4-13. The former one presents the average values and the latter one presents the evolution of friction coefficient during test.

It is clear that the PP thermal film decreases friction coefficient by about 30% while the ZDDP thermal film leads to an increase by about 30%. In order to understand the reason behind this finding; both the morphology and the chemistry of films must be considered. Thicker and patchy film is created by ZDDP (see Figs. 4-4 and 4-9) causes an increase in the friction coefficient. In addition, the presence of zinc particles might be also involved. The PP thermal film is thinner and consists of phosphorus based compounds only.

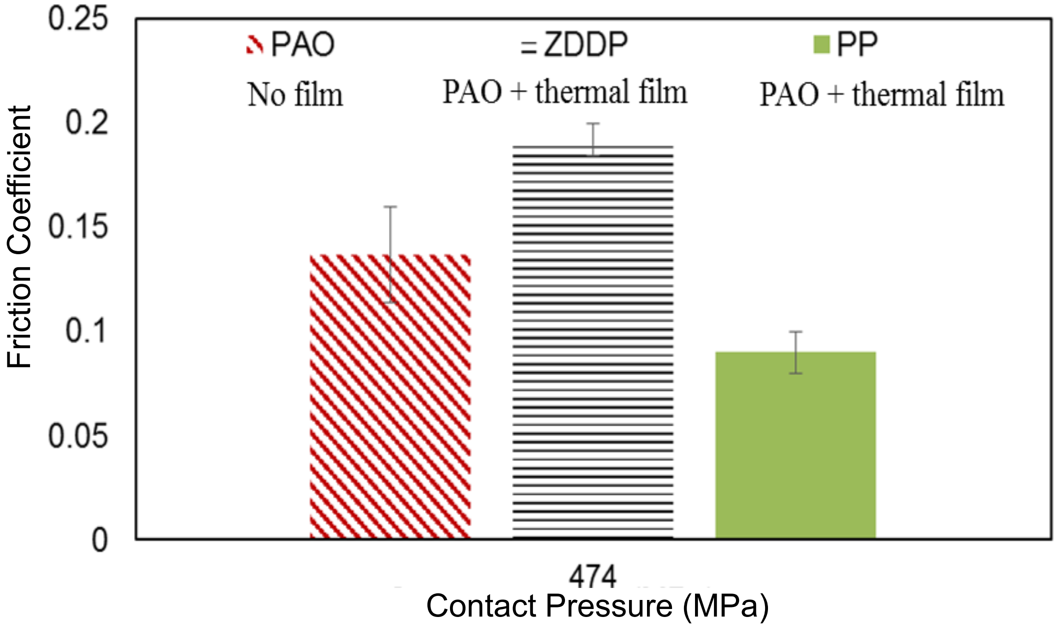

Figure 4-13: Average friction coefficients on surfaces of silicon in PAO before and after the formation of either ZDDP or PP thermal films.

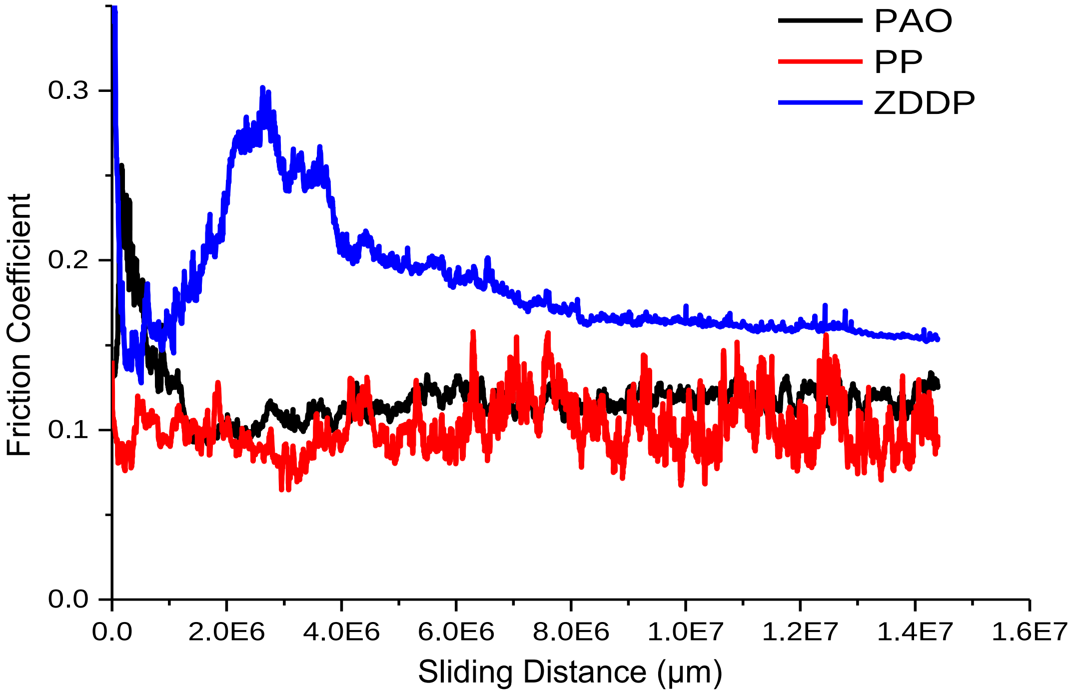

Figure 4-12: Friction coefficient behaviour during experiment.

Fig. 4-13 presents the friction coefficient evolution with the sliding distance. For the ZDDP thermal film, a high friction coefficient is obtained at the beginning and then the value is gradually decreased and becomes closer to the friction coefficient of silicon substrate before the generation of the thermal film. This behaviour suggests that the film exhibits high friction coefficient.

The decrease of friction coefficient with distance means that the destruction of film leads to decrease friction coefficient.

For the PP thermal film, a slight fluctuation in the friction coefficient is observed. This behaviour suggests that also a patchy film exists. However, the absence of zinc and the presence of a phosphorus based film decreased the friction coefficient. Lastly, the friction coefficient of silicon before the generation of thermal film shows a more stable behaviour than silicon containing the PP thermal film and lower values than silicon containing ZDDP thermal film.

Wear coefficients of the three samples are depicted in Fig. 4-14. The value of the wear coefficient is calculated by using the following equation: $wear\ coefficient = \frac{wear\ volume}{applied\ load \times sliding\ distance}$. It is clear that both films result in a substantial reduction in the wear coefficients. PP and ZDDP thermal films lead to decrease wear coefficient by about 75% and 85% respectively.

The presence of ZDDP thermal film shows the highest reduction in the wear coefficient. This can be resulted due its higher thickness in comparison with PP thermal film. In addition, the chemistry of film is also effective. The

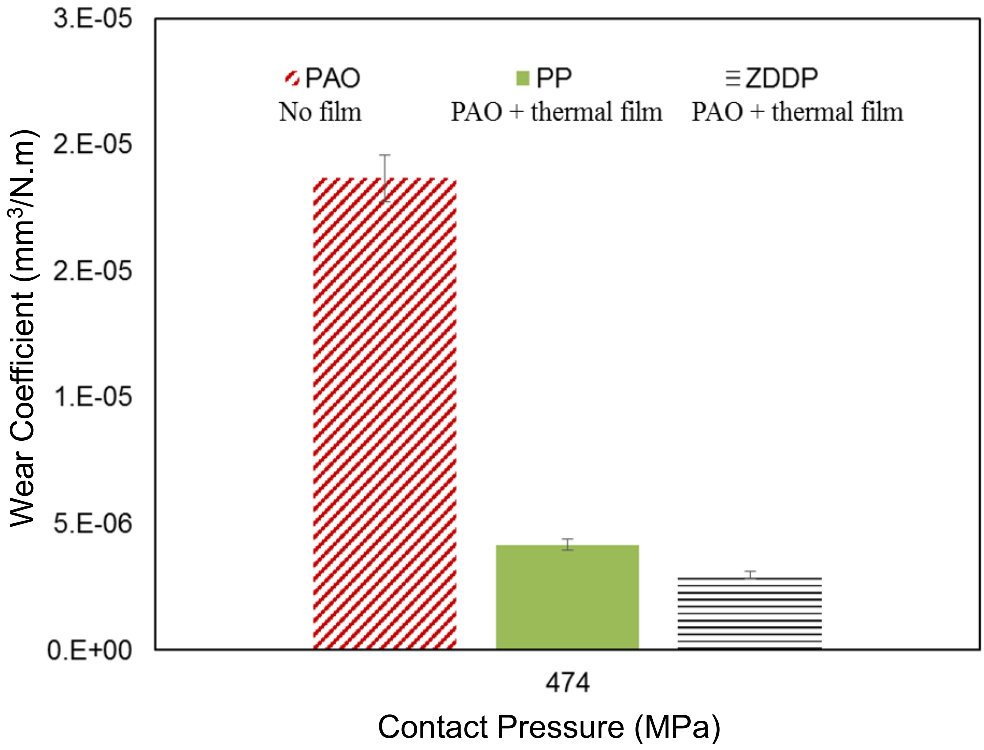

Figure 4-14: The wear coefficients of silicon surfaces before and after the formation of thermal films.

presence of zinc oxide might enhance the durability of the ZDDP thermal film. In contrast, the highest wear coefficient is obtained in the clear silicon sample due to the absence of any protective layer that can offer an anti-wear protection.

Lastly, the surface morphologies of the three samples are showed in Fig. 4-15. The ZDDP thermal film can be seen easily while PP thermal film cannot be recognized. This finding means that a transparent film is created. However, it is clear that the PP thermal film provides a considerable reduction in the wear coefficient. The presence of thermal film in both additives provides a considerable reduction against wear. ZDDP provides higher protection due to its higher thickness. In addition, film chemistry might also has a significant role.

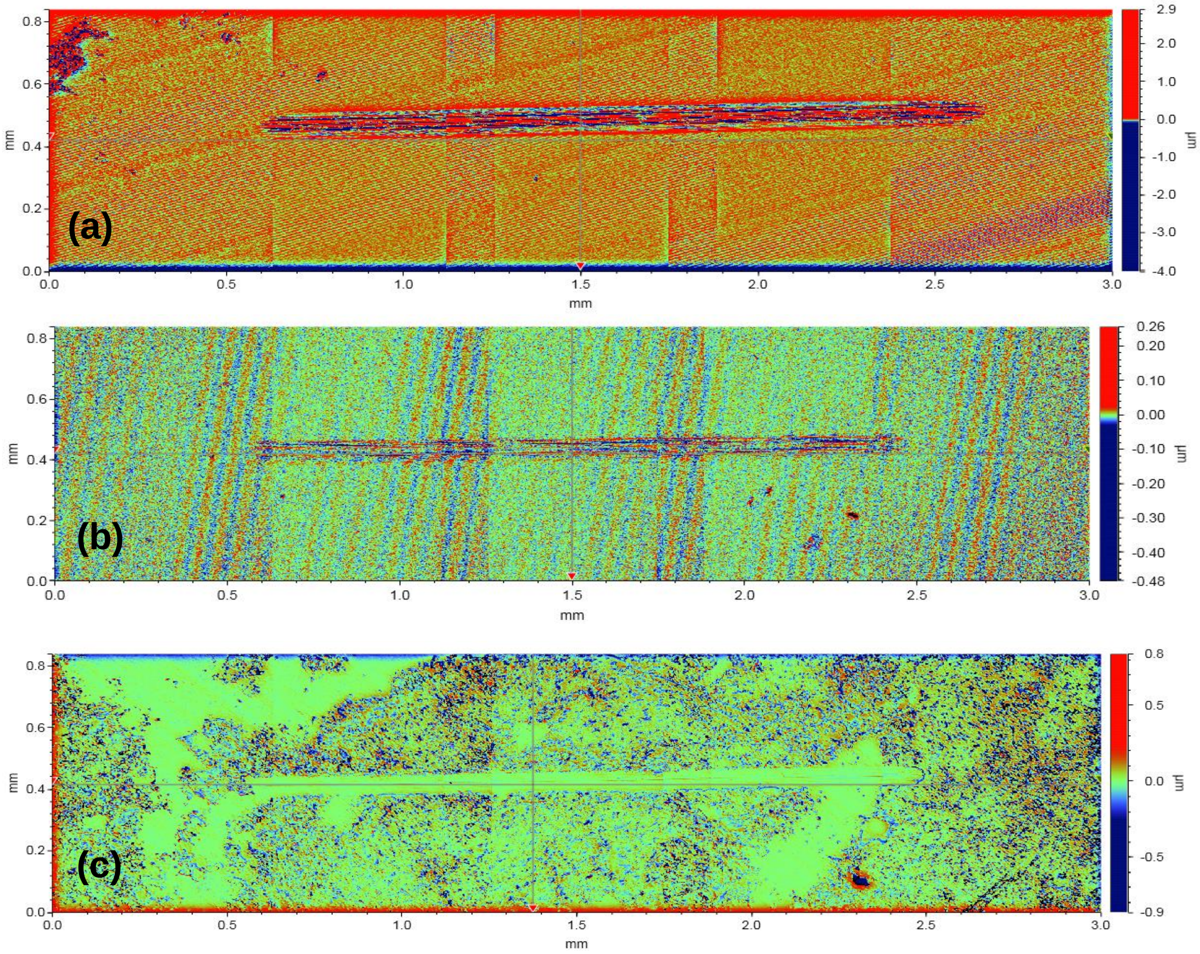

Figure 4-15: Surface morphologies of: (a) Silicon substrate without before the formation of thermal film, (b) silicon substrate contains PP thermal film and (c) silicon substrate contains ZDDP thermal film.

4.4 Discussion

4.4.1 Film Formation Mechanism

The ZDDP thermal film formation mechanism seems to follow the same mechanism as presented in [170] for a steel surface. Consequently, at 150 °C for 2h; three layers are formed which are ZnS (Figs. 4-66b and Figs. 4-7a), phosphate (Fig. 4-8b) and P-O-Si layers (Fig. 4-8b). The increase of time and temperature to 175°C for 6h shows that ZnS layer is replaced by ZnO as the sulfur peak is diminished as depicted in Fig. 4-6c and the Zn2p peak is shifted by 0.6 eV (Fig. 4-7b). This finding is confirmed when 6 spots are scanned by XPS for two silicon samples in the same conditions (175 °C for 6h). Further, the increase in time and temperature leads to an increase in the ratio of Si-O-P to phosphate which suggests the phosphate transformed to Si-O-P.

The formation mechanism of PP thermal film is summarized in Fig. 4-16. The reaction between PP and silicon surface at 150 °C for 2h results in the formation of phosphate and P-O-Si layers within the bulk of the thermal film (Fig. 4-11b). The increase of time and temperature to 175 °C and 6h seems to create a single layer thermal film consisting of P-O-Si as presented in Fig. 4-11c. This finding suggests that the phosphate layer is transforming to P-O-Si with the increase of time and temperature.

Despite the differences between the components of ZDDP and PP thermal films; both resulting phosphorus species being bond to the silicon surface as shown in Fig. 4-8 and Fig.4-11.

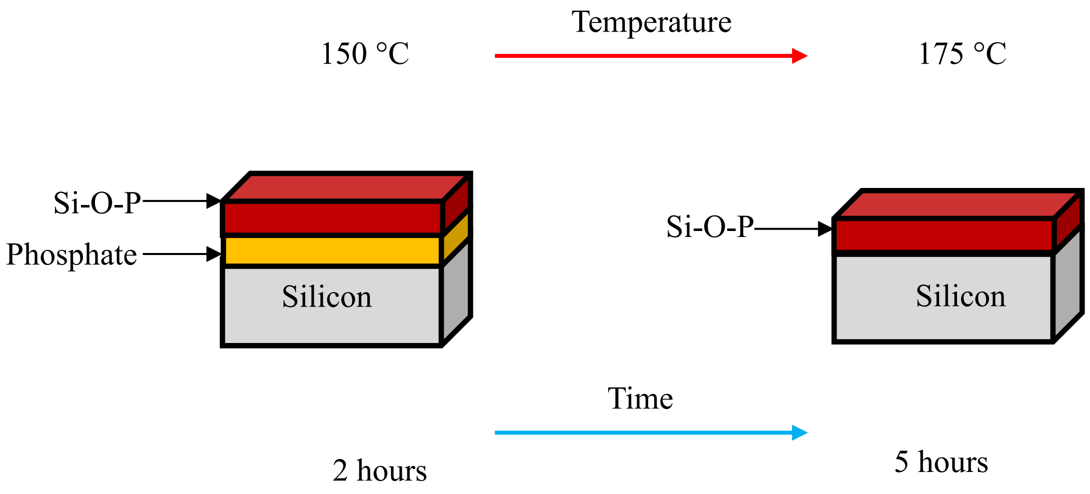

Figure 4-16: PP thermal film formation mechanism.

4.4.2 Film Thickness

Phosphonium phosphate thermal film remains undetectable by ATR-FTIR and EDS even at the longest time 24h and 150 ^{o}C. However, XPS results confirm the formation of the thermal film even at the shortest time of 2h and the lowest temperature of 150 ^{o}C. In contrast, ZDDP thermal film is detected by EDS and FTIR in three different conditions; 150 ^{o}C 24h, 175 ^{o}C 2h and 175 ^{o}C 6h (see Fig. 4-3). Therefore, it is clearly seen from the results that ZDDP thermal films are thicker than PP thermal films. The lower decomposition temperature of ZDDP additives compared to PP [171] can lead to a higher adsorption of ZDDP molecules to react with the silicon substrate which leads to form thicker films.

Formation of a thin thermal film by PP can also be related to the absence of metal cation, such as Zn^{2+} in ZDDP, to feed the chemical reaction. This means that the chemical reaction is not sustainable and PP reacts with silicon when they are in direct contact. To check the validity of this assumption, the time is increased into 24 hours but the film is still not thick enough to be detected by both ATR-FTIR and EDS. This finding is in agreement with the recent finding by Zhou at al [172] when the formation mechanism of PP tribofilm is studied and it is found that PP tribofilm formation is unsustainable unless a positive cation is provided from wear debris.

4.4.3 Tribological Behaviour

The generated thermal films of both additives result a reduction in the wear coefficient as shown in Fig. 4-14. This can be a confirmation to the ability of both additives to be employed as anti-wear additives. However, the higher thickness of the ZDDP thermal film results in a better anti-wear performance than the PP thermal film. Besides, the PP thermal film shows a reduction in the friction coefficient while the ZDDP thermal film shows an increasing in the friction coefficient when both are compared with silicon before the generation of thermal film.

These can be correlated to both films' morphologies and films' chemistries. Phosphorus moieties of both films are very comparable. This can suggest that the presence of zinc oxide provides ZDDP thermal film higher protection against wear.

However, for the same reason, the increase of friction coefficient might be resulted. Lastly, as concluded in section 4.1.1, again the presence of zinc in ZDDP results a higher film thickness than PP which lead to provide higher protection against wear.

4.5 Conclusions

A comparative study has been done to investigate the reactivity of oil-soluble IL and ZDDP with silicon surfaces at elevated temperatures and the following conclusions are obtained:

- Both additives have been reacted with silicon surfaces and form thermal film. However, the morphology and chemistry are quite different.
- Both additives have formed P-O-Si as a result of the chemical reaction between phosphorus and the silicon surface.
- The increase of time and temperature results in an increase in the ZDDP thermal film thickness and film homogeneity.
- For ZDDP the film chemistry, the increase of temperature lead to a change in the chemical state of Zn from ZnS to ZnO due to the dissociation of S and also an increase in the ratio of reacted phosphorus to adsorbed phosphorus.
- For the PP film chemistry, the increase of temperature lead to the adsorption of phosphorus being prevented and therefore only P-O-Si existed.
- The above findings confirm that, in contrast to ZDDP, the formation of the PP thermal film is not sustainable due to the absence of a positive ion that can feed the reaction to sustain it.
- The PP thermal film shows a considerable reduction in both friction and wear coefficients. However, The ZDDP thermal film shows a higher reduction in the wear coefficient.
- The ZDDP thermal film shows an increase in the friction coefficient in comparison with silicon substrate before the formation of the thermal film.

5. Chapter 5: Oil-soluble IL to lubricate silicon

5.1 Introduction

PP IL is soluble in non-polar lubricants and it has been proposed to be an effective alternative to ZDDP. Previously, PP has shown a better anti-wear performance than ZDDP only at certain conditions (high temperature and for long distances) [23, 28, 29, 162]. The lubrication mechanism of both additives needs to be understood. This will help to understand the reason behind the superior anti-wear performance of PP.

In this work, the tribological performance and the lubrication mechanism of PP are compared with ZDDP when lubricating silicon at various tribological conditions. Contact pressure, sliding distance and temperature are varied. A micro scale study is conducted using a nanotribometer (NTR); a steel ball against a silicon plate are employed as a tribopair. The selection of the tribopair aims to simulate the working of engines since silicon showed a very comparable tribological behaviour to aluminium-silicon alloy that is usually used in engines (in the manufacturing of cylinders) [155].

The results show that both additives provide a considerable reduction in both friction and wear coefficients. The reduction of wear coefficient is mainly controlled by the formation of tribofilm. ZDDP creates a thicker tribo/thermal film due to its higher reactivity which leads to a better anti-wear performance. However, ZDDP is depleted faster than PP. The depletion of ZDDP causes a decrease in the formation rate of its tribofilm. Therefore, PP provides a better tribological behaviour once the depletion of ZDDP starts.

This chapter is divided mainly into six sections as follows: chapter overview, introduction, experimental conditions, results, discussion and conclusions.

5.2 Experimental Conditions

The stroke length and velocity are kept constants; 2mm and 2 mm/s respectively. In contrast, four contact pressures are applied to reveal the influence of the contact pressure on the lubrication mechanism; 220 MPa, 474 MPa, 597 MPa and 700 MPa, see Table 5-1.

The calculation of the contact pressure and in addition to the calculation of both contact radius and lambda ratio are conducted based on the formula of Hamrock and Dowson [37] (see subsection 3-4-4). The contact radius is varied from 6 to 9 µm while lambda ratio is varied from 0.0045 to 0.006, which means that all experiments are conducted at the boundary lubrication regime.

Three sliding distances are applied which are 3.6 m, 14.4 m and 36 m at a constant contact pressure (700 MPa), see table 5-2. Temperature is also varied from the room temperature (25 ^{o}C) to high temperature (80 ^{o}C) at a constant contact pressure (700 MPa) and sliding distance (14.4 m). The selection of the maximum applicable contact pressure aims to obtain the most severe conditions that promote the formation of tribofilm.

The friction coefficient was measured in-situ by calculating the ratio of the friction force to the normal force. Each experiment is repeated at least two times and in most cases three times.

Table 5-1: The applied conditions to examine the formation mechanism of tribofilm for PP and ZDDP at various contact pressures.

Condition number	Contact pressure MPa	Lambda ratio	Contact radius µm	Sliding distance (m)	Temperature (^{o}C)
1	220	0.0058	6	14.4	25
2	474	0.0049	13	14.4	25
3	597	0.0047	16	14.4	25
4	700	0.0045	19	14.4	25

Table 5-2: The applied conditions to examine the formation mechanism of tribofilm for PP and ZDDP at various sliding distances.

Condition number	Contact pressure MPa	Lambda ratio	Contact radius µm	Sliding distance (m)	Temperature (°C)
1	700	0.0058	6	3.6	25
2	700	0.0049	13	14.4	25
3	700	0.0047	16	36	25

Table 5-3: The applied conditions to examine the formation mechanism of tribofilm for PP and ZDDP at various temperatures.

Condition number	Contact pressure MPa	Lambda ratio	Contact radius µm	Sliding distance (m)	Temperature (°C)
1	700	0.0058	6	14.4	25
2	700	0.0049	13	14.4	80

5.3 Results

The results are divided into three parts as follows; the effect of contact pressure, the effect of temperature and the effect of sliding distance.

5.3.1 Effect of Contact Pressure

5.3.1.1 Friction Coefficient

Friction coefficient is depicted in Figs. 5-1 and 5-2 when the former presents the average values and the latter demonstrates its evolution during experiments. It can be seen in average that the increase of the applied contact pressure leads to a decrease in the friction coefficient for PAO. This results from the reduction of surface roughness [173]. Adding PP leads to a decrease in friction coefficient and this reduction is decreased with the increase of contact pressure.

Adding ZDDP leads to a decrease in friction coefficient. Apart from the results at 220 MPa, the friction coefficients of both additives are comparable for the rest contact pressures.

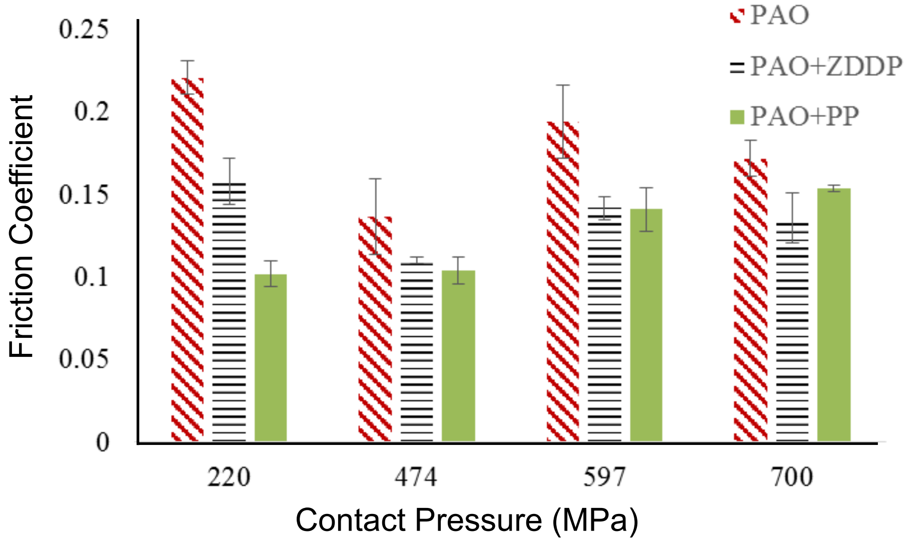

Figure 5-1: The average friction coefficient under various contact pressures**.**

The evolution of friction coefficient is also considered. PP demonstrates the highest stability at all contact pressures. In contrast, PAO shows the highest fluctuation. ZDDP implies a high fluctuation at the lowest contact pressure and a stable behaviour at the other contact pressures. This fluctuation can be as a result of the presence of wear debris (the presence of third body).

For PAO, the highest fluctuation is obtained at the highest contact pressure while the highest stability is obtained at contact pressure 474 MPa. The relationship between friction coefficient stability and the presence of wear debris will be evaluated by presenting wear track morphology.

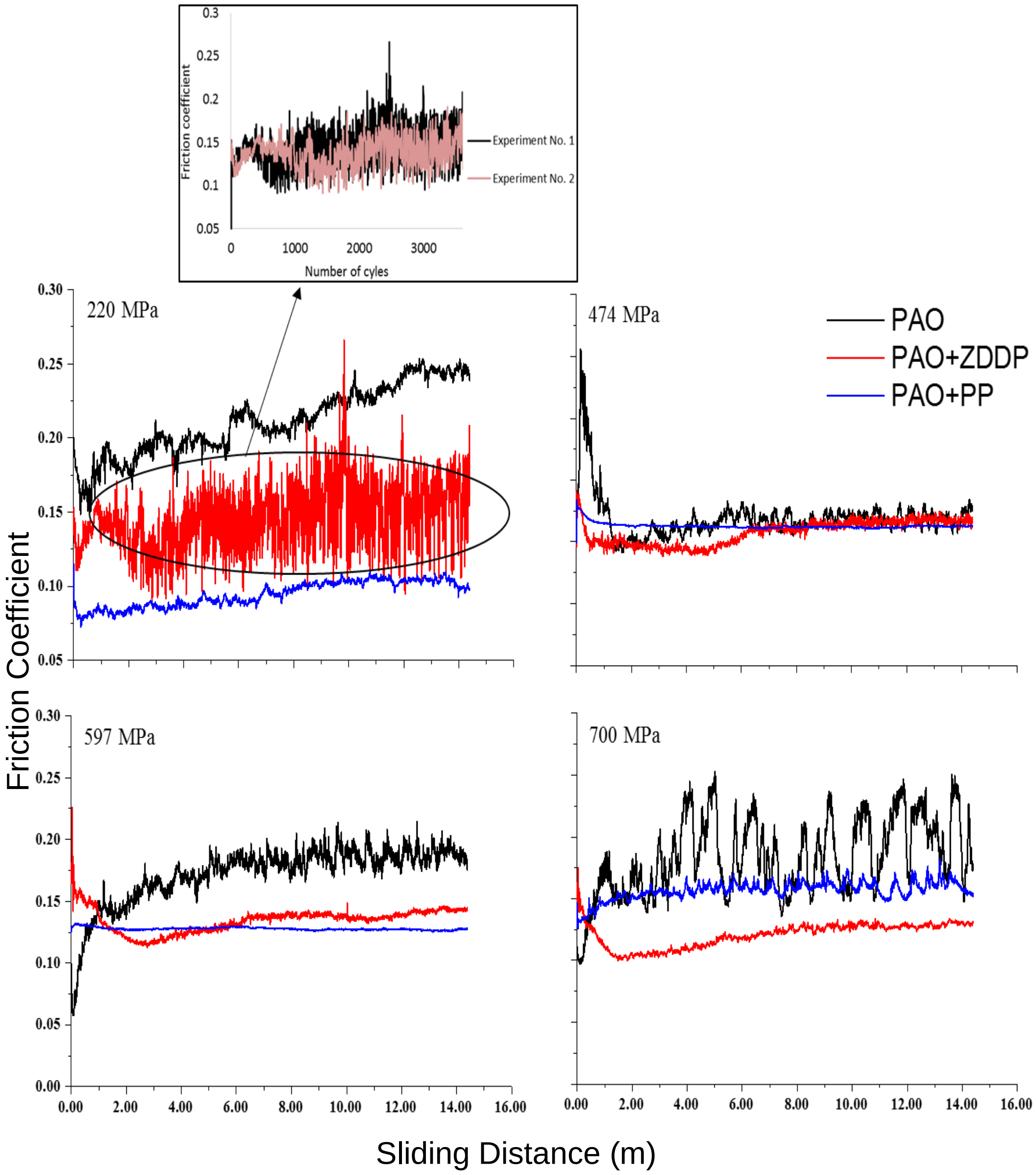

Figure 5-2: Evolution of friction coefficient during experiment at contact pressure: (a) 220 MPa, (b) 474 MPa, (c) 597 MPa

5.3.1.2 Wear Coefficient

Surface morphology is characterized using 3D optical microscopy including the quantification of wear volume. Fig. 5-3 depicts the wear coefficients for the examined lubricants. No measurable wear can be detected at the lowest contact pressure of 220 MPa. It is clear that both additives demonstrate a considerable reduction in the wear coefficient in comparison with neat PAO. However, ZDPP implies higher reduction in the wear coefficient than PP at all contact pressures.

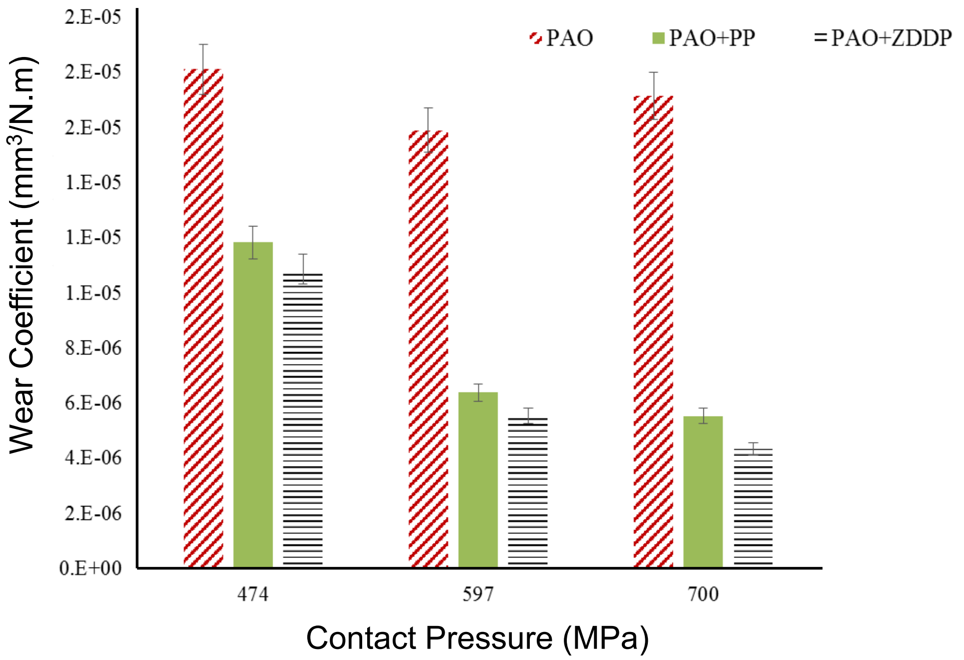

Figure 5-3: Wear coefficient at various contact pressures.

Fig. 5-4 presents a 3D view for surface morphology of silicon surfaces at the highest contact pressure. It can be clearly seen that the highest wear occurs when silicon is lubricated by neat PAO, as expected. Adding ZDDP decreases wear volume and the transference of material from the counter body; steel ball. PP also shows a significant reduction in the wear volume.

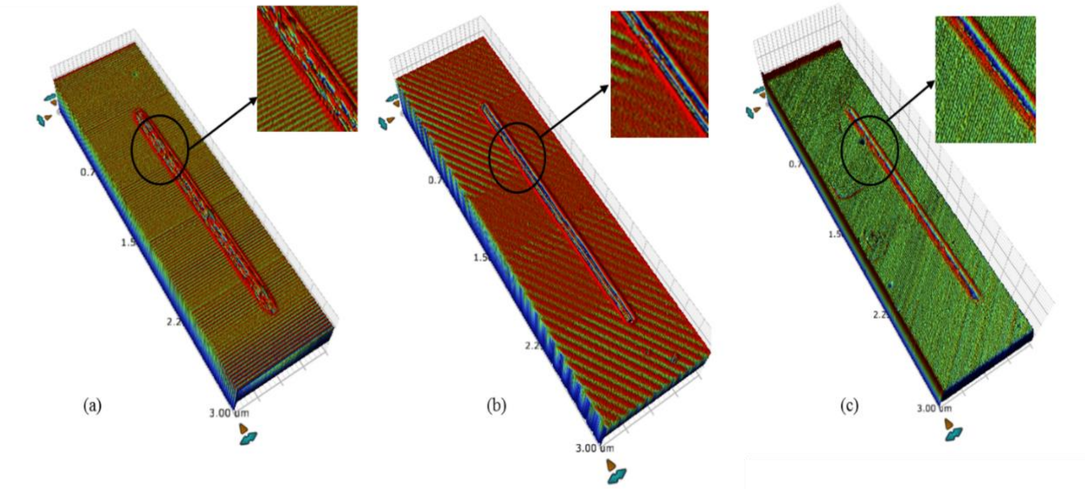

Figure 5-4: A 3D view for wear tracks at contact pressure 700MPa when lubricate with: (a) Neat PAO, (b) PAO+PP and (c) PAO+ZDDP.

Surface morphologies of wear tracks confirm that ZDDP provides better anti-wear performance than PP. The lowest wear depth is obtained when PP is added while the highest one is obtained when neat PAO is utilized. The width of wear track is also decreased when either PP or ZDDP is added.

5.3.1.3 Surface Chemistry

SEM-EDS is employed to evaluate surface chemistry for all samples and two spots are scanned; inside and outside wear track. Fig. 5-5 shows the scanned points (SEM images) for three samples at the maximum contact pressures. The same elements are obtained at the wear tracks for the rest two contact pressures.

The results demonstrate that only silicon, carbon and oxygen exist in all samples at all scanned spots. This finding suggests that the tribofilm is either not created or created but it is not thick enough to be detected by EDS. However, the only difference between the spots inside and outside wear track is the weight percentage of oxygen. The presence of oxygen is decreased inside wear track (See table 5.4). This reduction can be resulted from the destruction of the silicon oxide layer due to wear. Further, the absence of iron from wear track means that either no iron transfers into silicon or only a very small amount is transferred.

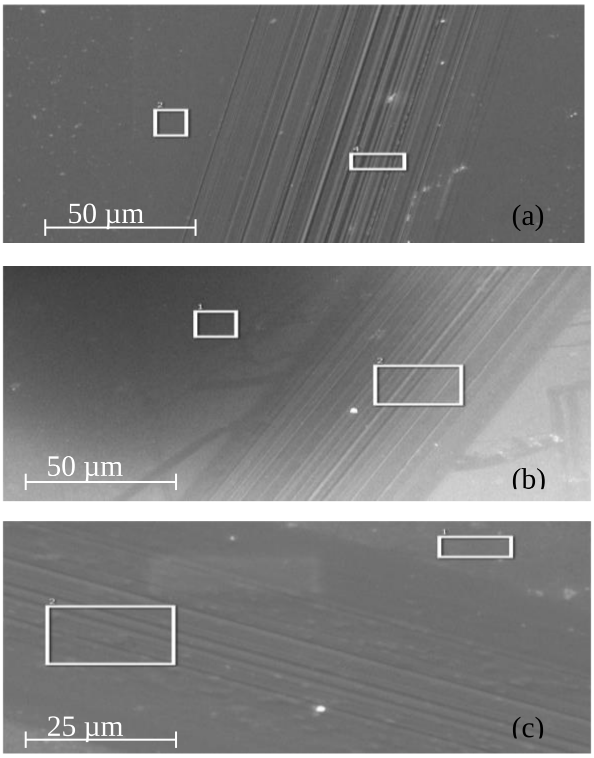

Figure 5-5: SEM images for wear tracks of silicon substrates when lubricated by: (a) neat PAO, PAO+PP and PAO+ZDDP.

Table 5-4: EDS results (atomic percentages) at contact pressure 700 MPa.

Lubricant	Inside wear track	Outside wear track
PAO	Silicon percentage 99% Carbon percentage 0.8% Oxygen percentage 0.2%	Silicon percentage 98.8% Carbon percentage 0.8% Oxygen percentage 0.4%
PAO+PP	Silicon percentage 71.8% Carbon percentage 22% Oxygen percentage 6.2%	Silicon percentage 71.3% Carbon percentage 22.4% Oxygen percentage 6.3%
PAO+ZDDP	Silicon percentage 72% Carbon percentage 19.5% Oxygen percentage 8.5%	Silicon percentage 71% Carbon percentage 20% Oxygen percentage 9%

To check the formation of tribofilm; XPS is employed and only samples that lubricated by PAO+ZDDP and PAO+PP are examined since the formation of tribofilm is expected to be formed as a result of the reaction/adsorption of additives. For ZDDP, referring to its structure (see section 3-3), three elements can reveal the formation of tribofilm which are zinc, phosphorus and sulfur. Fig. 5-6 presents XPS results for zinc.

It is clear that zinc exists inside the wear track which suggests that the tribofilm forms. The obtained peak of Zn 2p3/2 at 1022.6 eV can be assigned to ZnO [168]. XPS results for sulfur are shown in Fig. 5-7. No sulfur can be detected inside wear tracks at various conditions. This finding suggests that either sulfur is not included in the formation of tribofilm or it might be formed but then removed by rubbing (adsorbed at the top of the tribofilm).

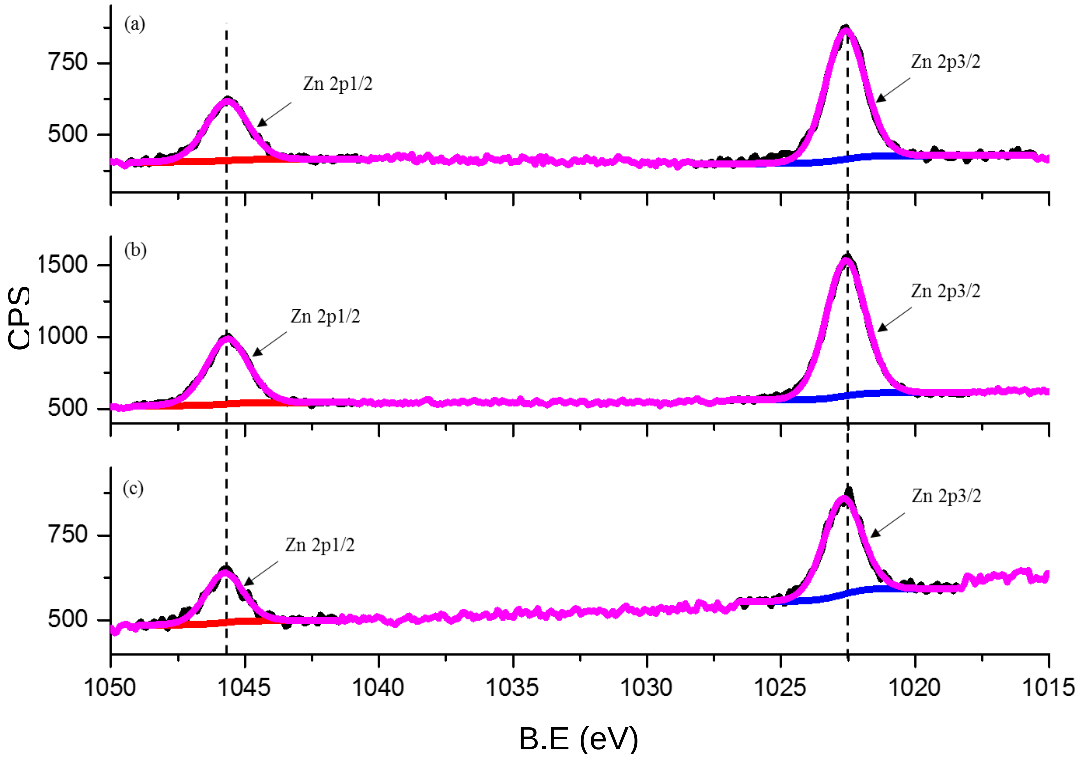

Figure 5-6: XPS results for Zn2p from inside wear track for samples lubricated by ZDDP at; (a) contact pressure 700 MPa, 25 ^{o}C and sliding distance 14.4 m, (b) contact pressure 700 MPa, 80 ^{o}C and sliding distance 14.4 m and (c) contact pressure 700 MPa, 25 ^{o}C and sliding distance 36 m.

Fig. 5-7 demonstrates XPS results for P2s before the experiment and inside the wear tracks that resulted at various tribological conditions. Phosphorus is scanned and the ratio of P2s to Si2s is calculated for silicon substrate before experiments since the n-type silicon contains phosphors. The ratio of P2s to Si2s is about 0.5 before experiment. The significant increase of this ratio is correlated to the increase of the phosphorus content inside wear track that comes from the formation of tribofilm. The results confirm that the tribofilm is formed by both additives at various conditions. The formation of tribofilm not only increases the presence of phosphorus but also results a new peak at 191.5 eV which is assigned to P-O-Si [148].

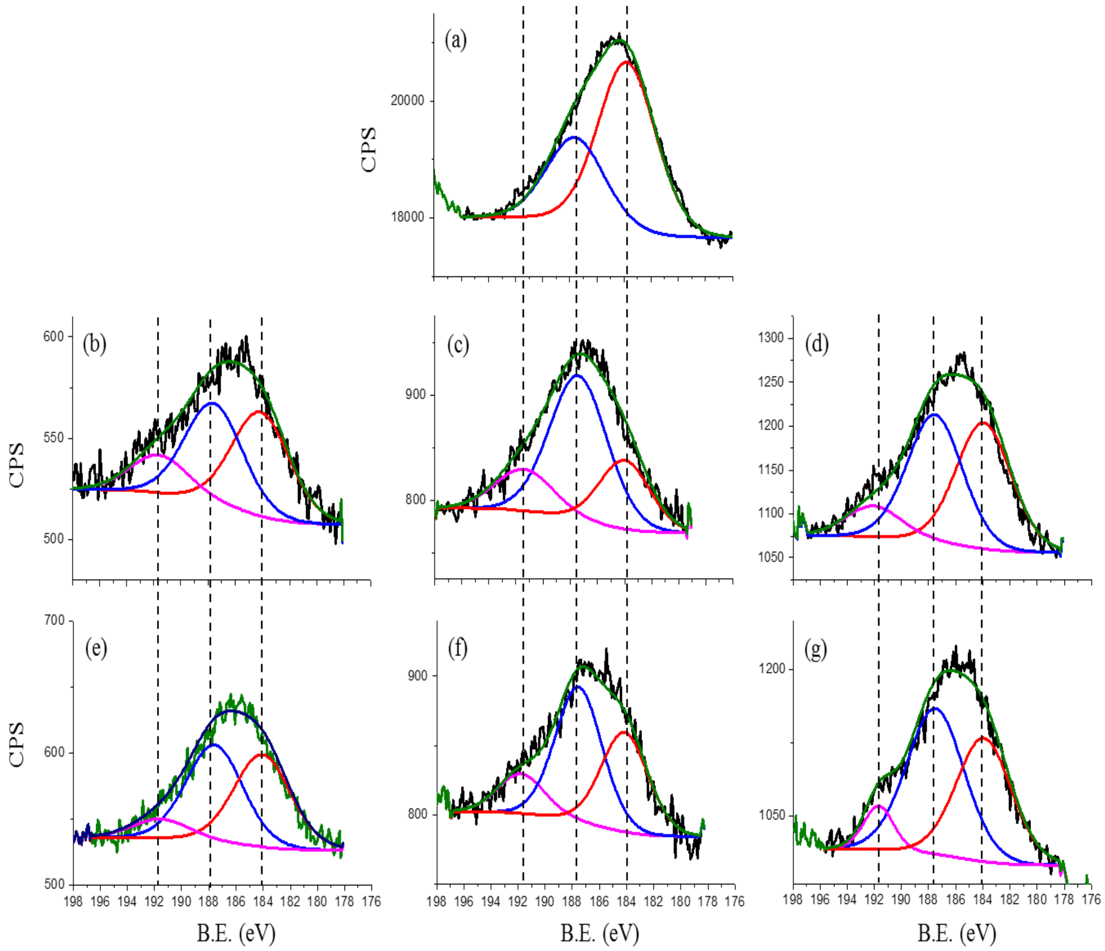

Figure 5-7: XPS results of P2s peak for: (a) silicon before experiments, the rest are inside wear track that resulted from (b) ZDDP tribofilm at contact pressure 700 MPa, 25 ^{o}C and sliding distance 14.4 m, (c) ZDDP tribofilm at contact pressure 700 MPa, 80 ^{o}C and sliding distance 14.4 m and (d) ZDDP tribofilm at contact pressure 700 MPa, 25 ^{o}C and sliding distance 36 m, (e) PP tribofilm at contact pressure 700 MPa, 25 ^{o}C and sliding distance 14.4 m, (f) PP tribofilm at contact pressure 700 MPa, 80 ^{o}C and sliding distance 14.4 m and (g) PP tribofilm at contact pressure 700 MPa, 25 ^{o}C and sliding distance 36 m.

5.3.2 Effect of Temperature

5.4.2.1 Friction Coefficient

The increase of temperature from room temperature (RT) to high temperature (HT), from 25 ^{o}C to 80 ^{o}C, leads to an increase in the friction coefficient of the sample lubricated by ZDDP. In contrast, it decreases in the sample lubricated by PP. Fig. 5-8 and 5-9 depict the effect of increasing temperature on the average friction coefficient and the evolution of friction coefficient during experiments respectively.

The increase of friction coefficient of ZDDP can be correlated to the increase of the tribofilm thickness. The XPS results support this finding (see Figs. 5-6 a and b). In contrast, the increase of phosphorus content in PP tribofilm (phosphorus and P-O-Si) leads to decrease friction coefficient (see Figs. 5-7 e and f). This finding is also in agreement with the results of the friction coefficient of ZDDP and PP thermal films in the previous chapter (see section 4.3.4).

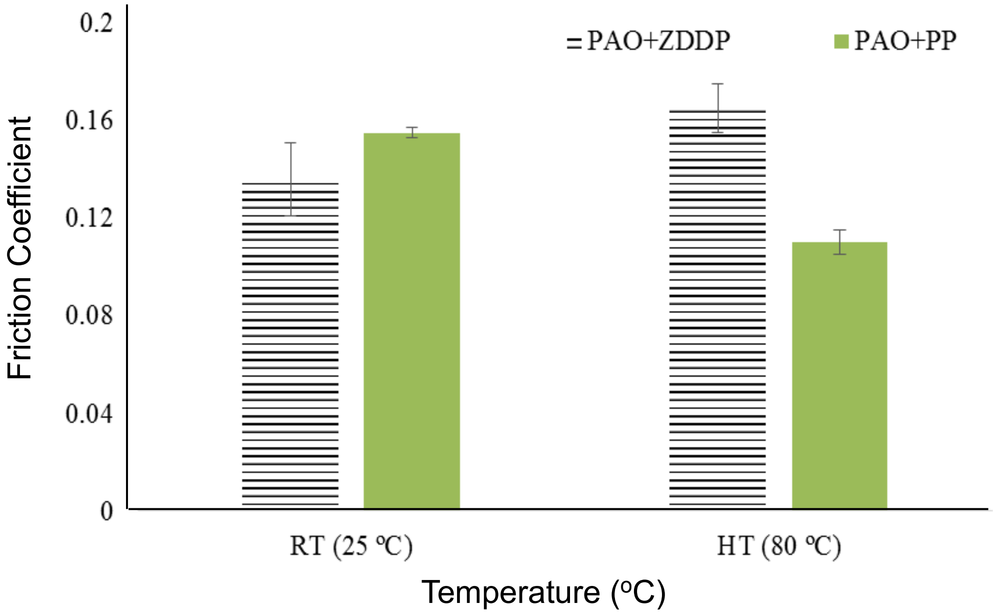

Figure 5-8: The average friction coefficients for PAO+ZDDP and PAO+PP at room temperature and at high temperature.

It is clear that the increase of temperature does not show a considerable effect on the stability of friction coefficients of both additives (see Fig. 5-9 and 5-2d).

The friction coefficients of both additives tend to decrease with sliding distance which can be related to either the reduction of surface roughness or the formation/destruction of tribofilm.

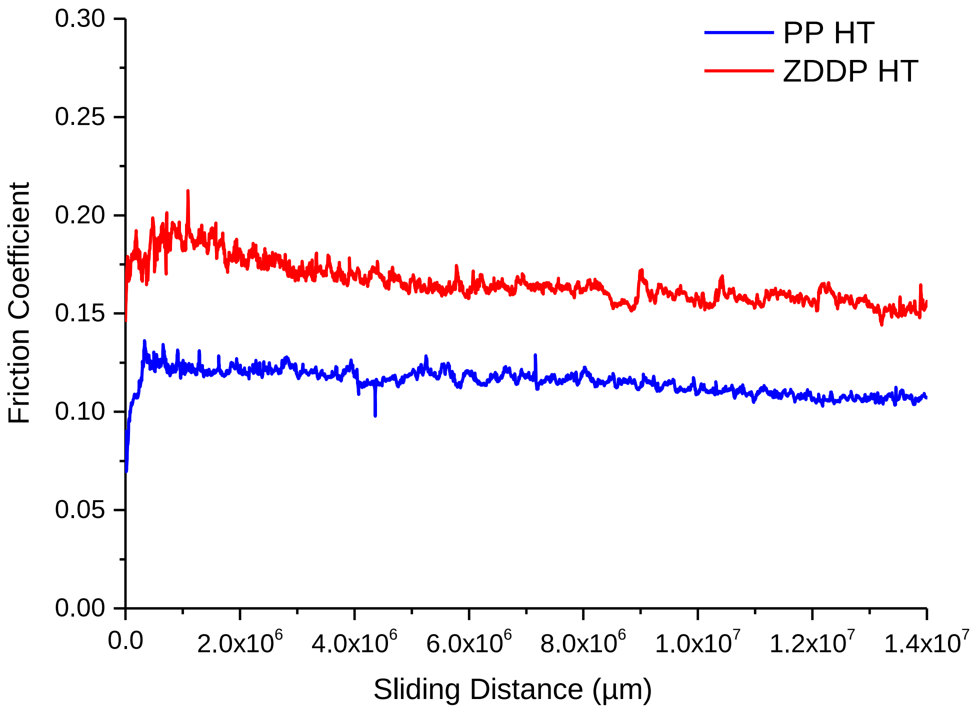

Figure 5-9: The evolution of friction coefficients for both PAO+ZDDP and PAO+PP at high temperature (80 °C).

5.4.2.2 Wear Coefficient

The increase of temperature causes a significant reduction in the wear coefficients of both additives as presented in Fig. 5-10. This reduction can be resulted due to the increase of the tribofilm formation rate. The increase of temperature leads to generating of the thermal film by both additives on silicon as presented in chapter 4. A higher reduction in wear coefficient is obtained by ZDDP which is expected since it is able to generate thicker thermal film and thus provide higher protection against wear (see section 4.4). In addition, the higher protection against wear of ZDDP thermal film (as presented in chapter 4) can justify this higher anti-wear performance (than PP) at higher temperature.

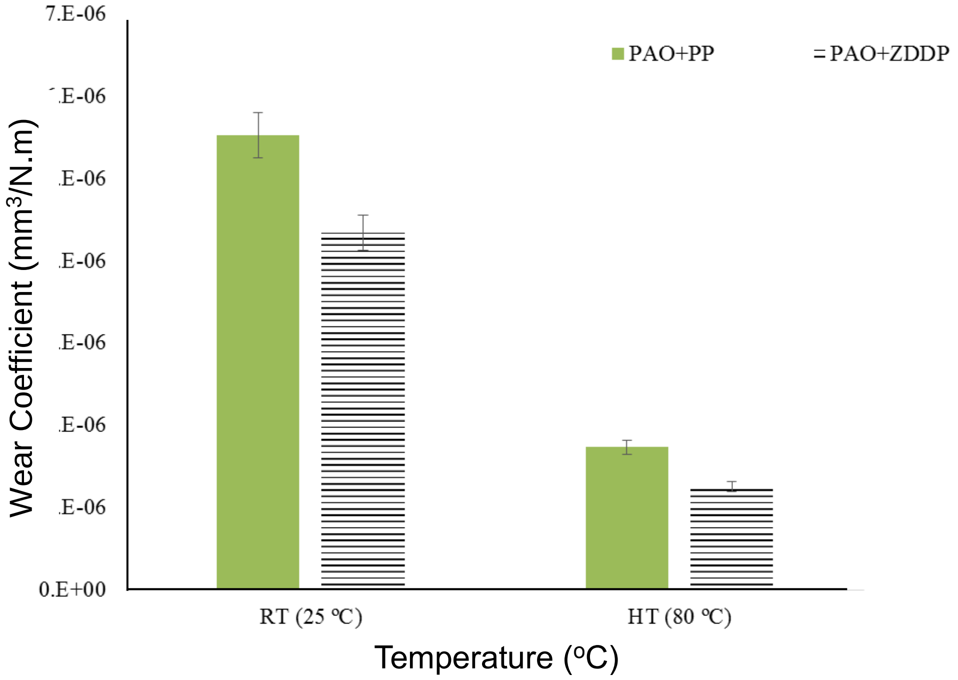

Figure 5-10: Wear coefficients for PAO+ZDDP and PAO+PP at room temperature and at high temperature.

5.4.2.3 Surface Chemistry

Only XPS is employed to detect the formation of tribofilm since the film was undetectable by EDS. Figs. 5-6b and 5-8c confirm the formation of ZDDP tribofilm. The increase of temperature leads to increase the thickness of the tribofilm since the ratio of Zn 2p3/2 to Si 2s is increased. In addition, the ratio of P2s to Si 2s increases as well. However, the obtained results by XPS suggested that the films' chemistry are the same since the related peaks of both zinc and phosphorus are obtained at the same binding energy. In addition, sulfur is still not existed. This could again suggest that it has been destructed as a result of rubbing (since it has been obtained in the thermal film).

For PP, the results also suggest that the thickness of tribofilm increases with temperature since the ratio of P2s to Si 2s shows a significant increase (see Figs. 5-8 e and f). The ratio of P-O-Si to phosphorus also increases which suggests that the formation of Si-O-P increases with temperature (see Figs. 5-7 e and f).

5.3.3 Effect of Sliding Distance

5.4.3.1 Friction Coefficient

The effect of sliding distance is investigated by applying three distances; 3.6 m, 14.4 m and 36 m to investigate the reason behind the fluctuation of friction coefficients and examine the durability of the generated tribofilms. Fig. 5-11 presents the average friction coefficients values for both additives at the aforementioned sliding distances. It can be seen clearly that both additives exhibit a comparable friction coefficients. However, ZDDP friction coefficient is slightly lower than PP (consider the error bars).

The increase of sliding distance from 3.6 m to 14.4 m shows an increase in the friction coefficients. The further increase of sliding distance to 36 m leads to a slight decrease in the friction coefficient of ZDDP while PP implies a comparable value to that obtained at 14.4 m. This can be correlated to the formation of tribofilm. The first increase in the sliding distance (to 14.4m) suggests an increase in the film thickness. Then, the further increase might lead to decrease the tribofilm thickness due to the depletion of ZDDP. This hypothesis will be either confirmed or refuted based on the results of surface chemistry (tribofilm formation mechanism).

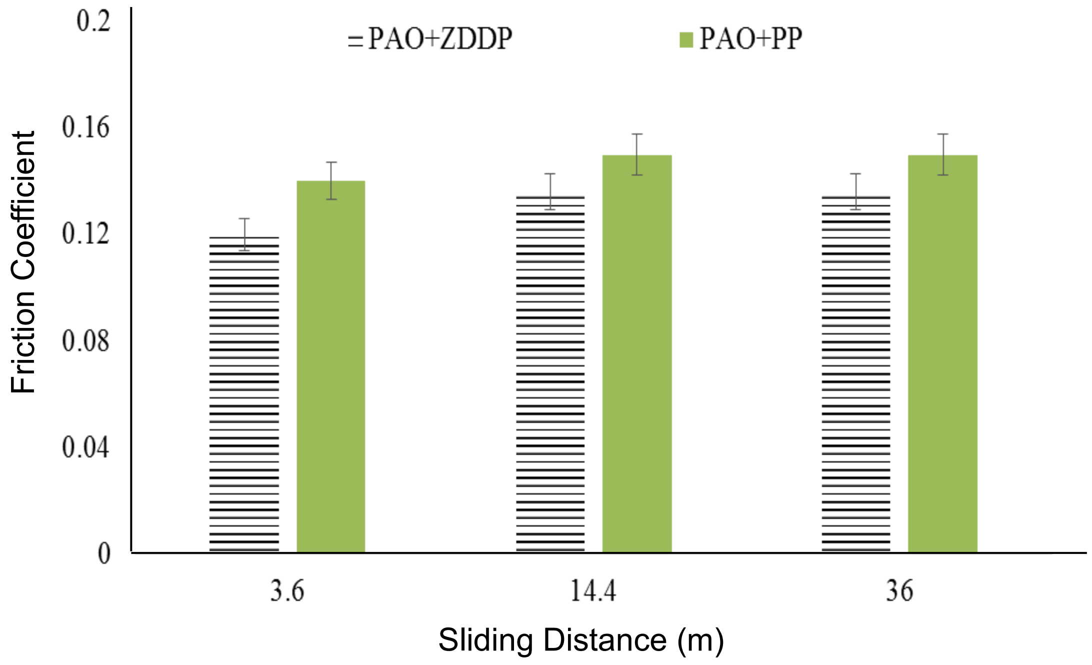

Figure 5-11: The average friction coefficients for both additives at various sliding distances.

The evolution of friction coefficients of both additives over 36 m of sliding is shown in Fig. 5-12. The friction coefficient of ZDDP starts with a low value and then increases until it reaches about 0.145 and then becomes quite stable. PP friction coefficient starts higher than ZDDP and increases slightly till reach about 0.165 and then decreases and becomes 0.125 at the end of the test (at 36 m of sliding). Again, this behaviour can be correlated to the formation mechanism of tribofilm and will be discussed in details in the discussion section.

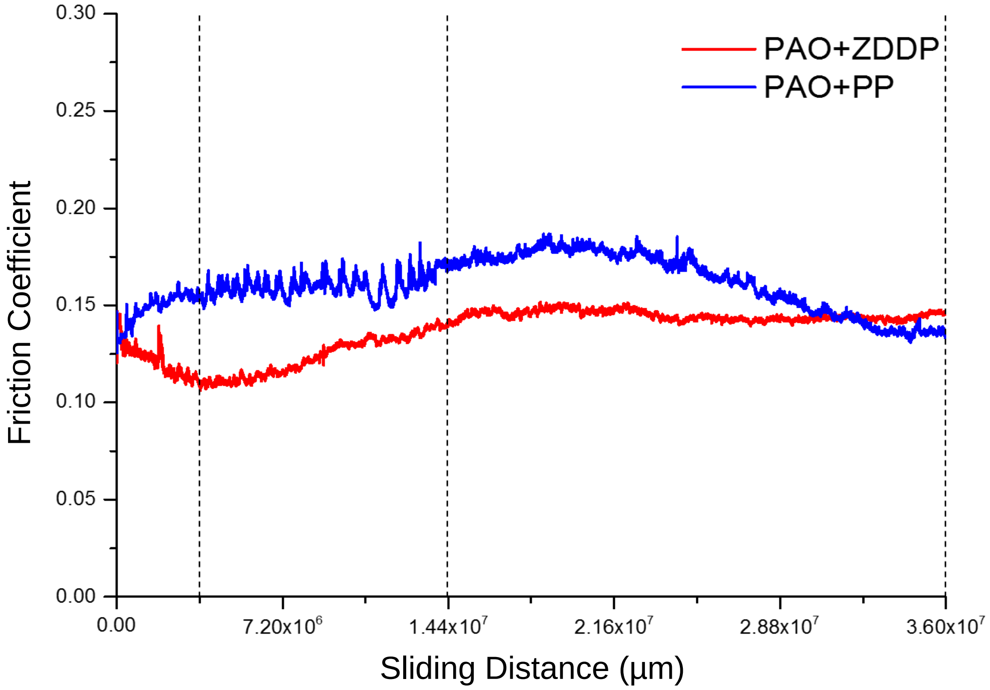

Figure 5-12: Friction coefficient evolution of both additives at three various sliding distances.

5.4.3.2 Wear coefficient

Fig. 5-13 depicts wear coefficients of both additives at two sliding distances (14.4 m and 36 m). No wear could be detected at the lowest sliding distance (3.6 m). A considerable reduction in the wear coefficient results from the increase of sliding distance to 36 m (wear volume is increased). This can be correlated to the formation of thicker tribofilm that leads to a higher protection against wear. PP shows higher wear protection than ZDDP at the highest sliding distance (36 m).

This might be resulted due to the depletion of ZDDP with time since it shows higher reactivity (thicker tribo/thermal film) in addition to its lower concentration in PAO (see section 3.3.1). This finding is in agreement with the results of friction coefficient.

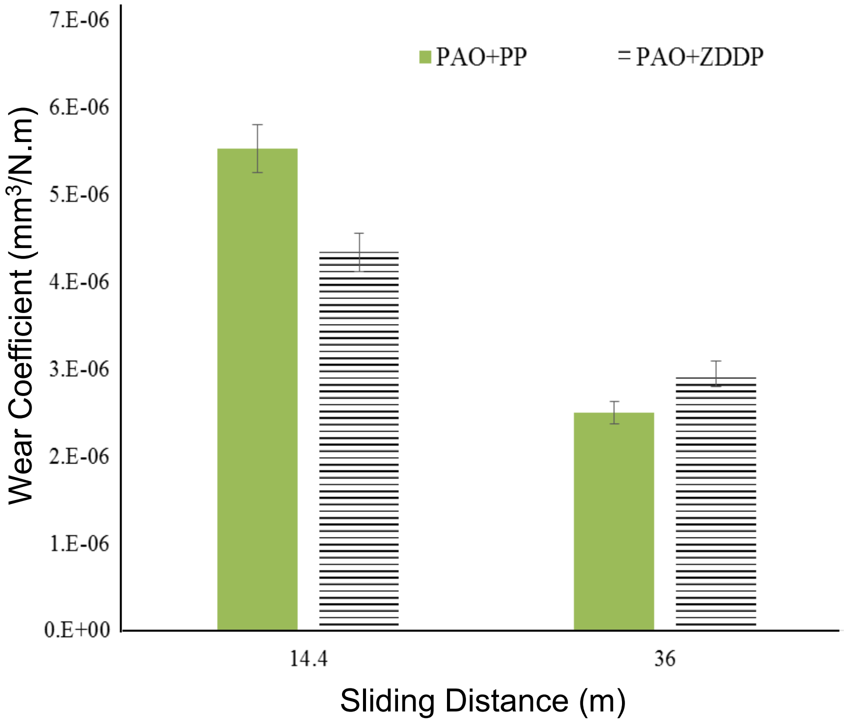

Figure 5-13: Wear coefficient behaviour of both additives at two various sliding distances.

5.4.3.3 Surface Chemistry

Referring to the XPS results in Figs. 5-6, 5-7 and 5-8. Sulfur again could not be detected (see Fig. 5-7c). It is clear that the thickness of ZDDP tribofilm decreases with the increase of sliding distance since the ratio of Zn 2p3/2 to Si 2s decreases (see Fig. 5-6c) and the ratio pf P2s to Si2s decreases (see Fig. 5-8d). In contrast, the results suggest that the thickness of PP tribofilm increases when the ratio of P2s to Si2s increases (see Fig. 5-8g). This finding confirms that the first increase in the sliding distance increases the formation rate of ZDDP tribofilm. The further increase leads to decrease the formation rate of ZDDP tribofilm. This can be correlated to the depletion of ZDDP from the bulk lubricant (ZDDP+PAO). In contrast, due to the higher concentration of PP and in addition to its lower tribofilm formation rate; the increase of sliding distance increases tribofilm thickness.

5.4 Discussion

5.5.1 Friction Coefficient

Friction coefficient can be mainly controlled by viscosity, surface roughness and the presence of third bodies that result from either the formation of tribofilm or wear debris [109, 173]. The effect of viscosity is negligible in this particular study since all lubricants exhibit the same viscosity; they have been measured and represented in [7]. Surface roughness shows a considerable effect on friction coefficient of neat PAO only (see table 5-5).

For neat PAO, the reduction of surface roughness leads to a decrease in friction coefficient and vice versa. This confirms that in the absence of any additive, the friction coefficient is mainly controlled by surface roughness. On the other hand, the lowest friction coefficients for both PAO+PP and PAO+ZDDP are obtained at contact pressure 474 MPa when the highest surface roughnesses exist. This finding supports that the formation of tribofilm controls the friction coefficient of PAO+PP and PAO+ZDDP rather than surface roughness.

The high stability of friction coefficient during experiments for both additives in comparison with PAO (see Fig. 5-2) suggests that no significant wear debris exists between the rubbed surfaces. The presence of wear debris causes a high fluctuation in the friction coefficient [173]. This means that the tribofilm is created and lead to decrease wear which results a reduction in the production of wear debris. The results of both wear coefficients and XPS confirms this finding when the wear coefficient is decreased and both additives create tribofilms.

The increase of ZDDP tribofilm thickness leads to increase friction coefficient (see Figs. 5-1, 5-9 and 5-12). The results of XPS confirm this finding. The increase of film thickness resulted by the increase of temperature leads to increase friction coefficient (see Figs. 5-1, 5-9, 5-8b and 5-8c). In contrast, the increase of temperature decreases friction coefficient of PP. These two findings can be correlated to the mechanical properties and the tribological behaviour of their films.

Table 5-5: Surface roughness inside wear track at various contact

Lubricants	474 MPa	597 MPa	700 MPa
PAO	80 nm ±5nm	168 nm ±7nm	150 nm ±5nm
PAO+ZDDP	73 nm ±8nm	37 nm ±4nm	35 nm ±3nm
PAO+PP	68 nm ±5nm	47nm ±8nm	18 nm ±1nm

5.5.2 Wear Coefficient

Wear coefficient is mainly controlled by viscosity and the formation of tribofilm. The viscosities of three lubricants are exactly same [7]. For neat PAO, wear coefficient increases when contact pressure increases from 474 MPa to 597 MPa and a further increase in contact pressure to 700 MPa shows a comparable wear rate to that obtained at 597 MPa.

Adding either ZDDP or PP demonstrates a significant reduction of both wear width and wear depth. The formation of tribofilm by both additives reduces wear coefficient (see Figs. 5-3 and 5-8). This finding is confirmed when the increase of temperature leads to increase tribofilm thickness of both additives which causes a decrease in the wear coefficients of both additives (see Figs. 5-3, 5-8b, 5-8c, 5-8e and 5-8f). The increase of sliding distance leads to decrease ZDDP tribofilm thickness and thus results in an increase in the wear coefficient (see Figs. 5-3, 5-8c and 5-8d).

These findings and in addition to the previous findings in the previous chapter and in [28, 162] suggests that ZDDP can form thicker tribofilm. However, ZDDP can be depleted faster than PP due its higher tribo/thermal film formation rate that resulted from the presence of zinc cation. The findings of the previous chapter and [28] confirmed that the formation of thermal/tribo film by PP is limited to the presence of either a direct contact with cationic surface or wear debris. In contrast, the presence of zinc in ZDDP leads to higher formation rate of thermal/tribo film. The higher reduction in wear by PP at elevated temperature (more sever condition) in [162] and at the highest sliding distance in this study confirms the faster depletion of ZDDP from the bulk oil (PAO+ZDDP).

5.5.3 Lubrication Mechanism

The relationship between the formation of tribofilm and the tribological behaviour of both additives. ZDDP tribofilm decreases friction coefficient in comparison with the neat PAO. However, the increase of ZDDP tribofilm leads to increase friction coefficient (see Figs 5-12, 5-6a and 5-6b). On the other hand, PP shows a reduction in friction coefficient in comparison with neat PAO. The increase of PP tribofilm demonstrates a comparable friction coefficient.

The difference of the relation between tribofilm and friction coefficient can be resulted from the difference in the films' chemistries. The formation of tribofilm decreases wear coefficient in both additives. The increase of tribofilm thickness decreases wear coefficient and vice versa. The reduction of friction coefficient that resulted from the formation of the tribofilm can be correlated to the reduction of the production of wear debris.

5.5 Conclusions

An experimental investigation has been conducted to compare between the tribological performance and the lubrication mechanism of PP and ZDDP when added into PAO to lubricate silicon substrate. Contact pressure, temperatures and sliding distance have been varied. The main conclusions are:

- Both additives provide a considerable reduction in the friction coefficient.
- Both additives exhibit comparable friction coefficients.
- Both additive enhance the stability of friction coefficient during experiments.
- The friction coefficient of neat PAO is mainly controlled by surface roughness.
- The formation of tribofilm controls the friction coefficient of PAO+PP and PAO+ZDDP.
- Both additives provide a substantial reduction in the wear coefficient.
- ZDDP exhibits lower wear coefficient than PP at all conditions except at the highest sliding distance.

- The depletion of ZDDP from the bulk oil is faster than PP due to not only its lower concentration in PAO but also due to the self-limited tribo/thermal film formation in PP.
- The superior anti-wear performance of PP than ZDDP at certain condition(s) is most probably resulted due to the faster depletion of ZDDP from the bulk lubricant rather than due to its higher viscosity.

6. Chapter 6: Thermal stability of neat ILs and their reactivity with the silicon surfaces at elevated temperature

6.1 Introduction

The main aim of lubricants is to enhance the tribological performance of the interacting surfaces in terms of reducing both wear and friction, managing energy dissipation and extending the lifetime of tribopairs. In the boundary lubrication regime, the formation of the protective layer controls the tribological performance (wear and friction coefficients). The protective layer can result from either the chemical/physical adsorption or chemical reaction of lubricant/additives with the interacting surfaces [39, 40]. To understand the formation mechanism of the protective film, the formation of thermal film in the absence of any tribological motion needs to be understood [174]. The reactivity of lubricant/additive with the solid surface at elevated temperature is strongly related to its thermal decomposition mechanism [174]. In addition, the thermal stability of lubricants needs to be defined in order to understand their working temperature limit [31].

Thus, the thermal stability of five ILs will be analysed in this chapter.

As mentioned in subsection 3.3, the selection of ILs aims to cover the effect of IL chemistry. After that, the reactivity of these ILs with the silicon surfaces at elevated temperature is investigated.

Silicon is the dominant material in the manufacturing of MEMS [24]. ILs are suggested to be the potential lubricants for MEMS [3-6].

Both static and dynamic thermal stabilities will be investigated in the first part of this chapter. FTIR and TGA are used for the static and the dynamic thermal stability respectively. Then, in the second part, the formation mechanism of the thermal film is studied at various temperatures and time intervals.

6.2 Experimental Conditions

In the dynamic thermal decomposition experiments, temperature is increased at a rate of 10 ^{o}C/min, which is the recommended heating rate in the literature [175]. The starting temperature is 55 ^{o}C and in addition, air is utilized to maintain the same environment at both the static and the dynamic thermal decomposition experiments.

In the static thermal decomposition experiments, both time and temperature are varied. Two temperatures are used (80 ^{o}C and 100 ^{o}C) for three periods (2 hours, 5 hours and 24 hours), see table 6-1. The same amount of IL is used in all experiments (2 ml). ILs are placed in the glass beakers. Then, a hot plate is utilized for the heating process when the pre-set temperature is maintained by using a feedback signal (see subsection 3.2.1). The error is about ± 2 ^{o}C. The hot plate is placed in a well ventilated place to exhaust the produced fumes directly.

The applied conditions to generate the thermal films are presented in Table 6-2. Four conditions are applied to reveal the influence of both time and temperature on the thermal film formation process. The formation procedure is illustrated in subsection 3.4.2.

Table 6-1: The applied conditions in the static thermal decomposition experiments.

Condition number	Temperature (^{o}C)	Time (hours)
1	80	2
2	80	5
3	80	24
4	100	2
5	100	5
6	100	24

Table 6-2: The applied conditions to generate the thermal films.

Condition number	Temperature (ºC)	Time (hours)
1	80	2
2	80	5
3	80	24
4	100	2

Lastly, the durability of the generated thermal films is examined by applying a 50 mN load in a dry contact condition. A borosilicate ball is rubbed against silicon plate containing a thermal film. The results of friction and wear coefficients are used to evaluate the durability of the generated thermal films.

6.3 Results

6.3.1 Thermal Decomposition of ILs

6.3.1.1 Dynamic Thermal Decomposition

The results of the dynamic thermal decomposition of the examined ILs are depicted in Fig. 6-1.

The effect of anion chain length is evaluated by comparing between EMIM ESU (both chains are ethyl) and EMIM OSU (cation chain is ethyl and anion chain is octyl).

The effect of cation chain length is evaluated by comparing between EMIM ESU and BMIM OSU (cation chain is butyl and anion chain is octyl). The results demonstrate that decreasing of either cation or anion chain length increases the dynamic thermal stability of IL. This can be as a result of the decrease of the stability of carbocation [61].

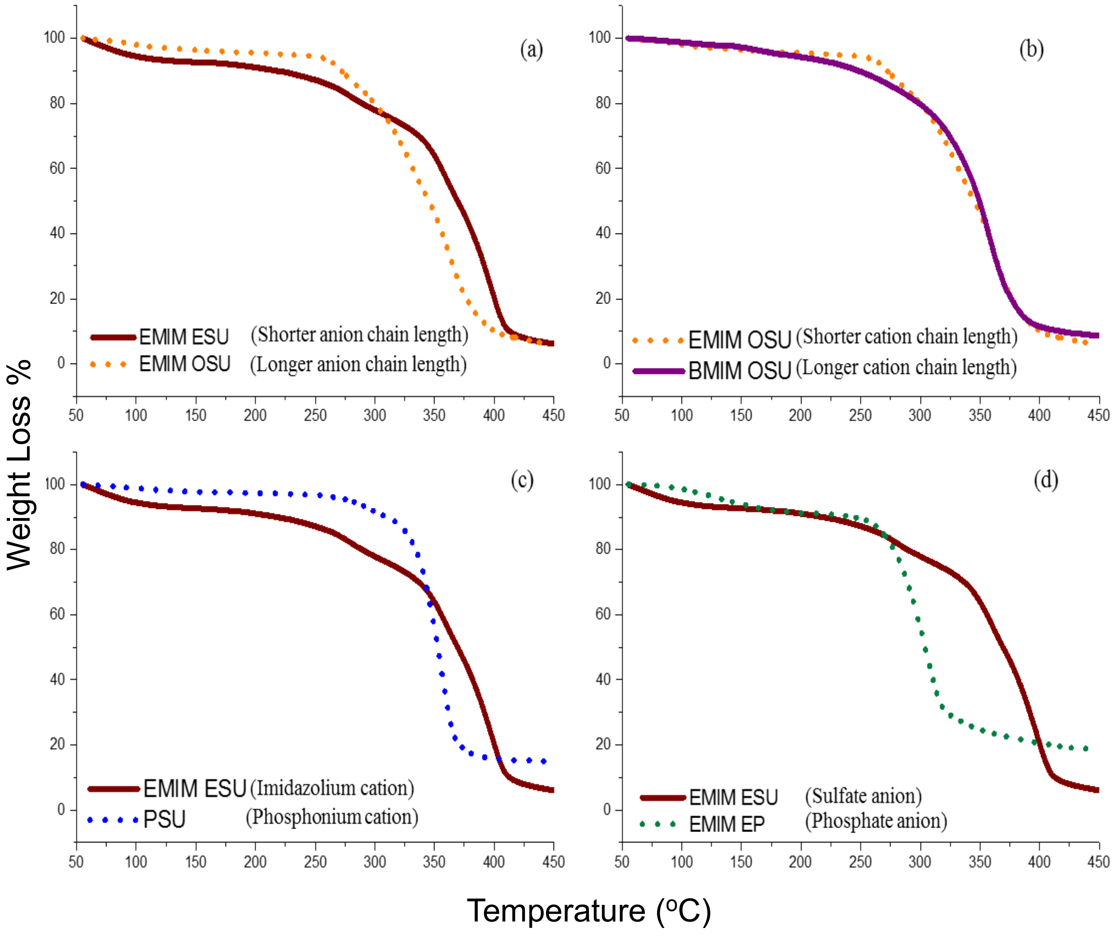

Figure 6-1: Dynamic thermal decomposition of the examined ILs to reveal the effect of: (a) anion chain length, (b) cation chain length, (c) cation type and (d) anion type.

The effect of anion chain length is significantly higher than cation chain length (see Figs. 6-1a and 6-1b). This finding is expected since the increase of anion chain length (from ethyl to octyl) is higher than that applied for cation chain length (from ethyl to butyl).

The effects of both the anion type and the cation type are considered by comparing EMIM ESU with PSU and EMIM EP respectively. Previous findings showed that the correlation between either anion type or cation type and the thermal stability cannot be determined precisely. Some ions (anion/cation) demonstrated a significant influence while other ions did not demonstrate any influence [176, 177]. However, in this study, both anion and cation demonstrate a considerable effect on the thermal stability. It is observed that the presence of phosphorus as either a cation (phosphonium cation) or anion (phosphate anion) instead of imidazolium or sulfate respectively, decreases the dynamic decomposition temperature (see Fig. 6-1). This finding is in agreement with the previous study that compared phosphonium with imidazolium when both were combined with a halogenic anion [177].

Both the onset temperature and the decomposition temperature are considered. The former is obtained when only a slight reduction in mass is detected which suggests that the decomposition is just started (see Fig. 6-2). The highest reduction in the mass was defined as the decomposition temperature [178] as presented in Fig. 6-2.

It is clear that the ILs' chemistry has a considerable effect not only on the decomposition temperature but also on the onset temperature (see Fig. 6-2). Longer cation or anion chain length appears to lead to a decrease in the decomposition temperature while there is no significant effect on the onset temperature. In addition, sulfate anion and imidazolium cation show a lower onset temperature in comparison with phosphate anion and phosphonium cation respectively (see Fig. 6-2).

Previous studies reported that the use of TGA to study the dynamic thermal decomposition of ILs can provided an overestimation for their thermal stability [139, 179]. In other word, the thermal decomposition can be started in a temperature by far lower than that estimated by TGA.

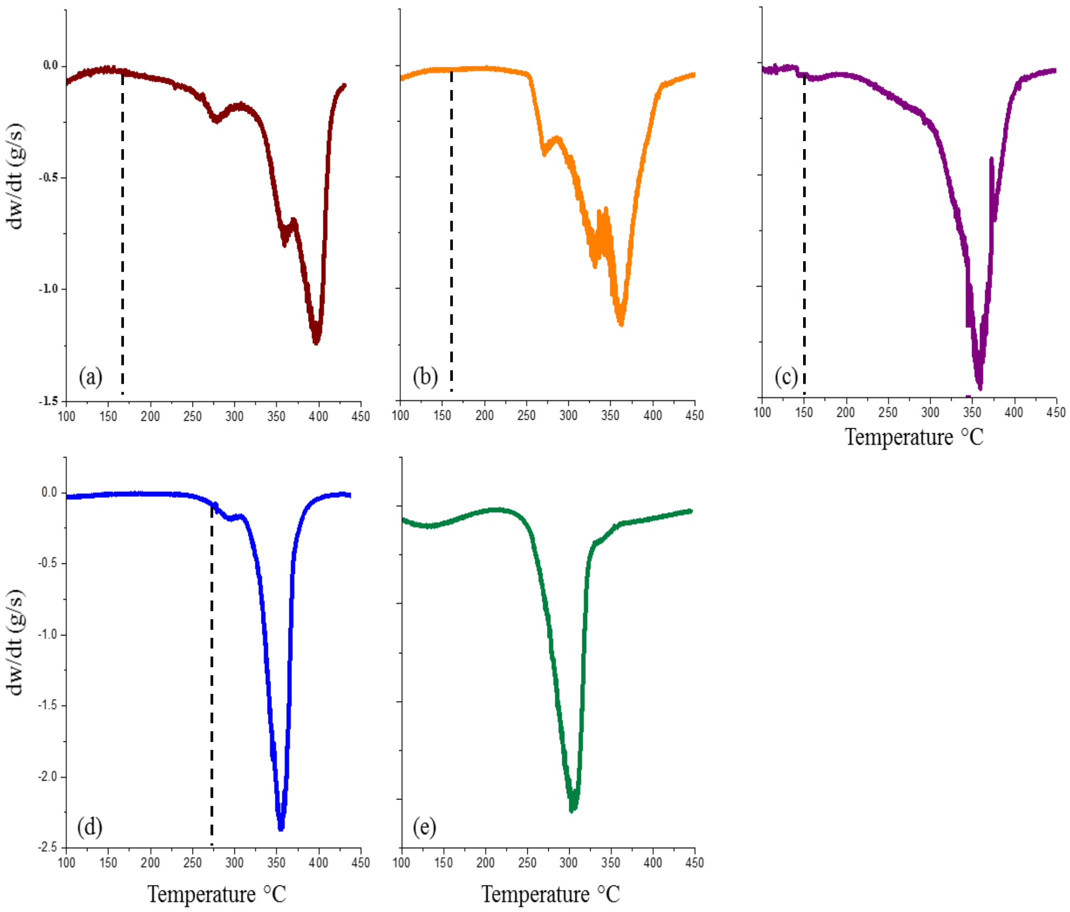

Figure 6-2: First derivative of the weight loss against surface temperature curve for: (a) EMIM ESU, (b) EMIM OSU, (c) BMIM OSU, (d) PSU and (e) EMIM EP.

Thus, the static thermal decomposition experiments are utilized in this study to obtain complementary information.

6.3.1.2 FTIR Results at Room Temperature

IR spectra for the examined ILs are depicted in Fig. 6-3. The analysis starts with EMIM ESU, because it is the only IL in this study that is widely analysed in the literature [139]. Table 6-3 demonstrates the assigned peaks for EMIM ESU, and all peaks are in agreement with [139, 140]. It can be clearly seen in Fig. 6-3 that the variation of anion chain length plays a more significant role than cation chain length. The intensities of peaks related to the hydrocarbons are increased with the increase of either anion or cation chain length (see Fig. 6-3).

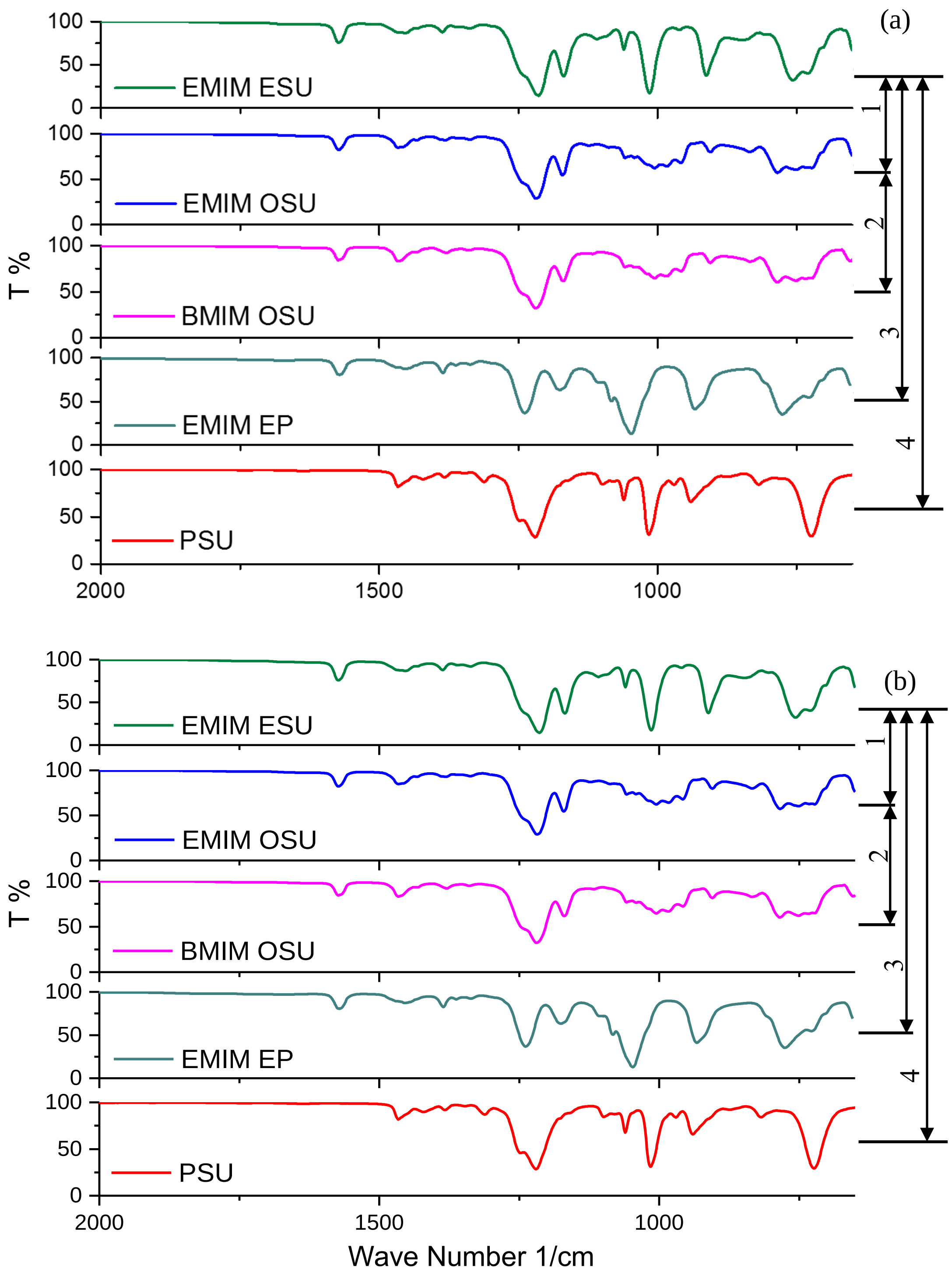

1: Anion chain length is increased, 2: cation chain length is increased, 3: Anion type is changed and 4: cation type is changed.

Figure 6-3: IR spectra of five ILs at room temperature; (a) spectra between 4000 cm^{-1} and 2000 cm^{-1} and (b) spectra between 2000 cm^{-1} and 650 cm^{-1}.

Table 6-3: The assigned peaks for EMIM ESU at room temperature.

Intensity	Wave number cm^{-1}	Assigned to
w	3150	HCCH ring
m	3100	CH_3(N) HCH
w	2980	H-C-H
w	2940	CH_3 HCH
w	2900	Ring CH3 HCH sym str
m	1574	CH3-N or CH2-N
w	1468	N-CH3 symmetric vibration
w	1380	C-H stretching, CH3 (N) bending
w	1360	CH_2 (N) or CH_3 (N) stretching
w	1330	CH_2 (N) stretching
s	1215	S-O stretching
s	1170	(N) with CH_2 or CH_3
w	1110	SO_4 asymmetric vibration
m	1060	O-C
s	1015	C-O-SO_3 stretching, S=O stretching
w	960	C-C stretching, CH bending
s	912	C-O-SO_3
w	847	CCH bending
s	757	C-O-S-O bending
m	729	S-O stretching
w	705	In plane bending resulted from imidazolium ring; CH_3(N), CH_2(N).

Referring to the Beer-Lambert law [138]; the increase of intensity (decrease the transmissivity) has a linear relationship with molar concentration. This means that the reduction of peaks' intensity suggests a reduction of the concentration of their related chemicals.

The increase of anion chain length leads to a decrease in the intensity (concentration) of both sulfate and imidazolium related peaks, as expected. In contrast, the intensities of the peaks related to chain lengths; such as C-C, C-H and CH-CH are increased. This finding is expected since the chain length is increased and the concentration of these bonds is increased. The same behaviour is obtained as a result of the increase of cation chain length (see Fig. 6-3).

Changing cation type from imidazolium to phosphonium leads to a full diminishing of imidazolium related peaks, as expected. Five new peaks are detected and assigned to the phosphonium cation. Three peaks are assigned to P-CH3 at 1421 cm^{-1} asymmetric vibration, 1313 cm^{-1} symmetric vibration and 939 cm^{-1} rocking vibration. For the last two peaks, the one at 729 cm^{-1} is assigned to P-C stretching vibration and the second one at 1090 cm-1 is assigned to the asymmetric stretching of P-C. Besides, the rest of the peaks are assigned to either sulfate anion or hydrocarbons exist. However, a new peak at 2825 cm^{-1} appears and is assigned to the stretching of OCH_3 that exists in methyl sulfate. The assignment of all these peaks are made based on the available data in [135].

Changing anion type from sulfate to phosphate leads the sulfate-related peaks being eliminated, as expected. Five new peaks appear; four of them are related to phosphate anion. The assignment of the phosphate related peaks are as follows: P-O stretching at 776 cm^{-1}, P-O-C symmetric stretching at 933 cm^{-1}, P-O-C asymmetric stretching at 1050 cm^{-1}, P=O at 1240 cm^{-1}. Further, the last peak is assigned to OH. The OH related peak can be as a result of the water content. Again, the assignments of all these peaks are made based on the available data in [135].

6.3.1.3 FTIR Results After Heating Process

ILs are heated up to 80 ^{o}C for 2 and 5 hours. The IL colour was changed to black after 30 minutes of heating (see Fig. 6-4).

The change of colour from transparent to black is a reported feature of the oxidation of lubricants [180]. In addition, a partial decomposition is observed when the intensity of anion and/or cation related peaks are decreased. The increase of time from 2 hours to 5 hours leads to a further decrease of anion and/or cation related peaks. The temperature is also increased to 100 ^{o}C for 2 and 5 hours. The results show that the increase of temperature also leads to a decrease of anion and/or cation related peaks. This finding suggests the increase of either time or temperature increases the amount of the decomposed species.

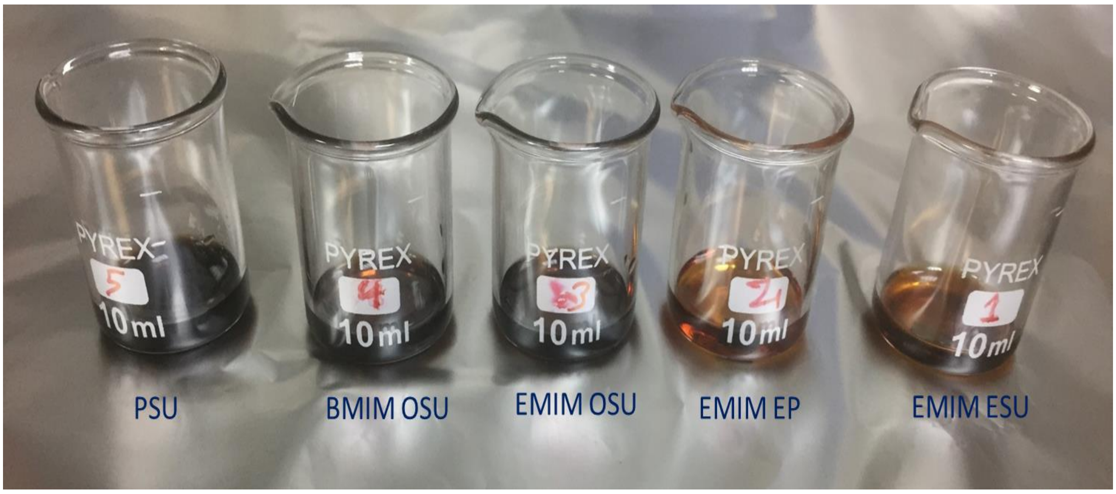

Figure 6-4: ILs after heating them into 80 ^{o}C and for 2 hours.

Fig. 6-5 presents the IR spectra of ILs after heating them to 100 ^{o}C for five hours. Starting from BMIM OSU, a broad weak peak was obtained between 3400 and 3600 cm^{-1}. This peak is assigned to OH [179]. This is likely to result from the decomposition of IL as pointed out in [139]. Subsequently, the intensities of peaks related to imidazolium and hydrocarbon peaks, CH_3-CH_2 and CH_3-HCH, are increased which means that their molar concentrations are increased. In contrast, three peaks related to the sulfate anion are diminished which are SO_4 at 1110 cm^{-1} and at 912 cm^{-1}, C-O-S-O and S=O at 757 cm^{-1}. This means that the decomposition process starts in the sulfate anion. This finding is in agreement with the previous studies [139, 181].

Decreasing cation chain length is expected to increase thermal stability of IL, based on TGA results (see Fig. 6-1b).

As expected, only one peak related to sulfate anion is diminished while the rest sulfate related peaks still exist with a considerable reduction in their intensities (see Fig. 6-5). In contrast, cation and hydrocarbon related peaks are increased. Similarly, the decrease of anion chain length leads to increase the thermal stability (see Fig. 3-5). This finding is again in agreement with TGA results (see Fig. 6-1a).

Changing anion type from sulfate to phosphate leads to an increase in the stability of IL. Thus, in EMIM EP no peaks are neither diminished nor produced due to the heating process (see Fig. 6-5). This outcome is in agreement with TGA results since the onset temperature of EMIM ESU is lower than EMIM EP (see Fig. 3-1d). However, a slight reduction in the intensities of the hydrocarbon related peaks occurs.

In addition, a noticeable increase of the intensity of OH related peak is observed. This finding suggests that a partial decomposition occurs in the anion/cation chain.

Changing cation type shows a slight influence on the static thermal stability. Again, only sulfate peak intensities are decreased (see Fig. 6-5). Further, a new peak appears at 1160 cm^{-1} which is assigned to methyl sulphoxides [135]. This suggests that the change of cation from imidazolium to phosphonium leads to higher oxidation as a result of heating. The phosphonium cation related peaks are almost the same before and after the heating process (see Fig. 6-5). These findings suggest that the anion has a more significant role in the thermal decomposition process than cation.

To investigate the influence of time and temperature on the decomposition process, BMIM OSU after exposure to various conditions is analysed, since it exhibits the lowest static thermal stability. Fig. 6-6 depicts the FTIR spectra for BMIM OSU at room temperature, after heating to 80 ^{o}C for 2 and 5 hours and after heating to 100 ^{o}C for 5 hours. The variation is mainly observed in sulfate related peaks rather than imidazolium ones. The intensity of OH peak increased with the increase of either time or temperature which confirms that this peak results from the decomposition process as reported before in [139].

The increase of either time or temperature leads to a reduction in the intensity (concentration) of the decomposed species (sulfate). It is obvious that the increase of temperature is more significant than time.

This could suggest that the increase of temperature increases the decomposition rate. The slight effect of longer exposure can be as a result of the increase of the amount of the decomposed species at constant decomposition rate.

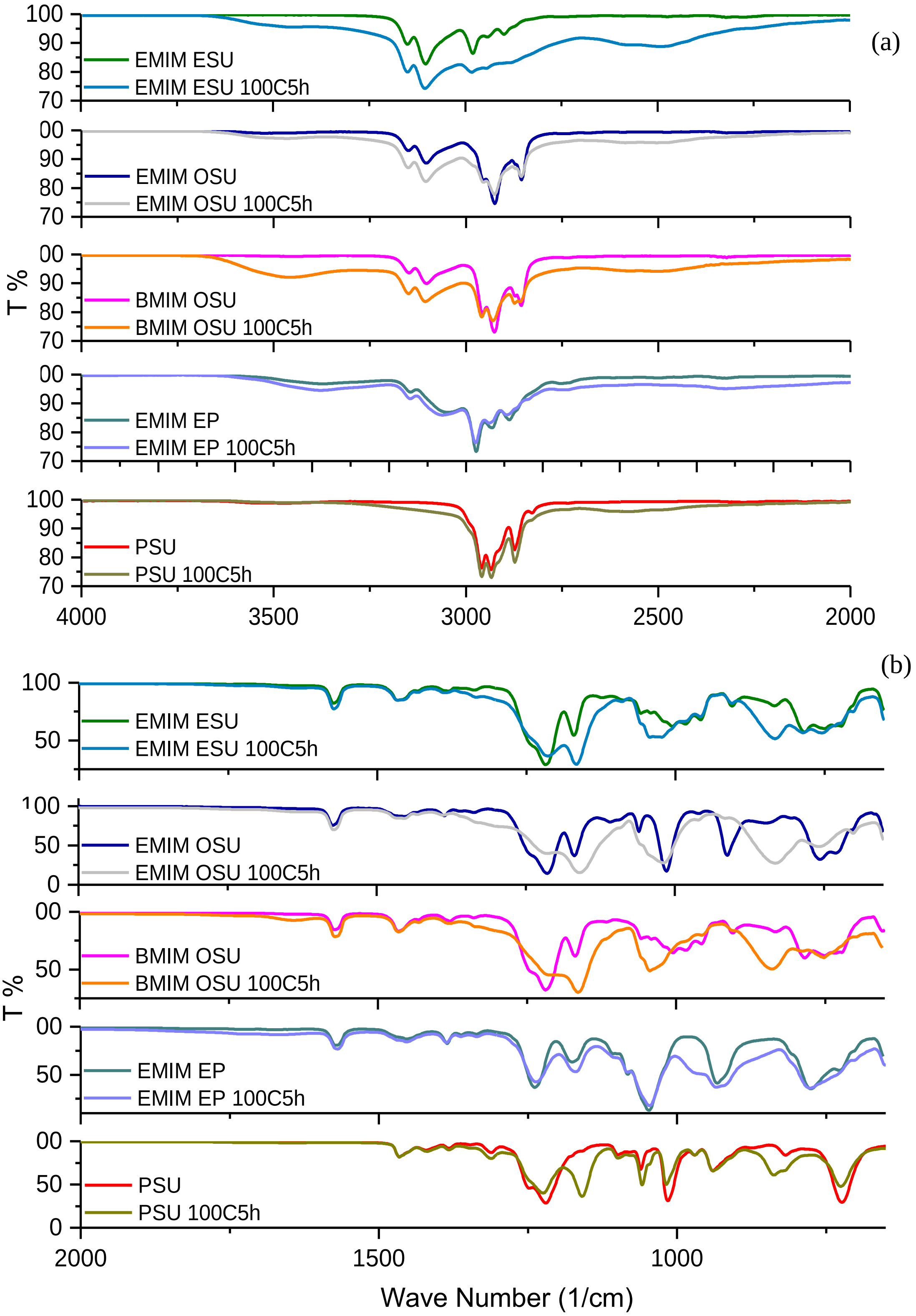

Figure 6-5: IR spectra of five ILs after heating into 100 °C for five hours; (a) spectra between 4000 cm^{-1} and 2000 cm^{-1} and (b) spectra between 2000 cm^{-1} and 650 cm^{-1}.

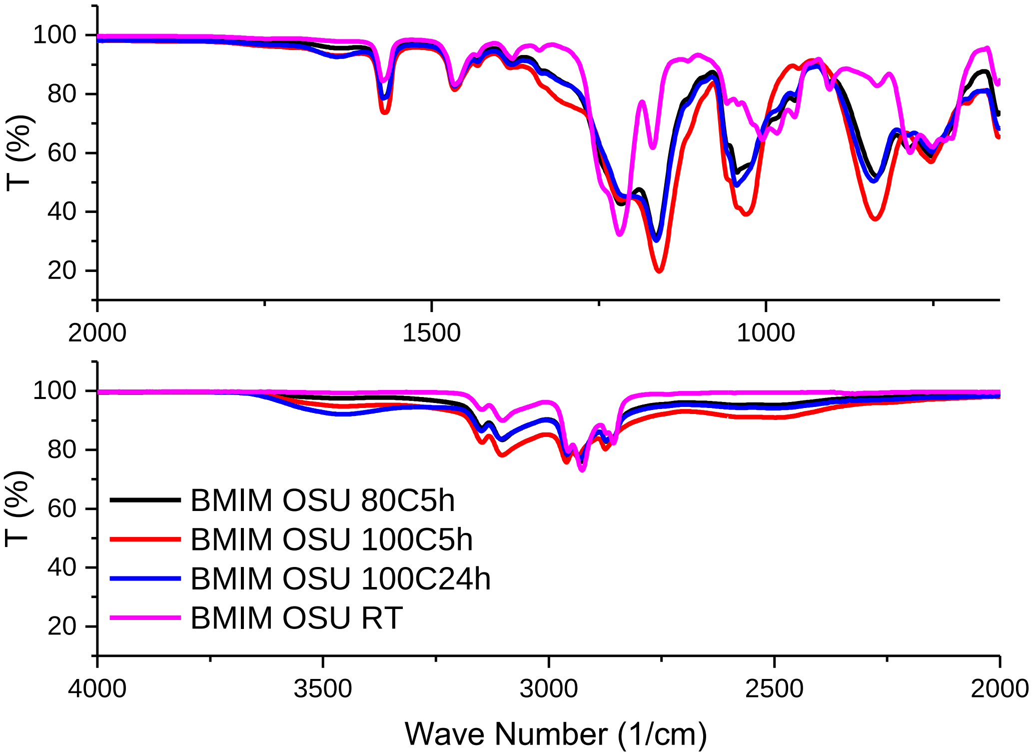

Figure 6-6: Effect of time and temperature on BMIM OSU IR spectra; (a) spectra between 4000 cm^{-1} and 2000 cm^{-1} and (b) spectra between 2000 cm^{-1} and 650 cm^{-1}.

6.3.2 Reactivity of ILs with Silicon Surface at Elevated Temperature.

6.3.2.1 Thermal Decomposition of ILs in the Presence of Silicon Surface

The thermal decomposition process of the examined ILs is investigated in details at the previous subsection (6.4.1). In addition, the effect of the presence of the silicon substrate on the decomposition process is investigated in this study. Fig. 6-7 presents the FTIR spectra of BMIM OSU at room temperature, high temperature (100 ^{o}C for 2h) and at high temperature (100 ^{o}C for 2h) in the presence of the silicon substrate. The assignments of all peaks can be found in the previous section (see table 6-3).

Basically, the heating process leads to a decrease in the intensities of anion (sulfate) related peaks while the intensities of cation (imidazolium) related peaks increase.

The FTIR results of the previous section (in the absence of silicon) suggest that the decomposition starts from the anion which leads to a decrease in the concentration of anion moieties and increase the concentration of cation moieties.

It is clear that the presence of silicon substrate decreases the intensities (concentration) of cation (imidazolium) related peaks at 3150 cm^{-1}, 3100 cm^{-1} and 1574 cm^{-1} (see Fig.6-7a). In contrast, the intensities of anion (sulfate) related peaks increase (see Fig. 6-7b). The rest of the peaks that are assigned to hydrocarbons show comparable intensities in both cases; either in the presence or absence of silicon.

These results suggest that the presence of silicon catalyses the cation to decompose. The increase of the intensities of anion-related peaks can be as a result of the reduction of the intensities of cation-related peaks. For the rest of the ILs, a similar behaviour is obtained since the presence of silicon also catalyses the decomposition of the phosphonium cation in PSU and the imidazolium cation in EMIM EP.

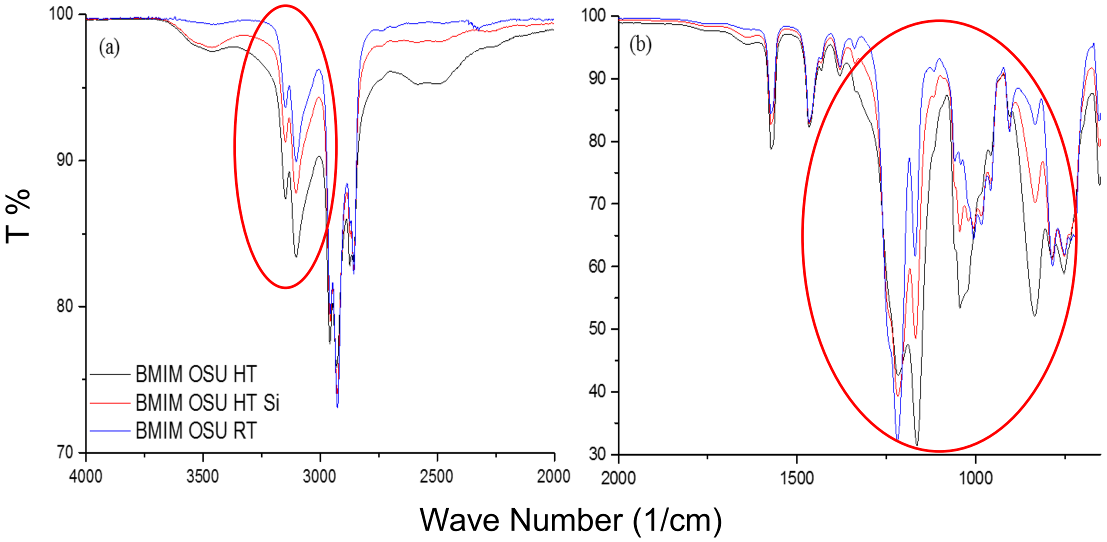

Figure 6-7: FTIR spectra for BMIM OSU IL at room temperature, 100 °C for 2h (HT) in the absence of silicon substrate and 100 °C for 2h (HT Si) in the presence of silicon substrate for (a) wave number between 4000 and 2000 cm^{-1} and (b) wave number

6.3.2.2 Thermal Film Chemistry

FTIR is employed to detect the formation of thermal film by scanning silicon sample before and after the generation of thermal films. However, the same spectra are obtained in both cases which means that the film is not thick enough to be detected by FTIR at the employed setup (see Fig. 6-8).

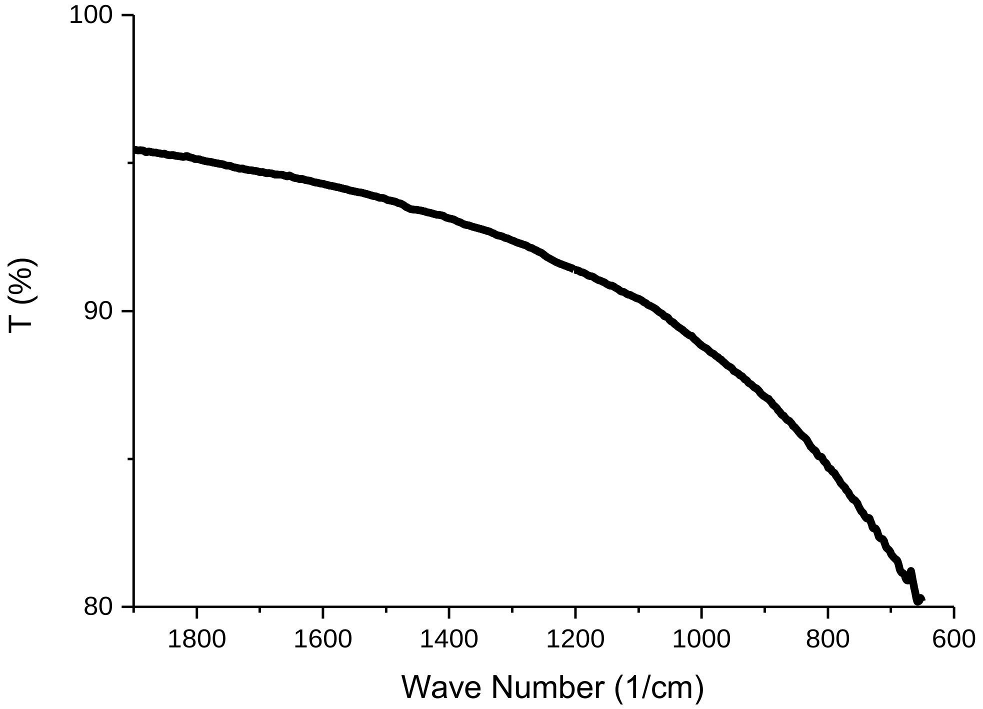

Figure 6-8: FTIR results for silicon substrate before after the generation of thermal films of all examined ILs.

XPS is then utilized to detect the formation of the thermal films and define their chemistry. The formation of the thermal films is detected based on the presence of either cation or anion elements; nitrogen, phosphorus and sulfur. However, phosphorus exists in the n-type silicon and thus the ratio of P2s to Si2s is calculated for silicon substrate before the generation of thermal film. The increase of this ratio means that phosphorus content is increased due to the formation of the thermal film.

For imidazolium sulfate ILs, both nitrogen and sulfur elements are scanned at high resolution regions when the former comes from the imidazolium cation and the latter comes from the sulfate anion. Fig. 6-9 presents XPS results of N1s for all imidazolium based ILs. It is clear that the thermal films generate from the first applied condition (80 ^{o}C for 2 hours).

N1s peaks are obtained from all imidazolium based ILs and are fitted with two peaks. The first peak is at 399.8 eV and the second one is at 401.6 eV. The former is assigned to SiNxOy and the latter to the nitrogen-containing hydrocarbons. The slight increase of the binding energy of SiNxOy peak can be as a result of the increase of the oxygen content. These assignments are in agreement with [182].

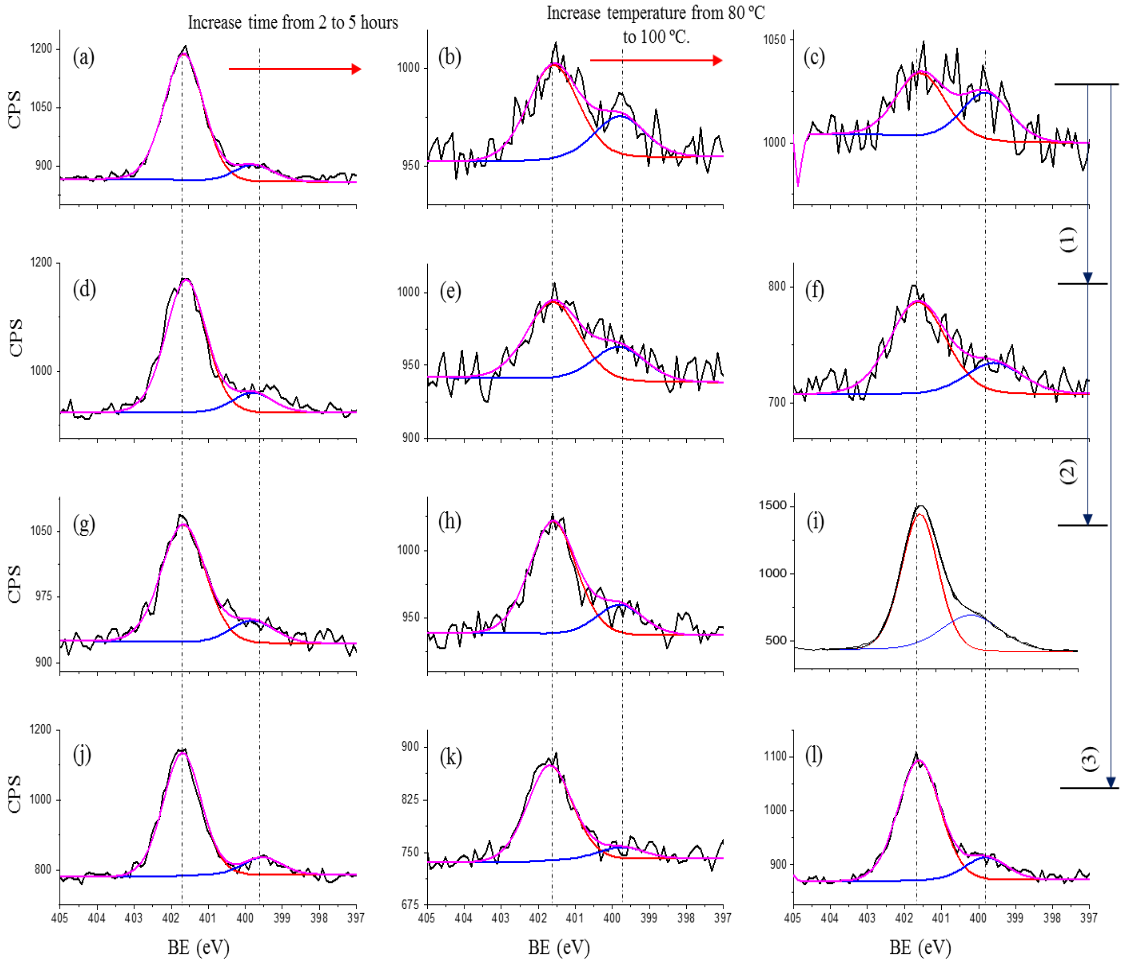

1: Increase anion chain length, 2: increase cation chain length and 3: change anion type.

Figure 6-9: N1s peaks for: (a) EMIM ESU at 80 ^{0}C 2h, (b) EMIM ESU at 100 °C 2h, (c) BMIM OSU at 100 °C 5h, (d) EMIM OSU at 80 °C 2h, (e) EMIM OSU at 100 °C 2h, (f) EMIM OSU at 100 °C 5h, (g) BMIM OSU at 100 ^{0}C 2h, (h) EMIM EP at 100 ^{0}C 2h, (i) EMIM ESU at 100 ^{0}C 5h, (j) EMIM OSU at 100 ^{0}C 5h, (k) BMIM OSU at 100 ^{0}C 5h and (l) EMIM EP at 100 ^{0}C 5h.

It is clear that the increase of either the cation chain length or the anion chain length leads to increase in the ratio of SiNxOy to nitrogen contains organics (increase the amount of the reacted nitrogen). This finding suggests that the increase of anion/cation chain length leads to an increase in the reactivity of IL. The change of the anion from sulfate to phosphate decreases the ratio of SiNxOy-related peak to nitrogen-containing hydrocarbons-related peak. This finding suggests that the reactivity of the imidazolium cation is higher when it is combined with the sulfate anion rather than the phosphate anion. The increase of either time or temperature also leads to a decrease in the ratio of SiNxOy-related peak to nitrogen-containing organic-related peak. This suggests that the increase of time and/or temperature leads to increase the adsorption rate in a rate higher than the reaction.

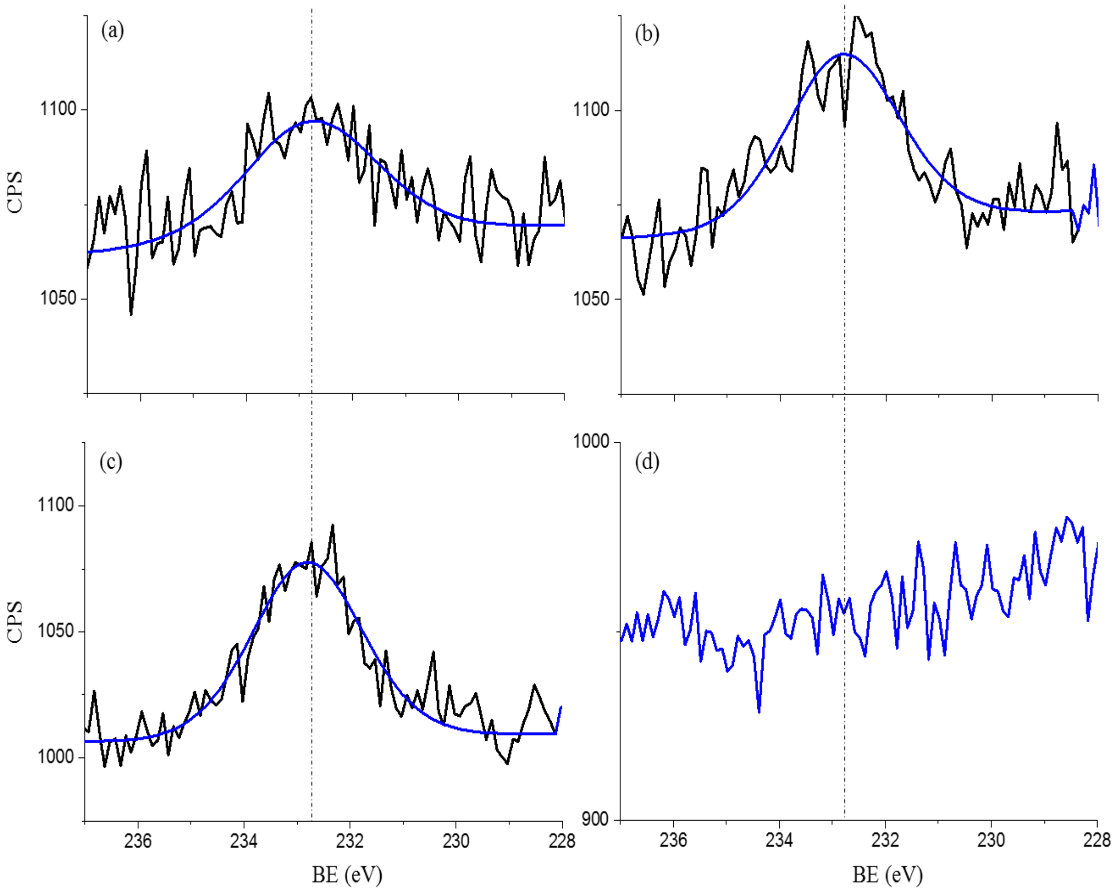

Figure 6-10: S2s peaks for: (a) EMIM ESU, (b) EMIM OSU, (c) BMIM OSU and (d) PSU.

S2s is scanned to detect the presence of the anion-related moieties in the thermal films of imidazolium sulfate ILs. The decomposition of sulfate at the applied temperatures is occurred (see Fig. 6-7).

However, the S2s peak is detected only in one spot out of three scanned spots. Fig. 6-10 depicts the obtained peaks for S2s in the thermal films generated at 100 ^oC and for 5h. It can be seen that only one peak at 232.8 eV is obtained. It is assigned to SO_3 [115]. A peak with the same binding energy is obtained at the rest applied conditions with lower intensity ratio (S2s to Si2s ratio). This finding suggests that SO_3 adsorbs to the silicon surface after the decomposition process. The intensities of the SO_3-related peaks are decreased as a result of the decomposition process (see table 6-3 and Fig. 6-5).

As expected, the increase of either anion chain length or cation chain length increases the adsorption rate due to the increase of the decomposition rate. SO_3 diminishes when the cation is changed from imidazolium to phosphonium. This finding is in agreement with the thermal decomposition results when phosphonium sulfate IL shows higher thermal stability than imidazolium sulfate.

Fig. 6-11 presents the XPS results of P2s peaks of silicon before the generation of the thermal film and after the generation of PSU and EMIM EP thermal films at 80 ^oC 2h, 100 ^oC 2h and 100 ^oC 5h. The intensity ratio of P2s to Si2s for silicon before the generation of thermal film is 0.5. The generation of thermal film results in an increase in the intensity ratio of P2s peak to Si2s peak which suggests that a surplus of phosphorus exists after the formation of the thermal film. This finding means that phosphorus adsorbs onto silicon. In addition, a new peak at 191.5 eV forms which is assigned to phosphorus that bonded with silicon through oxygen, Si-O-P [148]. The increase of temperature leads to an increase in the intensity ratio of Si-O-P to phosphorus peak which suggests the increase of temperature increases the formation process of Si-O-P (see Fig. 6-11). The increase of time from 2h to 5h at 100 ^oC leads to an increase in the intensity ratio of P2s peak to Si2s in PSU while Si2s is totally diminished in EMIM EP. This can be as a result of the increase of the adsorption rate of phosphorus.

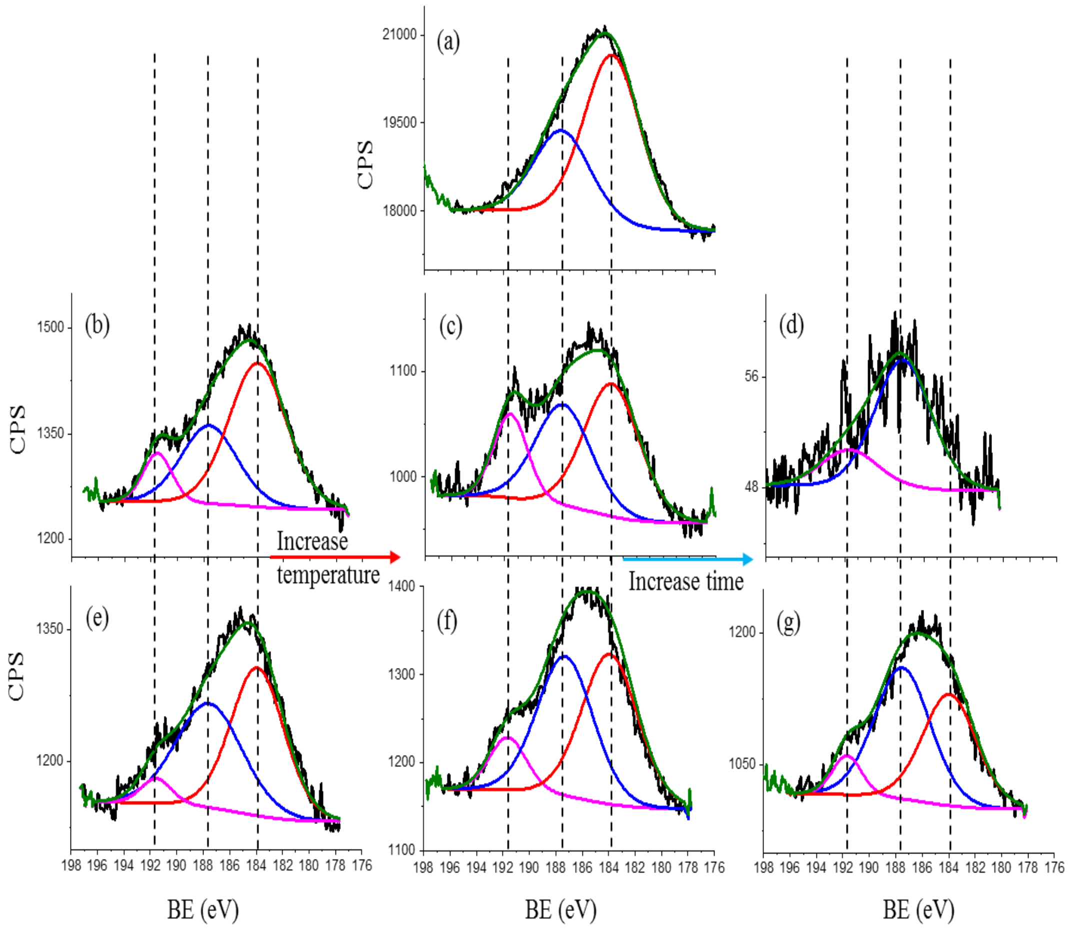

Figure 6-11: P2s peak for: (a) silicon before experiment, (b) EMIM EP 80 °C 2h, (c) EMIM EP 100 °C 2h, (d) EMIM EP 100 °C 5h, (e) PSU 80 °C 2h, (f) PSU 100 °C 2h and (g) PSU 100

6.3.2.3 Thermal Film Morphology

Film morphology is characterized by AFM since it could not be detected by White Light Interferometry due to its transparency. Fig. 6-12 depicts the morphology of silicon before after the formation of the thermal films. It is obvious that thin films are created by ILs; below 10 nm. However, both thickness and consistency are effected by IL chemistry.

It is clear that homogenous films are created with comparable thicknesses. However, the sulfate anion presents thinner film than the phosphate anion when both are combined with imidazolium. The phosphonium cation demonstrates thinner film than the imidazolium cation when both are combined with the sulfate anion. The increase of either anion chain length or cation chain length also leads to increase film thickness.

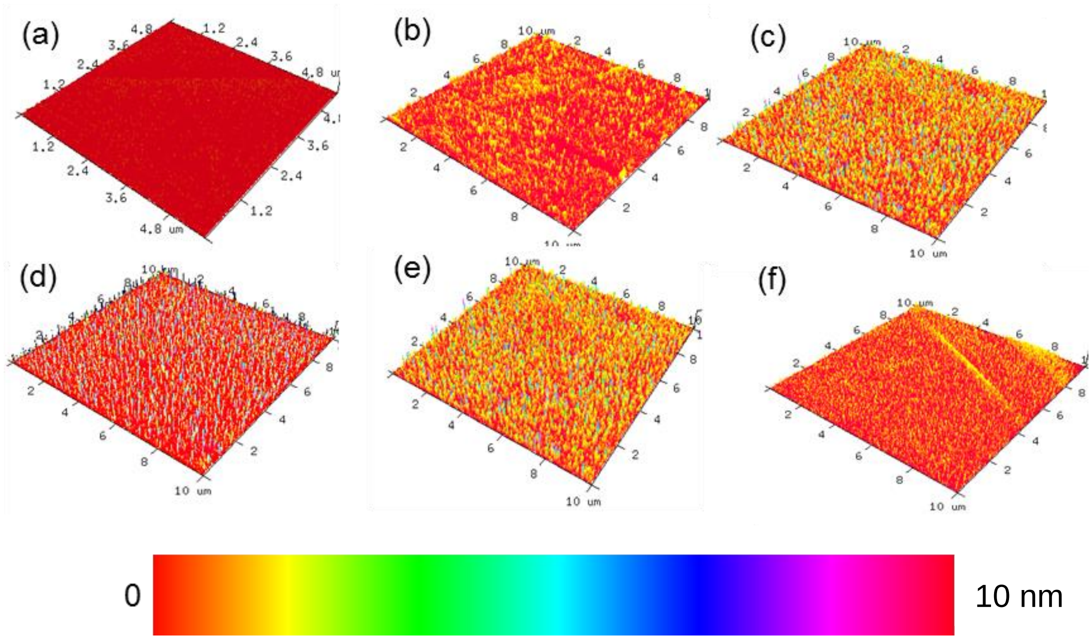

Figure 6-12: The surface morphology of (a) silicon before formation of thermal film and for thermal films that formed at 100 ^{o}C for 5 hours for: (b) EMIM ESU, (c) EMIM OSU, (d) BMIM OSU, (e) EMIM EP and (f) PSU.

6.3.2.4 Thermal Films Durability

A tribological motion has been applied to examine the durability of the created films. The results of friction and wear coefficients are presented in Fig. 6-13 and Fig. 6-14 respectively. It is obvious that the friction coefficients of all samples are very comparable (see Fig. 6-13). This might be as a result of the low thickness of the generated films (see Fig. 6-12).

The results of wear show that the presence of thermal film can provide a reduction in the wear coefficient in comparison with silicon sample without any thermal film.

It is clear that BMIM OSU presents the thermal film with the highest durability. A considerable reduction is also obtained the PSU thermal film. The wear coefficients for the rest three ILs thermal films are very comparable and slightly less than that obtained in the silicon without thermal film (see Fig. 6-14).

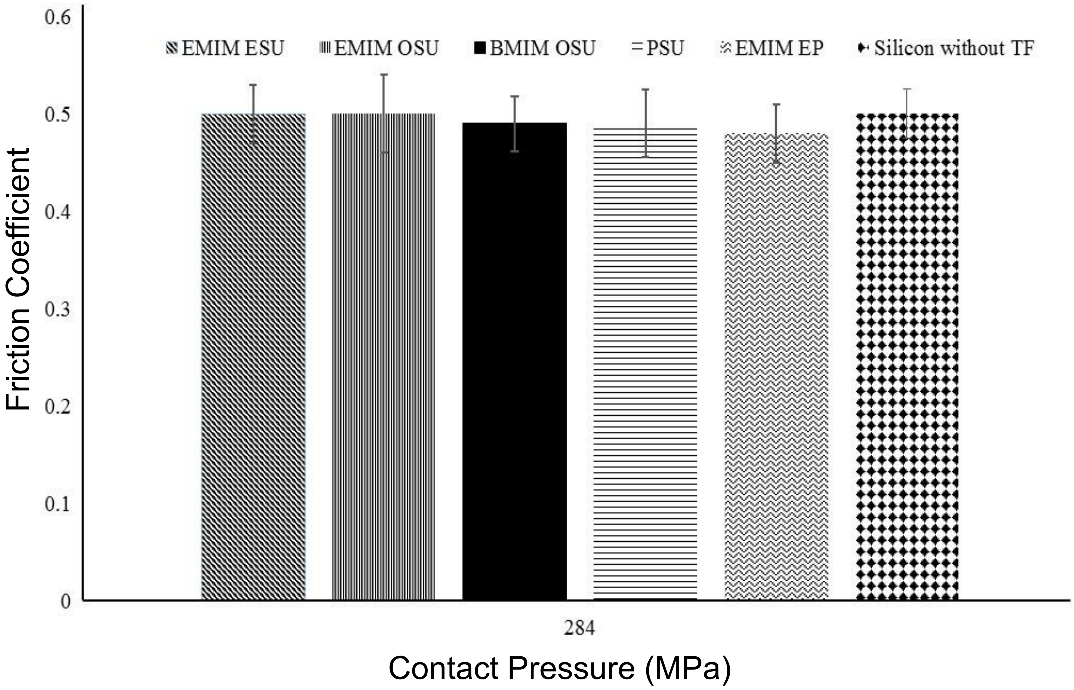

Figure 6-13: Friction coefficients for silicon before and after the generation of ILs' thermal films.

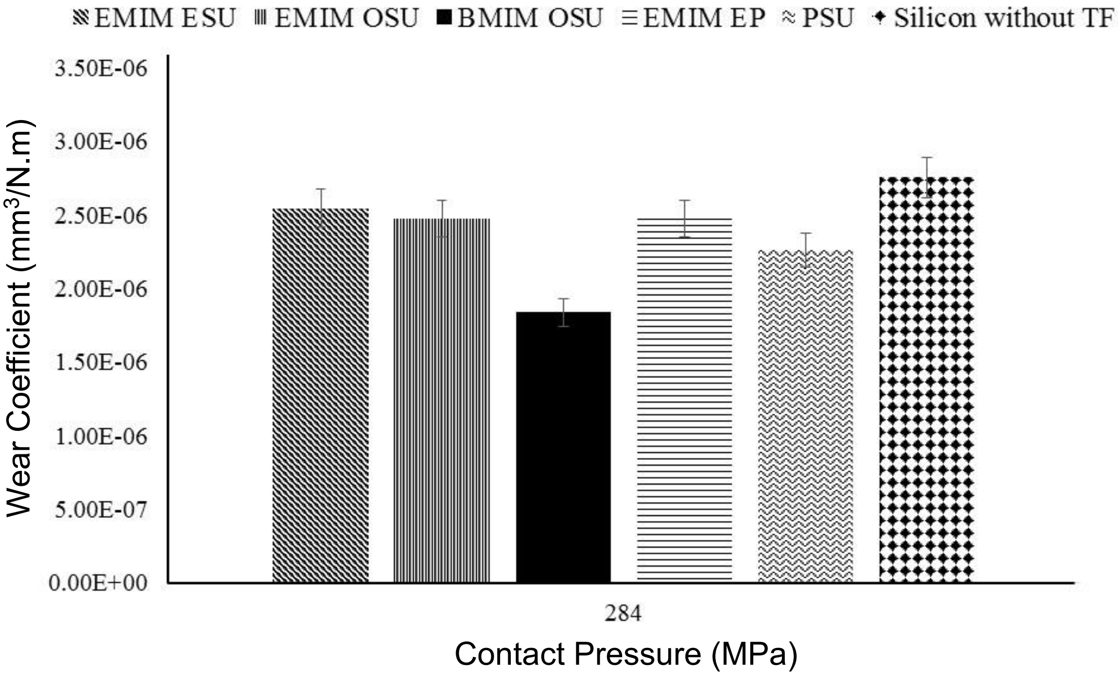

Figure 6-14: Wear coefficients for silicon before and after the generation of ILs' thermal films.

Lastly, it is clear that the increase of either anion or cation chain length enhances the durability of the generated film. The increase of cation chain length shows a more significant effect.

In terms of the effect of the anion type, the generated films that resulted from both anions (sulfate and phosphate) show a comparable durability. The effect of cation is more obvious and phosphonium cation’s thermal film shows a more durability than imidazolium one (in EMIM ESU).

6.4 Discussion

6.4.1 Comparison Between Dynamic and Static Thermal Decomposition

The use of TGA (in non-isothermal mode) to predict the thermal stability of ILs can result in an overestimation for their stability as also pointed out in [139, 179]. The use of FTIR to assess the thermal stability of ILs can provide more accurate results. The partial thermal decomposition can be captured by the static thermal decomposition (using FTIR).

However, the results of both techniques show that the thermal decomposition of ILs is strongly affected by IL chemistry. Consequently, the increase of either cation or anion chain length results in a reduction of the thermal stability of ILs in both techniques. In addition, phosphate anion is more stable than sulfate anion. This finding suggests that TGA overestimates the decomposition temperature but it can provide a good prediction when it is utilized for comparison purposes.

6.4.2 Thermal Decomposition Mechanism

The decomposition mechanisms are obtained from the static decomposition results. For imidazolium sulfate ILs, decomposition starts from the anion (see Figs. 6-5 and 6-15). The decomposition process starts when the concentrations (intensities) of the sulfate-related peaks decrease. The second step is the breaking of anion chain length when SO_4 and C-O-S-O peaks are diminished.

For EMIM EP, the decomposition only occurs in the hydrocarbons since a slight reduction in their intensities was observed. The increase of the intensity of OH peak confirmed that a partial decomposition occurs in the hydrocarbons (See Fig. 6-5). Besides, PSU IL demonstrates a partial decomposition in the sulfate anion results a formation of methyl sulphoxides (See Fig. 6-5). This suggested that the decomposed sulfur is bonded with CH_3 instead of O.

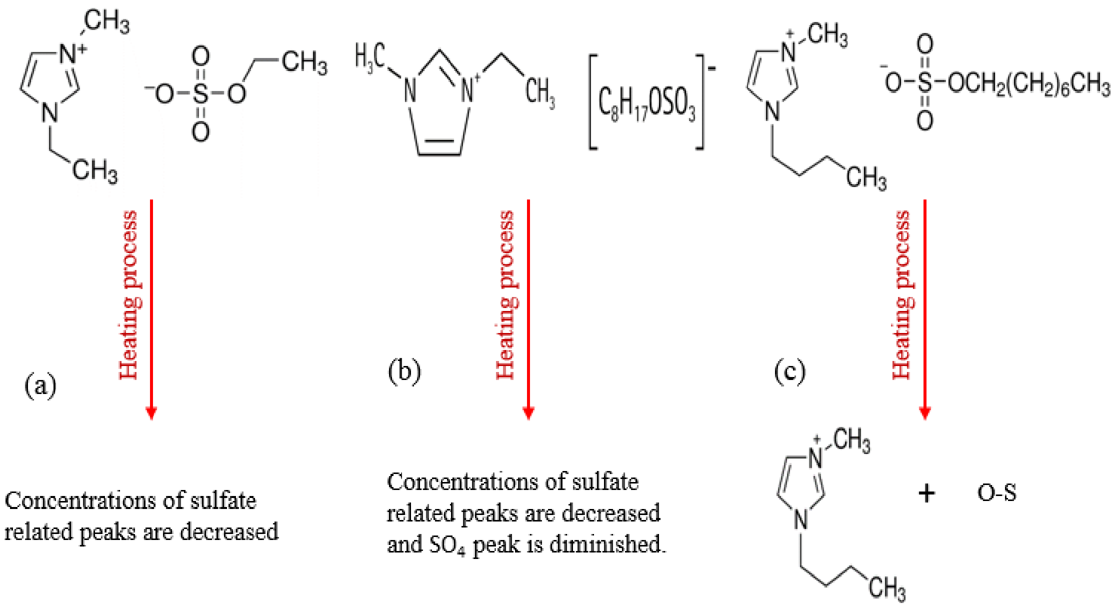

Figure 6-15: Thermal decomposition mechanism for: (a) EMIM ESU, (b) EMIM OSU and (c) BMIM OSU.

6.4.3 Effect of Time and Temperature on the Decomposition Process

The increase of either time or temperature demonstrates an increase in the concentration of the decomposed species. However, the increase of temperature demonstrates a higher influence than time, see Fig. 6-6. This finding suggests that at a particular temperature, the decomposition has a particular rate, and the increase of temperature leads to increase the decomposition rate. This finding is in agreement with Arrhenius equation [183] since it states that the rate constant is increased with temperature. The increase of time leads to an increase in the concentration of the decomposed bonds due to the increase of their amount at constant decomposition rate.

6.4.4 Film Formation Mechanism

For the imidazolium sulfate ILs, Fig. 6-16 summarizes the formation mechanism of their thermal films. The process starts when ILs are partially decomposed after heating them to 80 ^{o}C. Referring to Figs 6-7 and 6-8, SO_3 results from the partial decomposition of anion moiety adsorbs into silicon surface. Nitrogen results from the partial decomposition of the cation moiety and both adsorbs to and reacts with the silicon surface to form nitrogen-containing organic species and SiNxOy respectively (see Figs. 6-7 and 6-10).

The increase of either time or temperature leads to an increase in the ratio of SiNxOy peak to nitrogen-containing organic species peak. This suggests that the increase of the formation of SiNxOy is higher than the adsorption of nitrogen-containing hydrocarbons.

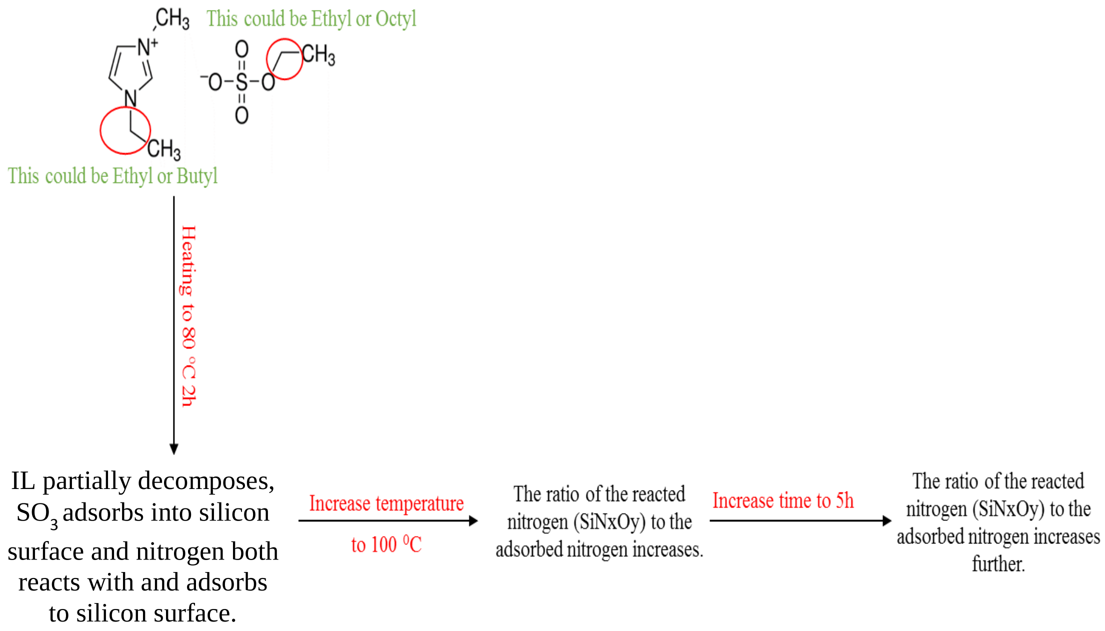

Figure 6-16: The formation mechanism of thermal film of imidazolium based ILs.

The formation mechanism of PSU thermal film is presented in Fig. 6-17. For both temperatures the anion moiety could not be detected. This finding is expected since PSU showed a higher thermal stability than imidazolium sulfate (see Figs. 6-1 and 6-3).

Phosphorus that comes from phosphonium cation reacts with and adsorbs to silicon (see Fig. 6-11).

The increase of either time or temperature increases the ratio of the adsorbed phosphorus to the Si2s. In addition, the increase of temperature increases the intensity ratio of Si-O-P related peak to P2s peak. However, the increase of time show a contrasting behaviour since it leads to increases the deposition of phosphorus.

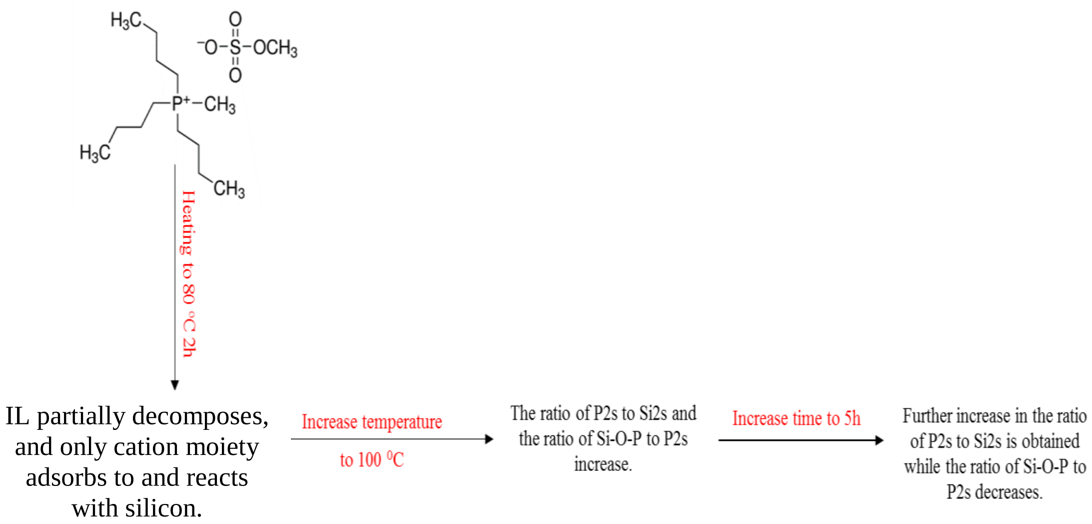

Figure 6-17: The formation mechanism of thermal film of PSU.

Fig 6-18 demonstrates the formation mechanism of EMIM EP thermal film. From the first applied temperature, 80 °C, both the imidazolium cation and the phosphate anion react with and adsorb to the silicon surface. These processes lead to format of a thermal film consisting of P, Si-O-P, SiNxOy and nitrogen-containing organic species (see Figs 6-9 and 6-10).

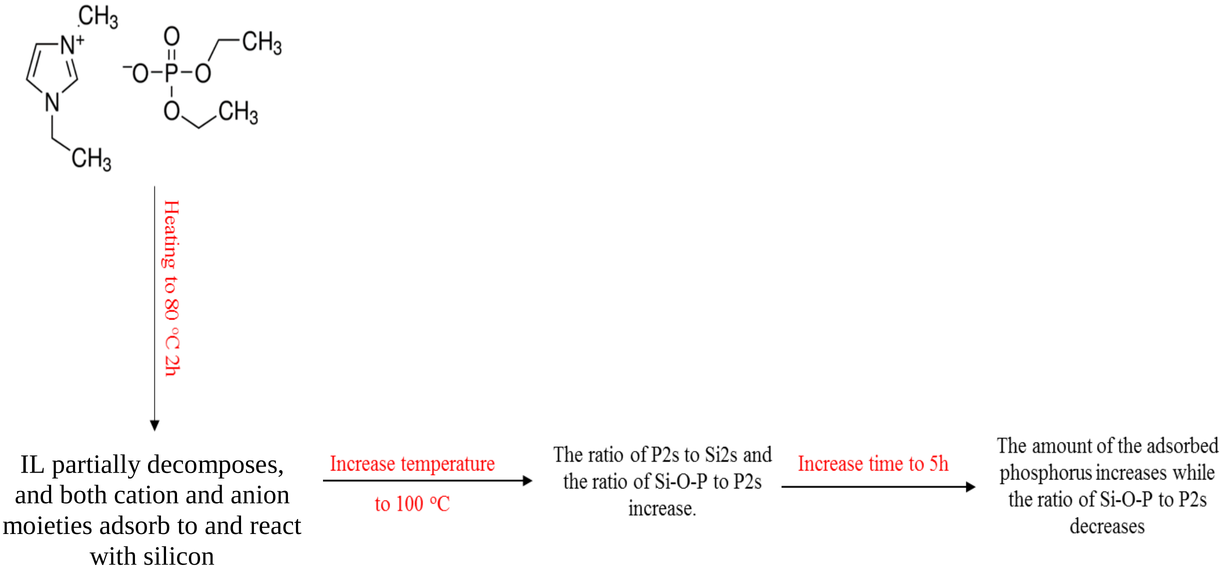

Figure 6-18: The formation mechanism of thermal film of EMIM EP.

The increase of either time or temperature shows a comparable ratio of the adsorbed nitrogen to the reacted nitrogen (SiNxOy). In contrast, the increase of either time or temperature increases the ratio of P2s to Si2s which means that the adsorption of phosphorus increases.

The increase of temperature from 80 ^{o}C 100 ^{o}C leads to increase the ratio of Si-O-P to P2s which means the formation rate of Si-O-P increases with temperature. However, the increase of time from 2h to 5h leads to decrease the ratio of Si-O-P to P2s which suggests that the formation of Si-O-P is limited as pointed out in chapter four.

6.4.5 Effect of IL Chemistry on the Formation of the Thermal Film.

The variation of ILs chemistry plays a crucial role in the formation mechanism and the chemistry of the generated thermal films. Starting from the effect of anion/cation chain length; its increase results in an increase in the reactivity of IL. This can be correlated to the reduction of the thermal stability of IL as a result of increasing anion/cation chain length (see Fig. 6-2). However, the same species are obtained in all imidazolium sulfate ILs regardless to the anion/cation chain length.

Besides, the variation of anion type being substantial; in contrast to the sulfate anion, the phosphate anion demonstrates an ability to react with silicon and form Si-O-P film in addition to the adsorption of phosphorus under all the applied conditions. However, imidazolium cation shows higher reactivity when it is combined with the sulfate anion rather than the phosphate anion. Fig. 6-9 confirms that when the ratio of SiNxOy to nitrogen-containing organic species is higher in the EMIM ESU thermal film than EMIM EP thermal film. In addition, the ratio of N1s peak to Si2s peak is slightly higher in the EMIM ESU.

The variation of cation type is again crucial and affects the formation mechanism of thermal film and its chemistry. Both the reactivity of cation and the ability of anion (sulfate) to adsorb into silicon are effected. Both cations demonstrate their reactivity with silicon and also their ability to be adsorbed into silicon. However, SO_3 is only detected when sulfate combines with imidazolium (see Fig. 6-10). This can be correlated to the higher thermal stability of PSU than EMIM ESU (see Fig. 6-2).

In addition, the chemistry of IL has a considerable effect of the durability of the generated film (see Fig. 6-14).

These findings together confirm that IL chemistry is crucial and the combination of anion-cation is also crucial. Sulfate showed higher reactivity when combined with imidazolium rather than phosphonium and imidazolium showed higher reactivity when combined with sulfate rather than phosphate.

6.5 Conclusions

In this chapter, both thermal stability and the reactivity of five ILs have been investigated. In addition, the influence of IL chemistry on their thermal stability and their reactivity has been considered. The following conclusions have been drawn:

- TGA provides an overestimation to the onset temperature of ILs. However, it provides an acceptable prediction to the effect of IL chemistry on their thermal decomposition.
- The increase of either cation chain length or anion chain length decreases the thermal stability of IL due to the decrease of the stability of carbocation.
- Both anion type and cation type influence on the thermal decomposition mechanism of IL. However, anion is more crucial in the determination of the thermal decomposition of IL.
- Phosphate anion is more stable than sulfate anion when both are combined with imidazolium cation.
- The decomposition is started from the anion rather than cation.
- The increase of temperature increases the thermal decomposition rate.
- All ILs have reacted with silicon surface and a thin thermal film has been created, a few nano meters.
- IL chemistry is crucial in the determination of the reactivity of IL, thermal film chemistry and the thermal film thickness.
- The increase of anion/cation chain length lead to enhance the reactivity of IL and then increase thermal film thickness.
- Phosphate anion showed higher reactivity than sulfate anion.

- The combination of anion-cation is also crucial since SO3 is only obtained when sulfate combined with imidazolium and higher amount of nitrogen is obtained when imidazolium combined with sulfate rather than phosphate.

7. Chapter 7: Lubrication mechanism of neat ILs in various tribological conditions

7.1 Introduction

The use of neat ILs as potential lubricants is not feasible in many applications due to their high cost. They have been recommended to be used as potential lubricants mainly in two applications; to lubricate MEMS or to lubricate moving parts in space vehicles. A small amount is required in the former application and the high cost can be afforded in the latter application [3-6]. In this chapter, silicon based materials are employed and a micro scale study is conducted to simulate the working of MEMS [109, 115].

Despite the large number of previous studies that examined the tribological performance of ILs, the relationship between their tribological performance and tribofilm formation ability is still not fully understood. Further, the relation between ILs' chemistry and their tribological behaviour is not fully understood. Previous studies focused mainly on the investigation of the tribological performance of various ILs (propose various ILs to lubricate various tribopairs) [3-6].

Some previous macro-scale studies considered the relation between the ILs' chemistry and their tribological performance. For instance, several studies [24-27] found that the increase of the cation chain length enhances the tribological performance of ILs. Other studies examined the effect of either anion or cation type.

They found that the halogen-free anions showed better tribological performance than halogenic ones. The phosphonium cation exhibited a lower friction coefficient than imidazolium [26, 107]. However, it should be noted that the occurrence of tribocorrosion processes in the previous studies due to the use of the halogenic ILs can affect the comparison (halogenic ILs show high friction and wear coefficients). To reveal the influence of anion/cation type, both ILs must be non-halogenic. Furthermore, there is a contrast in the literature whether the formation of tribofilm is started by either cation [24] or anion [26, 90]. Therefore, this study is conducted to reveal the effect of IL chemistry on their tribological performance and their ability to form a tribofilm.

To understand the relationship between the formation of tribofilm and the tribological behaviour (lubrication mechanism); a various tribological conditions are applied. The formation/destruction of the tribofilm that might result from the increase/decrease of contact pressure, sliding distance or temperature. In addition, the friction and wear coefficients and their relationship with the formation of tribofilm will be studied as well.

Therefore, this chapter will investigate the effect of IL chemistry on their lubrication mechanism at various conditions. The chapter is divided into three parts. The first one will illustrates the effect of contact pressure by applying for various contact pressures. The second one will present the effect of sliding distance by applying three various sliding distances. The last part will demonstrate the influence of temperature by applying two various temperatures.

7.2 Experimental Conditions

The viscosity is measured at temperatures ranging from 20 to 70 ^{o}C. The tribological experiments are conducted by applying a reciprocating motion using NTR with a ball-on-plate configuration.

For all experiments; the following parameters are kept constants: the sliding velocity is 2 mm/s, sliding amplitude is 2 mm and the lubrication regime is boundary (all calculations are provided in subsection 3.4.4). Table 7-1 presents the applied conditions in the investigation of the effect of contact pressure.

Table 7-1: The applied conditions to investigate the effect of contact pressure on the lubrication mechanism.

Condition number	Contact pressure MPa	Contact radius µm	Sliding distance (m)	Temperature (^{o}C)
1	142	6	14.4	25
2	306	13	14.4	25
3	386	16	14.4	25
4	451	19	14.4	25

Then, based on the results of the effect of contact pressure; the effect of sliding distance is conducted at contact pressure 386 MPa, see table 7-2.

Lastly, the effect of temperature is conducted by applying high temperature experiments using the bespoke design described in 3.2.2. Table 7-3 presents the applied conditions. Again, the selection of contact pressure is made based on the results of the effect of contact pressure.

Table 7-2: The applied conditions to investigate the effect of sliding distance on the lubrication mechanism.

Condition number	Contact pressure MPa	Contact radius µm	Sliding distance (m)	Temperature (°C)
1	386	16	3.6	25
2	386	16	14.4	25
3	386	16	36	25

Table 7-3: The applied conditions to investigate the effect of temperature on the lubrication mechanism.

Condition number	Contact pressure MPa	Contact radius µm	Sliding distance (m)	Temperature (°C)
1	386	16	14.4	25
2	386	16	14.4	80

7.3 Results

The results are divided into three main sections. The effect of contact pressure, sliding distance and temperature on the lubrication mechanism and they will be presented in the sections 7.3.1, 7.3.2 and 7.3.3 respectively.

7.3.1 Viscosity

The IL viscosities are measured across a temperature range between 20 and 70 °C and the results are presented in Fig. 7-1. The results reveal that ILs' viscosities decrease with the increase of temperature. On the other hand, the increase in chain length of either cation or anion, increases the viscosity due to the increase of both Van der Waals forces and ions' weight [184].

Furthermore, the results show that the phosphonium cation and phosphate anion exhibit a higher viscosity than imidazolium cation and sulfate anion respectively. This is expected due to their higher ions' weight.

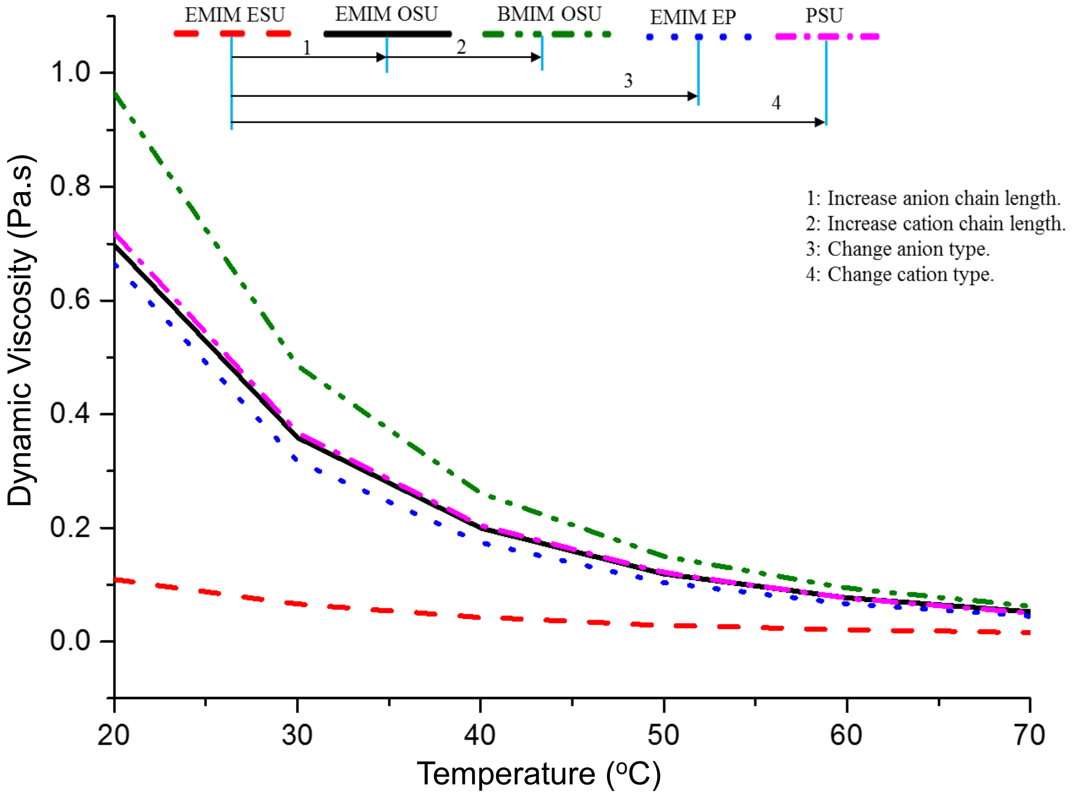

Figure 7-1: ILs viscosity at various temperatures.

7.3.2 Effect of Contact Pressure

7.3.2.1 Friction

Friction coefficients of ILs at various contact pressures are presented in Fig. 7-2. The friction coefficients of all lubricants fluctuate, i.e. either increases or decreases, with the increase in contact pressure. This can be related to the either flattening of the rubbed surfaces [173] or formation of a tribofilm [109].

The results indicate that the increase in chain length of anion or cation leads to a significant reduction in the friction coefficient. This reduction is decreased with the increase in the applied contact pressure. The results also show that anion type and cation type have a considerable effect on friction coefficient especially at the lowest contact pressure. This can be related to the considerable influence of IL viscosity at the lowest contact pressure (see Figs. 7-1 and 7-2).

At the lowest contact pressure, the phosphate anion shows a lower friction coefficient than the sulfate anion. However, at higher contact pressures, a comparable friction coefficient for both anions are obtained.

The phosphonium cation exhibits a lower friction coefficient than imidazolium cation especially at the lowest contact pressure. The increase in contact pressure decreases the difference between the friction coefficients of both cations (phosphonium and imidazolium) though the former continued to maintain its lower friction.

The behaviour of friction coefficients over the sliding distance is presented in Fig. 7-3. As mentioned in section 3.4, each experiment has been repeated at least two times and in most cases three times. The presented friction coefficients are the average of at least two tests (see Fig.7-3 the behaviour of EMIM ESU friction coefficient at 142 MPa). The increase in the chain length of either cation or anion results in a higher stability in the friction coefficient (less fluctuation). The phosphate anion shows higher stability in friction coefficient than sulfate anion at the lowest contact pressure (see Fig. 7-3a). However, at higher contact pressures, the sulfate anion exhibits higher stability than the phosphate anion (see Fig. 7-3a, b and c).

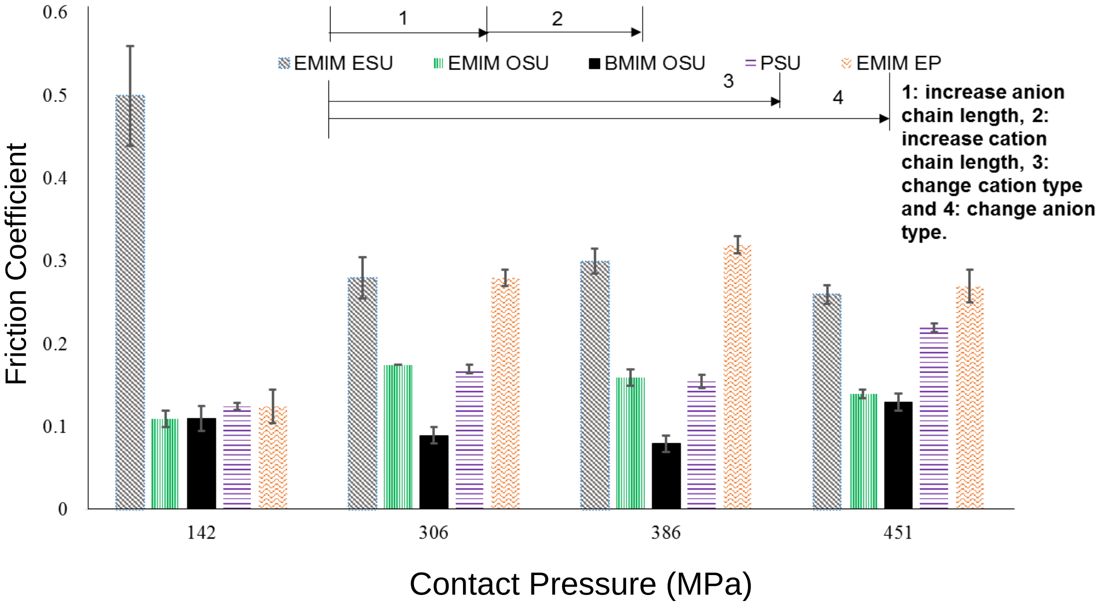

Figure 7-2: Friction coefficient values for five ILs at various contact pressures.

The phosphonium cation shows higher stability in friction coefficient than the imidazolium cation under all contact pressures except at the highest one (451 MPa) when imidazolium exhibits a higher stability.

The friction coefficient behaviour is affected by the presence of third bodies between the interacting surfaces. These can be either wear debris or a formed tribofilm. The presence of wear debris causes a rapid increase in friction coefficient which can be followed by a considerable decrease when debris are removed from the wear track [185]. The continuous fluctuation in friction coefficient suggests that the production of wear debris from silicon surface is still ongoing through the whole test (see Fig. 7-3). This behaviour in silicon was also obtained in [155].

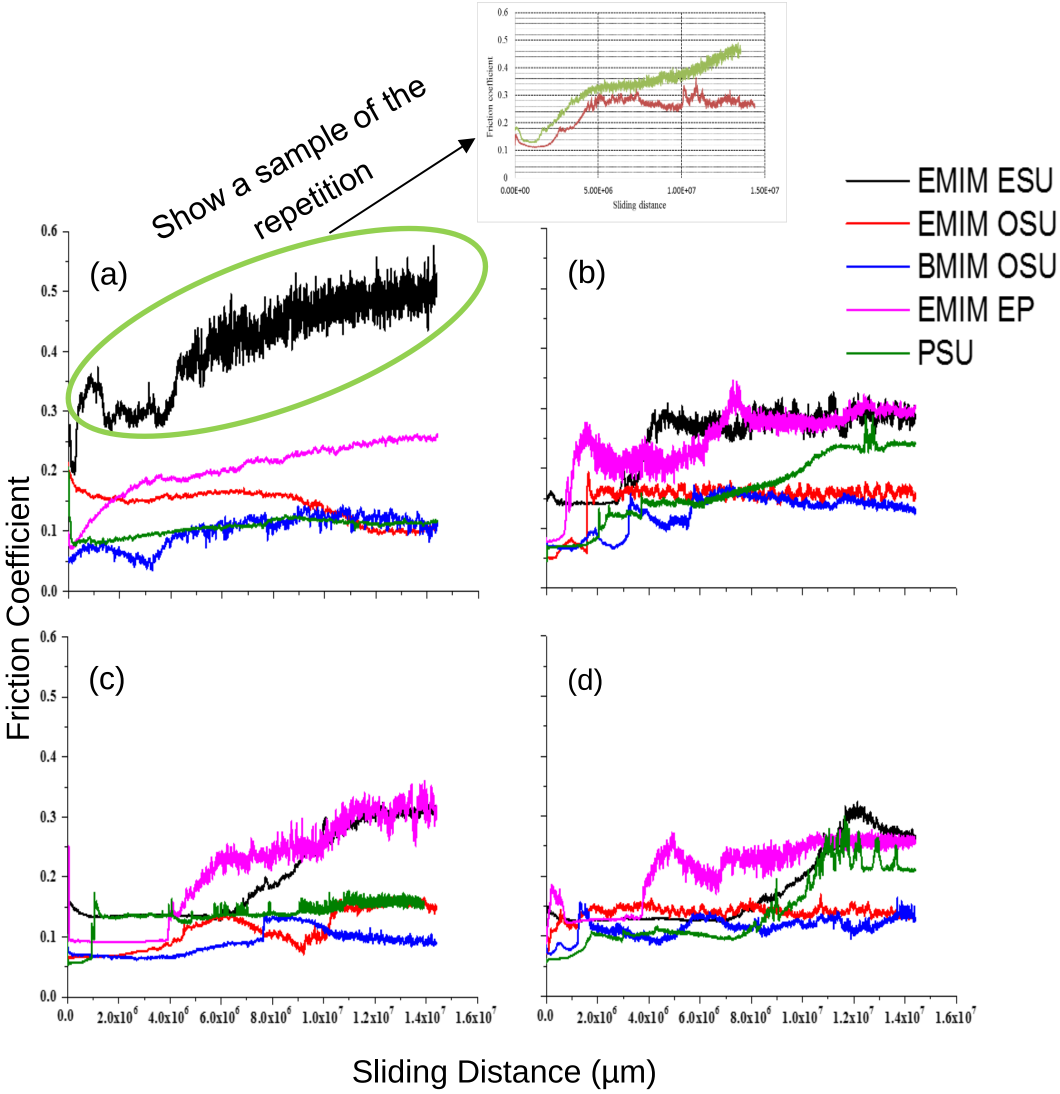

Figure 7-3: Variation of friction coefficient with sliding distance at various contact pressures; (a) 142 MPa, (b) 306 MPa, (c) 386 MPa and 451 MPa.

The instability in the friction coefficient might be also influenced by surface roughness. Table 7-4 presents the obtained average surface roughness values inside wear tracks.

It is obvious that friction coefficient does not controlled by surface roughness. Surface roughness values increase with contact pressure despite the reduction of friction coefficient with the increase of contact pressure.

Table 7-4: The average surface roughness inside wear tracks.

Contact Pressure MPa	EMIM ESU	EMIM OSU	BMIM OSU	PSU	EMIM EP
306	6.0 nm ±0.6	5.5 nm ±0.3	5.5 nm ±0.25	15.0 nm ±0.9	8.0 nm ±0.5
386	10.0 nm ±0.8	6.5 nm ±0.4	4.0 nm ±0.1	12.0 nm ±1.0	5.0 nm ±0.1
451	16.0 nm ±1.2	7.0 nm ±0.15	11.0 nm ±0.8	15.0 nm ±0.6	9.0 nm ±0.7

7.3.2.2 Wear

Surface morphology is characterized using 3D optical microscopy including the quantification of wear volume. No wear was detected at the lowest contact pressure. However, the higher contact pressures significantly alter the wear performance of ILs. Fig. 3.4 presents the wear coefficients for five ILs. The results clearly show that the longer the chain length of either cations or anions, the lower the wear of the system. Furthermore, the phosphonium cation showed lower wear coefficient than imidazolium at the lowest and moderate contact pressures (306 and 386 MPa). On the other hand, imidazolium shows lower wear coefficient at the highest contact pressure (451 MPa). In terms of the effect of anion type, phosphate anion also shows lower wear coefficient than sulfate anion at both low and moderate contact pressures (306 and 386 MPa). However, the sulfate anion IL shows lower wear coefficient than the IL with the phosphate anion at the highest contact pressure (451 MPa).

It is clear that the lowest wear coefficient for three of the tested ILs (BMIM OSU, EMIM EP and PSU) is obtained at the moderate load (386 MPa). This might suggest that at this contact pressure the tribofilm exists.

For EMIM ESU and EMIM OSU, the lowest wear rate is observed at the highest contact pressure, which suggests that the required load to form a tribofilm higher than the other tested ILs. The results of surface chemistry will either confirm or refute this hypothesis.

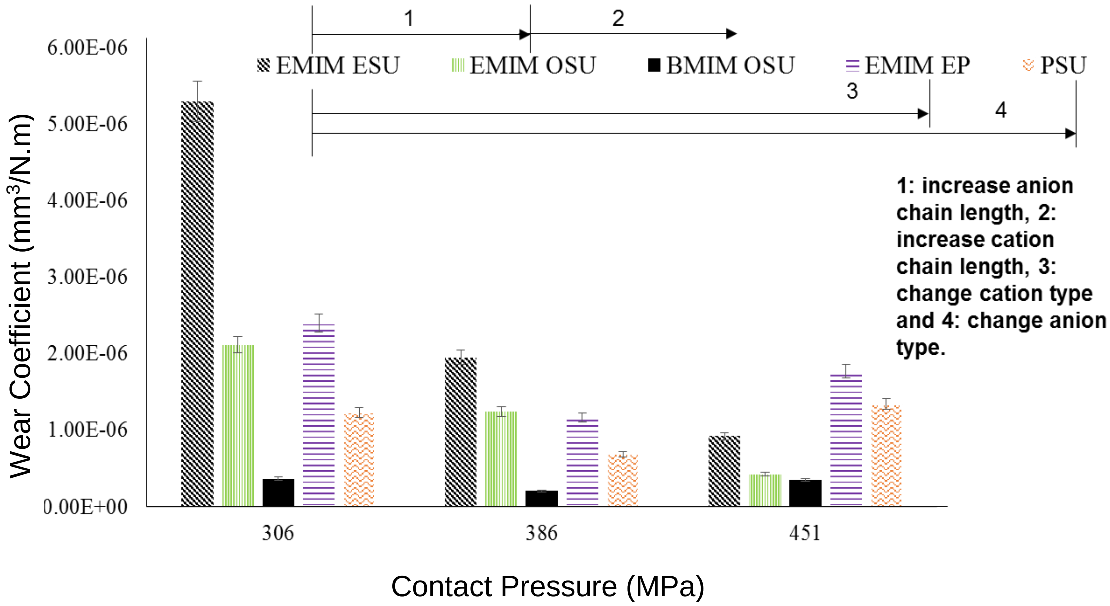

Figure 7-4: Wear coefficient values for five ILs at various contact pressures.

The surface morphology of the surfaces tested with EMIM ESU and EMIM EP ILs are shown in Figs. 7-5 and 7-6, respectively. The results show that the increase in contact pressure increases the width of the wear track, as expected. However, the depth of wear tracks decreases with the increases of contact pressure in EMIM ESU and EMIM OSU (see Fig. 7-5).

The highest depth of the wear track appears to occur at low contact pressure (306 MPa) in the case of BMIM, PSU EMIM EP. Although, the lowest depth of the wear track appears to occur at (386 MPa).

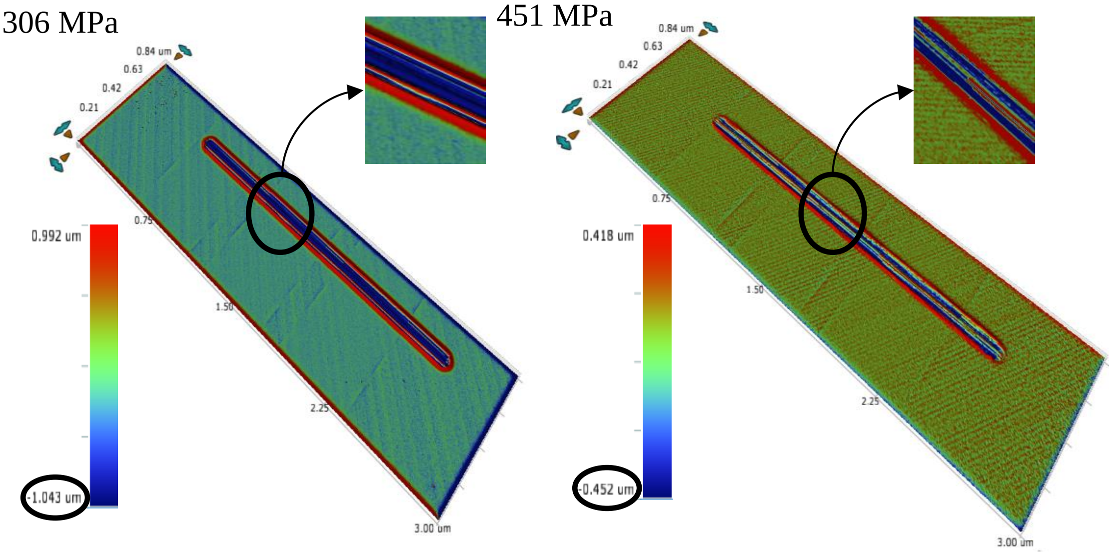

Figure 7-5: Surface topography of wear track for samples lubricated by EMIM ESU IL.

Further increase in contact pressure to 451 MPa leads to a slight increase in the wear track depth (see Fig. 7-6). This finding confirms that the highest reduction in the wear depth is obtained at the moderate contact pressure (386 MPa) for BMIM OSU, PSU and EMIM EP.

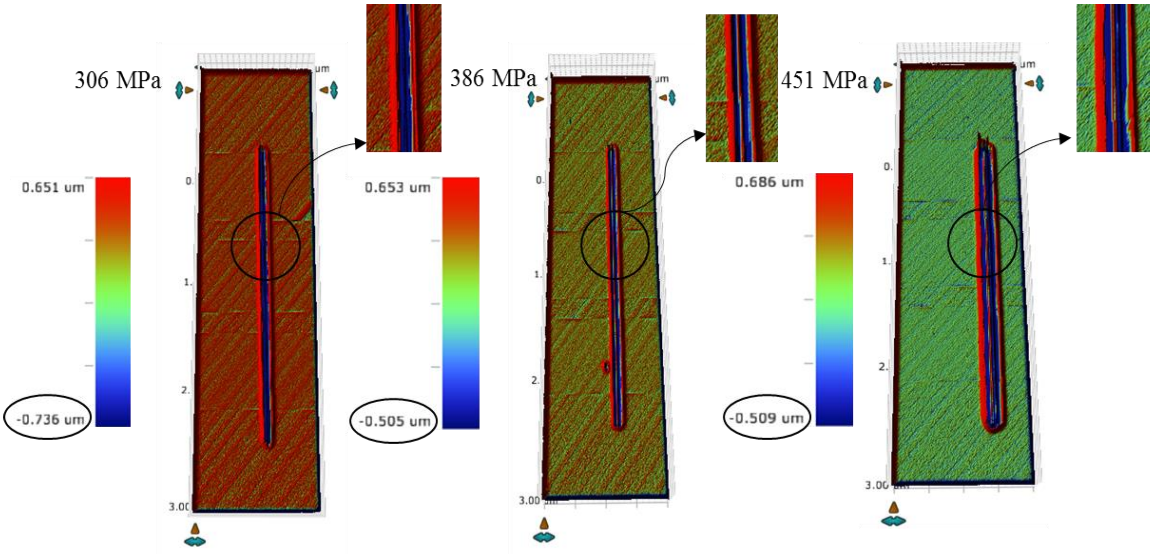

Figure 7-6: Surface topography of wear track for samples lubricated by EMIM EP IL.

7.3.2.3 Surface Chemistry

Samples showing a discernible wear track (all samples except those at the lowest contact pressure) are scanned by XPS to check the formation of the tribofilm.

The detection of these tribofilms is performed by scanning N 1s, S 2s and P 2s elements. The imidazolium sulfate ILs contain N and S elements, PSU contains P and S elements and EMIM EP contains N and P elements.

Starting from imidazolium sulfate ILs, both S2s and N1s were scanned for the samples tested under three different contact pressures. The results show that tribofilm cannot be detected for all ILs at 306 MPa; since neither N1s nor S2s are picked up (see Figs 7-7 and 7-8). The increase in contact pressure to 386 MPa results in a detectable tribofilm only in BMIM OSU. The N1s peak confirms the presence of a tribofilm (see Fig 7-7 (f)). The existence of N 1s at 399.6 eV can be assigned to SiNxOy [182].

However, an S2s peak is still not detected in imidazolium sulfate ILs. Fig. 7-8 shows the typical signal obtained for all the scanned samples. In addition, the further increase in contact pressure to 451 MPa shows that no tribofilm is detected since neither S2s nor N1s are picked up (see Figs 7-7 and 7-8).

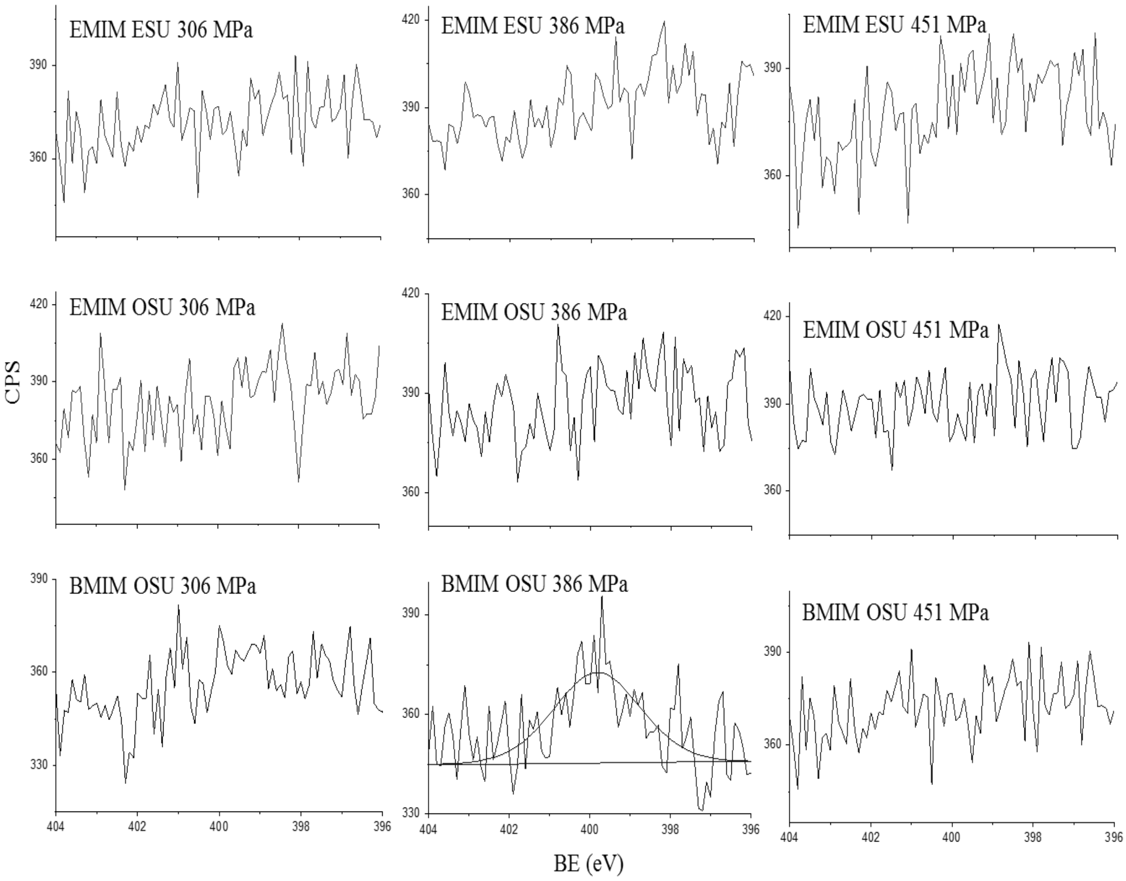

Figure 7-7: XPS results of N1s for samples lubricated by imidazolium sulfate ILs.

In addition to the presence of a Si2s peak that results from the plasmon effect in silicon, the n-type silicon contains phosphorus. Therefore, the ratio of P2s to Si2s is calculated for silicon wafer before the tribological experiments to compare it with the ratio observed inside the wear track (see Fig. 7-9). The increase of P2s to Si2s ratio suggests that phosphorus inside the wear track can be assigned to the formation of a tribofilm. The XPS data acquired inside the wear tracks of both PSU and EMIM EP at 306 MPa indicates that the ratio of P2s to Si2s remains constant before after the test. The increase in contact pressure to 386 MPa results in a significant increase in the ratio of P2s to Si2s (see Fig. 7-10). The further increase in contact pressure to 451 MPa results in a reduction in the ratio of P2s to Si2s inside the wear track for both PSU and EMIM EP.

However, the ratio is still higher than that for the silicon before the tribological test (See Fig. 7-10).

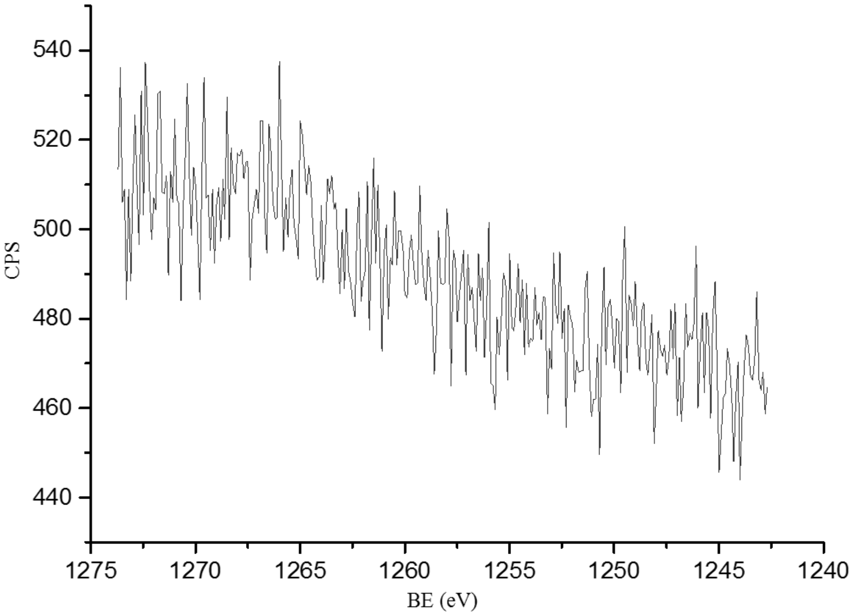

Figure 7-8: XPS result of S2s peak for all imidazolium sulfate ILs and phosphonium sulfate IL at three contact pressures; 306, 386 and 451 MPa.

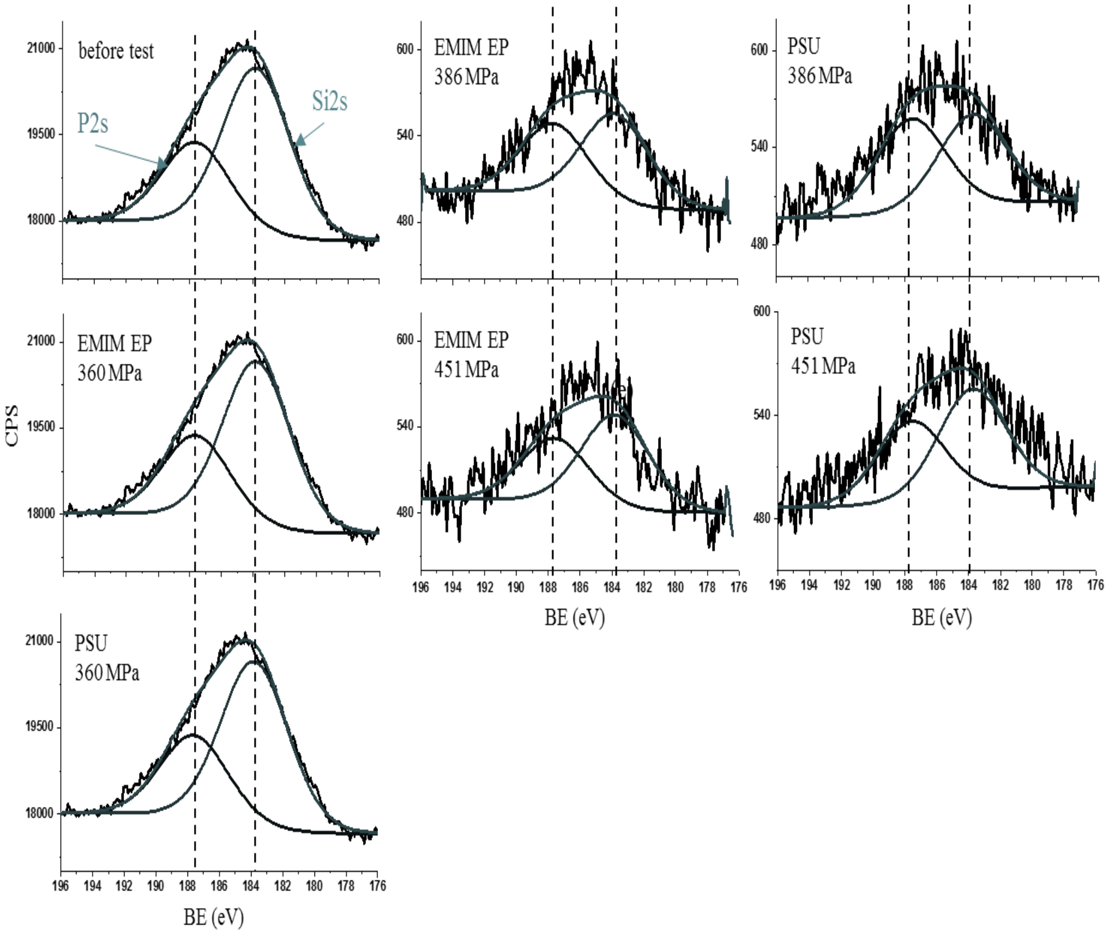

Figure 7-9: P2s peaks for silicon before test and inside the wear tracks of samples lubricated by either EMIM EP or PSU.

It is suggested that this is due to the increased removal of the tribofilm. The P2s peak at 187.8 eV for both EMIM EP and PSU is assigned to phosphorus element that is chemically/physically adsorbed into the silicon surface [186].

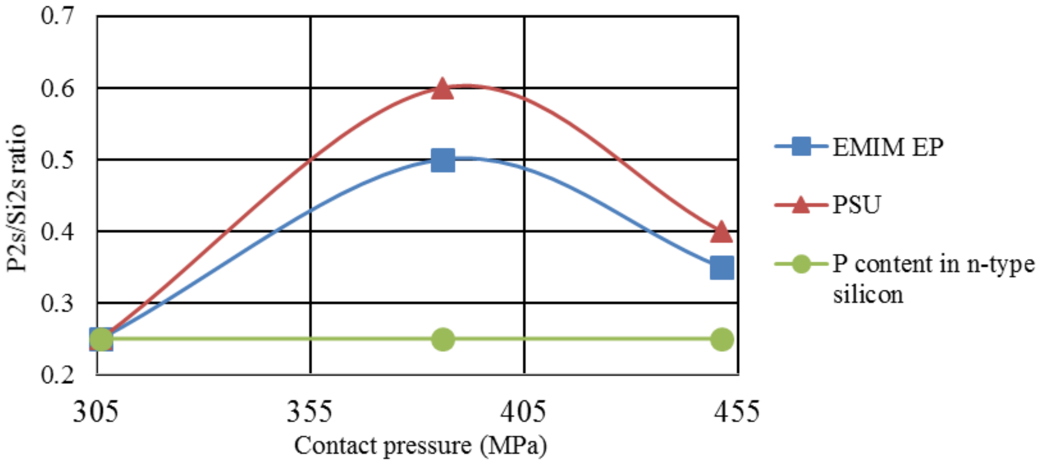

Figure 7-10: P2s to Si2s ratio for silicon before test and inside wear tracks of samples lubricated by either PSU or EMIM EP.

7.3.3 Effect of Sliding Distance

7.3.3.1 Friction

The friction coefficient is measured at three different sliding distances, 3.6 m, 14.4 m and 36 m. Fig. 7-11 presents the final friction coefficients. At the lowest sliding distance (3.6 m) the highest friction coefficient is obtained by EMIM ESU while the lowest value is obtained by EMIM OSU. In terms of the effect of ILs' chemistry; the only negligible effect is the cation chain length. In contrast, the increase of anion chain length, the use of phosphonium cation instead of imidazolium or the use of phosphate anion instead of sulfate anion leads to decrease friction coefficient.

The increase of sliding distance to 14.4 m causes a significant increase in the friction coefficients of EMIM ESU and EMIM EP. A considerable increase is also obtained in EMIM OSU and PSU while only a slight increase is obtained in BMIM OSU. This increasing is expected due to the initiation of wear that results an increase in the surface roughness and might result a wear debris as well [109, 173].

The effect of ILs' chemistry is clear at this condition (14.4 m). The increase of either cation chain length or anion chain length decreases friction coefficient. Cation type shows a significant effect when phosphonium cation exhibits lower friction coefficient than imidazolium cation. Besides, anion type shows only a slight effect when phosphate anion and sulfate anion exhibit comparable friction coefficients.

Further increase of sliding distance to 36 m demonstrates a comparable friction coefficients for EMIM ESU and PSU. Besides, friction coefficient is reduced in EMIM OSU, EMIM EP and EMIM OSU. The reduction in EMIM OSU is higher than that obtained in BMIM OSU. This finding means that the increase of cation chain length causes an increasing in the friction coefficient at the highest sliding distance. Sulfate anion exhibits lower friction coefficient than phosphate and the increase of anion chain length still shows a clear reduction in friction coefficient.

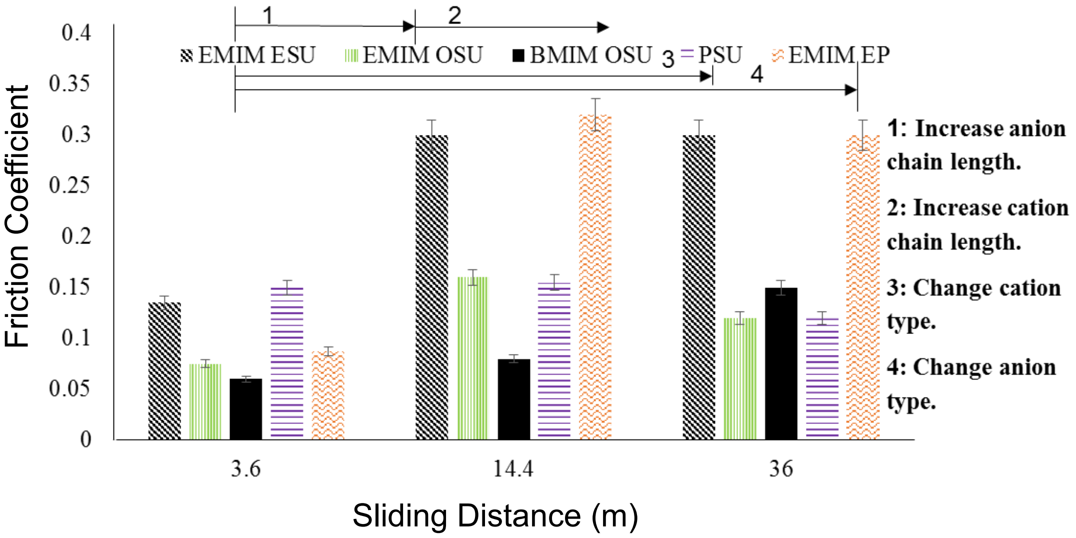

Figure 7-11: Friction coefficient at various sliding distances.

The evolution of friction coefficient is depicted in Fig. 7-12. It is clear that the effect of ILs' chemistry is oblivious even at the first 3.6 m. A stable friction coefficients are obtained for all ILs. At this sliding distance, the influence of cation type and cation chain length are negligible while anion type and anion chain length show a considerable influence. Phosphate anion exhibits lower friction coefficient than sulfate. The highest instability observes when the sliding distance between 3.6 m to 14.4 m. This can be related to the increase of surface roughness that resulted from the scratch and the presence of wear debris that resulted from wear [109, 173].

For both sliding distances (14.4 m and 36 m), the increase of anion chain length increases the stability of friction coefficient while the increase of cation chain length shows a slight decrease in the stability of friction coefficient at the longest sliding distance. The phosphonium cation depicts a higher stability than the imidazolium while both the sulfate anion and the phosphate anion depict a comparable stability.

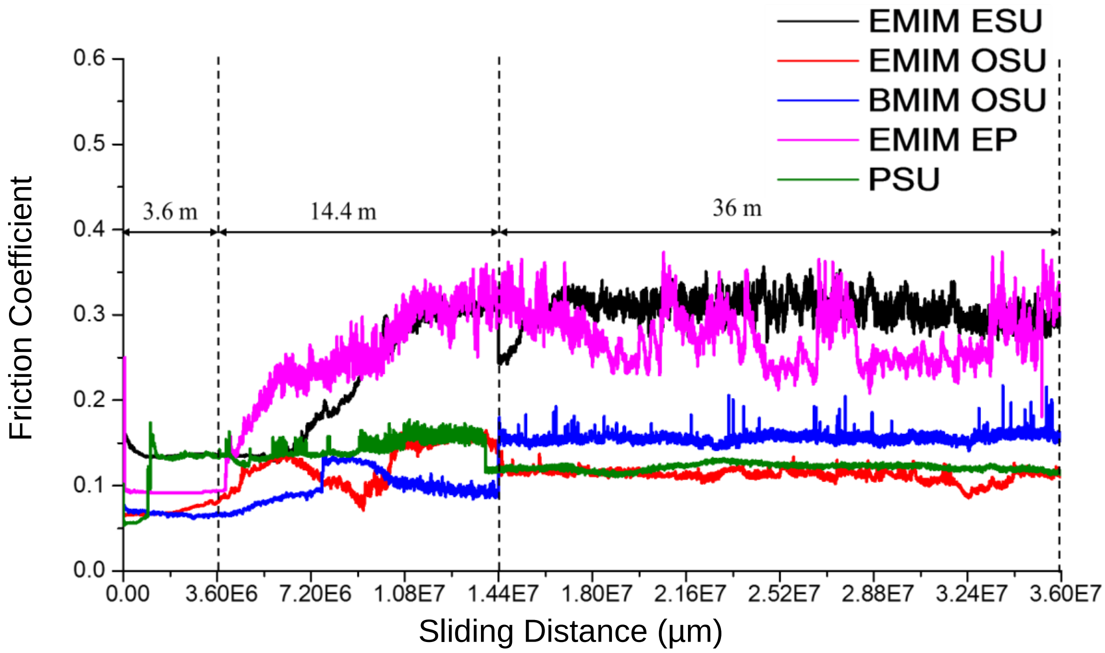

Figure 7-12: Friction coefficient behaviour at three various sliding distances.

The first increase of sliding distance (from 3.6 m to 14.4 m) leads to a significant increase in the surface roughness (see Table 7-5). This could justify the significant increase of the friction coefficient after increasing the sliding distance from 3.6 m to 14.4 m.

The further increase in the sliding distance to 36 m shows a substantial increase in the surface roughness while comparable friction coefficients are obtained (see Fig 7-11 and Table 7-5.)

Table 7-5: Surface roughness inside wear tracks at various sliding distances.

Sliding distance (m)	EMIM ESU	EMIM OSU	BMIM OSU	PSU	EMIM EP
3.6	0.2 nm ±0.05 nm	0.2 nm ±0.05 nm	0.2 nm ±0.05 nm	0.2 nm ±0.05 nm	0.2 nm ±0.05 nm
14.4	10 nm ±1.5 nm	6.5 n ±0.5 nm	4 nm ±0.5 nm	12 nm ±2 nm	5 nm ±2 nm
36	50 nm ±4 nm	13 nm ±2 nm	13 nm ±1 nm	27 nm ±4 nm	90 nm ±6 nm

7.3.3.2 Wear

At the lowest sliding distance (3.6m) no wear can be detected. Fig. 7-13 depicts wear coefficients for five ILs at two various sliding distances. Wear is detected in all ILs when sliding distance is increased to 14.4 m. The increase of either anion chain length or cation chain length causes a substantial decrease in wear coefficient. Anion type also implies a crucial influence when phosphate anion exhibits by far lower wear coefficient than sulfate anion. Cation type again plays a significant role in the determination of wear coefficient when phosphonium cation shows lower wear coefficient than imidazolium.

Further increase in sliding distance to 36 m causes a reduction in the wear coefficient in all ILs. However, wear volume is increased slightly and the reduction is occurred due to the increase of sliding distance (see the equation of wear coefficient 7.1). This increasing in sliding distance reduces the influence of cation chain length. However, the increase of cation chain length still shows a reduction in wear coefficient. The effect of anion type also decreases but phosphate anion still exhibits lower wear coefficient than sulfate anion. In contrast, the influence of anion chain length grows and the reduction of wear coefficient is increased in comparison with the previous sliding distance (14.4 m). Cation type is the only parameter that implies comparable influence and phosphonium cation still demonstrates lower wear coefficient.

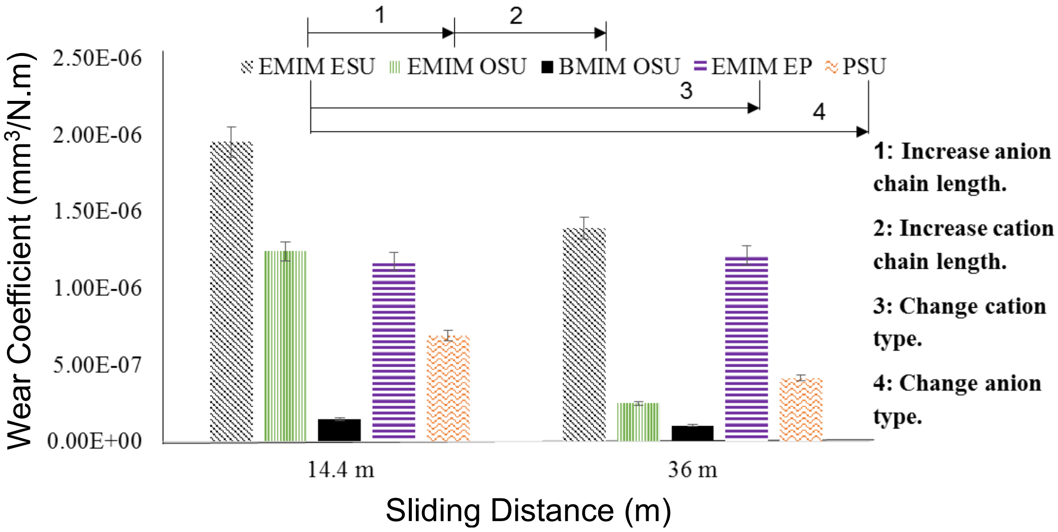

Figure 7-14: Wear coefficient at various sliding distances.

The increase of wear volume results from the increase of both wear depth and wear width. The increase of wear depth will lead to increase wear width since the penetration of the counter face (borosilicate ball) increases with sliding distance. Fig. 7-14 depicts a 3-dimensional view for the surface morphology of EMIM ESU to show the increase of wear volume that results from the increase o sliding distance.

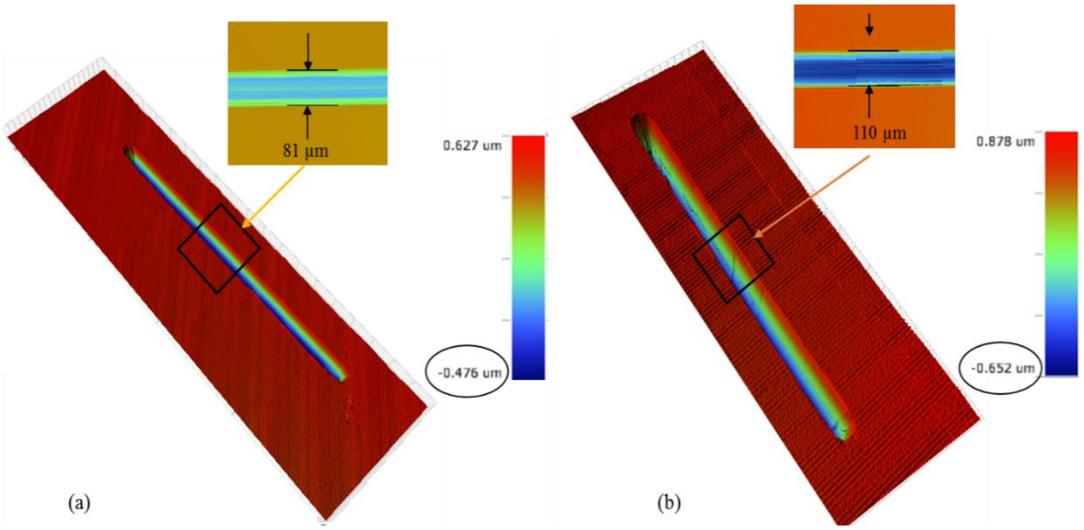

Figure 7-13: A 3D view of surface morphology and wear track for: (a) EMIM ESU after 14.4 m of sliding and (b) EMIM ESU after 36 m of sliding.

7.3.3.3 Surface Chemistry

In order to reveal whether the tribofilm is formed or not; three elements are scanned at high resolution region (N1s, S2s and P2s), even if they are not detected in the survey scan.

The presence of phosphorus refers to the presence of either phosphonium cation or phosphate anion and the presence of sulfur and nitrogen refer to the presence of sulfate anion and imidazolium cation respectively.

Tribofilm is not detected in the samples lubricated by EMIM ESU and EMIM OSU at both sliding distances, since neither N1s nor S2s is detected (see Figs 7-15 and 7-16). In contrast, nitrogen is detected at both sliding distances in BMIM OSU. At 14.4 m only one peak is obtained at 399.8 eV (see Fig.7-15a) which is assigned to SiNxOy [182].

The increase of sliding distance to 36 m a new peak is obtained at 401.7 eV (see Fig. 7-15b) which is assigned to nitrogen contains organic compounds [182]. However, no sulfur is detected for BMIM OSU.

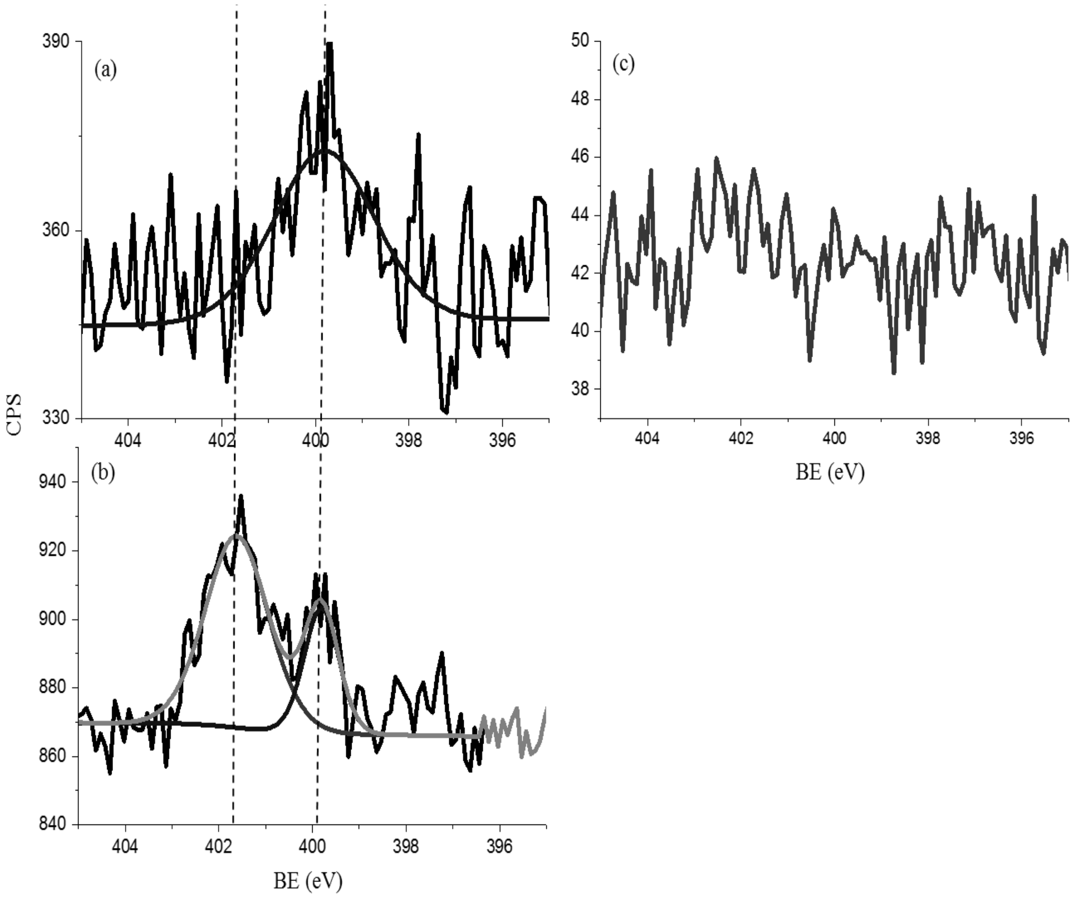

Figure 7-15: XPS scan of N1s inside wear track for samples lubricated by: (a) BMIM OSU at sliding distance 14.4 m, (b) BMIM OSU at sliding distance 36 m and (c) typical result of EMIM ESU, EMIM OSU and EMIM EP at both sliding distances.

The surface chemistry analysis for samples lubricated by either PSU or EMIM EP are also conducted. The results show that neither sulfur from PSU nor nitrogen from EMIM EP can be detected at both sliding distances (see Figs. 3-6 and 3-7). However, phosphorus element is detected which results from phosphonium cation in PSU and phosphate anion in EMIM EP at both sliding distances (see Fig. 3-8). Due to the presence of phosphorus in the n-type silicon, the ratio of P2s to Si2s is calculated for silicon surface before experiment. This ratio is compared with that obtained inside wear track and its increase means that the extra phosphorus content occurs due to the formation of tribofilm.

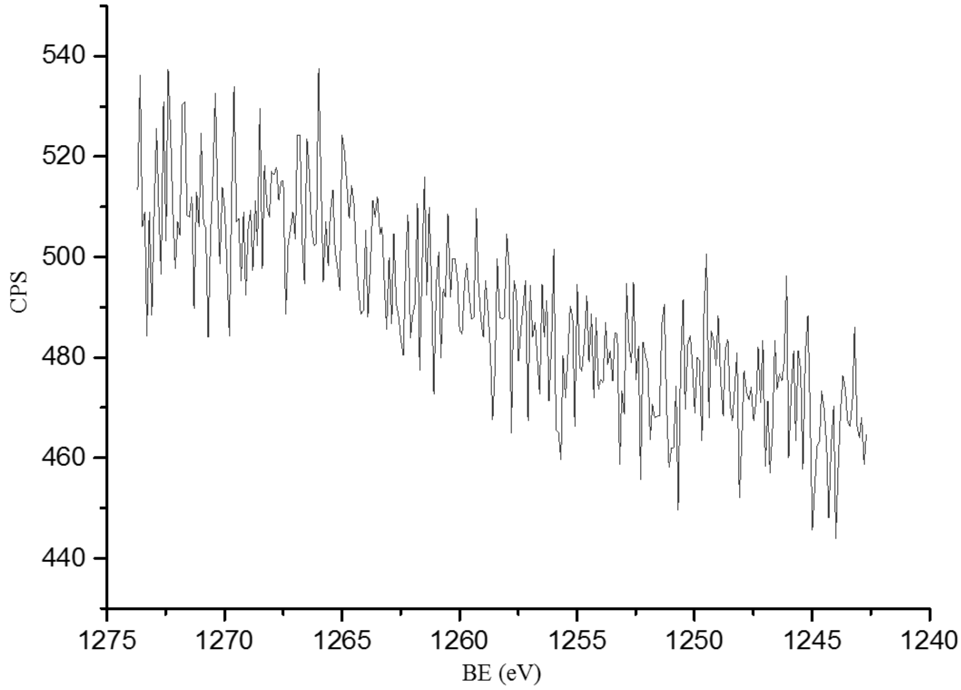

Figure 7-16: Typical result of XPS scan of S2s inside wear track of all imidazolium sulfate ILs and PSU at both sliding distances.

At a lower sliding distance (14.4 m), only adsorbed phosphorus is detected for both ILs (PSU and EMIM EP) since the ratio of P2s to Si2s increases as presented in Fig. 7-17. The increase of sliding distance to 36 m shows a comparable ratio of P2s to Si2s in EMIM EP (see Fig. 7-17). Besides, the increase of sliding distance in PSU results a significant increasing in the ratio of P2s to Si2s and also a new peak is appeared at 191.5 eV. This peak can be assigned to P-O-Si which is in agreement with [148].

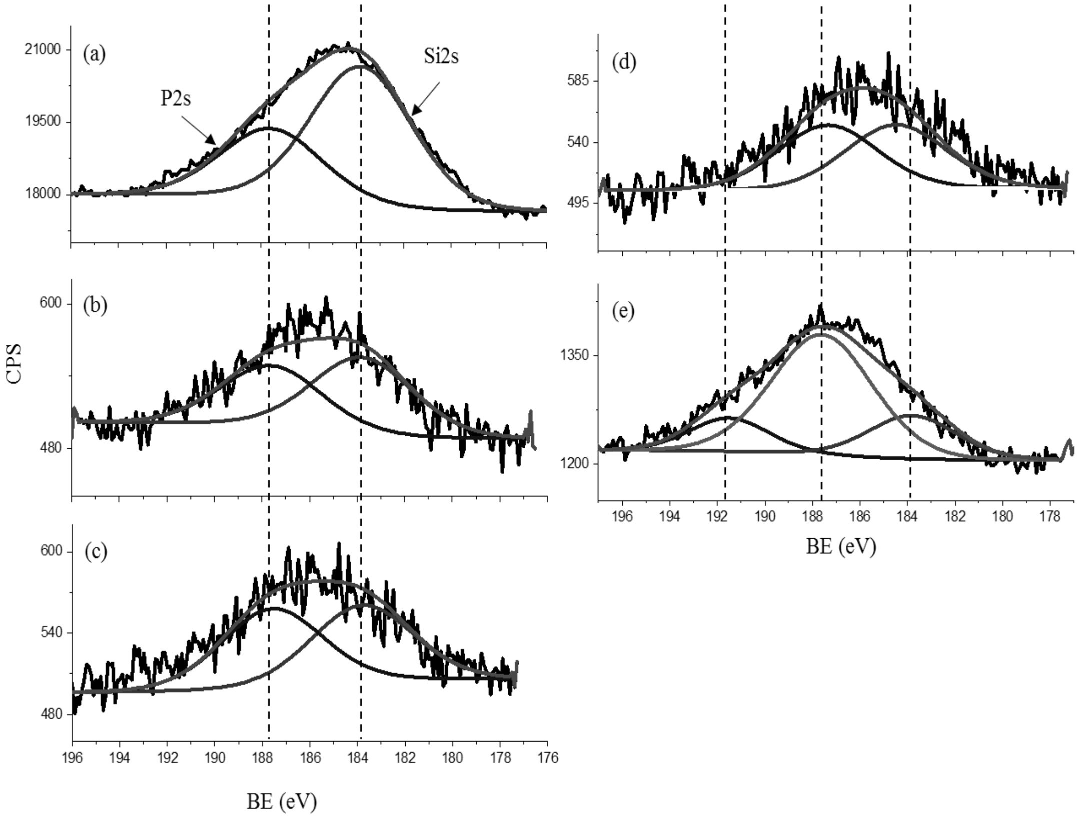

Figure 7-17: P2s peaks for: (a) silicon before experiment, (b) inside wear track of sample lubricated by EMIM EP at distance 14.4 m, (c) inside wear track of sample lubricated by PSU at distance 14.4 m, (d) inside wear track of sample lubricated by EMIM EP at distance 36 m and (e) inside wear track of sample lubricated by

7.3.4 Effect of Temperature

7.3.4.1 Friction

The effect of temperature is studied by comparing the results at room temperature (25 ^{o}C) with the results at high temperature (80 ^{o}C). Fig. 7-18 presents the results of the final friction coefficients for all ILs at two temperatures. The increase of temperature leads to increase friction coefficients of four ILs which are BMIM OSU, EMIM ESU, EMIM EP and PSU. Besides, for EMIM OSU a comparable friction coefficients are obtained at both temperatures.

The increase of temperature leads to increase the role of anion chain length on determination of friction coefficient. At high temperature, a higher reduction in the friction coefficient is resulted due to the increase of anion chain length.

In contrast, the influence of cation chain length decreases with the increase of temperature. At high temperature, a lower reduction in friction coefficient is resulted due to the increase of cation chain length.

In terms of the influence of cation type, phosphonium cation still exhibits lower friction coefficient than imidazolium. In contrast, in terms of the influence of anion type, sulfate anion shows a lower friction coefficient than phosphate anion after the increase of the temperature.

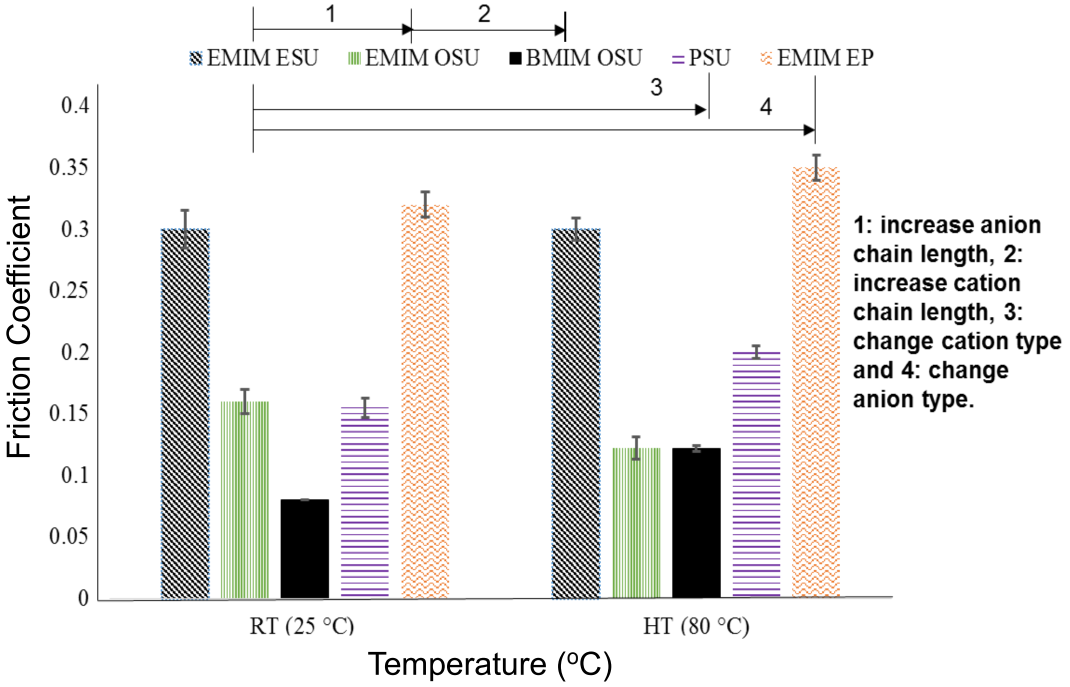

Figure 7-18: Friction coefficient values for five ILs at various contact pressures.

A considerable increasing in the surface roughnesses as a result of the increase of temperature is observed (see Table 7-6). This could contribute in the increase of friction coefficients. However, in EMIM OSU, the friction coefficient is decreased after the increase of temperature despite the considerable increase of surface roughness. This finding, again, confirms that the surface roughness might effect on friction coefficient but it is not the only factor that control it.

Table 7-6: Surface roughness inside wear tracks at two temperatures.

Temperature	EMIM ESU	EMIM OSU	BMIM OSU	PSU	EMIM EP
25 °C	10nm ±2 nm	6.5 nm ±1 nm	4 nm ±1.5 nm	12 nm ±1.5 nm	5 nm ±2 nm
80 °C	100 nm ±6 nm	10 nm ±2 nm	13 nm ±3 nm	37 nm ±2 nm	50 nm ±8 nm

The behaviour of friction coefficients during the experiments is demonstrated in Fig. 7-19. It can be seen clearly that the increase of temperature decrease the stability of friction coefficients for all the examined ILs. However, for EMIM ESU, the sudden increasing after about 6 m of sliding is disappeared. This behaviour is related to both the formation of tribofilm and the presence of wear debris, as discussed before. Lastly, at high temperature, the fluctuation of friction coefficients are comparable for all the examined ILs regardless to their chemistry.

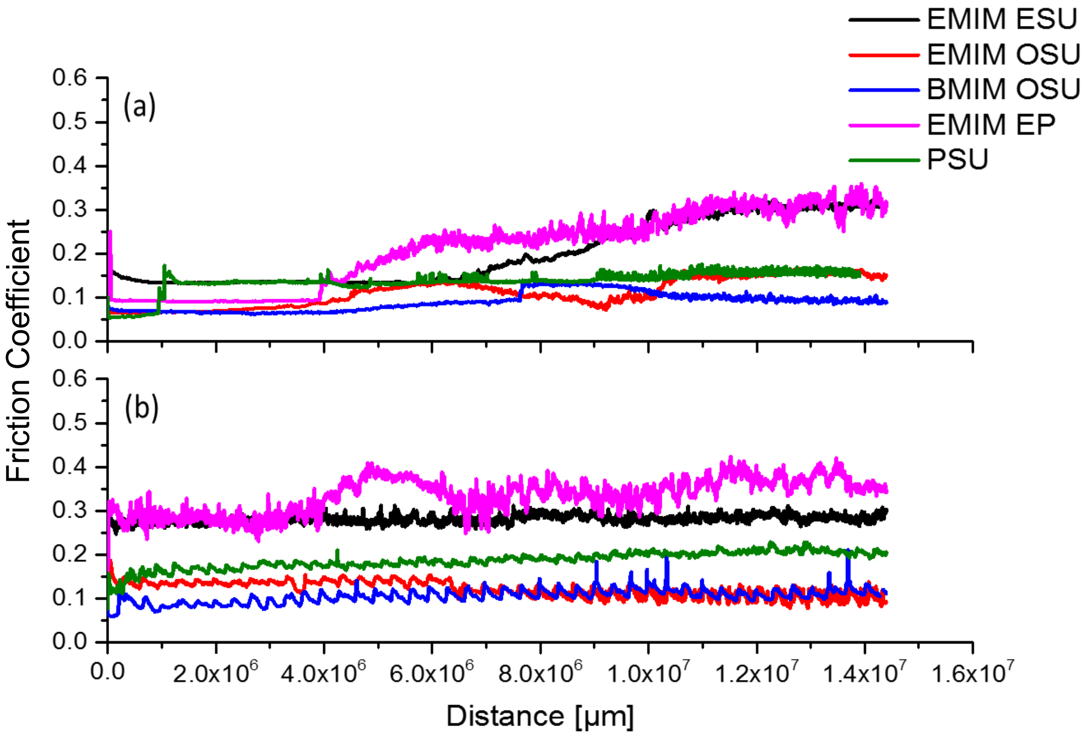

Figure 7-19: Variation of friction coefficient with sliding distance at: (a) at room temperature (25 °C) and (b) at high temperature (80 °C).

7.3.4.2 Wear

The results of wear coefficients for the examined ILs at both temperatures are depicted in Fig. 7-20. It is clear that the wear coefficients for EMIM ESU, EMIM EP and PSU increase with the increase of temperature. In contrast, the wear coefficients of both EMIM OSU and BMIM OSU decrease with the increase of temperature.

Besides, the influence of anion chain length is more significant at high temperature. A higher reduction in the wear coefficient is obtained as a result of the increase of anion chain length.

Besides, the influence of cation chain length decreases with the increase of temperature. However, the increase of cation chain length still results a reduction in the wear coefficient.

In terms of the effect of anion type and cation type; phosphate anion and phosphonium cation still show lower wear coefficients than sulfate anion and imidazolium cation respectively.

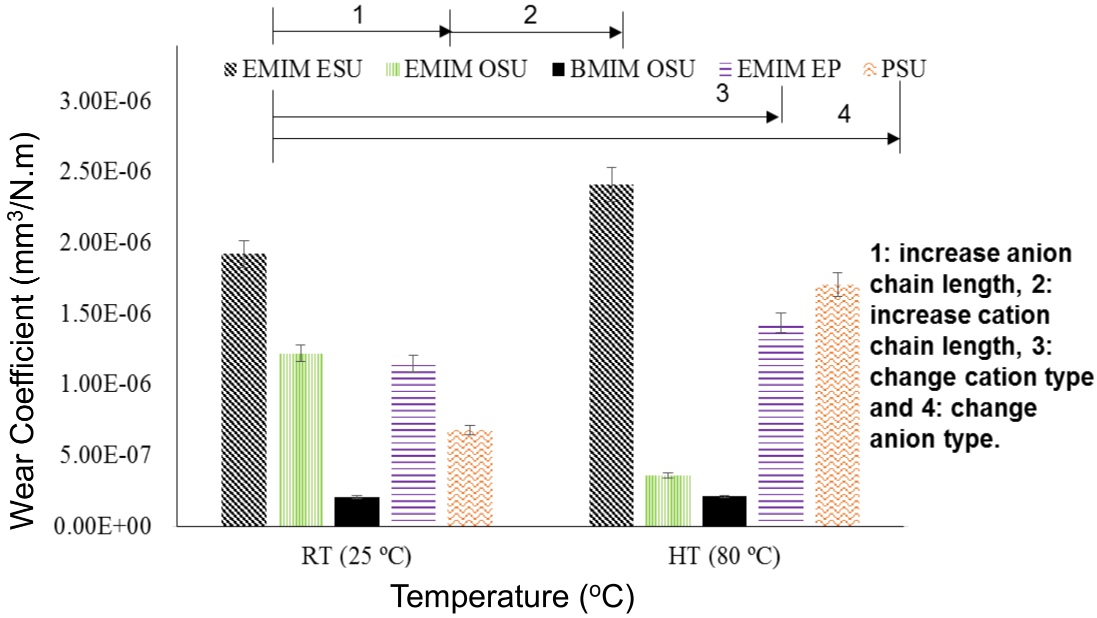

Figure 7-20: Wear coefficient values for five ILs at temperatures.

The morphologies of wear tracks are also analysed. Fig. 7-21 presents the wear track morphologies of samples lubricated by either EMIM OSU or PSU at both conditions (room and high temperatures). These samples are selected since the highest reduction and the highest increasing of wear volume are obtained in EMIM OSU and PSU respectively.

It is obvious that both the width and the depth of wear tracks are decreased with the increase of temperature for the sample lubricated by EMIM OSU (see Fig.7-21a and 7-21b). In contrast, the increase of temperature leads to increase both wear track width and depth for the sample lubricated by PSU (see Fig. 7-21c and 7-21d). Further, for PSU, a flatter wear track is observed which suggests that the tribofilm is destructed. This finding will be either confirmed or refuted by the results of surface chemistry in the next section. Lastly, the morphologies of the rest samples have a comparable behaviour to that presented for PSU.

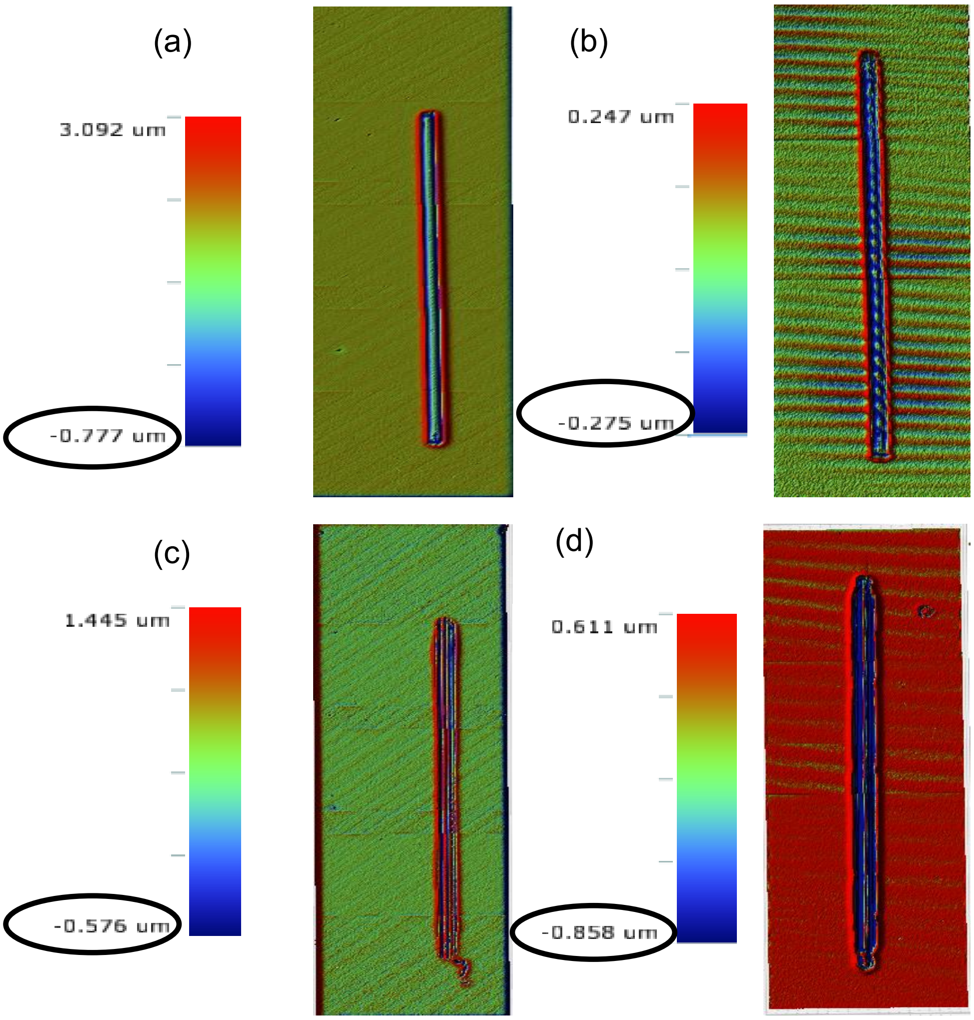

Figure 7-21: Surface morphologies for: (a) sample lubricated by EMIM OSU at room temperature, (b) sample lubricated by EMIM OSU at high temperature, (c) sample lubricated by PSU at room temperature and (d) sample lubricated by PSU at high temperature.

7.3.4.3 Surface Chemistry

Again, the following elements are scanned in high resolution region: N1s, S2s and P2s. The results show that no tribofilm can be detected inside the wear track of the samples that lubricated by either EMIM ESU or EMIM OSU (see Figs. 7-22 and 7-23). In contrast, the tribofilm is detected inside the wear track of the samples that lubricated by BMIM OSU (see Fig. 7-22). The chemistry of the tribofilm is changed with the increase of temperature. A new peak is obtained at 401.6 eV that is assigned to the presence of nitrogen contains hydrocarbons as assigned before in [182]. For PSU, the sulfur is still undetectable even after the increase of temperature (see Fig. 7-23).

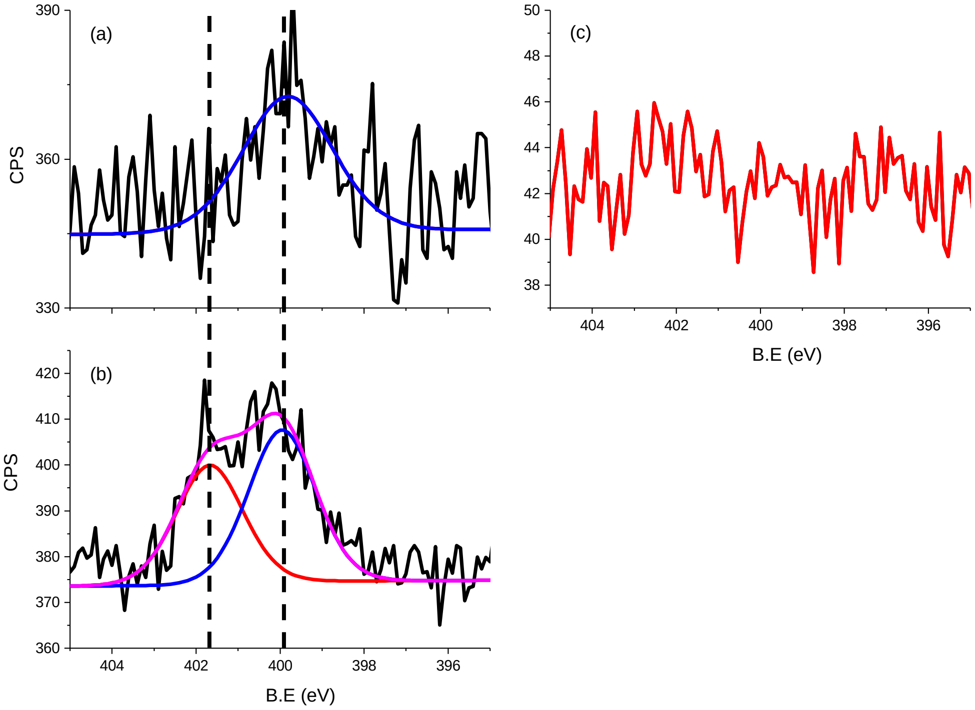

Figure 7-22: XPS results of N1s peak for: (a) sample lubricated by BMIM OSU at room temperature, (b) sample lubricated by BMIM OSU at high temperature and (c) The typical N1s peak for the samples that lubricated by EMIM ESU, EMIM OSU and EMIM EP at both temperatures.

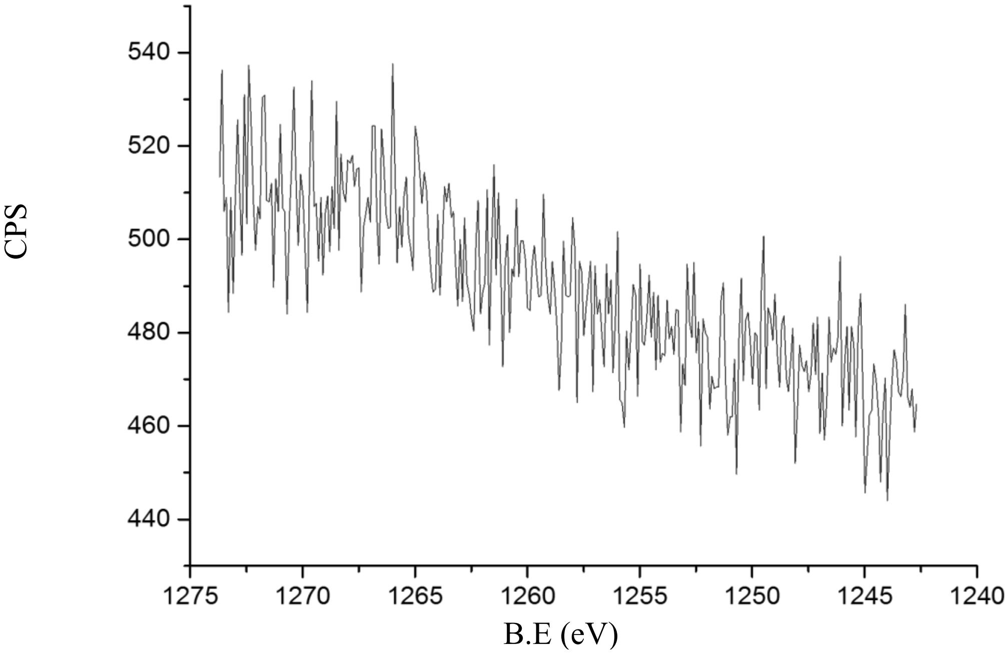

Figure 7-23: S2s typical peak for the samples that lubricated by EMIM ESU, EMIM OSU, BMIM OSU and PSU at both

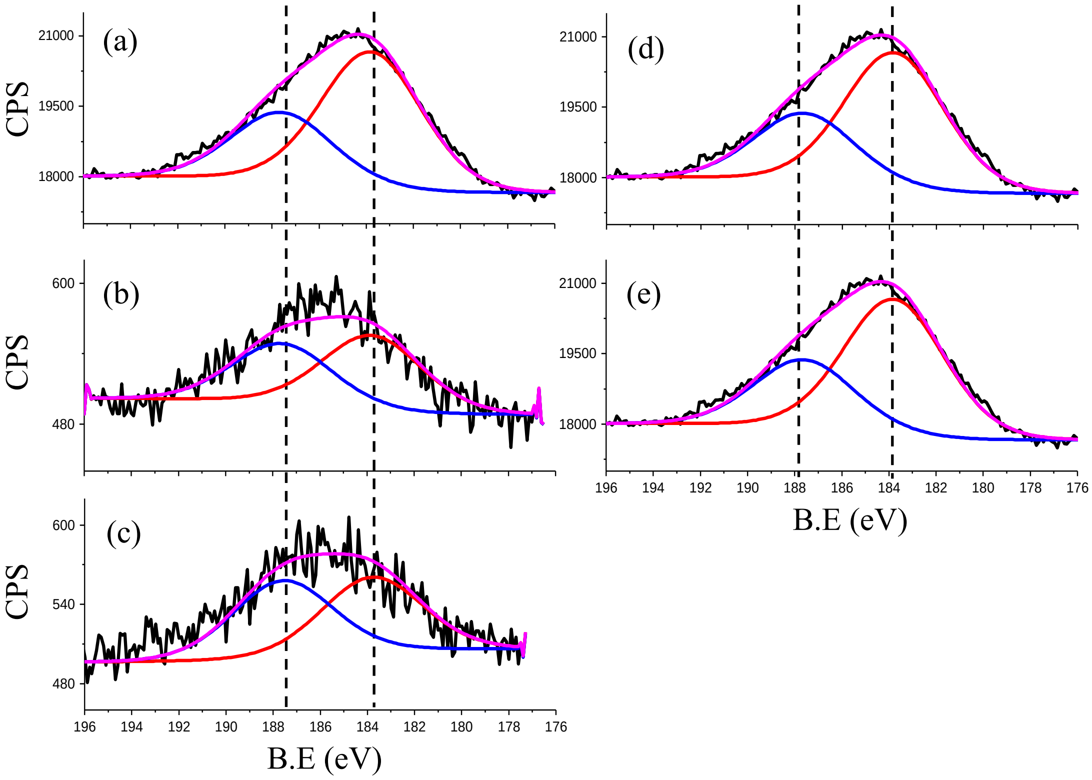

Figure 7-24: P2s peaks for: (a) silicon before test, (b) inside wear track of EMIM EP at contact pressure 386 MPa, (c) inside wear track of PSU at room temperature, (d) inside wear track of PSU at high temperature (e) inside wear track of EMIM EP at high temperature.

The ratio of P2s to Si2s decreases and it becomes same as that obtained in silicon sample before the experiment (see Fig. 7-24d). This finding suggests that the tribofilm is totally destructed. In similar manner, for EMIM EP, both the anion and cation moieties cannot be detected (see Figs 7-22c and 7-24e). This finding also suggested that the tribofilm is destructed after heating process.

7.4 Discussion

7.4.1 Friction Coefficient

Friction coefficient is greatly affected by surface roughness, viscosity and the presence of either a protective layer (tribofilm) or wear debris [27, 49, 187]. Silicon surface roughness is measured for all the samples inside and outside the wear tracks.

As presented in tables 7-4, 7-5 and 7-6 there is no clear correlation between the final friction coefficients and the average surface roughness values. This finding suggests that the influence of both the viscosity and tribofilm formation are more crucial in the determination of the friction coefficient.

The effect of viscosity is also not obvious except at the lowest contact pressure (see Figs. 7-1, 7-2, 7-11 and 7-18). The lowest friction coefficient is obtained by BMIM OSU that exhibits the highest viscosity and vice versa for EMIM ESU. For the other contact pressures (where wear is high), the effect of viscosity is strongly decreased. This suggests that in this regime the wear is dominating the friction coefficient. Despite their lower viscosities, EMIM ESU and EMIM OSU show a lower friction coefficient than EMIM EP and PSU respectively. These findings suggest that the viscosity might effect on the friction coefficient only at the lowest contact pressure. In addition, the increases of IL viscosity as a result of increasing their anion/cation chain length also contributes in the reduction of friction coefficient.

Lastly, the formation of tribofilm has an impact on the friction coefficient as well. The lowest friction coefficient of BMIM OSU, EMIM EP and PSU is obtained when a tribofilm is detected at a contact pressure of 386 MPa. The decrease in the tribofilm thickness of PSU and EMIM EP at the highest contact pressure (451 MPa) seems to increase the friction coefficient.

In addition, the increase of BMIM OSU tribofilm thickness leads to increase its friction coefficient (see Figs. 7-11, 7-18, 7-15, and 7-22). This would also confirm that the formation of tribofilm has a substantial influence on the friction coefficient.

7.4.2 Wear and Lubrication Mechanism

Wear is mainly affected by the reactivity of ILs with silicon to form a tribofilm which reduces the wear coefficient [23]. The surface chemistry results indicate that the minimum wear coefficient (for BMIM OSU, EMIM EP and PSU) is obtained when a tribofilm is detected on the rubbing surfaces (See Figs 7-4, 7-7f and 7-9). The results show that the lower the thickness of the tribofilm the higher the wear of the system (see Figs. 7-4, 7-10). For the rest of ILs, i.e. EMIM ESU and EMIM OSU, wear coefficient continuously decreases by increasing the contact pressure or sliding distance. However, no tribofilm is detected by XPS.

These findings suggest that the wear coefficient is significantly controlled by the reactivity of the ILs and their tribofilms formation. The formation of the tribofilm decreases both the wear and friction coefficients. The minimum wear coefficient for BMIM OSU, EMIM EP and PSU are observed at contact pressure 386 MPa. At this contact pressure, the largest tribofilm thickness is formed on the surface for PSU and EMIM EP. This observation suggests that the tribofilm formation rate is considerably higher than the removal rate. This finding is in a high agreement with the previous finding by Yagi *et al* [15] when they studied the lubrication mechanism of ammonium IL.

For EMIM ESU and EMIM OSU, the wear coefficient is continuously decreasing by increasing the contact pressure, which might be related to the increase of the formation rate of the tribofilm. However, it could not be detected because the removal rate is still higher than formation rate. This suggestion is in agreement with [67] when they examined a few bis(trifluoromethylsulfonyl)amide based ILs. In addition, the increase of sliding distance/temperature (increase the severity of the contact) leads to decrease the wear coefficient of EMIM OSU (see Figs. 7-13 and 7-20). This can again confirm the proposed assumption (the formation rate increases with severity but it is still lower than the formation rate).

These findings suggest that the tribofilm formation process starts with the decomposition of ILs on the surface followed by either a chemical reaction or a chemical/physical adsorption on silicon surface. This finding is supported by XPS results since only anion/cation moiety can be detected inside wear tracks. In addition, this suggestion is also confirmed by previous studies; e.g. in [90] only anion moieties are detected inside wear track and in [24] only cation moieties are detected inside wear track.

The formation of the tribofilm seems to start by either cation or anion moieties depending on the combination of anion-cation. For both BMIM OSU and PSU the formation starts from cation moieties while it starts from anion moieties for EMIM EP (see Figs. 7-7, 7-8 and 7-9). This might be related to the reactivity of the elements that anion/cation consisted of. In other word, the formation of tribofilm seems to be started after the decomposition of IL and followed by a reaction/adsorption of either anion or cation moiety. The more reactive moiety will start the reaction/adsorption process. This finding can reveal the reason behind the conflict in the literature since the formation of the tribofilm was reported to be controlled by cation moiety in [24] or anion moiety in [26, 90].

7.5 Conclusions

A comprehensive study have been conducted to investigate the effect of ILs' chemistry of their lubrication mechanism. The formation mechanism of the tribofilm and its influence on the tribological performance at various conditions have been examined. The following conclusions are drawn:

- ILs' chemistry is crucial in the determination of their tribological behaviour due to their significant influence on both ILs' viscosity and ILs' reactivity.
- The increase of either anion or cation chain length leads to enhance the tribological performance.
- The phosphate anion shows better tribological performance than sulfate anion at all conditions except at high contact pressure (from 386 MPa and higher).
- The phosphonium cation shows better tribological performance than imidazolium cation under all the examined conditions.
- Wear coefficient is controlled by the formation of tribofilm.

- The phosphonium cation exhibits higher reactivity than imidazolium cation at all the examined conditions.
- The phosphate anion exhibits higher reactivity than sulfate anion under all conditions except at high contact pressure (higher than 386 MPa).
- The formation of the tribofilm can be started from either the anion moiety or cation moiety. It depends on the chemistry of the both ions and their combination.

8. Chapter 8: Discussion

8.1 Chapter Overview

This chapter aims to make a link between the findings of the previous results chapters and proposes the lubrication mechanism of ILs. This is achieved by linking the formation of ILs thermal films and the formation of ILs tribofilms. In other words, the full story of the lubrication mechanism can be obtained when the results of both thermal and tribofilms are linked and discussed. Based on this discussion, the full story of the effect of ILs chemistry on their lubrication mechanism is presented.

8.2 The Link between Thermal and Tribo Films of Neat ILs (The Lubrication Mechanism of IL as Potential Lubricant To Lubricate MEMS)

The thermal decomposition of ILs starts from the anion which suggests that IL firstly decomposes and then the anion moiety, the cation moiety or both moieties reacted/adsorbed into the surface (see Fig. 6-15). This finding is confirmed by the results of the formation of thermal films when both moieties are detected in EMIM EP and only the cation moieties in PSU (see Figs. 6-17 and 6-18). In addition, the detected tribofilms only result from the reaction/adsorption of either anion moiety (in EMIM EP) or cation moiety (in BMIM OSU and PSU) as depicted in Figs. 7-7 and 7-9. The previous findings also confirmed this finding since the obtained tribofilm consisted of only cation moiety in [24] or anion moiety in [26, 90].

Herein, it is believed that the ILs decompose firstly and then react/adsorb with the silicon surfaces. The tribological behaviour is mainly controlled by the formation of the tribo/thermal film that results from the reaction/adsorption of ILs.

Fig. 8-1 shows the relationship between the formation of tribofilm and the tribological behaviour of ILs. It is obvious that the lowest friction and wear coefficients are obtained when the tribofilm is detectable. The lowest wear and friction in Fig. 8-1b confirm this finding. In contrast, the absence of tribofilm causes a higher wear and friction (see Fig 8-1a and 8-1c).

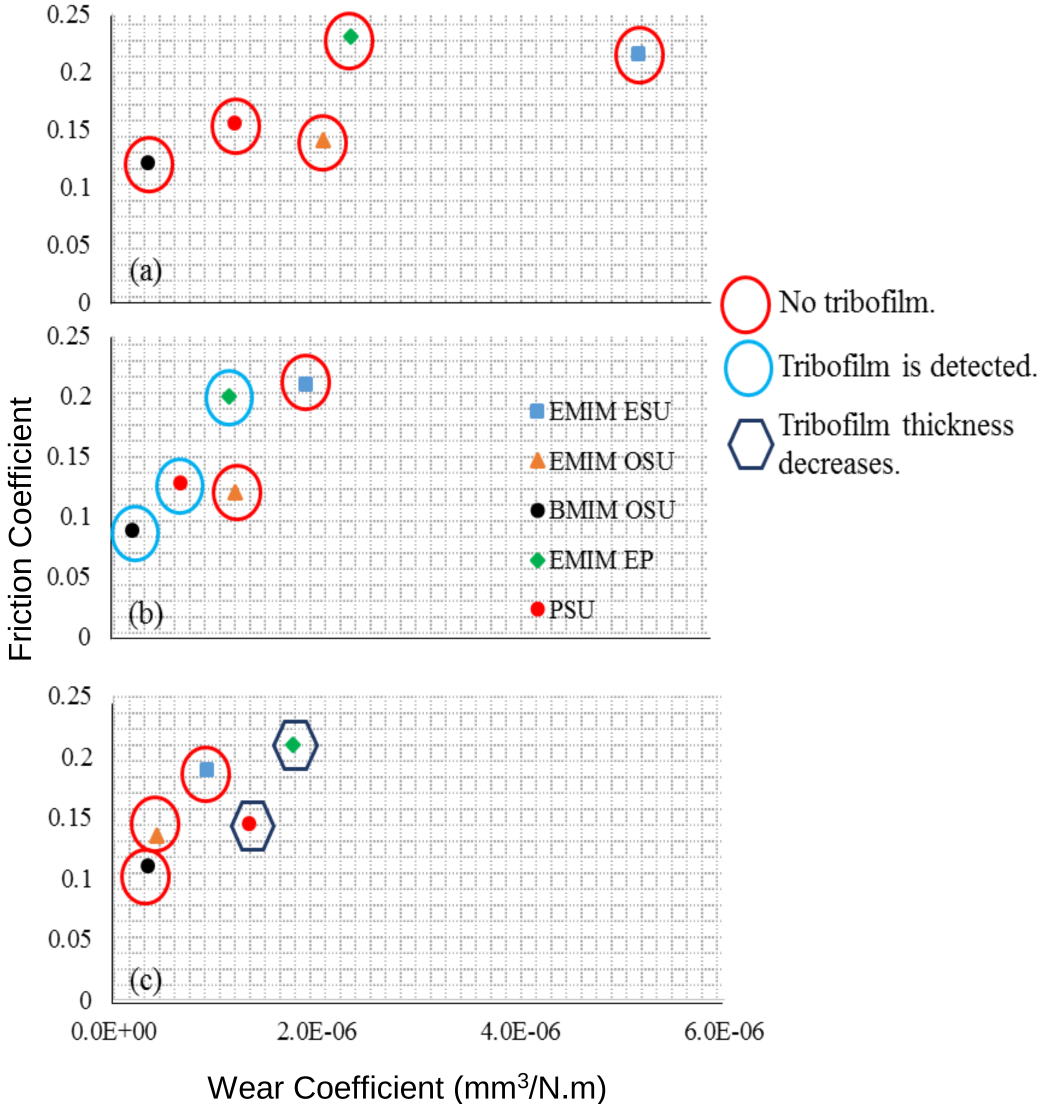

Figure 8-1: The relationship between the formation of the tribofilm and the tribological performance of ILs at various contact pressures: (a) at 306 MPa, (b) at 386 MPa and (c) at 451 MPa.

The tribofilm can be only detected when the formation rate of the tribofilm is higher than the destruction rate. This finding has been pointed out before in [15] and [67]. This can be occurred when either IL is highly reactive and the formation rate is very high or the generated tribofilm is durable.

The durability of the thermal films is examined (see Fig. 6-14). It is clear that the films resulted from EMIM ESU, EMIM OSU and EMIM EP have a comparable durability. Besides, BMIM OSU film has the highest durability and PSU has higher durability than the other three ILs.

This can completely justify the detection of BMIM OSU tribofilm since it is highly reactive and highly durable (refereeing to the thickness and durability of its thermal film in chapter 6).

The increase of contact pressure, sliding distance or temperature results either an increasing or a decreasing in the tribofilm thickness. This can be assigned again to the relationship between the formation rate and the destruction rate of the tribofilm. The increase of contact pressure from 386 MPa to 451 MPa (see Fig. 8-1) results a decreasing in the friction and wear coefficients of EMI ESU and EMIM OSU. This suggests that the increase of contact pressure increases the formation rate of the tribofilm, but it is still lower than the destruction rate which makes them undetectable.

To check the validity of this finding (the relationship between the formation and destruction rate of tribofilm), a more sever conditions are applied. Fig. 8-2 depicts the relationship between the formation rate of the tribo and the thermal films and the tribological performance of ILs at various temperatures and sliding distances. The results again confirm that the increase of the severity of the applied conditions can lead to increase both the formation and the destruction rate of the tribofilm.

It can be seen that the increase of the severity of the tribological conditions increases the formation rate of tribofilm (see the results of BMIM OSU in Fig. 8-2a and 8-2b). However, the destruction rate of tribofilm also increases with the severity of the tribological conditions (see the results of PSU in Fig. 8-2a and 8-2b). This finding suggests that there is an optimum condition that the formation rate of tribofilm is higher than the destruction rate. The use of a low severity might be not enough to make the formation rate of the tribofilm higher than the destruction rate. In contrast, the use of a high severity increases the destruction rate of the tribofilm and make it higher than the formation rate.

These findings all together lead to propose that the formation of the thermal/tribo film starts after the partial decomposition of IL. The formation might be started from either the anion moieties or the cation moieties. This mainly depends on the IL chemistry (i.e., which ion is more reactive). The formation of the thermal/tribofilm enhances the tribological performance.

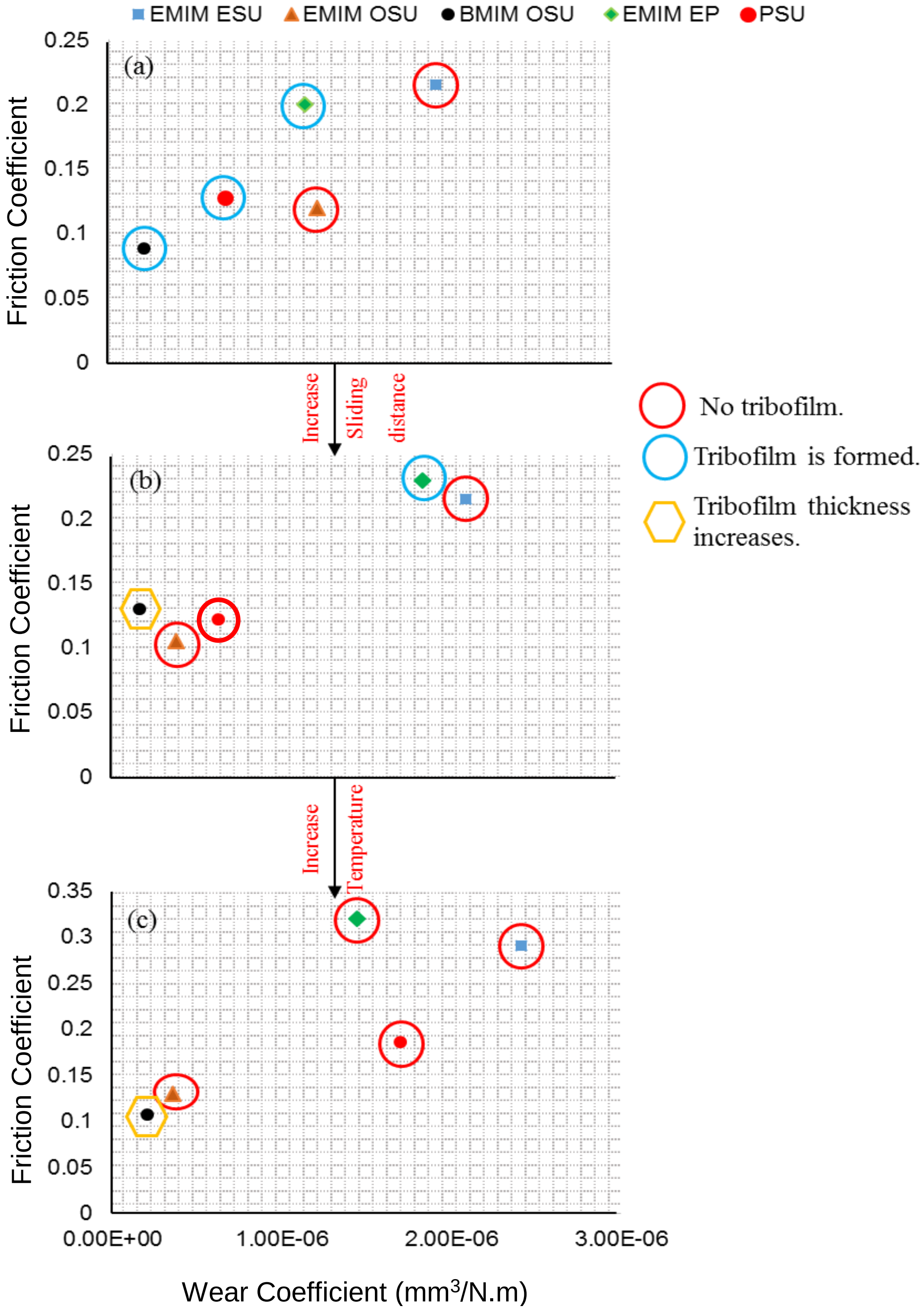

Figure 8-2: The relationship between the formation of the tribofilm and the tribological performance of ILs at various conditions: (a) at 386 MPa, sliding distance 14.4 ma and 25 ^{o}C, (b) at 386 MPa, sliding distance 36 m and 25 ^{o}C and (c) at 386 MPa, sliding distance 14.4m and 80 ^{o}C.

8.3 Effect of Neat ILs Chemistry on Their Lubrication Mechanism

ILs chemistry is crucial in determining of the tribological performance since both ILs viscosity and reactivity are substantially influenced by their chemistry. The viscosity and reactivity show a considerable effect on the friction coefficient (see Figs. 7-1, 8-1 and 8-2). In addition, the reactivity of ILs indicates a significant effect on the wear coefficient (see Figs. 8-1 and 8-2).

Several studies showed that the increase in the chain length of either the cation or the anion enhances the tribological performance of ILs in terms of decreasing both friction coefficient and wear [24, 49, 52, 90]. However, the reason behind that is still not well understood. For halogenic ILs, the increase in the chain length of either the cation or the anion causes a reduction in tribocorrosion which leads to decrease wear volume [49, 52]. In this study, for halogenic-free ILs, the longer in the chain length of either the cation or anion the higher the IL viscosity, thermal film durability and reactivity (see Figs. 7-1, 8-1, 6-14 and 8-2). This behaviour will enhance the tribological behaviour of the lubricated tribopairs.

The cation type is also important in the determination of the tribological performance. For instance, the phosphonium cation shows lower friction coefficient than imidazolium at all the tested conditions (see Figs. 8-1 and 8-2). The phosphonium cation demonstrates higher viscosity, more durable thermal film and higher reactivity than imidazolium cation (see Figs. 6-14, 7-1, 8-1 and 8-2). Therefore, the phosphonium cation also exhibits lower wear coefficient. However, the imidazolium cation exhibits lower wear coefficient than the phosphonium cation at only one condition (451 MPa, 14.4 m and 25 ^{0}C). Nevertheless, it was pointed out by several studies [24, 107] that the cation type does not demonstrate a considerable effect on the tribological performance of ILs. Imidazolium and pyridinium were used in those two studies when both cations contain nitrogen atom. This can be the reason behind the comparable tribological performance in those two cations.

The anion type also have a substantial effect on the performance of ILs as lubricants. Apart from the effect of tribocorrosion that might be occurred in halogenic anions [23].

In this study both anions are halogen-free, and the results show that the anion type has a significant role on the tribological performance of ILs (see Figs. 8-1 and 8-2). The phosphate anion exhibits higher reactivity and viscosity than sulfate anion. However, the durability of the thermal films of both ILs is comparable. The phosphate anion shows superior tribological performance in comparison with the sulfate anion. However, the sulfate anion shows better tribological performance at only one condition (451 MPa, 14.4 m and 25 ^{o}C).

In addition, IL chemistry controls the tribofilm formation mechanism. The presence of either nitrogen (in BMIM OSU tribofilm) or phosphorus (in PSU tribofilm) rather than sulfur suggests that the tribofilm formation starts first in the cation. However, the presence of phosphorus rather than nitrogen (in EMIM EP tribofilm) suggests that the formation starts in the anion. This finding again confirms that the tribofilm formation mechanism mainly depends on the IL chemistry in addition to the combination of anion-cation. This conclusion explains the contrast in the literature whether the reaction is started by cation [24] or by anion [26, 90].

8.4 The Link between Thermal and Tribo Films of Oil-Soluble IL (The Lubrication Mechanism of Oil-Soluble IL).

Firstly, the results of the formation of thermal films confirmed two main findings:

- ZDDP can form thicker thermal film than PP since the formation of PP thermal film is self-limited (see Figs. 4-4 and 4-9).
- Fig. 8-3 shows that the thermal films of both additives can provide a considerable reduction in wear. However, ZDDP thermal film can provide better anti-wear performance but it exhibits higher friction coefficient.

These two findings can help to define the mechanism of the anti-wear mechanism of both additives. The higher protection of ZDDP thermal film means that ZDDP protective film is more durable. Similarly, ZDDP tribofilm provides a higher protection against wear at various contact pressures (see Fig. 8-4).

The increase of contact pressure increases the formation rate of the tribofilms for both additives. However, ZDDP shows higher protection against wear at both contact pressures. These findings are in agreement since the thicker and the more durable thermal/tribo film by ZDDP leads to a better anti-wear performance.

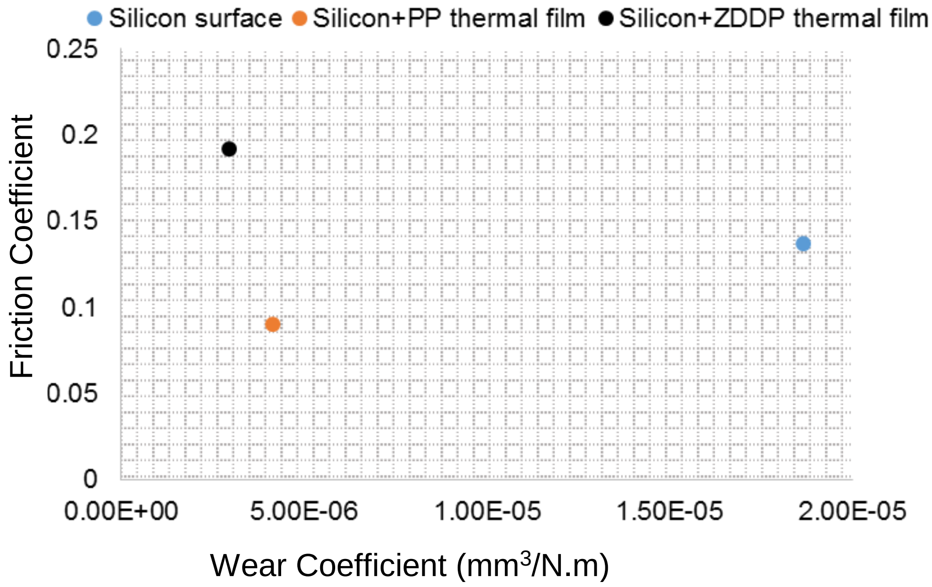

Figure 8-3: The tribological properties of PP and ZDDP thermal films.

PP thermal film shows lower friction coefficient than ZDDP one (see Fig. 8-3). This has been assigned to the effect of film chemistry (the presence of zinc in ZDDP thermal film). ZDDP still shows a higher reduction in wear after the increase of temperature to 80 ^{o}C. This finding is in contrast to the previous findings in [162]. However, the applied sliding distances in [162] is 4000 m while only 14.4 m is applied in the current study. Besides, for PP, a lower friction coefficient is obtained after the increase of temperature.

This can be related to the increase of the tribofilms thicknesses (ZDDP and PP). This increase lead to decrease wear (the presence of wear debris) and thus the friction coefficient in PP is decreased. In contrast, the increase of ZDDP tribofilm thickness leads to a slight increase in friction coefficient. This can be resulted from the high friction nature of ZDDP protective film (see Fig. 8-3).

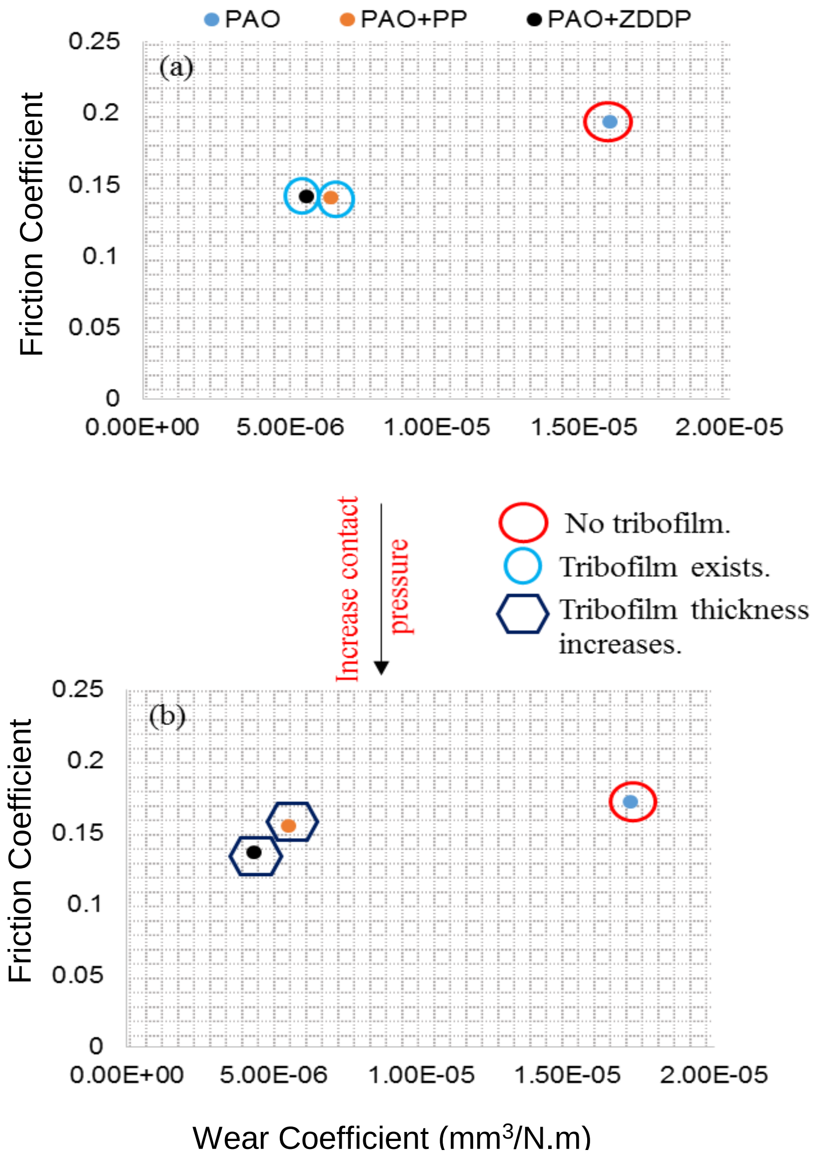

Figure 8-4: The relationship between the ZDDP and PP tribofilms formation with their tribological behaviour at: (a) 597 MPa and (b) at 700 MPa.

After that, the increase of sliding distance reveals a new behaviour (see Fig. 8-5). PP shows a better anti-wear performance after increasing the sliding distance (from 14.4m to 36m). This results from the depletion of ZDDP.

The higher tribofilm formation rate of ZDDP causes a faster depletion. Thus, PP shows a higher protection against wear. Another confirmation to this finding, Qu *et al* in [162] reported that the tribofilm that lubricated by PAO+ZDDP got failure after 400 m of sliding while PP kept the system working for 4000 m.

Lastly, after these findings the differences between the lubrication mechanisms of PP and ZDDP can be identified. Both additives react with the silicon surfaces and form an anti-wear layer (tribo/thermal film). The formation rate of ZDDP thermal/tribo film is higher and thus a thicker film can be obtained (see Figs. 4-4, 4-9 and 5-8). As a result, ZDDP provides a higher protection against wear. However, the higher formation rate leads to a faster depletion in ZDDP form the bulk lubricant (PAO+ZDDP) than PP from the bulk lubricant (PAO+PP). This finding can clarify and confirm the previous findings in [23, 28, 29, 162] when PP showed a better anti-wear performance at certain conditions.

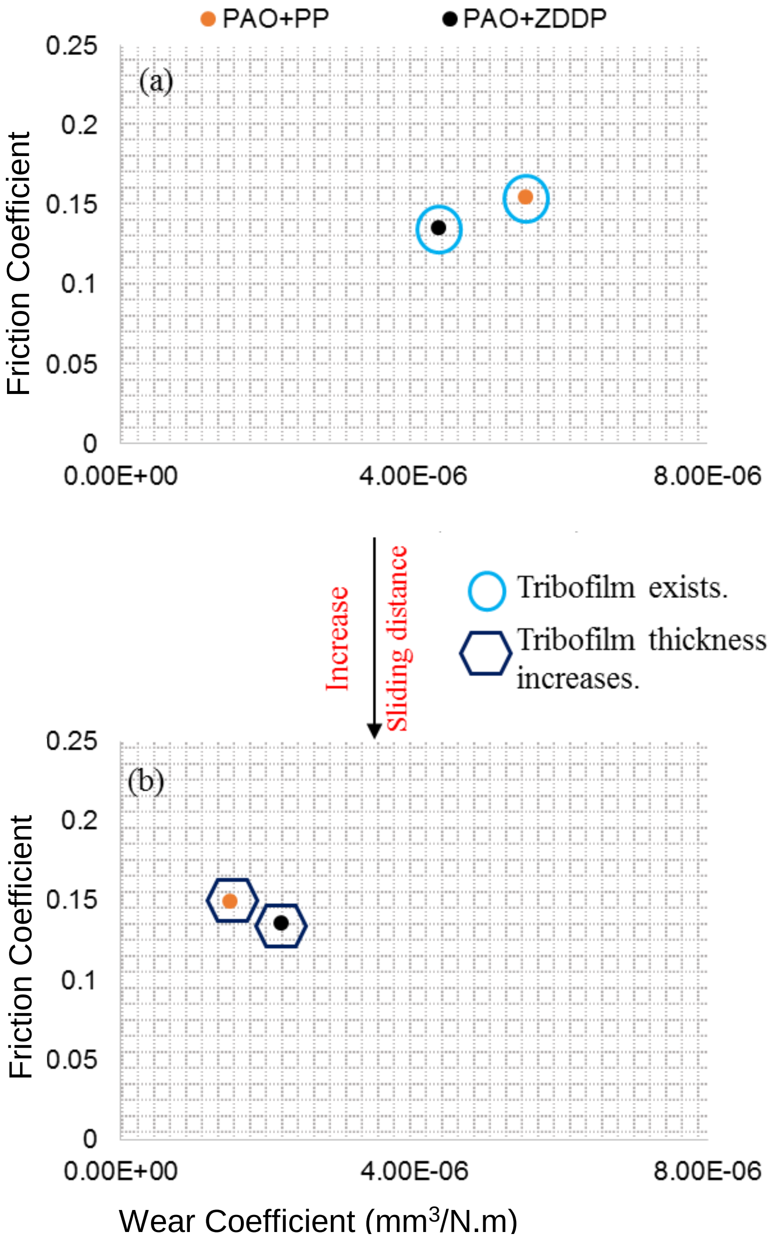

Figure 8-5: The relationship between the ZDDP and PP tribofilms formation with their tribological behaviour at: (a) 14.4 m and (b) 36 m.

9. Chapter 9: Conclusions and Future Work

9.1 Conclusions

A wide study has been conducted to understand the lubrication mechanism of ILs when they are used as either additives or potential lubricants. In order to understand the lubrication mechanism: the formation of thermal films, the durability of thermal films and the formation of tribofilms at various conditions are studied.

At the first part of this study; the use of oil-soluble IL as additive has been compared with the common anti-wear additive ZDDP when lubricating engines. Thus, steel against silicon in ball on plate configuration is used.

Both anti-wear additives have reacted and formed thermal films. However, ZDDP is capable to form thicker and more durable thermal film than PP at the same applied conditions. This results from the chemistry of ZDDP since the presence of zinc (as a metallic cation) can feed the reaction of the formation of thermal film. In contrast, away from the silicon surface, there is no positive cation to sustain the formation of the PP thermal film (after the decomposition process). In addition to its higher thickness, the presence of zinc at the ZDDP thermal film results a more durable film. The same behaviour has been observed for the formation of the tribofilms at various tribological conditions. The formation of the thermal/tribo films controls the tribological performance of both additives. The thicker thermal/tribo films leads to a better anti-wear performance.

These lead to make ZDDP provide better anti-wear performance than the oil-soluble IL. Nevertheless, the higher formation rate of therma/tribo films of ZDDP causes a faster depletion. Thus, at particular conditions, especially after long sliding distance and at sever conditions the oil-soluble IL might show better tribological performance (due to the depletion of the ZDDP).

After that, the lubrication mechanism of ILs as potential lubricants is studied when lubricating MEMS. Thus, borosilicate ball against silicon in ball on plate configuration is used. Five ILs have been used in order to reveal the influence of ILs chemistry on their lubrication mechanism.

The use of FTIR to assess the thermal stability of ILs is more accurate than TGA. The partial decomposition can be noticed and the decomposition mechanism can be studied. All ILs have been decomposed before the formation of the thermal/tribo film. Despite the high reactivity of the examined ILs with the silicon surfaces, since they form thermal films at all conditions, the resulted films are very thin and they are not durable. Thus, the films have been destructed by the tribological motion. The films has been detected after the test only when the formation rate of the tribofilm is higher than the destruction rate. The higher formation rate of the tribofilm leads to a better tribological performance since the presence of the tribofilm reduces both friction and wear coefficients.

In terms of the influence of the ILs chemistry, the longer anion/cation chain length leads to a better tribological performance due to not only the higher viscosity but also due to the higher reactivity. The anion type and the cation type are very crucial in the determination of the tribological performance. Thus, the more reactive anion/cation moiety can provide better triological performance. This will lead to a high formation rate of the tribofilm and therefor better tribological performance.

9.2 Future Work

Several studies can be conducted in the future which can be linked with the obtained results in this study, as follow:

- The use of IL to coat silicon substrate and compare the results with the use of IL as liquid lubricant. The use of coating instead of liquid lubricant is easier to be applied in MEMS. This work will be started in a collaboration with another research group.
- Manufacturing MEMSs and lubricate them with IL. This can result a correlation between the results of nanotribometer and the real MEMS. This work will be started once the manufacturing process is offered by one of the MEMSs' manufacturers.
- The use of ILs as microcapsules in the base lubricant can offer many advantages. The insolubility issue will be solved and the release mechanism can be controlled. This work is already undergoing.
- Verify the contact area by loading the ball on the surface and measure the real area of contact.
- Conduct an in-situ study through the use of synchrotron in order to observe the formation of the tribofilm in-situ.
- MD simulation for prediction of the effect of anion/cation chain length on the reactivity of ILs. The results can be validated by comparing them with the available experimental data.

Lastly, apart from this study, ILs can be used to lubricate the compressors in the vapour compression systems. The high polarity of ILs will make them highly soluble in the refrigerants. In addition, the non-flammable, low vapour pressure and high thermal conductivity are strongly desirable in the vapour compression systems.

10. References

1. Holmberg, K., *et al*., *Global energy consumption due to friction in trucks and buses.* Tribology International, 2014. **78**: p. 94-114.
2. Holmberg, K., P. Andersson, and A. Erdemir, *Global energy consumption due to friction in passenger cars.* Tribology International, 2012. **47**: p. 221-234.
3. Minami, I., *Ionic liquids in tribology.* Molecules, 2009. **14**(6): p. 2286-2305.
4. Somers, A.E., *et al*., *A review of ionic liquid lubricants.* Lubricants, 2013. **1**(1): p. 3-21.
5. Palacio, M. and B. Bhushan, *A review of ionic liquids for green molecular lubrication in nanotechnology.* Tribology Letters, 2010. **40**(2): p. 247-268.
6. Zhou, Y. and J. Qu, *Ionic Liquids as Lubricant Additives – a Review.* ACS Applied Materials & Interfaces, 2016.
7. Erdemir, A. and O. Eryilmaz, *Achieving superlubricity in DLC films by controlling bulk, surface, and tribochemistry.* Friction, 2014. **2**(2): p. 140-155.
8. Ala'A, A.-A., *et al*., *Nano-texture for a wear-resistant and near-frictionless diamond-like carbon.* Carbon, 2014. **73**: p. 403-412.
9. Pensado, A., M. Comunas, and J. Fernandez, *The pressure–viscosity coefficient of several ionic liquids.* Tribology Letters, 2008. **31**(2): p. 107-118.
10. Ye, C., *et al*., *Room-temperature ionic liquids: a novel versatile lubricant.* Chemical Communications, 2001(21): p. 2244-2245.
11. Street, K.W., *et al*., *Evaluation of Vapor Pressure and Ultra-High Vacuum Tribological Properties of Ionic Liquids.* Tribology Transactions, 2011. **54**(6): p. 911-919.
12. Wang, H., *et al*., *Friction and wear behaviors of ionic liquid of alkylimidazolium hexafluorophosphates as lubricants for steel/steel contact.* Wear, 2004. **256**(1–2): p. 44-48.
13. Liu, W., *et al*., *Tribological Performance of Room-Temperature Ionic Liquids as Lubricant.* Tribology Letters, 2002. **13**(2): p. 81-85.

14. Omotowa, B.A., *et al*., *Phosphazene-Based Ionic Liquids: Synthesis, Temperature-Dependent Viscosity, and Effect as Additives in Water Lubrication of Silicon Nitride Ceramics.* Inorganic Chemistry, 2004. **43**(17): p. 5466-5471.
15. Yagi, T., *et al*., *Lubricity and chemical reactivity of ionic liquid used for sliding metals under high-vacuum conditions.* Proceedings of the Institution of Mechanical Engineers, Part J: Journal of Engineering Tribology, 2009. **223**(7): p. 1083-1090.
16. Totolin, V., *et al*., *Tribological investigations of ionic liquids in ultra-high vacuum environment.* Lubrication Science, 2014. **26**(7-8): p. 514-524.
17. Shah, F.U., *et al*., *Novel halogen-free chelated orthoborate–phosphonium ionic liquids: synthesis and tribophysical properties.* Physical chemistry chemical physics, 2011. **13**(28): p. 12865-12873.
18. Minami, I., T. Inada, and Y. Okada, *Tribological properties of halogen-free ionic liquids.* Proceedings of the Institution of Mechanical Engineers, Part J: Journal of Engineering Tribology, 2012. **226**(11): p. 891-902.
19. Wu, J., *et al*., *Halogen-free ionic liquids as excellent lubricants for PEEK-stainless steel contacts at elevated temperatures.* Tribology International, 2016. **104**: p. 1-9.
20. Totolin, V., *et al*., *Halogen-free borate ionic liquids as novel lubricants for tribological applications.* Tribology International, 2013. **67**: p. 191-198.
21. Gusain, R., *et al*., *Halogen-free imidazolium/ammonium-bis (salicylato) borate ionic liquids as high performance lubricant additives.* RSC Advances, 2014. **4**(3): p. 1293-1301.
22. Phillips, B.S. and J.S. Zabinski, *Ionic Liquid Lubrication Effects on Ceramics in a Water Environment.* Tribology Letters, 2004. **17**(3): p. 533-541.
23. Yu, B., *et al*., *Oil-miscible and non-corrosive phosphonium-based ionic liquids as candidate lubricant additives.* Wear, 2012. **289**: p. 58-64.

24. Nainaparampil, J.J., *et al*., *Ionic-liquid lubrication of sliding MEMS contacts: comparison of AFM liquid cell and device-level tests.* Journal of microelectromechanical systems, 2007. **16**(4): p. 836.
25. Pagano, F., *et al*., *Dicationic ionic liquids as lubricants.* Proceedings of the Institution of Mechanical Engineers, Part J: Journal of Engineering Tribology, 2012. **226**(11): p. 952-964.
26. Minami, I., *et al*., *The Tribological Properties of Ionic Liquids Composed of Trifluorotris(pentafluoroethyl) Phosphate as a Hydrophobic Anion.* Tribology Letters, 2008. **30**(3): p. 215-223.
27. Itoh, T., *et al*., *Design of Alkanesulfonate Ionic Liquids for Lubricants.* Chemistry Letters, 2009. **38**(1): p. 64-65.
28. Zhou, Y., *et al*., *Understanding Tribofilm Formation Mechanisms in Ionic Liquid Lubrication.* Scientific Reports, 2017. **7**.
29. Qu, J., *et al*., *Comparison of an oil-miscible ionic liquid and ZDDP as a lubricant anti-wear additive.* Tribology International, 2014. **71**: p. 88-97.
30. Archard, J., *Surface topography and tribology.* Tribology, 1974. **7**(5): p. 213-220.
31. Torbacke, M., A.K. Rudolphi, and E. Kassfeldt, *Lubricants: introduction to properties and performance*. 2014: John Wiley & Sons.
32. Dresel, T.M.a.W., ed. *Lubricants and Lubrication*. 2nd ed. Completely Revised and Extended Edition. 2007, WILEY. 890.
33. Jost, P., *Lubrication (Tribology) Education and Research. UK Department of Education and Science*. 1966, HMSO.
34. Committee, A.I.H., *ASM handbook: Friction, lubrication, and wear technology*. Vol. 18. 1992: ASM International.
35. Johnson, K.L. and K.L. Johnson, *Contact mechanics*. 1987: Cambridge university press.
36. Stribeck, R. and M. Schröter, *Die wesentlichen Eigenschaften der Gleit-und Rollenlager: Untersuchung einer Tandem-Verbundmaschine von 1000 PS*. 1903: Springer.
37. Hamrock, B.J. and D. Dowson, *Ball bearing lubrication: the elastohydrodynamics of elliptical contacts.* 1981.

38. Archard, J., *Contact and rubbing of flat surfaces.* Journal of applied physics, 1953. **24**(8): p. 981-988.
39. Comstock, M.J., *Surface Science Investigations in Tribology, Copyright, ACS Symposium Series, Foreword*, in *Surface Science Investigations in Tribology*, M.J. Comstock, Editor. 1992, American Chemical Society. p. i-vi.
40. Zhang, J. and H. Spikes, *On the mechanism of ZDDP antiwear film formation.* Tribology Letters, 2016. **63**(2): p. 1-15.
41. Castañeda Ugarteburu, M., *Assessment of the water content in several ionic liquids using the coulometric Karl Fischer technique.* 2015.
42. Patel, D.D. and J.M. Lee, *Applications of ionic liquids.* The Chemical Record, 2012. **12**(3): p. 329-355.
43. Zhang, S. and K. Dong, *Structures and interactions of ionic liquids*. Vol. 151. 2013: Springer.
44. Qu, J., *et al.*, *Ionic liquids with ammonium cations as lubricants or additives.* Tribology Letters, 2006. **22**(3): p. 207-214.
45. Lu, Q., *et al.*, *Room temperature ionic liquid 1-ethyl-3-hexylimidazolium-bis(trifluoromethylsulfonyl)-imide as lubricant for steel–steel contact.* Tribology International, 2004. **37**(7): p. 547-552.
46. López-Sánchez, F., *et al.*, *Tribological Behavior of Two 1-Ethyl-3-methylimidazolium Alkyl Sulfates as Neat Lubricants for a Steel–Steel Contact.* Tribology Transactions, 2016: p. 1-10.
47. Li, H., *et al.*, *Combined Nano-and Macrotribology Studies of Titania Lubrication Using the Oil-Ionic Liquid Mixtures.* ACS Sustainable Chemistry & Engineering, 2016. **4**(9): p. 5005-5012.
48. Qu, J., *et al.*, *Tribological characteristics of aluminum alloys sliding against steel lubricated by ammonium and imidazolium ionic liquids.* Wear, 2009. **267**(5–8): p. 1226-1231.
49. Jiménez, A.E., *et al.*, *1-N-alkyl -3-methylimidazolium ionic liquids as neat lubricants and lubricant additives in steel–aluminium contacts.* Wear, 2006. **260**(7–8): p. 766-782.

50. Somers, A.E., *et al*., *A comparison of phosphorus and fluorine containing IL lubricants for steel on aluminium.* Physical Chemistry Chemical Physics, 2012. **14**(22): p. 8224-8231.
51. Bermúdez, M. and A. Jiménez, *Surface interactions in lubrication of titanium, aluminium, and titanium–aluminium alloys with the ionic liquid [C2mim]Tf2N under increasing temperature.* Proceedings of the Institution of Mechanical Engineers, Part J: Journal of Engineering Tribology, 2012. **226**(11): p. 977-990.
52. Jiménez, A.-E. and M.-D. Bermúdez, *Ionic liquids as lubricants for steel–aluminum contacts at low and elevated temperatures.* Tribology Letters, 2007. **26**(1): p. 53-60.
53. Jiménez, A.E. and M.D. Bermúdez, *Ionic Liquids as Lubricants of Titanium–Steel Contact. Part 2: Friction, Wear and Surface Interactions at High Temperature.* Tribology Letters, 2010. **37**(2): p. 431-443.
54. Kondo, Y., *et al*., *Lubricity and corrosiveness of ionic liquids for steel-on-steel sliding contacts.* Proceedings of the Institution of Mechanical Engineers, Part J: Journal of Engineering Tribology, 2012. **226**(11): p. 991-1006.
55. Chen, *et al*., *Tribological performance of an ionic liquid as a lubricant for steel/aluminium contacts.* Journal of Synthetic Lubrication, 2003. **20**(3): p. 217-225.
56. Zhang, L., D. Feng, and B. Xu, *Tribological Characteristics of Alkylimidazolium Diethyl Phosphates Ionic Liquids as Lubricants for Steel–Steel Contact.* Tribology Letters, 2009. **34**(2): p. 95-101.
57. Song, Z., *et al*., *Green Ionic Liquid Lubricants Prepared from Anti-Inflammatory Drug.* Tribology Letters, 2015. **60**(3): p. 38.
58. Bermudez, M.-D. and A.-E. Jimenez, *Surface interactions and tribochemical processes in Ionic Liquid lubrication of aluminium-steel contacts.* International Journal of Surface Science and Engineering, 2007. **1**(1): p. 100-110.
59. Lu, R., *et al*., *Study of tribochemical decomposition of ionic liquids on a nascent steel surface.* Applied Surface Science, 2009. **255**(22): p. 8965-8971.

60. Xiao, H., *et al*., *Film Thickness of Ionic Liquids Under High Contact Pressures as a Function of Alkyl Chain Length.* Tribology Letters, 2011. **41**(2): p. 471-477.
61. Montanino, M., *et al*., *The role of the cation aliphatic side chain length in piperidinium bis (trifluoromethansulfonyl) imide ionic liquids.* Electrochimica Acta, 2011. **57**: p. 153-159.
62. Wu, J., *et al*., *High load capacity with ionic liquid-lubricated tribological system.* Tribology International, 2016. **94**: p. 315-322.
63. Jiang, D., L. Hu, and D. Feng, *Crown-Type Ionic Liquids as Lubricants for Steel-on-Steel System.* Tribology Letters, 2011. **41**(2): p. 417-424.
64. Mu, Z., *et al*., *Effect of the functional groups in ionic liquid molecules on the friction and wear behavior of aluminum alloy in lubricated aluminum-on-steel contact.* Tribology International, 2005. **38**(8): p. 725-731.
65. Mu, Z., *et al*., *Investigation of Tribological Behavior of Al–Si Alloy Against Steel Lubricated With Ionic Liquids of 1-Diethylphosphonyl-n-propyl-3- Alkylimidazolium Tetrafluoroborate.* Journal of Tribology, 2008. **130**(3): p. 034501-034501.
66. Fan, M., *et al*., *DOSS– Based QAILs: As Both Neat Lubricants and Lubricant Additives with Excellent Tribological Properties and Good Detergency.* Industrial & Engineering Chemistry Research, 2014. **53**(46): p. 17952-17960.
67. Battez, A.H., *et al*., *Friction, wear and tribofilm formation with a [NTf 2] anion-based ionic liquid as neat lubricant.* Tribology International, 2016. **103**: p. 73-86.
68. Qu, J., *et al*., *Nanostructure and Composition of Tribo-Boundary Films Formed in Ionic Liquid Lubrication.* Tribology Letters, 2011. **43**(2): p. 205-211.
69. Otero, I., *et al*., *Ionic Liquids Based on Phosphonium Cations As Neat Lubricants or Lubricant Additives for a Steel/Steel Contact.* ACS Applied Materials & Interfaces, 2014. **6**(15): p. 13115-13128.

70. Liu, X., *et al*., *Tribological performance of phosphonium based ionic liquids for an aluminum-on-steel system and opinions on lubrication mechanism.* Wear, 2006. **261**(10): p. 1174-1179.
71. Somers, A.E., *et al*., *Transition in Wear Performance for Ionic Liquid Lubricants under Increasing Load.* Tribology Letters, 2010. **40**(2): p. 279-284.
72. Saurín, N., *et al*., *Study of the effect of tribo-materials and surface finish on the lubricant performance of new halogen-free room temperature ionic liquids.* Applied Surface Science, 2016. **366**: p. 464-474.
73. Otero, I., *et al*., *Tribo-chemical reactions of anion in pyrrolidinium salts for steel–steel contact.* Tribology International, 2014. **77**: p. 160-170.
74. Taher, M., *et al*., *Halogen-free pyrrolidinium bis (mandelato) borate ionic liquids: some physicochemical properties and lubrication performance as additives to polyethylene glycol.* RSC Advances, 2014. **4**(58): p. 30617-30623.
75. González, R., *et al*., *Lubrication of TiN, CrN and DLC PVD Coatings with 1-Butyl-1-Methylpyrrolidinium tris(pentafluoroethyl)trifluorophosphate.* Tribology Letters, 2010. **40**(2): p. 269-277.
76. Yu, G.Q., *et al*. *Tribological Investigation of Guanidinium Ionic Liquids as Lubricants for Steel/Bronze Contacts*. in *Materials Science Forum*. 2016. Trans Tech Publ.
77. Otero, I., *et al*., *Friction and anti-wear properties of two tris(pentafluoroethyl)trifluorophosphate ionic liquids as neat lubricants.* Tribology International, 2014. **70**: p. 104-111.
78. Jiménez, A.E. and M.-D. Bermúdez, *Ionic Liquids as Lubricants of Titanium–Steel Contact.* Tribology Letters, 2009. **33**(2): p. 111-126.
79. Guo, Y., *et al*., *Application of Alkylphosphate Ionic Liquids as Lubricants for Ceramic Material.* Industrial & Engineering Chemistry Research, 2015. **54**(51): p. 12813-12825.
80. Weng, L., *et al*., *Effect of tetraalkylphosphonium based ionic liquids as lubricants on the tribological performance of a steel-on-steel system.* Tribology Letters, 2007. **26**(1): p. 11-17.

81. Minami, I., *et al*., *Tribo-Chemistry of Phosphonium-Derived Ionic Liquids.* Tribology Letters, 2010. **40**(2): p. 225-235.

82. Fan, M., *et al*., *An Investigation on the Friction and Wear Properties of Perfluorooctane Sulfonate Ionic Liquids.* Tribology Letters, 2016. **63**(1): p. 11.

83. Matczak, L., *et al*., *Effect of cation nature on the lubricating and physicochemical properties of three ionic liquids.* Tribology International, 2018. **124**: p. 23-33.

84. Qu, J., *et al*., *Antiwear Performance and Mechanism of an Oil-Miscible Ionic Liquid as a Lubricant Additive.* ACS Applied Materials & Interfaces, 2012. **4**(2): p. 997-1002.

85. Mistry, K., M.F. Fox, and M. Priest, *Lubrication of an electroplated nickel matrix silicon carbide coated eutectic aluminium—silicon alloy automotive cylinder bore with an ionic liquid as a lubricant additive.* Proceedings of the Institution of Mechanical Engineers, Part J: Journal of Engineering Tribology, 2009. **223**(3): p. 563-569.

86. Cai, M., *et al*., *Alkyl Imidazolium Ionic Liquids as Friction Reduction and Anti-Wear Additive in Polyurea Grease for Steel/Steel Contacts.* Tribology Letters, 2010. **40**(2): p. 215-224.

87. Battez, A.H., *et al*., *Tribological behaviour of two imidazolium ionic liquids as lubricant additives for steel/steel contacts.* Wear, 2009. **266**(11–12): p. 1224-1228.

88. Cai, M., *et al*., *Imidazolium Ionic Liquids As Antiwear and Antioxidant Additive in Poly(ethylene glycol) for Steel/Steel Contacts.* ACS Applied Materials & Interfaces, 2010. **2**(3): p. 870-876.

89. Jiménez, A.-E. and M.-D. Bermúdez, *Imidazolium ionic liquids as additives of the synthetic ester propylene glycol dioleate in aluminium–steel lubrication.* Wear, 2008. **265**(5–6): p. 787-798.

90. Pejaković, V., *et al*., *Influence of concentration and anion alkyl chain length on tribological properties of imidazolium sulfate ionic liquids as additives to glycerol in steel–steel contact lubrication.* Tribology International, 2016. **97**: p. 234-243.

91. Wang, Y., *et al.*, *Ibuprofen-Based Ionic Liquids as Additives for Enhancing the Lubricity and Antiwear of Water–Ethylene Glycol Liquid.* Tribology Letters, 2017. **65**(2): p. 55.

92. Blanco, D., *et al.*, *Lubrication of CrN Coating With Ethyl-Dimethyl-2-Methoxyethylammonium Tris(pentafluoroethyl)Trifluorophosphate Ionic Liquid as Additive to PAO 6.* Tribology Letters, 2011. **41**(1): p. 295-302.

93. Blanco, D., *et al.*, *Use of ethyl-dimethyl-2-methoxyethylammonium tris(pentafluoroethyl)trifluorophosphate as base oil additive in the lubrication of TiN PVD coating.* Tribology International, 2011. **44**(5): p. 645-650.

94. Zheng, G., *et al.*, *Fatty acid based phosphite ionic liquids as multifunctional lubricant additives in mineral oil and refined vegetable oil.* Tribology International, 2018. **123**: p. 316-324.

95. Qu, J., *et al.*, *Characterization of ZDDP and ionic liquid tribofilms on non-metallic coatings providing insights of tribofilm formation mechanisms.* Wear, 2015. **332**: p. 1273-1285.

96. Huang, G., *et al.*, *Oil-soluble ionic liquids as antiwear and extreme pressure additives in poly-α-olefin for steel/steel contacts.* Friction, 2017: p. 1-14.

97. Qu, J., *et al.*, *Synergistic Effects Between Phosphonium-Alkylphosphate Ionic Liquids and Zinc Dialkyldithiophosphate (ZDDP) as Lubricant Additives.* Advanced Materials, 2015. **27**(32): p. 4767-4774.

98. Landauer, A.K., W.C. Barnhill, and J. Qu, *Correlating mechanical properties and anti-wear performance of tribofilms formed by ionic liquids, ZDDP and their combinations.* Wear, 2016. **354**: p. 78-82.

99. Seymour, B.T., *et al.*, *Improved Lubricating Performance by Combining Oil-Soluble Hairy Silica Nanoparticles and an Ionic Liquid as an Additive for a Synthetic Base Oil.* ACS applied materials & interfaces, 2018. **10**(17): p. 15129-15139.

100. Khemchandani, B., *et al.*, *A biocompatible ionic liquid as an antiwear additive for biodegradable lubricants.* Tribology International, 2014. **77**: p. 171-177.

101. Wang, Z., J. Chang, and C. Cai, *Tribological Performance of Phosphonium Ionic Liquids as Additives in Lithium Lubricating Grease.* Lubricants, 2018. **6**(1): p. 23.

102. Pejaković, V., *et al*., *Pyrrolidinium sulfate and ammonium sulfate ionic liquids as lubricant additives for steel/steel contact lubrication.* Proceedings of the Institution of Mechanical Engineers, Part J: Journal of Engineering Tribology, 2012.

103. Schneider, A., *et al*., *Capacity of selected ionic liquids as alternative EP/AW additive.* Lubrication Science, 2010. **22**(6-7): p. 215-223.

104. Sharma, V., *et al*., *Mechanism of tribofilm formation with P and S containing ionic liquids.* Tribology International, 2015. **92**: p. 353-364.

105. Sharma, V., N. Doerr, and P.B. Aswath, *Chemical–mechanical properties of tribofilms and their relationship to ionic liquid chemistry.* RSC Advances, 2016. **6**(27): p. 22341-22356.

106. Jiménez, A.E., *et al*., *Room temperature ionic liquids as lubricant additives in steel–aluminium contacts: Influence of sliding velocity, normal load and temperature.* Wear, 2006. **261**(3–4): p. 347-359.

107. Kronberger, M., *et al*., *How anion and cation species influence the tribology of a green lubricant based on ionic liquids.* Proceedings of the Institution of Mechanical Engineers, Part J: Journal of Engineering Tribology, 2012.

108. Bhushan, B., *Handbook of micro/nano tribology*. 1998: CRC press.

109. Stoyanov, P. and R.R. Chromik, *Scaling effects on materials tribology: from macro to micro scale.* Materials, 2017. **10**(5): p. 550.

110. Li, H., *et al*., *Ionic liquid adsorption and nanotribology at the silica–oil interface: Hundred-fold dilution in oil lubricates as effectively as the pure ionic liquid.* The journal of physical chemistry letters, 2014. **5**(23): p. 4095-4099.

111. Hjalmarsson, N., R. Atkin, and M.W. Rutland, *Is the boundary layer of an ionic liquid equally lubricating at higher temperature?* Physical Chemistry Chemical Physics, 2016. **18**(13): p. 9232-9239.

112. Ku, I., *et al*., *Wear of silicon surfaces in MEMS.* Wear, 2011. **271**(7-8): p. 1050-1058.

113. Reddyhoff, T., *et al*., *Friction modifier behaviour in lubricated MEMS devices.* Tribology letters, 2011. **41**(1): p. 239-246.

114. Leong, J.Y., *Lubrication and tribological performance optimizations for micro-electro-mechanical systems.* 2013.

115. Amorim, P.M., *et al*., *Imidazolium-based ionic liquids used as additives in the nanolubrication of silicon surfaces.* Beilstein Journal of Nanotechnology, 2017. **8**: p. 1961.

116. Bhushan, B., M. Palacio, and B. Kinzig, *AFM-based nanotribological and electrical characterization of ultrathin wear-resistant ionic liquid films.* Journal of colloid and interface science, 2008. **317**(1): p. 275-287.

117. Kondo, H., *et al*., *Thin Film Properties of Ammonium Sulfonate Ionic Liquids Having a Long Alkyl Chain.* Bulletin of the Chemical Society of Japan, 2016.

118. Gosvami, N., *et al*., *Mechanisms of antiwear tribofilm growth revealed in situ by single-asperity sliding contacts.* Science, 2015. **348**(6230): p. 102-106.

119. Palacio, M. and B. Bhushan, *Nanotribological properties of novel lubricants for magnetic tapes.* Ultramicroscopy, 2009. **109**(8): p. 980-990.

120. Pu, J., *et al*., *Preparation and characterization of ultrathin dual-layer ionic liquid lubrication film assembled on silica surfaces.* Journal of colloid and interface science, 2011. **354**(2): p. 858-865.

121. Zhao, W., *et al*., *Influence of heat treatment on the micro/nano-tribological properties of ultra-thin ionic liquid films on silicon.* Colloids and Surfaces A: Physicochemical and Engineering Aspects, 2010. **361**(1–3): p. 118-125.

122. Yu, B., *et al*., *Tribological properties of ultra-thin ionic liquid films on single-crystal silicon wafers with functionalized surfaces.* Tribology International, 2006. **39**(9): p. 879-887.

123. Perkin, S., *Ionic liquids in confined geometries.* Physical Chemistry Chemical Physics, 2012. **14**(15): p. 5052-5062.

124. Elbourne, A., *et al*., *Ion structure controls ionic liquid near-surface and interfacial nanostructure*.

125. Li, H., F. Endres, and R. Atkin, *Effect of alkyl chain length and anion species on the interfacial nanostructure of ionic liquids at the Au (111)–ionic liquid interface as a function of potential.* Physical Chemistry Chemical Physics, 2013. **15**(35): p. 14624-14633.
126. Howlett, P.C., *et al.*, *An Investigation of a Phosphinate-Based Ionic Liquid for Corrosion Protection of Magnesium Alloy AZ31.* Australian Journal of Chemistry, 2007. **60**(1): p. 43-46.
127. Zhang, Q.B. and Y.X. Hua, *Corrosion inhibition of mild steel by alkylimidazolium ionic liquids in hydrochloric acid.* Electrochimica Acta, 2009. **54**(6): p. 1881-1887.
128. Stachowiak, G. and A.W. Batchelor, *Experimental methods in tribology*. Vol. 44. 2004: Elsevier.
129. Binnig, G., C.F. Quate, and C. Gerber, *Atomic force microscope.* Physical review letters, 1986. **56**(9): p. 930.
130. Yablon, D.G., *Overview of Atomic Force Microscopy.* Scanning Probe Microscopy in Industrial Applications: Nanomechanical Characterization, 2013: p. 1-14.
131. Balthazar, J.M., *et al.*, *On an Overview of Nonlinear and Chaotic Behavior and Their Controls of an Atomic Force Microscopy (AFM) Vibrating Problem*. Nonlinearity, Bifurcation and Chaos - Theory and Applications. 2012.
132. Palacio, M.L. and B. Bhushan, *Normal and lateral force calibration techniques for AFM cantilevers.* Critical Reviews in Solid State and Materials Sciences, 2010. **35**(2): p. 73-104.
133. Pejaković, V., M. Kronberger, and M. Kalin, *Influence of temperature on tribological behaviour of ionic liquids as lubricants and lubricant additives.* Lubrication Science, 2014. **26**(2): p. 107-115.
134. Li, H., *et al.*, *Addition of low concentrations of an ionic liquid to a base oil reduces friction over multiple length scales: a combined nano-and macrotribology investigation.* Physical Chemistry Chemical Physics, 2016. **18**(9): p. 6541-6547.
135. Socrates, G., *Infrared and Raman characteristic group frequencies: tables and charts*. 2004: John Wiley & Sons.

136. Nyquist, R.A., *Interpreting infrared, Raman, and nuclear magnetic resonance spectra*. 2001: Academic Press.

137. Meier, R.J., *Calculating the vibrational spectra of molecules: An introduction for experimentalists with contemporary examples.* Vibrational spectroscopy, 2007. **43**(1): p. 26-37.

138. Swinehart, D., *The beer-lambert law.* J. Chem. Educ, 1962. **39**(7): p. 333.

139. Wheeler, J.L., *et al*., *Thermal Breakdown Kinetics of 1-Ethyl-3-Methylimidazolium Ethylsulfate Measured Using Quantitative Infrared Spectroscopy.* Applied Spectroscopy, 2017: p. 0003702817727293.

140. Kiefer, J., J. Fries, and A. Leipertz, *Experimental vibrational study of imidazolium-based ionic liquids: Raman and infrared spectra of 1-ethyl-3-methylimidazolium bis (trifluoromethylsulfonyl) imide and 1-ethyl-3-methylimidazolium ethylsulfate.* Applied spectroscopy, 2007. **61**(12): p. 1306-1311.

141. Paschoal, V.H., L.F. Faria, and M.C. Ribeiro, *Vibrational Spectroscopy of Ionic Liquids.* Chemical reviews, 2017. **117**(10): p. 7053-7112.

142. Zhang, Q.-G., N.-N. Wang, and Z.-W. Yu, *The hydrogen bonding interactions between the ionic liquid 1-ethyl-3-methylimidazolium ethyl sulfate and water.* The Journal of Physical Chemistry B, 2010. **114**(14): p. 4747-4754.

143. Buffeteau, T., J. Grondin, and J.-C. Lassègues, *Infrared spectroscopy of ionic liquids: quantitative aspects and determination of optical constants.* Applied spectroscopy, 2010. **64**(1): p. 112-119.

144. Radetic, T., *Fundamentals of Scanning Electron Microscopy and Energy Dispersive X-ray Analysis in SEM and TEM.* Faculdade de Tecnologia e Metalurgia, Universidade de Belgrado, Servia, 2011.

145. Mukhopadhyay, S.M., *Sample preparation for microscopic and spectroscopic characterization of solid surfaces and films.* Sample Preparation Techniques in Analytical Chemistry, 2003. **162**(9): p. 377-411.

146. Watts, J.F. and J. Wolstenholme, *An introduction to surface analysis by XPS and AES.* An Introduction to Surface Analysis by XPS and

AES, by John F. Watts, John Wolstenholme, pp. 224. ISBN 0-470-84713-1. Wiley-VCH, May 2003., 2003: p. 224.

147. Watts, J.F., *X-ray photoelectron spectroscopy.* Vacuum, 1994. **45**(6-7): p. 653-671.

148. Gouzman, I., *et al*., *Monolayer vs. multilayer self-assembled alkylphosphonate films: X-ray photoelectron spectroscopy studies.* Surface Science, 2006. **600**(4): p. 773-781.

149. Scofield, J., *Hartree-Slater subshell photoionization cross-sections at 1254 and 1487 eV.* Journal of Electron Spectroscopy and Related Phenomena, 1976. **8**(2): p. 129-137.

150. Tanuma, S., C. Powell, and D. Penn, *Calculations of electron inelastic mean free paths.* Surface and Interface Analysis, 2005. **37**(1): p. 1-14.

151. Reilman, R.F., A. Msezane, and S.T. Manson, *Relative intensities in photoelectron spectroscopy of atoms and molecules.* Journal of Electron Spectroscopy and Related Phenomena, 1976. **8**(5): p. 389-394.

152. Gabbott, P., *Principles and applications of thermal analysis*. 2008: John Wiley & Sons.

153. Yu, G., *et al*., *Viscosity of ionic liquids: Database, observation, and quantitative structure‐property relationship analysis.* AIChE Journal, 2012. **58**(9): p. 2885-2899.

154. Wasserscheid, P. and T. Welton, *Ionic liquids in synthesis*. 2008: John Wiley & Sons.

155. Burkinshaw, M., *et al*., *Calcium sulphonate and its interactions with ZDDP on both aluminium–silicon and model silicon surfaces.* Tribology International, 2012. **46**(1): p. 41-51.

156. Hamrock, B.J. and D. Dowson, *Minimum film thickness in elliptical contacts for different regimes of fluid-film lubrication.* 1978.

157. Arcifa, A., A. Rossi, and N.D. Spencer, *Adsorption and Tribochemical Factors Affecting the Lubrication of Silicon-Based Materials by (Fluorinated) Ionic Liquids.* The Journal of Physical Chemistry C, 2017.

158. Harris, K.R., M. Kanakubo, and L.A. Woolf, *Temperature and Pressure Dependence of the Viscosity of the Ionic Liquids 1-Hexyl-3-*

methylimidazolium Hexafluorophosphate and 1-Butyl-3-methylimidazolium Bis (trifluoromethylsulfonyl) imide. Journal of Chemical & Engineering Data, 2007. **52**(3): p. 1080-1085.

159. Gaciño, F.M., *et al*., *Effect of the pressure on the viscosities of ionic liquids: Experimental values for 1-ethyl-3-methylimidazolium ethylsulfate and two bis (trifluoromethyl-sulfonyl) imide salts.* The Journal of Chemical Thermodynamics, 2012. **54**: p. 302-309.
160. Mangolini, F., A. Rossi, and N.D. Spencer, *Influence of metallic and oxidized iron/steel on the reactivity of triphenyl phosphorothionate in oil solution.* Tribology International, 2011. **44**(6): p. 670-683.
161. Zhang, Z., *et al*., *Tribofilms generated from ZDDP and DDP on steel surfaces: Part 1, growth, wear and morphology.* Tribology Letters, 2005. **19**(3): p. 211-220.
162. Qu, J., *et al*., *Antiwear performance and mechanism of an oil-miscible ionic liquid as a lubricant additive.* ACS applied materials & interfaces, 2012. **4**(2): p. 997-1002.
163. Akbari, S., J. Kovač, and M. Kalin, *Effect of ZDDP concentration on the thermal film formation on steel, hydrogenated non-doped and Si-doped DLC.* Applied Surface Science, 2016. **383**: p. 191-199.
164. Mangolini, F., *Reactivity of environmentally compatible lubricant additives: an In Situ and Ex Situ Investigation*. 2011, Politecnico di Milano (Italy.
165. Mangolini, F., A. Rossi, and N.D. Spencer, *Chemical reactivity of triphenyl phosphorothionate (TPPT) with iron: an ATR/FT-IR and XPS investigation.* The Journal of Physical Chemistry C, 2010. **115**(4): p. 1339-1354.
166. Crobu, M., *et al*., *Chain-length-identification strategy in zinc polyphosphate glasses by means of XPS and ToF-SIMS.* Analytical and bioanalytical chemistry, 2012. **403**(5): p. 1415-1432.
167. Langer, D. and C. Vesely, *Electronic core levels of zinc chalcogenides.* Physical Review B, 1970. **2**(12): p. 4885.
168. Gaarenstroom, S. and N. Winograd, *Initial and final state effects in the ESCA spectra of cadmium and silver oxides.* The Journal of Chemical Physics, 1977. **67**(8): p. 3500-3506.

169. Bruker, *Attenuated Total Reflection (ATR) – a versatile tool for FT-IR spectroscopy* B. Optics, Editor. 2011, Bruker Optics BOPT-4000352-01.
170. Johnson, D. and J. Hils, *Phosphate Esters, Thiophosphate Esters and Metal Thiophosphates as Lubricant Additives.* Lubricants, 2013. **1**(4): p. 132.
171. Improving Wind Turbine Gearbox Reliability, W.M., S. Butterfield, B. McNiff, NREL/CP-500-41548, European Wind Energy Conference, Milan, Italy, May 2007.
172. Zhou, Y., *et al*., *Understanding Tribofilm Formation Mechanisms in Ionic Liquid Lubrication.* Scientific reports, 2017. **7**(1): p. 8426.
173. *Elastic deformation and the laws of friction.* Proceedings of the Royal Society of London. Series A. Mathematical and Physical Sciences, 1957. **243**(1233): p. 190-205.
174. Spikes, H., *The history and mechanisms of ZDDP.* Tribology letters, 2004. **17**(3): p. 469-489.
175. Van Valkenburg, M.E., *et al*., *Thermochemistry of ionic liquid heat-transfer fluids.* Thermochimica Acta, 2005. **425**(1): p. 181-188.
176. Parajó, J.J., *et al*., *Thermal stability of aprotic ionic liquids as potential lubricants. Comparison with synthetic oil bases.* The Journal of Chemical Thermodynamics, 2017.
177. Ferreira, A.F., P.N. Simões, and A.G. Ferreira, *Quaternary phosphonium-based ionic liquids: Thermal stability and heat capacity of the liquid phase.* The Journal of Chemical Thermodynamics, 2012. **45**(1): p. 16-27.
178. Gonfa, G., *et al*. *Thermophysical Properties of Ionic Liquid with Thiocyanate Anion: Effect of Cations*. in *Advanced Materials Research*. 2013. Trans Tech Publ.
179. Maton, C., N. De Vos, and C.V. Stevens, *Ionic liquid thermal stabilities: decomposition mechanisms and analysis tools.* Chemical Society Reviews, 2013. **42**(13): p. 5963-5977.
180. Snyder Jr, C.E. and R.E. Dolle Jr, *Development of polyperfluoroalkylethers as high temperature lubricants and hydraulic fluids.* ASLE TRANSACTIONS, 1976. **19**(3): p. 171-180.

181. Feng, W.-q., *et al*., *Thermal stability of imidazolium-based ionic liquids investigated by TG and FTIR techniques.* Journal of Thermal Analysis and Calorimetry, 2016. **125**(1): p. 143-154.
182. Arcifa, A., *et al*., *Lubrication of Si-Based Tribopairs with a Hydrophobic Ionic Liquid: The Multiscale Influence of Water.* The Journal of Physical Chemistry C, 2018.
183. Laidler, K.J., *The development of the Arrhenius equation.* Journal of Chemical Education, 1984. **61**(6): p. 494.
184. Seddon, K.R., A. Stark, and M.-J. Torres, *Viscosity and density of 1-alkyl-3-methylimidazolium ionic liquids*. 2002, ACS Publications.
185. Denape, J. and J. Lamon, *Sliding friction of ceramics: Mechanical action of the wear debris.* Journal of Materials Science, 1990. **25**(8): p. 3592-3604.
186. Schaerli, M. and J. Brunner, *Bremsstrahlung-induced Auger transitions and photoemission in elemental red phosphorus.* Zeitschrift für Physik B Condensed Matter, 1981. **42**(4): p. 285-289.
187. Ghalme, S., A. Mankar, and Y. Bhalerao, *Effect of lubricant viscosity and surface roughness on coefficient of friction in rolling contact.* Tribology in Industry, 2013. **35**(4): p. 330-336.

11. Appendix 1: XPS data process

CasaXPS has been used to process XPS results, and the following steps show the full process:

1- The process starts with the scan of the survey, as follows:

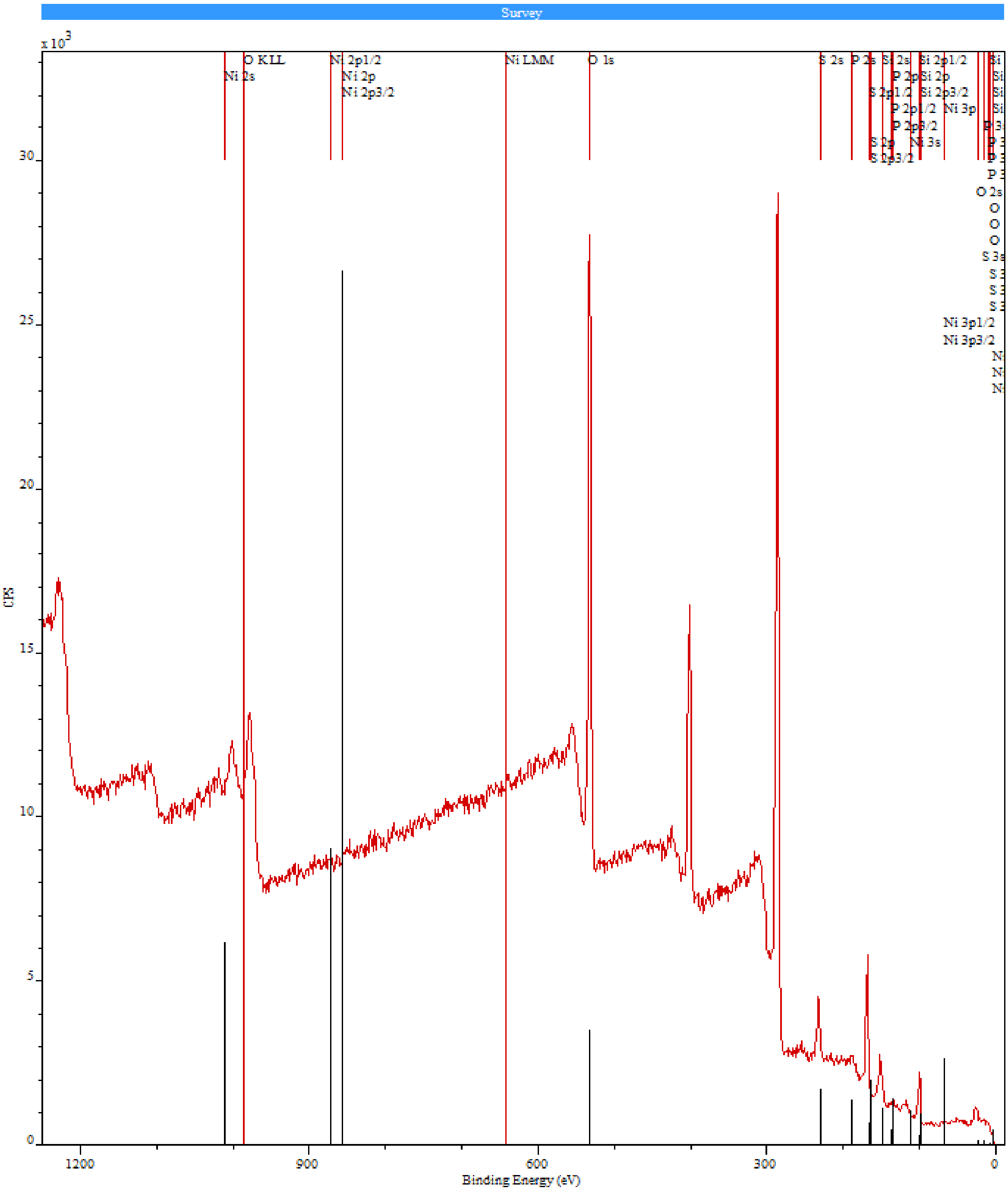

2- All peaks have been scanned at the high resolution region. Some other peaks has been scanned at the high resolution (those expected but have not been shown on survey).

3- The calibration process has been made based on the binding energy of the C1s peak when it is shifted to 285 eV. This process is applied for all peaks.

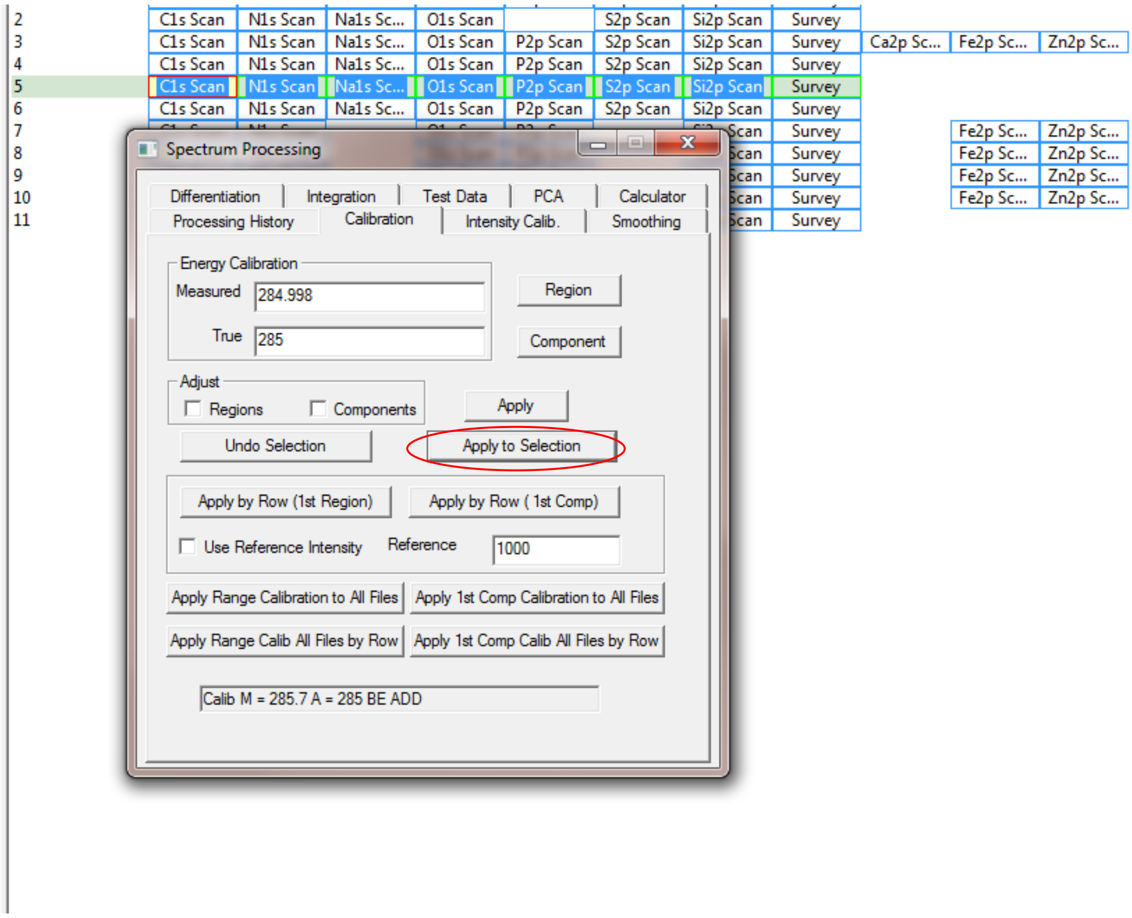

Measured 284.998

True 285

Reference 1000

Calib M = 285.7 A = 285 BE ADD

4- Shirley back ground was applied.

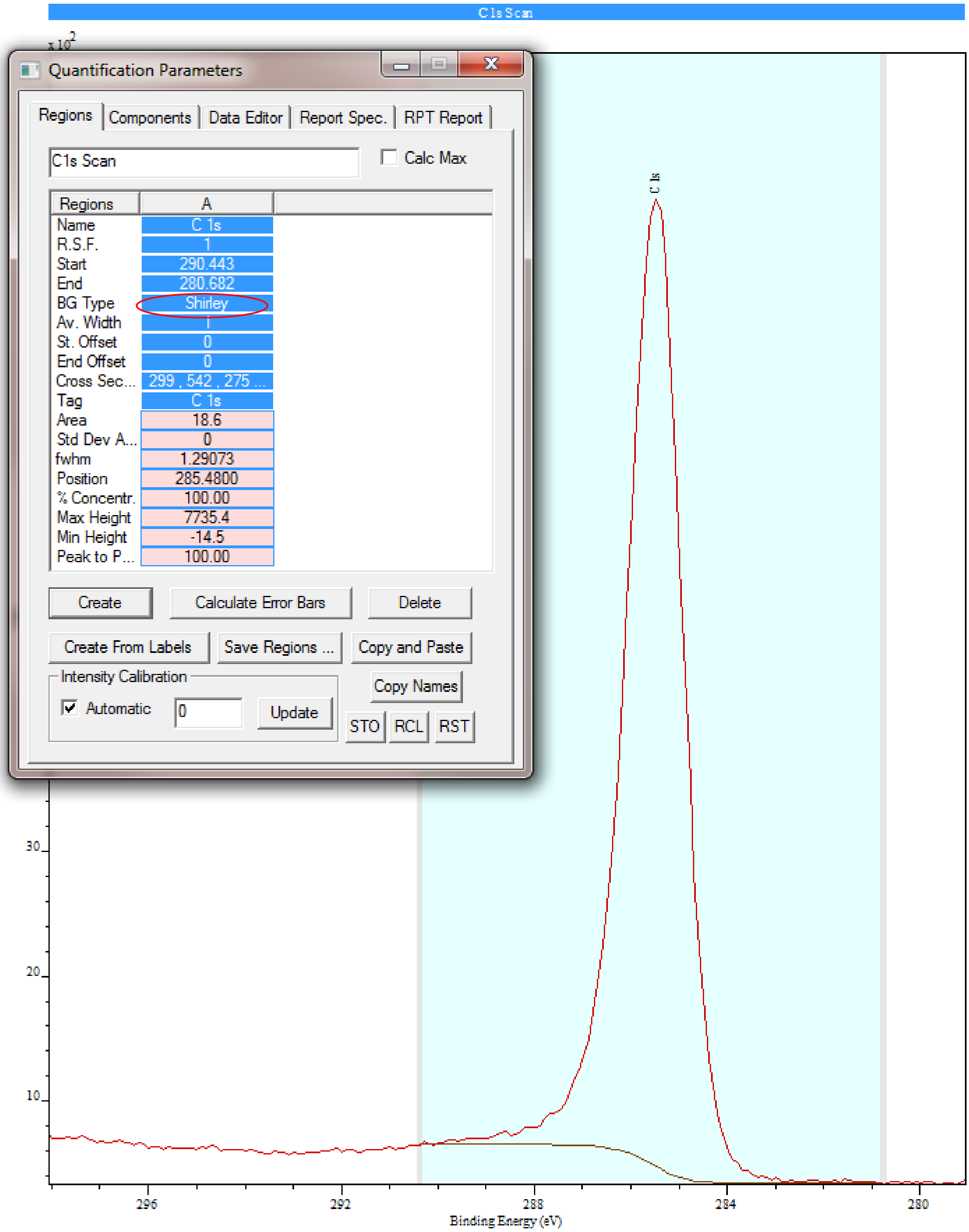

C1s Scan

☐ Calc Max

Regions	A
Name	C 1s
R.S.F.	1
Start	290.443
End	280.682
BG Type	Shirley
Av. Width	1
St. Offset	0
End Offset	0
Cross Sec...	299 , 542 , 275 ...
Tag	C 1s
Area	18.6
Std Dev A...	0
fwhm	1.29073
Position	285.4800
% Concentr.	100.00
Max Height	7735.4
Min Height	-14.5
Peak to P...	100.00

Intensity Calibration

☑ Automatic 0

5- The Full Width Half Maximum was kept the same for all peaks during the curve fitting for each element.

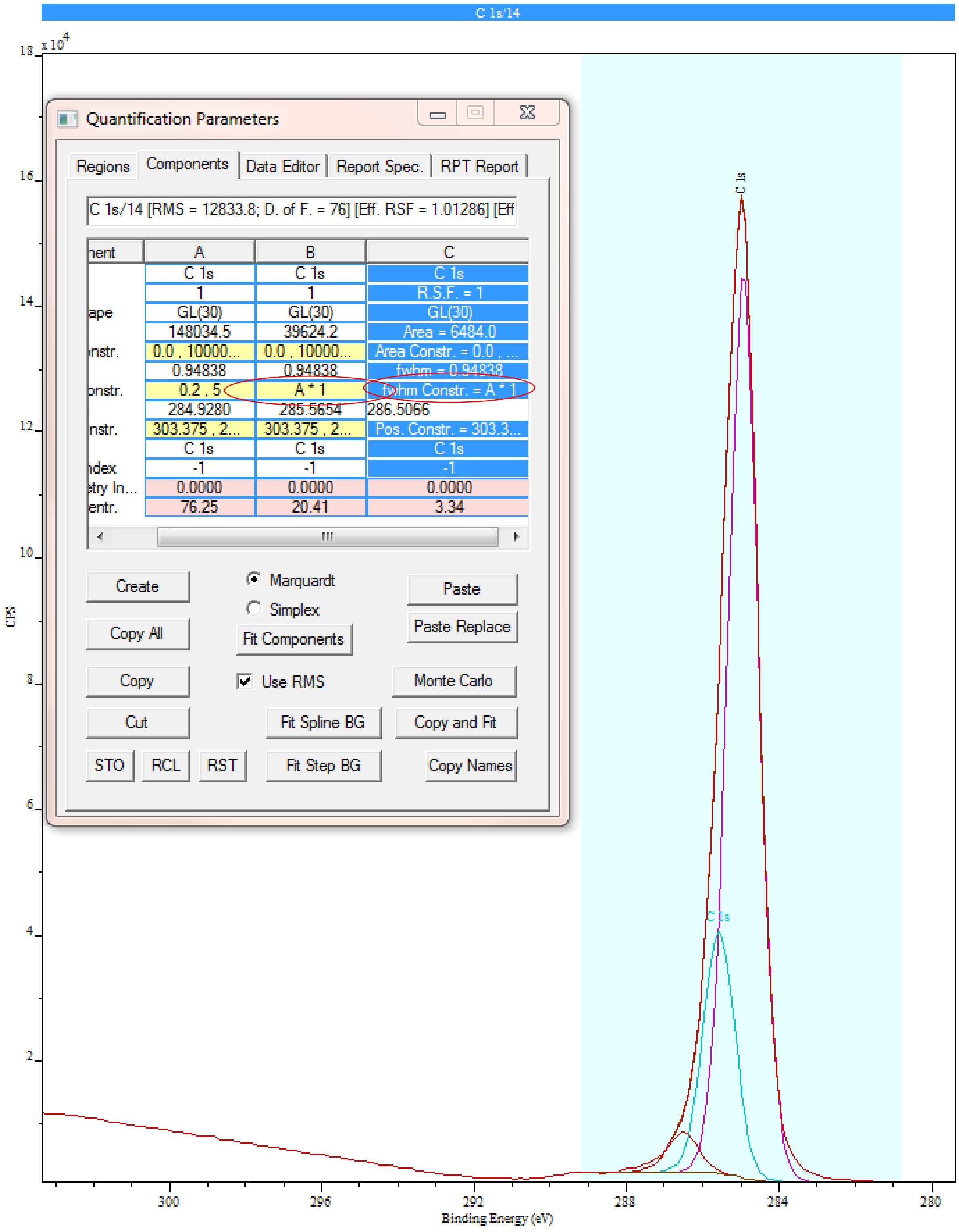

C 1s/14 [RMS = 12833.8; D. of F. = 76] [Eff. RSF = 1.01286] [Eff

nent	A	B	C
	C 1s	C 1s	C 1s
	1	1	R.S.F. = 1
ape	GL(30)	GL(30)	GL(30)
	148034.5	39624.2	Area = 6484.0
nstr.	0.0 , 10000...	0.0 , 10000...	Area Constr. = 0.0 , ...
	0.94838	0.94838	fwhm = 0.94838
onstr.	0.2 , 5	A * 1	fwhm Constr. = A * 1
	284.9280	285.5654	286.5066
nstr.	303.375 , 2...	303.375 , 2...	Pos. Constr. = 303.3...
	C 1s	C 1s	C 1s
ndex	-1	-1	-1
etry In...	0.0000	0.0000	0.0000
entr.	76.25	20.41	3.34

● Marquardt
○ Simplex
☑ Use RMS

6- Then, all data was export to the OriginPro in order to plot it and present it.

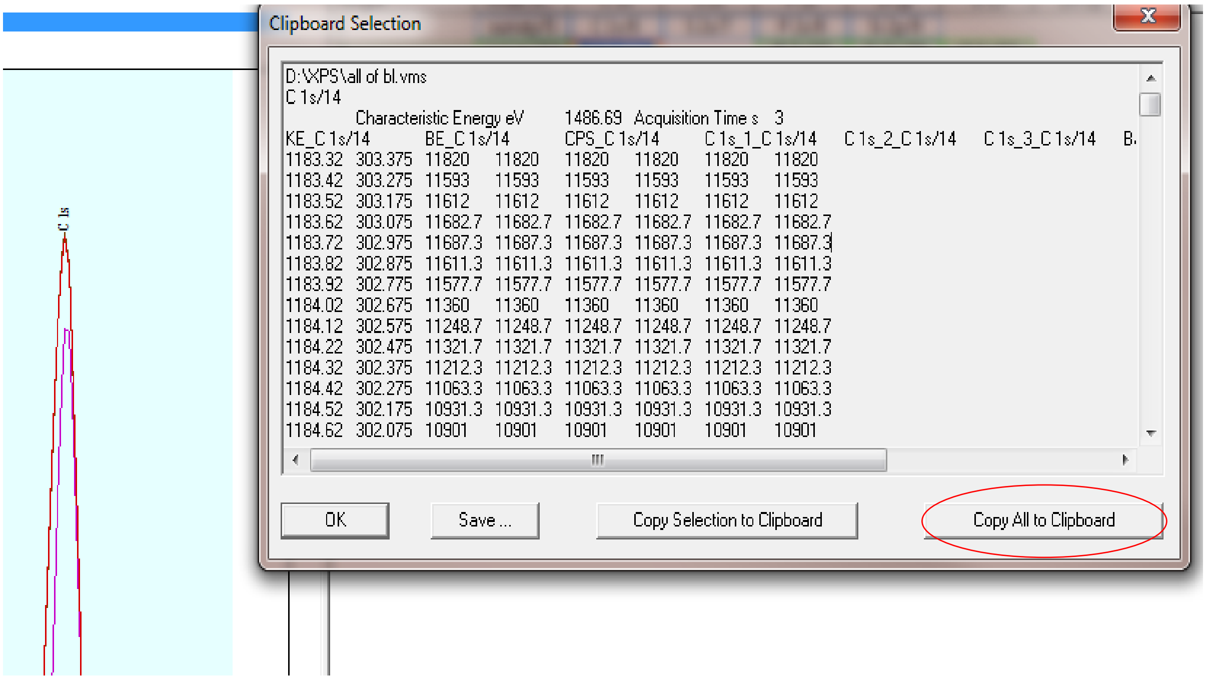

```
D:\XPS\all of bl.vms
C 1s/14
          Characteristic Energy eV      1486.69  Acquisition Time s   3
KE_C 1s/14          BE_C 1s/14          CPS_C 1s/14         C 1s_1_C 1s/14      C 1s_2_C 1s/14      C 1s_3_C 1s/14      B.
1183.32  303.375  11820    11820    11820    11820    11820    11820
1183.42  303.275  11593    11593    11593    11593    11593    11593
1183.52  303.175  11612    11612    11612    11612    11612    11612
1183.62  303.075  11682.7  11682.7  11682.7  11682.7  11682.7  11682.7
1183.72  302.975  11687.3  11687.3  11687.3  11687.3  11687.3  11687.3
1183.82  302.875  11611.3  11611.3  11611.3  11611.3  11611.3  11611.3
1183.92  302.775  11577.7  11577.7  11577.7  11577.7  11577.7  11577.7
1184.02  302.675  11360    11360    11360    11360    11360    11360
1184.12  302.575  11248.7  11248.7  11248.7  11248.7  11248.7  11248.7
1184.22  302.475  11321.7  11321.7  11321.7  11321.7  11321.7  11321.7
1184.32  302.375  11212.3  11212.3  11212.3  11212.3  11212.3  11212.3
1184.42  302.275  11063.3  11063.3  11063.3  11063.3  11063.3  11063.3
1184.52  302.175  10931.3  10931.3  10931.3  10931.3  10931.3  10931.3
1184.62  302.075  10901    10901    10901    10901    10901    10901
```